

Iron isotope fractionation in soils

From phenomena to process identification

Doctoral Thesis

Author(s):

Wiederhold, Jan Georg

Publication date:

2006

Permanent link:

<https://doi.org/https://doi.org/10.3929/ethz-a-005275890>

Rights / license:

[In Copyright - Non-Commercial Use Permitted](#)

DISS. ETH NO. 16849

**IRON ISOTOPE FRACTIONATION IN SOILS -
FROM PHENOMENA TO PROCESS
IDENTIFICATION**

Jan G. Wiederhold



Zurich, 2006

DISS. ETH NO. 16849

**IRON ISOTOPE FRACTIONATION IN SOILS -
FROM PHENOMENA TO PROCESS IDENTIFICATION**

A dissertation submitted to

ETH ZURICH

for the degree of
Doctor of Natural Sciences

presented by

JAN GEORG WIEDERHOLD

Dipl.-Geoökol., University of Karlsruhe (TH)

born 06.09.1975

citizen of Germany

accepted on the recommendation of

Prof. Dr. Ruben Kretzschmar, examiner

PD Dr. Stephan M. Kraemer, co-examiner

Dr. Nadya Teutsch, co-examiner

Prof. Dr. Alex N. Halliday, co-examiner

2006

***Und so sag ich zum letzten Male:
Natur hat weder Kern noch Schale;
Du prüfe dich nur allermeist,
Ob du Kern oder Schale seist!***

*And so for the last time this I tell:
Nature has neither core nor shell;
Better search yourself once more,
Whether you are crust or core!*

Johann Wolfgang von Goethe, 1749-1832, German poet and natural scientist
The iron oxide mineral goethite was named after him in 1815.

TABLE OF CONTENTS

Summary	VII
Zusammenfassung	IX
1. Introduction	1
1.1 Objectives and approach.....	3
2. Iron in soils	5
2.1 Pedogenic iron transformations.....	6
2.2 Dissolution of iron oxide minerals.....	11
References.....	14
3. Iron isotopes	17
3.1 Iron isotope analysis.....	21
3.2 State of research on iron isotopes.....	26
References.....	35
4. Iron isotope fractionation in oxic soils by mineral weathering and podzolization	43
4.1 Introduction.....	44
4.2 Methods.....	
4.2.1 Sampling sites.....	47
4.2.2 Soil sampling and sample preparation.....	49
4.2.3 Iron isotope measurement.....	50
4.3 Results and Discussion.....	
4.3.1 Iron concentration profiles in total soil digests.....	52
4.3.2 Iron isotope ratios in total soil digests.....	54
4.3.3 Sequential extraction methods in iron isotope studies.....	56
4.3.4 Iron concentration profiles in sequential extraction samples.....	58
4.3.5 Iron isotope ratios in sequential extraction samples.....	62
4.3.6 Comparison with available literature data.....	63
4.3.7 Fractionation mechanisms.....	65
4.4 Conclusions.....	66
References.....	67

5. Iron isotope fractionation during pedogenesis in redoximorphic soils	71
5.1 Introduction	72
5.2 Materials and Methods	
5.2.1 Sampling sites	75
5.2.2 Soil sampling and sample preparation	78
5.2.3 Iron isotope measurement	80
5.3 Results and Discussion	
5.3.1 Iron concentration profiles in total soil digests	81
5.3.2 Iron isotope ratios in total soil digests	83
5.3.3 Sequential extraction methods in iron isotope studies	85
5.3.4 Iron concentration profiles in sequential extraction samples	86
5.3.5 Iron isotope ratios in sequential extraction samples	88
5.3.6 Interpretation of iron isotope effects	91
5.4 Conclusions	94
References	95
6. Iron isotope fractionation during proton-promoted, ligand-controlled and reductive dissolution of goethite	99
6.1 Introduction	100
6.2 Experimental Section	
6.2.1 Material and reagents	103
6.2.2 Setup of batch dissolution experiments	103
6.2.3 Sample preparation for isotope analysis	104
6.2.4 Analytical methods	105
6.2.5 Modeling approach	106
6.3 Results and Discussion	
6.3.1 Dissolution kinetics	107
6.3.2 Iron isotopes	108
6.3.3 Model results	110
6.3.4 Fractionation mechanism	111
6.3.5 Late stage dissolution	112
6.3.6 Environmental significance	115
References	116
7. Conclusions	119
Appendix 1 (referring to work presented in chapter 4)	123
Appendix 2 (referring to work presented in chapter 5)	129
Appendix 3 (referring to work presented in chapter 6)	137
Acknowledgements	145
Curriculum Vitae	147

Summary

Iron is a key element for biogeochemical processes in the pedosphere. It is not only an essential nutrient for almost all organisms, but also exerts an important control on the behavior and fate of other elements in the environment. Moreover, iron is a very dynamic element in soils. Iron transformations in soils, which are governed by the prevailing geochemical and pedogenetic conditions, represent fundamental processes of weathering and soil formation.

The distribution of the four stable iron isotopes (^{54}Fe , ^{56}Fe , ^{57}Fe , ^{58}Fe) in nature is influenced by isotope fractionations during biogeochemical iron cycling. Thus, the iron isotope signature of a soil sample offers valuable clues on past and present pedogenetic processes and iron transformations in nature. The analytical methods required to resolve the small variations of iron isotope ratios in natural samples were developed only a few years ago. Hence, the available data on iron isotope variations in nature is still very limited, despite the intense current research activities. Furthermore, the fractionation mechanisms which govern the behavior of iron isotopes in biogeochemical reactions are only partially understood up to now. The objective of this thesis was to apply iron isotopes as a new geochemical tool to soil systems and to establish mechanistic links from the observed iron isotope fractionation effects to pedogenic processes and mineral weathering reactions.

Iron isotope ratios were measured by multiple collector inductively coupled plasma mass spectrometry (MC-ICPMS). Five soil profiles, characterized by well-defined and contrasting geochemical conditions, were studied in detail. The analysis of bulk soil samples was complemented by the investigation of individual iron mineral pools separated by sequential extractions. In addition, dissolution experiments under controlled laboratory conditions were performed to gain insight into iron isotope fractionation during mineral weathering at a mechanistic level.

Significant variations in the iron isotope signature of natural soils were found and linked to pedogenic processes. The range in $\delta^{57}\text{Fe}$, describing variations of the isotope ratio $^{57}\text{Fe}/^{54}\text{Fe}$ relative to the iron isotope standard IRMM-014 in parts per thousand (per mil), amounts to more than one per mil for bulk soil samples, which exceeds the variability of iron isotope ratios in igneous rocks by more than one magnitude. The investigation of individual iron mineral pools separated from the soil

samples revealed even larger variations of more than three per mil in $\delta^{57}\text{Fe}$. It was found that light iron isotopes are preferentially translocated within the soil during pedogenesis. This effect was observed both during podzolization, a pedogenic iron translocation occurring in oxic soils under the influence of organic ligands and acidic conditions, and during reductive iron transformations in hydromorphic soils. The observed directions and magnitudes of iron isotope fractionation induced by abiotic and biotic iron transformations, or by ligand-controlled and redox-controlled processes, respectively, have important implications for the interpretation of natural iron isotope signatures.

As a result of the laboratory experiments, it was demonstrated for the first time that different dissolution mechanisms of iron oxide minerals cause distinct iron isotope fractionation effects. Ligand-controlled and reductive dissolution result in strong enrichments of light iron isotopes in solution during the initial reaction phase. A model describing the evolution of iron isotope ratios at the mineral surface and in solution was developed to understand and quantify the observed kinetic isotope effect. An enrichment of heavy iron isotopes in solution was observed during later stages of dissolution, which points toward the occurrence of equilibrium iron isotope fractionation between organic complexes in solution and the mineral surface. In contrast, no iron isotope fractionation was observed during proton-promoted dissolution, which could be explained by a different bond-breakage scheme compared to the other two mechanisms.

In summary, the presented thesis represents the first comprehensive investigation of iron isotope fractionations in soils. It provides new important insights into pedogenic iron transformations and mineral dissolution mechanisms by elucidating the associated iron isotope effects. Thus, this thesis will be useful for the further development of iron isotopes as a tracer for the past and present biogeochemical iron cycle in natural systems.

Zusammenfassung

Eisen ist ein Schlüsselement für biogeochemische Prozesse in der Pedosphäre. Es ist nicht nur ein essentieller Nährstoff für nahezu alle Lebewesen, sondern übt auch eine wichtige Kontrolle über das Verhalten und den Verbleib anderer Elemente in der Umwelt aus. Zudem ist Eisen ein sehr dynamisches Element in Böden. Umwandlungen von Eisen im Boden, die durch die vorherrschenden geochemischen und pedogenetischen Bedingungen bestimmt werden, stellen fundamentale Prozesse der Verwitterung und Bodenbildung dar.

Die Verteilung der vier stabilen Eisenisotope (^{54}Fe , ^{56}Fe , ^{57}Fe , ^{58}Fe) in der Natur wird durch Isotopenfraktionierungen während des biogeochemischen Eisenkreislaufs beeinflusst. Daher bietet die Eisenisotopensignatur einer Bodenprobe wertvolle Hinweise auf vergangene oder gegenwärtige bodenbildende Prozesse und Eisenumwandlungen in der Natur. Die benötigten analytischen Methoden zur Auflösung der kleinen Variationen der Eisenisotopenverhältnisse wurden erst vor wenigen Jahren entwickelt. Somit sind die verfügbaren Daten über Eisenisotopenvariationen in der Natur trotz der gegenwärtigen intensiven Forschungsaktivitäten noch sehr begrenzt. Überdies sind die Fraktionierungsmechanismen, welche das Verhalten von Eisenisotopen in biogeochemischen Reaktionen bestimmen, bisher nur teilweise verstanden. Die Zielsetzung dieser Arbeit war es, Eisenisotope als neues geochemisches Hilfsmittel auf Bodensysteme anzuwenden, und mechanistische Zusammenhänge zwischen den beobachteten Eisenisotopen-Fraktionierungen sowie pedogenen Prozessen und Mineralverwitterungsreaktionen herzustellen.

Eisenisotopenverhältnisse wurden mithilfe der Multikollektor-Plasma-Massenspektrometrie (MC-ICPMS) gemessen. Fünf Bodenprofile, gekennzeichnet durch eindeutige und kontrastierende geochemische Bedingungen, wurden detailliert untersucht. Die Analyse von Gesamtbodenproben wurde ergänzt durch die Untersuchung von einzelnen Eisenmineral-Pools, die mithilfe sequentieller Extraktionen getrennt wurden. Zusätzlich wurden Auflösungsexperimente unter kontrollierten Laborbedingungen durchgeführt, um Einblicke in die Fraktionierung von Eisenisotopen auf einer mechanistischen Ebene zu erhalten.

Signifikante Variationen in der Eisenisotopensignatur von Böden wurden festgestellt und mit pedogenen Prozessen verknüpft. Die Spanne in $\delta^{57}\text{Fe}$, einem Wert der die Abweichung des Eisenverhältnisses $^{57}\text{Fe}/^{54}\text{Fe}$ relativ zu dem Eisenisotopen-Standard IRMM-014 in Promille beschreibt, beträgt mehr als ein Promille in den Gesamtbodenproben, was die Variabilität in magmatischen Gesteinen um mehr als eine Grössenordnung übertrifft. Die Untersuchung der einzelnen Eisenmineral-Pools, die aus den Bodenproben abgetrennt wurden, ergab sogar noch grössere Variationen in $\delta^{57}\text{Fe}$ von mehr als drei Promille. Es wurde herausgefunden, dass leichte Eisenisotope bevorzugt während der Pedogenese im Boden verlagert werden. Dieser Effekt wurde sowohl während der Podsolierung, einer pedogenen Eisenverlagerung, die in oxischen Böden unter dem Einfluss von organischen Liganden und sauren Bedingungen abläuft, und während reduktiver Eisenumwandlungen in hydromorphen Böden festgestellt. Die beobachteten Richtungen und Grössenordnungen der Eisenisotopenfraktionierung, die durch abiotische und biotische, respektive liganden-kontrollierte und redox-kontrollierte Prozesse hervorgerufen wurden, haben wichtige Auswirkungen auf die Interpretation von natürlichen Eisenisotopensignaturen.

Mithilfe der Laborexperimente konnte erstmals gezeigt werden, dass verschiedene Auflösungsmechanismen von Eisenoxidmineralen unterschiedliche Eisenisotopen-Fraktionierungseffekte bewirken. Liganden-kontrollierte und reduktive Auflösung rufen während der initialen Reaktionsphase eine starke Anreicherung der leichten Eisenisotope in Lösung hervor. Ein Modell, das den Verlauf der Eisenisotopen-Verhältnisse an der Mineraloberfläche und in Lösung beschreibt, wurde entwickelt, um den beobachteten kinetischen Isotopeneffekt zu verstehen und zu quantifizieren. Während der späteren Auflösungsphasen wurde eine Anreicherung von schweren Eisenisotopen in Lösung festgestellt, was auf das Auftreten von Gleichgewichts-Eisenisotopenfraktionierungen zwischen organischen Komplexen in Lösung und der Mineraloberfläche hindeutet. Im Gegensatz dazu wurden während der protonen-kontrollierten Auflösung keine Eisenisotopenfraktionierung festgestellt, was durch ein unterschiedliches Brechen von Bindungen gegenüber den beiden anderen Mechanismen erklärt werden könnte.

Zusammenfassend kann gesagt werden, dass die vorliegende Arbeit die erste umfassende Untersuchung von Eisenisotopenfraktionierungen in Böden darstellt. Sie

bietet neue wichtige Einblicke in pedogene Eisentransformationen und Mineralauflösungsmechanismen durch die Aufklärung der assoziierten Eisenisotopen-Effekte. Somit wird diese Arbeit für die weitere Entwicklung von Eisenisotopen als Tracer für den früheren oder gegenwärtigen biogeochemischen Eisenkreislauf in natürlichen Systemen hilfreich sein.

1. INTRODUCTION

Stable iron isotopes provide a new geochemical tool that holds promise to be useful for many basic and applied problems of earth and environmental sciences. The analytical methods to resolve mass-dependent variations of iron isotopes in nature have only been developed less than a decade ago. In consequence, the existing knowledge regarding the behavior of iron isotopes in the natural biogeochemical iron cycle is still very limited. The pioneering work on iron isotope geochemistry over the last few years has delivered some initial insight into the variations of iron isotope ratios in different natural systems and the fractionation mechanisms, which govern the distribution of iron isotopes during biogeochemical processes. The fundamental concept of the application of iron isotopes as a geochemical tracer is based on the homogeneous distribution of iron isotopes in magmatic rocks, which is only variable within a very small range. In contrast, a much wider range of iron isotope ratios exists in low-temperature environments such as sediments, soils, and the biosphere. Many geochemical processes including biologically-mediated reactions are able to induce significant fractionations of iron isotopes. Thus, the iron isotope signature of a natural sample represents an image of the processes and conditions which have influenced the genesis and the fate of the sample during biogeochemical iron cycling. Iron is a very dynamic element both in the geosphere and in the biosphere. It is for example removed from rocks by chemical weathering, transformed into pedogenic oxide minerals, mobilized in reduced sediments, or taken up by organisms and incorporated into enzymes and proteins. Due to its ubiquitous abundance and high reactivity, iron also exerts a major influence on the fate of other elements in nature. Moreover, iron is an essential nutrient element for organisms and involved in fundamental metabolic processes such as respiration and photosynthesis. The key role of iron in many geochemical and biological processes has led to extensive research on the behavior and fate of iron and iron-bearing compounds in the environment. However, there still remain many open questions and problems, which includes for instance the relative importance of biotic and abiotic iron transformations in nature, the role of iron in microbial metabolic processes, the surface reactivity of iron oxide minerals, or the bioavailability of iron in terrestrial and marine systems. Stable iron isotope geochemistry has the potential to elucidate some of the involved processes and

mechanisms and to provide new insights into iron cycling in modern and past environments. The applicability of iron isotopes as a tracer is still held back by the incomplete understanding of iron isotope geochemistry during fractionating reactions in natural systems. However, the current work in many research groups worldwide is constantly expanding the knowledge on iron isotopes which contributes to the development of this new geochemical tool.

The pedosphere is an integral part of terrestrial ecosystems. Soils are located at the interface of lithosphere, hydrosphere, biosphere, and atmosphere. They consist of a mixture of solid, liquid, and gaseous phases, are made up of inorganic and organic compounds, and are formed by a variety of abiotic and biotic processes. From a geochemical point of view, many reactions in soils are kinetically controlled and cannot be described sufficiently by thermodynamical considerations. Moreover, soils are highly heterogeneous systems and very variable in space and time. In summary, the study of soil biogeochemistry represents a challenging task and requires multidisciplinary approaches. Iron has a key role in many biogeochemical processes in the pedosphere. It is a major constituent of chemical weathering reactions in soils. Secondary iron oxide phases are important pedogenic minerals which exert a major influence on soil development and soil properties. Iron in soils is used as electron acceptor in anaerobic microbial respiration and required by organisms as essential nutrient element. Despite the knowledge on the pivotal role of iron in soil biogeochemistry and comprehensive research activities, there are still many open questions. The important role of microorganisms as the driving force for pedogenic iron transformations in water-saturated soils has been recognized relatively recently and is still only partially understood. Secondly, the elaborate iron acquisition strategies, executed by plants and microorganisms in order to gain access to the limiting nutrient iron in calcareous soils, still hold many secrets. Moreover, the formation and surface reactivity of pedogenic iron oxide minerals, which influence the fate of pollutant elements in the environment, is subject of intense research. These examples only highlight a few topics of current work on the biogeochemistry of iron in soil ecosystems. It is evident that stable iron isotopes have the potential to be applied as a geochemical tracer in the pedosphere. The isotope signature of iron in different soil profiles, soil horizons, or individual iron mineral pools in the soil offers information on pedogenic processes that was previously not

available. However, the geochemistry of iron isotopes in soils represents a new and almost completely unexplored scientific field. Thus, the motivation for the work presented in this thesis was to explore the new geochemical tool of iron isotopes in soils.

1.1 Objectives and approach

The first main objective of the presented thesis was to perform a systematic study of iron isotope variations in the pedosphere. The occurrence, magnitude and spatial distribution of iron isotope fractionation in natural soil environments was to be investigated in detail. However, the goal of this dissertation project was not only to report the existence of iron isotope fractionation in soils, but also to construct a link to pedogenic processes which are responsible for the observed phenomena. Since soils are often influenced by a multitude of geochemical reactions and different pedogenic processes which occur in parallel, it was necessary to perform a very careful selection of the investigated field sites. The selected soil profiles are characterized by distinct geochemical conditions (e.g., soil pH, redox potential) and dominated by a single pedogenic iron transformation process. Using this approach, it was possible to assess the effect of individual pedogenic processes on the iron isotope signature of soils. The studied processes include oxic mineral weathering reactions, podzolization, and redox transformations of iron under different pH conditions. The study presented in chapter 4 focused on oxic soil environments. The detailed sampling and investigation of two well-drained Podzol profiles and one Cambisol profile explored the influence of acidic pH and organic ligands on iron isotope fractionation in soils. In contrast, the study presented in chapter 5 focused on iron redox transformations in soils. A permanently water-saturated soil with high soil pH was compared to a seasonally water-saturated soil exhibiting very acidic soil conditions. Therefore, a systematic assessment of iron isotope fractionation induced by pedogenic iron transformation processes is provided by the field data presented in this thesis.

The second main objective of this thesis was to determine to what extent non-enzymatic weathering reactions of iron oxide minerals result in iron isotope fractionation. The dissolution behavior of iron oxide minerals plays an important role in pedogenic processes. The detailed understanding of iron oxide dissolution kinetics

at a mechanistic level is essential for the study of pedogenic iron transformations. It had been shown before that microbially-mediated dissolution of iron oxide minerals results in significant iron isotope fractionation. However, no information was available on the effect of non-enzymatic weathering reactions on iron isotopes. In order to address this objective, dissolution experiments under controlled laboratory conditions were performed. Iron isotope fractionation during proton-promoted, ligand-controlled and reductive dissolution mechanisms was investigated. The results of this part of the thesis are presented in chapter 6. Isotope fractionation during mineral dissolution reactions is complicated by the fact that dissolution proceeds only within a relatively small reaction front at the surface of the mineral. Therefore, isotope depletions and enrichments are occurring between this transient surface pool and the solution. A model, which describes isotope fractionation during mineral dissolution, was developed to approach this system and to understand the interactions between the involved iron pools.

The results of the laboratory-based dissolution experiments and the modeling approach provide important clues for the interpretation of the iron isotope field data. Thus, this thesis approaches the topic of iron isotope fractionation in soils from different perspectives. The combination of field and laboratory work enables a comprehensive view on the geochemistry of iron isotopes in soils by combining the relevance of field data with the detailed mechanistic understanding attained in laboratory studies. In consequence, the overall objective of this thesis was to bridge the gap between the observation of phenomena and the identification of processes and mechanisms concerning iron isotope fractionation in soils. A short discussion of the most important findings and conclusions of this thesis and a brief outlook to future research needs is provided in chapter 7. The next two chapters are intended to give some important background information on the topic of this thesis and to outline the development of the scientific field. They contain general information on iron in soils (chapter 2) and iron isotopes (chapter 3) based on a review of the recent literature.

2. IRON IN SOILS

Iron is a key element in soils and natural systems in general, not only due to its ubiquitous abundance but also due to its high reactivity in geochemical processes and its importance for biological systems. Iron is believed to be the most abundant element per weight in the Earth as a whole. Iron atoms were formed by stellar nucleosynthesis and the high geochemical abundance can be explained by the extremely stable configuration of iron nuclei which possess a maximum nuclear binding energy per nucleon. However, the major part of iron on Earth is concentrated as metallic iron in the Earth's core. Iron is the fourth most abundant element in the Earth's crust with an average content of about 5 % per weight, exceeded only by oxygen, silicon and aluminum (Kümmel and Papp, 1990). The iron content in rocks ranges from less than 1 % in limestones to about 10 % in ultramafic rocks (Marshall and Fairbridge, 1999). Accordingly, the iron content of soils depends initially on the primary composition of its lithogenic parent material. During soil development, iron concentrations in the soil can both decrease and increase depending on the pedogenetic conditions which may induce iron depletion or enrichment processes. Iron also represents a very important element in biological systems. It is required as an essential nutrient by virtually all living organisms, except a few groups of microorganisms (Andrews et al., 2003). The iron content of plants and other organisms is very variable, but the average iron concentration of biomass is estimated to be about 100 ppm (Murad and Fischer, 1988).

To understand the distribution and the biogeochemical behavior of iron in nature, one must consider the two different oxidation states of iron. Speciation of iron is highly dependent on redox potential and pH (Stumm and Morgan, 1996). Ferrous iron (Fe^{II}) is the stable form under reduced or strongly acidic conditions, whereas ferric iron (Fe^{III}) dominates in most surface environments with contact to the atmosphere. Ferrous iron has a fairly high solubility, whereas ferric iron compounds are generally characterized by a very low solubility (Cornell and Schwertmann, 2003). In consequence, transformation processes between ferrous and ferric iron govern the geochemical behavior of iron in natural surface environments. Iron in magmatic rocks, which were formed under high temperature and pressure conditions in the lithosphere, occurs primarily in the ferrous oxidation state. The exposure of these rocks to the atmosphere as a result of tectonic and geomorphologic processes

shifts the thermodynamic stability for iron compounds from ferrous toward ferric compounds. Thus, the ratio of ferrous to ferric iron compounds generally decreases with sustained weathering and soil formation. Redox transformations between ferrous and ferric iron also represent the key factor in the biological iron cycle where the main role of iron consists in the catalysis of electron transfer reactions in enzymes and proteins. In addition, microorganisms can use iron compounds in their respiration. Iron-oxidizing bacteria, most abundant in acidic environments, gain energy from the chemolithotrophic oxidation of ferrous to ferric iron (Weber et al., 2006) whereas iron-reducing bacteria, occurring under anaerobic conditions, couple the oxidation of organic matter to dissimilatory iron reduction by using ferric iron as terminal electron acceptor (Lovley et al., 2004).

2.1 Pedogenic iron transformations

One of the first processes in pedogenesis is the chemical weathering of the lithogenic parent material. As mentioned above, iron in the lithosphere is dominated by ferrous iron, though in some sedimentary rocks the ferric form is also present in considerable amounts. The most important iron-bearing phases in magmatic rocks are silicate minerals such as olivine, pyroxene, amphibole and biotite. The contact of these minerals with water, oxygen, and acids under atmospheric conditions results in weathering reactions that involve the oxidation of ferrous to ferric iron (Wilson, 2004). Iron oxidation occurs either within the mineral structure, which weakens the stability of the crystal lattice due to the smaller ionic radius of ferric iron, or in soil solution where ferrous iron, which was released from weathered silicate minerals, oxidizes rapidly resulting in the precipitation of secondary ferric iron oxide phases.

Iron oxides are, besides clay minerals, the major product of weathering reactions in soils and its formation, transformation, and dissolution processes exert an important influence on the development of soils and soil properties (Stucki et al., 1988; Cornell and Schwertmann, 2003). Poorly-crystalline iron oxyhydroxide phases such as ferrihydrite ($\text{Fe}_5\text{HO}_8 \cdot 4 \text{H}_2\text{O}$) are usually the first solid products of ferric iron precipitation. This is in accordance with the Ostwald step rule postulating that the least stable solid phase, i.e., the precipitate with the highest solubility, will form first in a consecutive precipitation reaction (Stumm and Morgan, 1996). Transformation reactions into thermodynamically more stable phases, which are often associated

with the elimination of crystal water, result in the formation of crystalline iron oxide phases. The most important crystalline iron oxides in soils are goethite (α -FeOOH) and hematite (α -Fe₂O₃). Lepidocrocite (γ -FeOOH) also occurs in soils, mainly in redoximorphic environments, but is less stable than goethite. Magnetite (Fe₃O₄) occurs mainly as lithogenic primary mineral in soils, although pedogenic magnetite formation has been described both by biotic and abiotic processes (Cornell and Schwertmann, 2003). However, magnetite and its oxidation product maghemite (γ -Fe₂O₃), which is mainly formed during forest fires, are only minor iron oxide phases in soils. Mixed-valence iron oxyhydroxide phases, which contain a mixture of ferrous and ferric iron, are summarized under the term 'green rust' and have been described in redoximorphic soils. Under permanently reducing conditions, ferrous iron compounds can be formed in soils with siderite (FeCO₃), vivianite (Fe₃(PO₄)₂ • 8 H₂O), and different iron sulfide phases representing the most important minerals. Iron oxide minerals are characterized by their intense colors. Apart from the dark color of soil organic matter which occurs mainly in the topsoil horizons, soil colors are dominated by iron oxides. The yellowish-brown colors of goethite and the bright red colors of hematite that are found in soils worldwide provide an apparent visible indication of pedogenic iron oxide formation. In addition, iron oxide minerals, which are like all pedogenic minerals characterized by small particle sizes and large surface areas, influence the physical and chemical properties of soils by for instance providing adsorption sites for nutrient and pollutant elements (Cornell and Schwertmann, 2003).

The development of brown colors in the weathering horizon is an important criteria in the classification of soils types. Soil profiles that exhibit such a weathered B horizon (Bw) as their main characteristic feature are classified as Cambisols (from the Latin word *cambiare* meaning "changing") according to the World Reference Base for Soil Resources (WRB, 2006) or as Braunerde (meaning "brown earth") in the German soil classification system. The main pedogenic iron transformation occurring in these soils are the formation of secondary iron oxides (e.g., ferrihydrite, goethite) as a result of silicate weathering under the influence of water, oxygen and acids. Acidification is an important natural process in pedogenesis which controls for instance the release of essential nutrient elements for plant growth. On the one hand, acidity is introduced into the soil by carbon dioxide which equilibrates with the soil

solution by forming carbonic acid and which originates from the atmosphere or from organic matter decomposition in the soil. On the other hand, organic acids are released into the soil environment by plants and microorganisms. Moreover, organic acids are produced during the degradation of organic matter. The introduced protons react in the soil environment with different buffer systems (e.g., carbonates, cation exchange sites, silicate minerals) promoting chemical weathering processes. In consequence, soil pH generally decreases with continued soil development in a humid climate. In some soils, extreme acidity in combination with organic ligands leads to another important pedogenic iron transformation process which is called podzolization.

Podzolization is a pedogenic process which leads to a vertical downward transport of iron in the soil profile, together with aluminum and organic matter (Van Breemen and Buurman, 2004). The translocation is induced by a combination of very acidic conditions (soil pH < 4) and high concentrations of organic ligands. General prerequisites for podzolization are a well-drained substrate that is poorly-buffered against acidification (typically quartz-rich sands or granite) and a cool humid climate. In addition, a vegetation which generates poorly-degradable litter (e.g., coniferous forests or heath) is essential for the podzolization process due to the release of organic ligands. The typical horizon sequence of Podzols consists of a dark organic surface layer (O) on top, followed by a grey depleted eluvial horizon (E) and enriched illuvial B horizons that are colored by organic matter (Bh) and iron oxides (Bs). Organic acids that are released from the organic surface layer (O horizon) under very acidic conditions (pH < 4) form metal-ligand-complexes with iron and aluminum thereby leaching the upper mineral soil which creates the grey depleted E horizon. The Fe-Al-organic complexes are then transported vertically downward until their reprecipitation in the B horizon. Often, an organic rich black Bh horizon is overlying a reddish sesquioxide-rich Bs horizon. The pedogenesis of Podzols has been studied for a long time. However, the exact mechanisms which are involved in podzolization are still discussed intensively in the literature (Anderson et al. 1982; Lundström et al., 2000; Buurman and Jongmans, 2005; Jansen et al., 2005). The main controversy focuses on the relative importance of organic acid complexes and inorganic colloidal sols in the downward transport of aluminum and iron (Lundström et al., 2000). The podzolization process has important consequences on many physical and chemical

soil properties and influences ecosystem functions and land use. Podzolization also changes the distribution of many elements other than iron and aluminum (e.g., Tyler, 2004; Donisa et al., 2005). It is generally assumed that pedogenic iron transformations during podzolization proceed without a change in the oxidation state of iron, at least in well-drained oxic soils. The mobility of ferric iron in Podzols is enabled by the extreme acidity and the presence of organic ligands which form stable complexes with ferric iron in soil solution. However, in soils which are temporarily or permanently saturated with water, hydromorphic conditions develop which initiates another important set of processes involved in pedogenic iron transformation.

Soil microorganisms and plant roots consume oxygen by aerobic respiration. However, oxygen supply by diffusion from the atmosphere into the soil is impeded to a great extent under water-saturated conditions. In consequence, anaerobic microorganisms take over the degradation of organic matter by using alternate electron acceptors. After the removal of nitrate by denitrification, dissimilatory metal-reducing bacteria start to use oxidized iron and manganese compounds in the soil as electron acceptor in their respiration. The active role of microorganisms in reductive iron transformations processes in these environments has been discovered relatively late (Lovley and Phillips, 1986). It is now generally accepted that microbial activity is the driving force for the biogeochemical iron cycle in hydromorphic soils. The most important groups of dissimilatory iron-reducing bacteria are the facultative anaerobic *Shewanella* species and the obligate anaerobic *Geobacter* species which couple the oxidation of organic matter to the reduction of ferric iron compounds (Lovley et al., 2004). However, the exact mechanisms of the electron transfer reactions which result in the reduction of ferric to ferrous iron are still subject to intense research (Hernandez and Newman, 2001; Rosso et al., 2003; Reguera et al., 2005). It is also still unclear which ferric iron phases are used by bacteria in natural environments. Laboratory studies have shown that dissimilatory iron-reducing bacteria are able to use different forms of iron oxide minerals, including crystalline magnetite and hematite (Dong et al., 2000; Gonzalez-Gil et al., 2005), or even structural ferric iron in clay minerals (Kostka et al., 1999; Stucki et al., 2006). It is generally assumed that poorly-crystalline iron oxyhydroxides such as ferrihydrite are preferentially utilized for thermodynamic reasons (Bonneville et al., 2004). However, recent reports indicate that mineralogical properties are less important in the control of microbial iron

reduction compared to the overall surface site availability which is influenced by secondary processes such as sorption or surface precipitation of ferrous iron (Roden, 2006). In any case, the dissolution of iron oxide minerals results in the generation of ferrous iron which is mobile within the soil. It is transported by diffusive and advective processes until it reaches zones of the soil profile where remaining oxygen leads to the reoxidation and precipitation of ferric iron (oxyhydr)oxide phases. This happens, depending on the temporal and spatial variability of the soil water regime, in characteristic horizons of the soil profile and results in the formation of typical iron depletion and enrichment zones. The corresponding soils are generally referred to as redoximorphic or hydromorphic soils (Schlichting and Schwertmann, 1973). They are formed by pedogenic processes that are summarized by the term redoximorphosis and they are characterized by typical redoximorphic features (Vepraskas, 1996). An example of redoximorphic features in a soil profile is displayed in Figure 2.1.

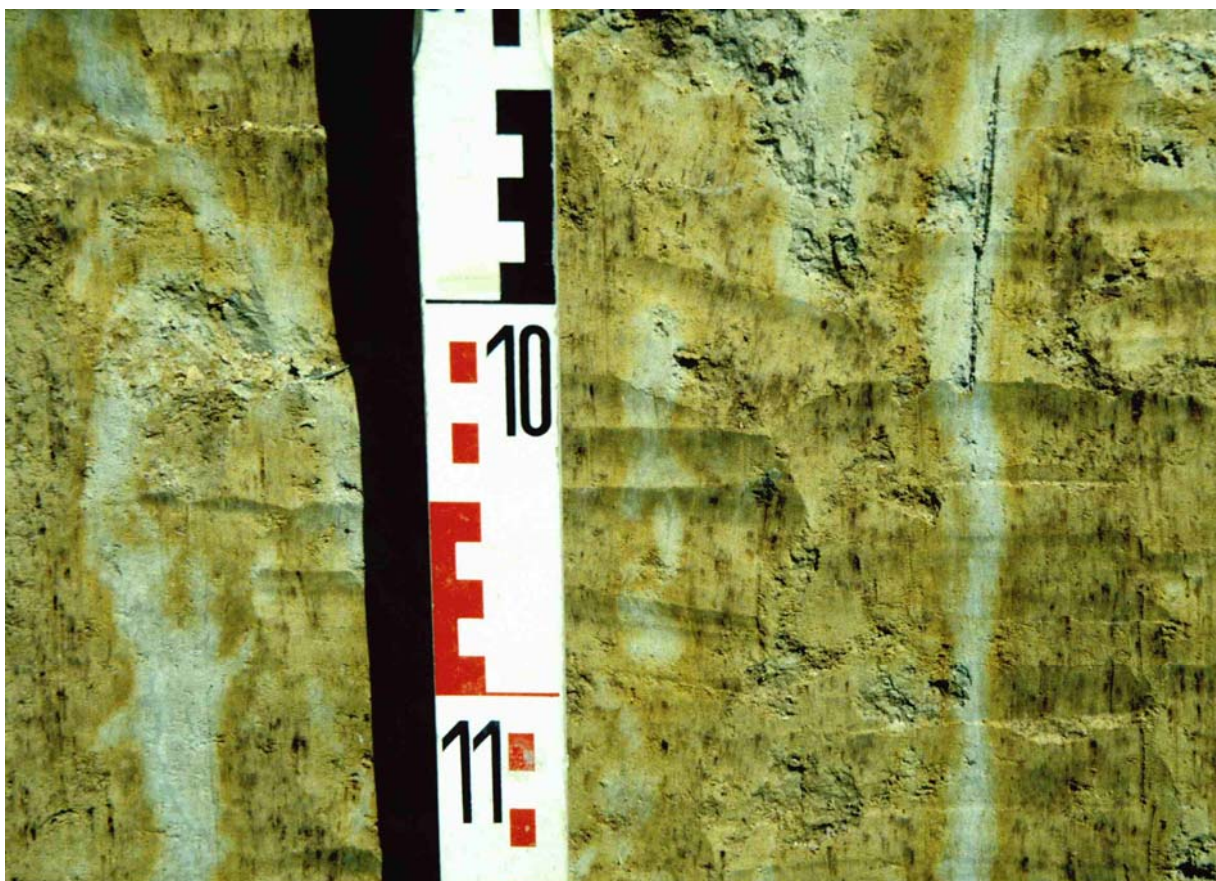


Figure 2.1 Photograph of redoximorphic features in a Stagnic Cambisol profile near Rafz (Canton Zurich, Switzerland). Grey iron depletion zones are clearly visible along preferential water flow paths, contrasting to brown iron enrichment zone in the adjacent soil matrix. Numbers on scale bar indicate 10 cm sections. (Photograph by courtesy of Ruben Kretzschmar)

In soils that are permanently water-saturated, mainly at locations with a high groundwater table, iron enrichments occur in a distinct horizon corresponding to the capillary fringe, whereas iron depletion zones are found predominantly in the soil horizons below the ground water table. In contrast, soils that are only seasonally water-saturated, typically due to stagnant water above a dense layer which inhibits vertical drainage, exhibit a different pattern of redoximorphic features. Here the depletion zones are mainly found in the vicinity of larger pores and along preferential flow paths where water infiltrates rapidly and reducing conditions are generated first. The enrichment zones are then mainly found in the interior of soil aggregates and in the soil matrix where remaining oxygen results in the precipitation of iron(oxyhydr)oxide minerals, often in the form of nodules or concretions (Vepraskas, 1996). These redistribution processes of iron within hydromorphic soils are not only interesting in terms of soil morphology and classification but also influence the fate of other elements of environmental interest such as phosphorus (Szilas et al., 1998), arsenic (Cummings et al., 1999), or other trace metals (Cooper et al., 2006; Thompson et al., 2006). In summary, redoximorphic processes represent, besides podzolization, the most important pedogenic iron transformation.

Iron transformations also occur during other pedogenic processes, but those are less important for the overall iron budget of soils. Iron is taken up by plant roots and microorganisms as essential nutrient element from the soil and iron contained in plant litter is redeposited on top of the soil in organically-bound form. Iron is also transported within soil profiles together with clay minerals in Luvisols during pedogenic clay translocation (Blume, 1988). However, this process consists mainly of a physical translocation of soil colloid particles at moderately acidic pH, and the involvement of iron is only caused by the small size of pedogenic iron oxide minerals which usually fall in the clay size fraction of soils.

2.2 Dissolution of iron oxide minerals

The important role of iron oxide minerals in soils has been illustrated in the previous section. The very low solubility of ferric iron in oxic environments, controlled by the precipitation of iron oxide phases, has a major impact on the bioavailability of iron. Therefore, despite its high abundance in soils, iron is often a limiting nutrient element for plants and microorganisms. Iron deficiency is especially widespread in

calcareous soils exhibiting a high soil pH. In consequence, plants and microorganisms have developed different strategies to overcome this geochemical barrier by enhancing the dissolution of iron oxide minerals. Thus, the study of dissolution mechanisms of iron oxide minerals plays a crucial role in understanding iron nutrition. In addition, reductive dissolution of iron oxide minerals occurs during microbial respiration by dissimilatory iron-reducing bacteria, as described in the previous section.

Mineral dissolution reactions in soils are surface processes which are governed by thermodynamic and kinetic constraints at the solid-solution interface (Stumm, 1992). Iron oxide dissolution occurs mainly by three different mechanisms (Zinder et al., 1986) which will be explained in the following (schematic overview in Figure 2.2).

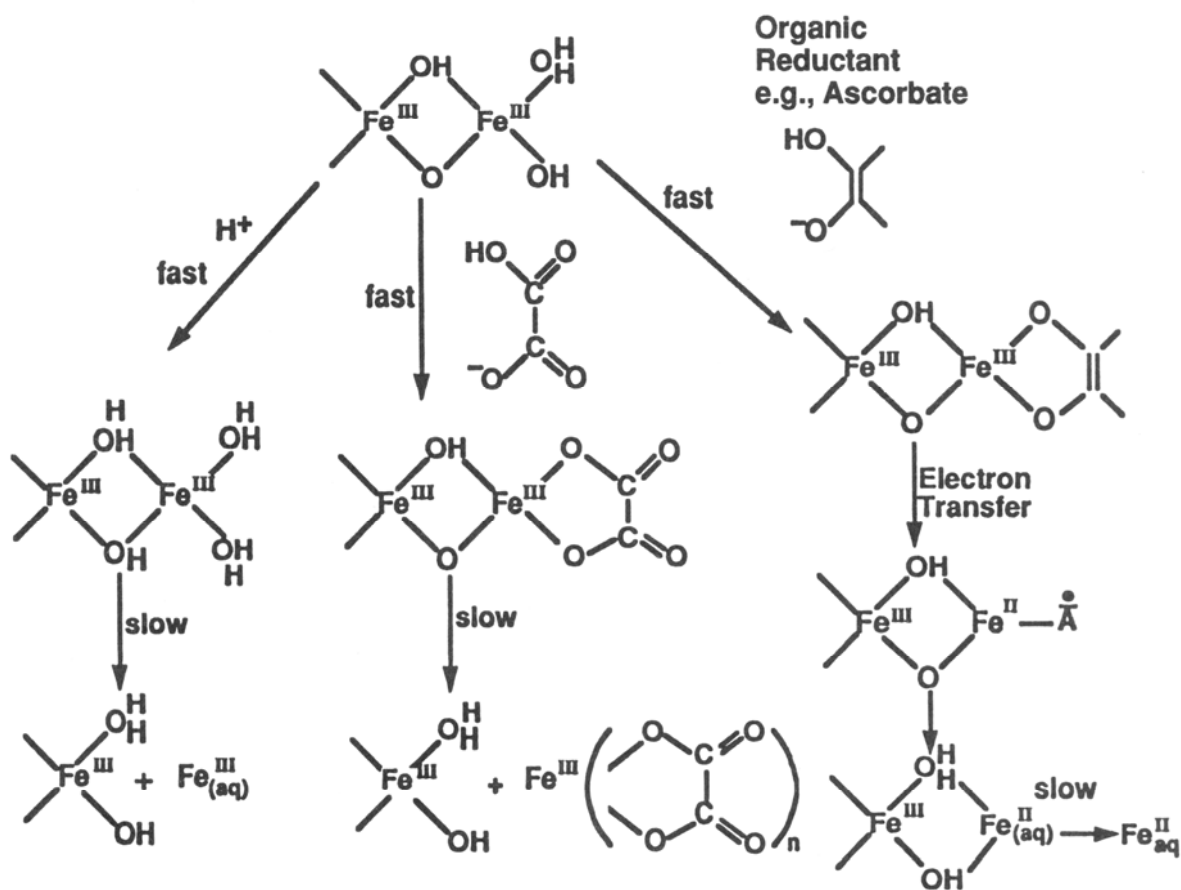


Figure 2.2 Schematic overview of iron oxide dissolution mechanisms (adapted from Stumm and Morgan, 1996). Arrows denoted as slow indicate the rate-limiting step of the particular dissolution reaction.

The essential part of all three mechanisms is the transfer of iron atoms, which are octahedrally coordinated by oxygen atoms in most iron oxide minerals, from the crystal surface into solution (Casey and Ludwig, 1996). Proton-promoted dissolution is driven by the reaction of protons with oxygen atoms and hydroxyl groups at the mineral surface. As a result of this proton adsorption, iron-oxygen bonds are weakened, probably by polarization, which promotes the detachment of iron atoms from the surface into solution (Cornell and Schwertmann, 2003). However, it is a very slow process and plays only a minor role in iron mobilization in nature except in environments with very acidic pH conditions.

The presence of molecules that form stable Fe(III)-ligand complexes can strongly accelerate the dissolution of iron oxides (Kraemer, 1997). These ligands include for instance organic acids, such as oxalate or citrate, but also specific iron-binding molecules which are called siderophores. Siderophores form a group of organic compounds which possess a very high affinity and specificity to form complexes with ferric iron. The functional units in siderophores include α -hydroxycarboxylate, hydroxamate, catecholate, carboxylate and amine binding groups. (Kraemer, 2004). The ligand molecules adsorb to the iron oxide and form surface complexes. The subsequent detachment of these surface complexes and release of Fe(III)-ligand-complexes represents the rate-limiting step for ligand-controlled dissolution (Cornell and Schwertmann, 2003). In natural soil environments, ligand-controlled dissolution exerts a major influence on iron cycling in Podzols or other soils rich in organic matter, but also in calcareous soils with low iron bioavailability.

However, the third dissolution mechanism of iron oxide minerals, reductive dissolution, is probably the most important mechanism in nature. Electron transfer to ferric iron atoms on the oxide surface generates ferrous iron which is readily released into solution. Reductive dissolution can be mediated by both biotic and abiotic processes. Dissimilatory iron reducing bacteria couple the oxidation of organic matter to the reduction of iron oxides by using ferric iron as terminal electron acceptor, as described in the last section. Besides microbially-mediated reactions, reductive dissolution of iron oxides can also occur non-enzymatically with a variety of different electron donors, such as phenolic compounds (LaKind and Stone, 1989) and is promoted by photochemical processes (Sulzberger and Laubscher, 1995; Borer et

al., 2005). In the presence of light, photolysis of Fe(III)-ligand-complexes results in electron transfer reactions and the formation of soluble ferrous iron. Reductive dissolution of iron oxide minerals is strongly accelerated in the presence of ferrous iron or Fe(II)-ligand-complexes (Suter et al., 1988).

Different iron oxide minerals phases exhibit different dissolution kinetics which has been the subject of numerous laboratory studies (e.g., Postma, 1993; Larsen and Postma, 2001; Roden, 2004). The different reactivities can be explained both by mineralogical properties which influence the crystal stability and surface parameters such as specific surface area.

REFERENCES

- Anderson HA, Berrow ML, Farmer VC, Hepburn A, Russell JD, Walker AD (1982) A reassessment of podzol formation processes. *J. Soil. Sci.* **33**, 125-136.
- Andrews SC, Robinson AK, Rodriguez-Quinones F (2003) Bacterial iron homeostasis. *FEMS Microbiol. Rev.* **27**, 215-237.
- Blume HP (1988) The fate of iron during soil formation in humid-temperate environments. p. 749-777. In Stucki JW, Goodman BA, Schwertmann U (eds.) *Iron in soils and clay minerals*. D. Reidel, Dordrecht, The Netherlands.
- Bonneville S, Van Cappellen P, Behrends T (2004) Microbial reduction of iron(III) oxyhydroxides: effects of mineral solubility and availability. *Chem. Geol.* **212**, 255-268.
- Borer PM, Sulzberger B, Reichard P, Kraemer SM (2005) Effect of siderophores on the light-induced dissolution of colloidal iron(III) (hydr)oxides. *Mar. Chem.* **93**, 179-193.
- Buurman P, Jongmans AG (2005) Podzolisation and soil organic matter dynamics. *Geoderma* **125**, 71-83.
- Casey WH, Ludwig C (1996) The mechanism of dissolution of oxide minerals. *Nature* **381**, 506-509.
- Cooper DC, Picardal FF, Coby AJ (2006) Interactions between microbial iron reduction and metal geochemistry: Effect of redox cycling on transition metal speciation in iron bearing sediments. *Environ. Sci. Technol.* **40**, 1884-1891.
- Cornell RM, Schwertmann U (2003) The iron oxides – structure, properties, reactions, occurrence and uses. Second edition. VCH, Weinheim, Germany.
- Cummings DE, Caccavo, Jr. F, Fendorf S, Rosenzweig RF (1999) Arsenic mobilization by the dissimilatory Fe(III)-reducing bacterium *Shewanella* alga BrY. *Environ. Sci. Technol.* **33**, 723-729.
- Dong HL, Fredrickson JK, Kennedy DW, Zachara JM, Kukkadapu RK, Onstott TC (2000) Mineral transformation associated with the microbial reduction of magnetite. *Chem. Geol.* **169**, 299-318.

- Donisa C, Steinnes E, Sjobakk TE (2005) Nitric-acid soluble fractions of 21 elements in Norwegian podzols: Factors affecting regional differences in vertical distribution. *Appl. Geochem.* **20**, 1258-1267.
- Gonzalez-Gil G, Amonette JE, Romine MF, Gorby YA, Geesey GG (2005) Bioreduction of natural specular hematite under flow conditions. *Geochim. Cosmochim. Acta* **69**, 1145-1155.
- Hernandez ME, Newman DK (2001) Extracellular electron transfer. *Cell. Mol. Life Sci.* **58**, 1562-1571.
- Jansen B, Nierop KGJ, Verstraten JM (2005) Mechanisms controlling the mobility of dissolved organic matter, aluminium and iron in podzol B horizons. *Eur. J. Soil. Sci.* **56**, 537-550.
- Kostka JE, Haefele E, Viehweger R, Stucki JW (1999) Respiration and dissolution of iron(III) containing clay minerals by bacteria. *Environ. Sci. Technol.* **33**, 3127-3133
- Kraemer SM (1997) Ligand controlled weathering kinetics of aluminum oxide and goethite. Dissertation, Technical University Darmstadt, Darmstadt, Germany.
- Kraemer SM (2004) Iron oxide dissolution and solubility in the presence of siderophores. *Aquat. Sci.* **66**, 3-18.
- Kümmel R, Papp S (1990) Umweltchemie - eine Einführung. Second edition. Deutscher Verlag für Grundstoffindustrie, Leipzig, Germany.
- LaKind JS, Stone AT (1989) Reductive dissolution of goethite by phenolic reductants. *Geochim. Cosmochim. Acta* **53**, 961-971.
- Larsen O, Postma D (2001) Kinetics of reductive bulk dissolution of lepidocrocite, ferrihydrite, and goethite. *Geochim. Cosmochim. Acta* **65**, 1367-1379.
- Lovley DR, Phillips EJP (1986) Organic matter mineralization with reduction of ferric iron in anaerobic sediments. *Appl. Environ. Microbiol.* **51**, 683-689.
- Lovley DR, Holmes DE, Nevin KP (2004) Dissimilatory Fe(III) and Mn(IV) reduction. *Adv. Microb. Physiol.* **49**, 219-286.
- Lundström US, van Breeman N, Bain D (2000) The podzolization process - a review. *Geoderma* **94**: 91-107.
- Marshall CP, Fairbridge RW (eds.) (1999) Encyclopedia of geochemistry. Kluwer Academic, Dordrecht, The Netherlands.
- Murad E, Fischer WR (1988) The geobiochemical cycle of iron. p. 1-18. In Stucki JW, Goodman BA, Schwertmann U (eds.) *Iron in soils and clay minerals*. D. Reidel, Dordrecht, The Netherlands.
- Postma D (1993) The reactivity of iron-oxides in sediments - a kinetic approach. *Geochim. Cosmochim. Acta* **57**, 5027-5034.
- Reguera G, McCarthy KD, Mehta T, Nicoll JS, Tuominen MT, Lovley DR (2005) Extracellular electron transfer via microbial nanowires. *Nature* **435**, 1098-1101
- Roden EE (2004) Analysis of long-term bacterial vs. chemical Fe(III) oxide reduction kinetics. *Geochim. Cosmochim. Acta* **68**, 3205-3216.

- Roden EE (2006) Geochemical and microbiological controls on dissimilatory iron reduction. *C.R.Geosci.* **338**, 456-467
- Rosso KM, Zachara JM, Fredrickson JK, Gorby YA, Smith SC (2003) Nonlocal bacterial electron transfer to hematite surfaces. *Geochim. Cosmochim. Acta* **67**, 1081-1087.
- Schlichting E, Schwertmann U (eds.) 1973. Pseudogley and Gley - Genesis and use of hydromorphic soils. VCH, Weinheim, Germany.
- Stucki JW, Goodman, BA, Schwertmann U (eds.) 1988. Iron in soils and clay minerals. D. Reidel, Dordrecht, The Netherlands.
- Stucki JW, Kostka JE (2006) Microbial reduction of iron in smectite. *C.R.Geosci.* **338**, 468-475.
- Stumm W (1992) Chemistry of the solid-water interface: processes at the mineral-water and particle-water interface in natural systems. Wiley, New York, US.
- Stumm W, Morgan JJ (1996) Aquatic Chemistry - Chemical Equilibria and Rates in Natural Systems. Third edition. Wiley, New York, US.
- Sulzberger B, Laubscher H (1995) Reactivity of various types of iron(III) (hydr)oxides towards light-induced dissolution. *Mar. Chem.* **50**, 103-115.
- Suter D, Siffert C, Sulzberger B, Stumm W (1988) Catalytic dissolution of iron(III) (hydr)oxides by oxalic acid in the presence of Fe(II). *Naturwissenschaften* **75**, 571-573.
- Szilas CP, Borggaard OK, Hansen HCB, Rauer J (1998) Potential iron and phosphate mobilization during flooding of soil material. *Water, Air, and Soil Pollution* **106**: 97-109.
- Thompson A, Chadwick OA, Boman S, Chorover J (2006) Colloid mobilization during soil iron redox oscillations. *Environ. Sci. Technol.* **40**, 5743-5749.
- Tyler G (2004) Vertical distribution of major, minor, and rare elements in a Haplic Podzol. *Geoderma* **119**, 277-290.
- Vepraskas MJ (1996) Redoximorphic features for identifying aquic conditions. North Carolina Agricultural Research Service, Technical Bulletin 301, Raleigh, North Carolina, US.
- Weber KA, Achenbach LA, Coates JD (2006) Microorganisms pumping iron: anaerobic microbial iron oxidation and reduction. *Nature Rev. Microbiol.* **4**, 752-764
- Wilson MJ (2004) Weathering of the primary rock-forming minerals: processes, products and rates. *Clay Min.* **39**, 233-266.
- WRB (2006) World Reference Base for Soil Resources 2006 - a framework for international classification, correlation and communication. World Soil resources reports 103. Food and Agriculture Organization of the United Nations, Rome, Italy.
- Zinder B, Furrer G, Stumm W (1986) The coordination chemistry of weathering: II. Dissolution of Fe(III) oxides. *Geochim. Cosmochim. Acta* **50**, 1861-1869.

3. IRON ISOTOPES

The chemical element iron (Fe) has the atomic number 26 which means that every atom containing 26 protons in its atomic nucleus is by definition an iron atom. The positive charge of the protons is balanced by the negative charge of electrons which surround the atomic core in equal numbers in the zerovalent state. In addition, uncharged neutrons are required to stabilize the atomic nucleus by absorbing the repulsive forces between the positively charged protons. However, for many elements this can be achieved by a different number of neutrons, which explains the existence of isotopes. Isotopes are atoms of an element which contain a different number of neutrons in their nucleus. There are for instance 13 different known isotopes of iron with atomic masses ranging from 49 to 62 (Goodman, 1988) corresponding to a neutron number of 23 to 36. However, most of these isotopes are not stable, and they decay by radioactive processes. Only four stable iron isotopes exist with the atomic masses 54, 56, 57, and 58. The work presented in this thesis is only concerned with these four stable isotopes and their relative distributions. Nevertheless, some interesting applications of radioactive iron isotopes in recent studies of earth and environmental sciences will be mentioned briefly here.

The radioactive isotopes ^{55}Fe and ^{59}Fe , which possess half lives of 2.7 years and 44.6 days, respectively, are used in tracer studies. Recent applications of this method include for instance the study of iron absorption and translocation in barley plants (Alam et al., 2005), surface transformation studies of iron oxide minerals (Reichard et al., 2005, Pedersen et al., 2005), iron speciation kinetics in seawater (Fischer et al., 2006), and the release of arsenic during iron oxide dissolution (Pedersen et al., 2006). The suitability of ^{55}Fe as a tracer for microbial iron reduction in aquatic sediments was evaluated by Roden and Lovley (1992). The impact of the release of radioactive ^{55}Fe in the discharge of nuclear power stations on the environment was investigated by Warwick et al. (2001). The radioactive iron isotope with the longest half life is ^{60}Fe (1.49 Myrs) which makes it relevant for cosmochemistry, for instance in meteorite studies (Quitté et al., 2006). It is an extinct radionuclide in the solar system, but can be generated inside a supernova. Studies on marine ferromanganese crusts report the existence of supernova produced ^{60}Fe on Earth (Knie et al., 1999) that could only be measured by accelerator mass spectrometry (Gartenmann et al., 1997). The stable isotope ^{57}Fe deserves special

attention due to its nuclear spin configuration which makes it useful in spectroscopic studies. Mössbauer spectroscopy represents the main application and has been used in many studies on iron, especially due to the possibility to obtain information on the iron oxidation state in solid samples (e.g., Amonette et al., 2003; Williams and Scherer, 2004; Williams et al., 2004; van der Zee et al., 2005; Feder et al., 2005; Dyar et al., 2006). The nuclear spin of ^{57}Fe also potentially enables studies with nuclear magnetic resonance (NMR) spectroscopy (Goodman, 1988), but the applicability to earth and environmental science appears limited.

In the following, we will focus on the four stable iron isotopes. The average relative distribution in nature, which is originally caused by nucleosynthetic constraints, is ^{54}Fe (5.84 %), ^{56}Fe (91.76 %), ^{57}Fe (2.12 %), and ^{58}Fe (0.28 %). The atomic mass of iron of 55.845 g/mole is deduced from the weighted average of the four isotopes. Every iron compound, regardless of being part of, for instance, a mantle rock, a heme protein, a manufactured steel, or a soil mineral consists of all of these four iron isotopes. However, the relative distribution of the four isotopes is variable to a very small degree caused by isotope fractionation processes. The deviations from the average relative distribution are so small that the ratio between two iron isotopes changes only on the order of per mil or parts per thousand (‰). The work presented in this thesis and all other studies discussed in the next section are investigating these small variations in the distribution of stable iron isotopes. A simplified illustration of the magnitude of iron isotopes fractionation in nature is presented in Figure 3.1.

The chemical behavior of elements in reactions is mainly controlled by their electronic structure. Isotopes of an element behave similar in most chemical reactions because of the similarity in number and configuration of electrons. However, their small mass differences due to the different number of neutrons in the atomic nucleus cause a slightly different behavior in certain processes in which physical properties are important. Typical examples of such processes are phase transitions, such as distillation or condensation, and the formation or cleavage of chemical bonds (Criss, 1999). These processes lead to isotope fractionations which are manifested by relative enrichments and depletions of isotopes between different pools. Stable isotope geochemistry describes the fractionations occurring in natural systems and tries to explain the origin of these fractionation processes (Hoefs, 2004).

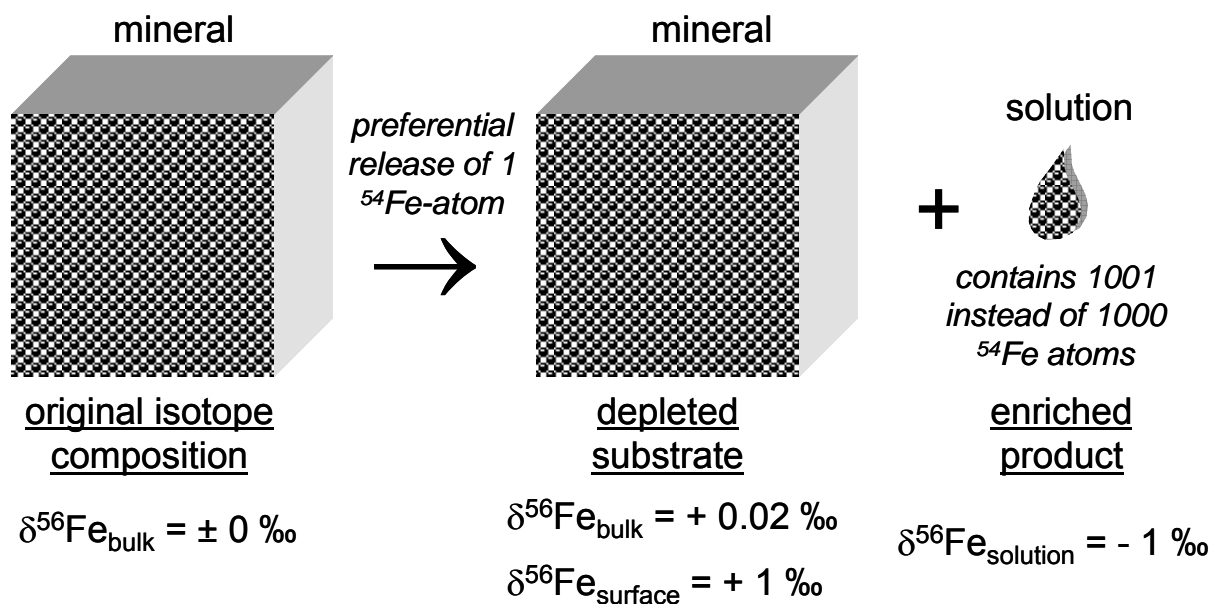


Figure 3.1 Schematic illustration of iron isotope fractionation during mineral dissolution and the effect on $\delta^{56}\text{Fe}$ of the involved pools (simplified boundary conditions: original pool size 1 million Fe atoms; distribution: 950,000 ^{56}Fe + 50,000 ^{54}Fe ; dissolved fraction = 2 % of total pool = $\frac{1}{2}$ size of surface monolayer). In the presented example, a small fraction (2%) of a schematic iron mineral pool (1 million Fe atoms) is dissolved. Without isotope fractionation, the dissolved pool would contain 1000 ^{54}Fe atoms. However, iron isotope fractionation manifests itself by the preferential release of one light ^{54}Fe atom resulting in a $\delta^{56}\text{Fe}$ value of -1 ‰ in solution. The influence on the isotopic signature of the bulk mineral is negligible (+0.02 ‰). However, a relative enrichment of heavy isotopes is created at the mineral surface. The extent of this isotope effect depends on the relative size of the surface pool compared to the dissolved fraction. The general magnitude of iron isotope fractionation illustrated in this example is similar to fractionation effects occurring in nature. However, in order to compare the dimensions, one has to envision that one gram of soil material usually contains about 10^{20} Fe atoms.

Knowledge regarding isotope fractionation processes provides a powerful tool in the interpretation of complex geochemical processes in past and present. Stable isotopes of light elements (e.g., hydrogen, carbon, oxygen, nitrogen, and sulfur) have been widely used in the investigation of many basic and applied problems in earth and environmental sciences. Stable isotope studies have been successfully applied

for instance in the discovery of biological element pathways, to determine the origin of geologic samples or to reconstruct past climate conditions (Hoefs, 2004). Isotope fractionations are generally more pronounced among isotopes of lighter elements because the relative mass difference between the different isotopes is higher. The mass difference between the two hydrogen isotopes protium (^1H) and deuterium (^2D) is 100 % and in the case of oxygen (^{18}O and ^{16}O) 12.5 %, whereas the difference between the two major iron isotopes ^{54}Fe and ^{56}Fe amounts to only 3.7 %. Until recently, mass-dependent isotope fractionations of heavier chemical elements, such as iron, were not believed to be possible, or at least insignificant, due to their smaller relative mass difference. However, the development of very precise analytical tools for the determination of isotope ratios in natural samples during the last decade has revealed that mass-dependent isotope fractionations also occur among heavier elements and that the magnitude of isotope fractionation is not simply a function of relative mass difference (Johnson et al., 2004a). In the meantime, significant mass-dependent fractionations of stable isotopes have been reported for elements with atomic masses above 200, such as mercury (Xie et al., 2005) and thallium (Rehkämper et al., 2002).

Isotope fractionation effects are generally divided into kinetic and equilibrium effects (Criss, 1999; Hoefs, 2004). Kinetic isotope effects are occurring during unidirectional reactions. Generally, light isotopes react faster which can be expressed in a quantitative manner by different reactions rate constants for the different isotopes. A good example for such a process is diffusion, where one can envision the lighter isotopes as being slightly faster than heavier isotopes. Kinetic isotope effects are only manifested in different isotope signatures between pools if a physical separation of substrate and product occurred and the reaction did not proceed quantitatively. Equilibrium isotope effects are occurring in situations where a chemical equilibrium between different phases exists and isotopes partition preferentially into one of the phases. The driving force for these isotope exchange processes are energetic differences between the bonding environments of the reaction partners. The pool which provides the stronger bonding environment will be enriched in heavy isotopes. The theoretical basis for equilibrium isotope effects can be deduced from differences of the vibrational energies of chemical bonds between light and heavy isotopes (Criss, 1999). Equilibrium isotope effects are temperature

dependent and decrease in magnitude with increasing temperature. In natural systems, it is often difficult to unravel whether isotope fractionations were caused by kinetic or equilibrium effects. It is even possible that kinetic and equilibrium isotope effects during different stages of a reaction cause fractionations which are opposite in direction. An example of such a situation will be presented in chapter 6. An interesting theoretical approach to differentiate between kinetic and equilibrium isotope effects, which results in a slightly different slope of data points in a three isotope-plot, was recently presented by Young et al. (2002). However, its application to natural systems proves to be difficult and in the case of iron isotopes probably impossible.

The delta-notation is commonly used in stable isotope geochemistry to describe isotope fractionation relative to a standard. This reference of measured isotope ratios to a certified standard, which should be available worldwide, enables the comparison of data between different laboratories and is an essential requirement for stable isotope studies. The international iron isotope standard is IRMM-014, which is a pure iron metal supplied by the Institute for Reference Materials and Measurements in Geel, Belgium (IRMM, 1999). Iron isotope ratios of samples are commonly expressed as $\delta^{56}\text{Fe}$ or $\delta^{57}\text{Fe}$ which are defined as

$$\delta^{56}\text{Fe} [\text{‰}] = \left(\frac{(^{56}\text{Fe}/^{54}\text{Fe})_{\text{sample}}}{(^{56}\text{Fe}/^{54}\text{Fe})_{\text{IRMM-014}}} - 1 \right) \cdot 10^3 \quad \text{or} \quad \delta^{57}\text{Fe} [\text{‰}] = \left(\frac{(^{57}\text{Fe}/^{54}\text{Fe})_{\text{sample}}}{(^{57}\text{Fe}/^{54}\text{Fe})_{\text{IRMM-014}}} - 1 \right) \cdot 10^3.$$

The two values can be easily converted into each other by the approximation $\delta^{57}\text{Fe} = 1.5 \times \delta^{56}\text{Fe}$ because the observed fractionation effects are mass-dependent. The epsilon-notation was used in some of the early publications to report iron isotope fractionation. In this case, deviations are expressed in terms of parts per ten thousand which can be converted to the delta-notation by the relation $\epsilon^{56}\text{Fe} = 10 \times \delta^{56}\text{Fe}$.

3.1 Iron isotope analysis

Isotope analysis is based on mass spectrometry. The separation of charged ions in a magnetic field according to their atomic masses and the subsequent simultaneous detection of the different isotopes constitute the fundament of this analytical technique. There are different analytical designs that were developed for isotope ratio mass spectrometry and which are constantly improved in terms of

precision and required sample size. The common method to measure isotope ratios of light elements (e.g., C, O, H, N, S) is the use of gas source mass spectrometers (Hoefs et al., 2004). However, this method is only applicable for elements which can be conveniently converted into a gaseous form. Some attempts were made to measure iron isotope ratios in the gas phase by introducing iron as $\text{Fe}(\text{PF}_3)_5$ compound in the mass spectrometer (Taylor et al., 1993), the achieved precision of the method was relatively poor. Iron can be easily brought in solution and the measurement of iron isotope ratios in liquid samples is the main method used in all subsequent studies, except for the recent application of laser ablation techniques allowing the in-situ analysis of solid samples, which will be briefly discussed at the end of this section. Iron isotope analysis of liquid samples requires highly purified solutions which only contain pure iron in a dilute acid matrix. In order to dissolve iron in solid samples (e.g., rock and soil material), different digestion and extraction techniques are used.

The further sample preparation requires a separation of iron from matrix elements. This is commonly achieved by a column separation procedure using an anion exchange resin in a hydrochloric acid medium. The basic principles of this method, which is used until today, were already developed many decades ago (Kraus and Moore, 1953). In a concentrated hydrochloric acid medium, iron is quantitatively present as FeCl_4^- anion which is retained on the functional groups of the anion-exchange resin (e.g., positively charged quaternary ammonium groups) on the column. The majority of other elements can be rinsed from the column by repeated additions of hydrochloric acid in high concentrations (e.g., 6 M HCl) (Strelow, 1980). Afterwards, iron can be eluted by the addition of a dilute solution (e.g., 0.05 M HCl) in which the negatively charged iron complexes are destroyed and the iron is transformed into neutral or positively charged species which are not attracted to the resin. If matrix elements are present which also bind to the resin in the form of chloro-complexes (e.g., Cu, Zn), the iron elution scheme can be adapted in a way to separate the different elements according to their distribution coefficients. Slightly different resin types and acid molarities are used in iron isotope studies. In the work presented in this thesis, 6 M HCl and an anion exchange resin with 4% crosslinkage (Biorad AG1 X4, 200-400 mesh) were used. Other matrix separation procedures using cation exchange resins, liquid extraction or iron precipitation are

principally also applicable, but are less frequently used (Dauphas et al., 2004; Schönberg and von Blanckenburg, 2005). In any case, sample purification represents a crucial part of iron isotope analysis both in terms of required working time and the quality of the obtained results. Iron isotope analysis is very sensitive to matrix effects which can be introduced for instance by incomplete destruction of organic compounds in the sample solutions or the presence of other elements which affect the mass bias of the sample during the measurement. The deteriorating influence of matrix effects on the obtained iron isotope data can be very difficult to detect and a thorough sample preparation is essential for accurate and precise iron isotope analysis of natural samples (Schönberg and von Blanckenburg, 2005). Secondly, the yield of the chromatographic separation procedure needs to be checked carefully, since an incomplete recovery could result in isotope fractionation effects (Anbar, 2000).

The history of iron isotope analysis dates back almost 60 years to a publication of a study on iron isotope ratios in terrestrial and meteoritic iron (Valley and Anderson, 1947). However, no significant differences could be detected by the available analytical equipment at the time. In the following, the lack of precise analytical tools to measure iron isotope ratios resulted in a long period of stagnancy in the scientific progress of the field. A few studies on iron isotope ratio measurements by thermal ionization mass spectrometry (TIMS) were undertaken (Völkening and Papanastassiou, 1989; Dixon et al., 1993) but the precision of the obtained results was still relatively low. The main drawbacks were the low ionization efficiency of iron and the variability of mass-dependent fractionation during the analysis. Dixon et al. (1992) stated that significant iron isotope variations should exist in natural systems and that their analysis could be helpful for geochemical problems. Walczyk (1997) presented a new analytical method for iron isotope analysis based on negatively charged FeF_4^- molecular ions (negative TIMS) which provided an improvement by a factor of three to four in precision compared to the previous positive TIMS methods.

However, the major breakthrough in the development of iron isotope analytics, which sparked the future rapid development of the field, was the application of a double-spike technique combined with positive TIMS (Bullen and McMahon, 1998; Johnson and Beard, 1999). As mentioned before, a major problem in the application

of TIMS consists of the variable mass-dependent fractionation during ionization which affects the precision of the measured isotope ratios. This problem can be corrected to a great extent by adding a spike of two isotopes in a known ratio to the sample. After the measurement of the spiked sample, the instrumentally produced fractionation can be subtracted from the ratio of the sample. The implementation of the mathematical fundament behind the double-spike method is relatively complex and involves multiple iterative steps in the calculation of the true ratio of the sample. A derivation of the most important principles is provided in Johnson and Beard (1999). The method can only be applied for elements which have at least four stable isotopes. In the case of iron, both $^{58}\text{Fe}/^{54}\text{Fe}$ and $^{58}\text{Fe}/^{57}\text{Fe}$ spikes are possible and have been used. The analytical precision in the determination of iron isotope ratios by double-spike TIMS exceeded the previous method by far. A reproducibility of about $\pm 0.3\text{‰}$ in $\delta^{56}\text{Fe}$ was achieved and this precision was sufficient to detect and to study significant naturally-occurring variations of iron isotope ratios (Bullen and McMahon, 1998; Beard and Johnson, 1999; Beard et al., 1999; Mandernack et al., 1999). However, the double-spike method is a very tedious and time-consuming procedure. In addition, the sample throughput of TIMS measurements is relatively low due to the individual loading of samples on filaments which are heated afterwards in order to ionize the samples.

An alternative ionization method in mass spectrometry is provided by an argon plasma, which has been developed and applied successfully for concentration analysis by inductively coupled plasma mass spectrometry (Montaser, 1998). These ICP mass spectrometers for concentration measurements are usually only equipped with a single collector which is moved during analysis from mass to mass. However, this setup is not suitable for high-precision isotope ratio analysis due to small instabilities of the plasma. Isotope analysis requires the simultaneous detection of different masses to determine precise ratios. This is achieved in TIMS by a set of multiple collectors which are configured in a way to detect different isotopes at the same time. A major progress in the development of isotope analytical methods was the combination of the front end of ICP-MS (plasma ionization) with the back end of TIMS (multiple collectors). In consequence, a new analytical technique, multiple collector inductively coupled plasma mass spectrometry (MC-ICPMS), was developed (Walder and Freedman, 1992; Halliday et al., 1998).

A major advantage of MC-ICPMS compared to TIMS is the higher ionization efficiency which allows the analysis of much more chemical elements. The instrumentally-produced mass fractionation (mass bias) which is introduced during ionization was found to be relatively large, but much less variable over time compared to TIMS. In addition, a higher sample throughput could be achieved due to the easier sample introduction by solution nebulizers. MC-ICPMS rapidly developed to be the method of choice for many applications in isotope geochemistry. The relatively constant mass bias enables the application of standard-sample-standard bracketing methods which represent a convenient way to correct for instrumental mass fractionation and machine drift. Standard solutions of known isotope composition are measured before and after every sample. The measured isotope ratios of the samples are expressed relative to the average of the isotope ratios of the standards measured before and after the samples. Alternative approaches to perform mass bias corrections during plasma source iron isotope analysis are based on doping the samples with another element which is assumed to behave similar during the ionization, such as copper (Arnold et al., 2004) or nickel (Malinovsky et al., 2003), or again by using a double spike (Dideriksen et al., 2006). However, a recent study reported no increase in precision using element doping to correct for instrumental mass bias compared to standard bracketing (Schoenberg and von Blanckenburg, 2005).

A major difficulty for iron isotope analysis by plasma source mass spectrometry is based on the use of argon as carrier gas and plasma source. Polyatomic argide ions (e.g., ArN^+ , ArO^+ , ArOH^+), which are formed by the reaction of argon with oxygen and nitrogen from air or the solvent, appear at the same position of the mass spectrum as the major iron isotopes ^{54}Fe , ^{56}Fe and ^{57}Fe . These interferences represent a serious problem for precise iron isotope measurements. However, different approaches were developed to overcome this problem and iron isotope measurements with MC-ICPMS became feasible (Belshaw et al., 2000; Anbar et al., 2000). First of all, the intensity of the argide interferences can be greatly reduced by the use of a so-called dry plasma. In this case the sample solution is introduced into a desolvating system prior to the ionization in the plasma. During this step the solvent matrix is removed from the sample by a membrane process at about 160°C. This procedure achieves a major reduction of argide interferences to controllable levels.

The intensity of argide interferences can also be manipulated by other methods such as a reduced power of the plasma (cold plasma, Kehm et al., 2003) or the choice of acid matrix, nebulizers and cones. However, in order to reduce the argide interferences to insignificant levels, relatively high iron concentrations in the lower ppm range have to be used in the sample solutions. An alternative method to minimize argide interferences is the operation of a collision cell in which a collision gas (e.g., hydrogen) is used to eliminate the interfering polyatomic ions (Vogl et al., 2003; Beard et al., 2003). The most effective and elegant solution to solve the problem of argide interferences during iron isotope measurement is the use of high-resolution mass spectrometry (e.g., Weyer and Schwieters., 2003; Malinovsky et al., 2003; Arnold et al., 2004; Williams et al., 2005). The slightly different masses of ^{54}Fe compared to ArN and ^{56}Fe compared to ArO make it possible to separate the peaks on a high-resolution mass scan. A mass resolution $M/\Delta M$ (10 % valley definition) of at least 2500 is required to measure iron isotopes without argide interferences.

Another analytical challenge of iron isotope ratio measurements consists of the in-situ analysis of solid samples by laser ablation techniques. Initial attempts to measure iron isotopes by laser ablation MC-ICPMS were published by Hirata and Ohno (2001), but the achieved reproducibility did not reach the required precision on the per mil level to resolve natural variations. An improved data quality was reported by Hirata et al. (2003). Graham et al. (2004) applied laser ablation MC-ICPMS to measure iron isotope ratios in ore samples. In the following, Kosler et al. (2005) used a UV (213 nm) laser coupled to high-resolution MC-ICPMS to investigate sulfide and meteorite samples. However, the quality of their data was subsequently challenged by Horn et al. (2006a) because of potential analytical artifacts that may have influenced the reported isotope ratios. The best currently available method to determine iron isotope ratios in solid samples with high accuracy and precision appears to be the use of a femtosecond (196 nm) laser which was recently demonstrated convincingly by Horn et al. (2006b).

3.2 State of research on iron isotopes

Iron isotope geochemistry is a rapidly evolving scientific field. Any attempt to review the scientific progress can only represent a snapshot of the current knowledge. This is of course true for most scientific disciplines, but particularly valid

in areas such as iron isotope geochemistry, where many basic principles are still poorly understood and new interpretations evolve constantly from the limited, but rapidly growing set of available data. Recent reviews on iron isotopes were presented by Anbar (2004), Beard and Johnson (2004), Johnson et al. (2004b) and Dauphas and Rouxel (2006). In the following, a brief overview of the state of research, which is particularly relevant for the work presented in this thesis, will be given. The development of iron isotope geochemistry was sparked by the pioneering work of Brian Beard and Clark Johnson at the University of Wisconsin, Madison, USA (Johnson and Beard, 1999; Beard and Johnson, 1999; Beard et al., 1999) and Thomas Bullen at the US Geological Survey, Menlo Park, USA (Bullen and McMahon, 1998; Mandernack et al., 1999). Since then, the number of publications on iron isotope geochemistry has risen almost exponentially (Figure 3.2).

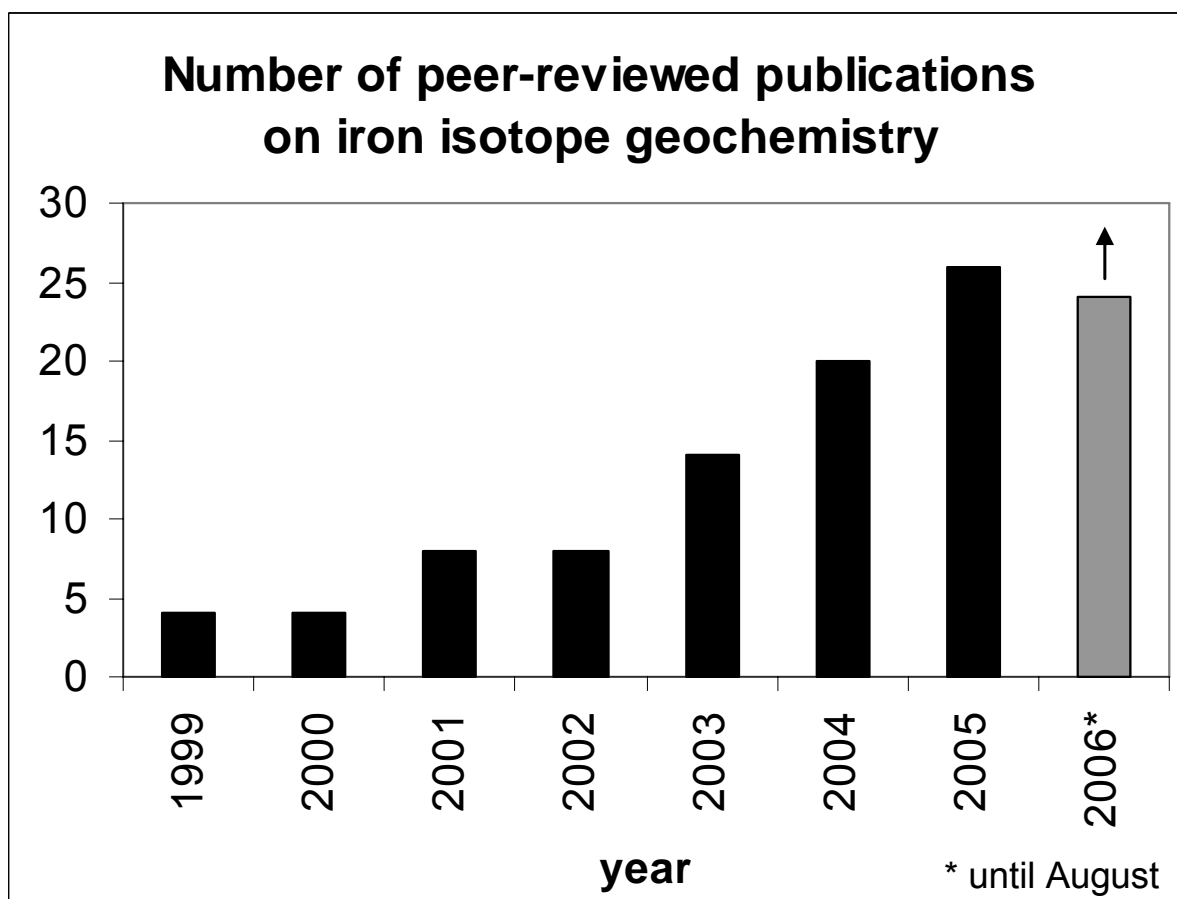


Figure 3.2 Development of the number of peer-reviewed publications on iron isotope geochemistry between 1999 and 2006. Please note that the number for 2006 includes only publications that were in press until the end of August. This number will certainly increase until the end of 2006.

An important milestone in the study of iron isotope variations in nature was the finding that bulk igneous rocks are relatively homogeneous in their iron isotope composition (Beard and Johnson, 1999). The range of $\delta^{56}\text{Fe}$ values in igneous rocks was given as $\pm 0.3\text{‰}$ (1SD) which was identical within the analytical precision available at that time using double-spike TIMS methods. However, this terrestrial baseline value was refined in the following due to the analytical advances and was reported to be only variable in $\delta^{56}\text{Fe}$ by $\pm 0.05\text{‰}$ (1SD) (Beard and Johnson, 2004; Poitrasson et al., 2004). It was suggested to use this average isotopic composition of igneous rocks as reference standard to report iron isotope data. This value was subsequently used in many studies and referred to as “Earth-Moon”, “Whole Earth Average”, or “Bulk Earth Baseline”. However, most research groups are now reporting their data relative to IRMM-014 which makes sense for several reasons. The IRMM-014 standard is a pure iron metal which is certified and supplied by the Institute for Reference Materials and Measurements in Geel, Belgium (IRMM, 1999). The iron isotope composition of IRMM-014 differs only slightly from the suggested terrestrial baseline value by 0.09‰ in $\delta^{56}\text{Fe}$ (Dauphas and Rouxel, 2006). Thus, data can be converted easily from one scale to the other if necessary. Most importantly, IRMM-014 is a standard that is available to everybody and certified for its homogeneity. In addition, recent studies have questioned the homogeneity of iron isotope ratios in terrestrial rocks. It is now clear that small, but resolvable iron isotope variations exist between different mineral phases of igneous rocks and even between different rock types (Williams et al., 2004; Weyer et al., 2005; Williams et al., 2005). Iron isotope signatures of granites that are significantly heavier compared to the average of bulk igneous rocks were reported by Poitrasson and Freydier (2005) and correlated with low magnesium and high SiO_2 contents of the rock, respectively. Their interpretations were subsequently questioned by Beard and Johnson (2006) and the question of the iron isotope homogeneity level of the continental crust remains highly debated (Poitrasson, 2006).

The first attempt to apply iron isotopes to an environmental science problem was performed by Bullen and McMahon (1998). They found significant variations of iron isotopes in a contaminated aquifer and interpreted the data as a result of microbially-mediated iron isotope fractionation during dissimilatory iron reduction. However, a much broader impact was attained by the following publication of

laboratory experiments with *Shewanella* cultures and ferrihydrite in which an enrichment of light iron isotopes in solution by about 1 ‰ in $\delta^{56}\text{Fe}$ was reported (Beard et al., 1999). This study initiated the idea of using iron isotopes as a biosignature based on the assumption that only biotic processes are able to change the isotopic composition of iron. This tool was designated to solve many important biogeochemical questions including life on Mars or the origin of banded-iron formations. However, it turned out very soon that the application of iron isotopes as a biosignature is not that simple. An ideal isotopic biosignature has to meet two basic criteria. On the one hand, all biological processes should result in an isotope fractionation. On the other hand, no abiotic process should be able to create significant isotope fractionations. It could be demonstrated that both criteria are not met in the case of iron isotopes. First it was reported that magnetite crystals which were precipitated by magnetotactic bacteria showed no iron isotope fractionation despite a significant fractionation of oxygen isotopes (Mandernack et al., 1999). The absence of iron isotope fractionation effects was explained by the different reaction mechanism compared to dissimilatory iron reduction. The rate-limiting step in the biotic synthesis of magnetite crystals is supposed to be the passive binding of iron atoms to the external surface of bacteria cells. This process does not make a difference between the different atomic masses of iron and therefore no iron isotope fractionation occurs.

Secondly, abiotic iron isotope fractionation was demonstrated both in laboratory studies (Anbar et al., 2000) and field studies (Bullen et al., 2001). The oxidative precipitation of ferrihydrite in a natural river, which is supposed to be mainly an abiotic process, was found to cause a significant fractionation of iron isotopes. The heavier ^{56}Fe isotope was enriched in the ferrihydrite and the river water was depleted in ^{56}Fe . A similar iron isotope effect was found in an analog laboratory setup of abiotic oxidative ferrihydrite precipitation (Bullen et al., 2001). The iron isotope fractionation was explained by a kinetic effect between different iron complexes in solution. The complex with the stronger bonding environment, hence enriched in ^{56}Fe , oxidizes more rapidly which results in the observed enriched of heavy iron isotopes in the precipitate. However, this interpretation was subsequently challenged by Johnson et al. (2004b) who attributed the observed effect to a combination of an equilibrium isotope effect between ferrous and ferric iron and a kinetic isotope effect

during precipitation. Modeling approaches for the described system were provided by Anbar (2004) and Dauphas and Rouxel (2006). Another obvious demonstration of abiotic iron isotope effects was provided in a laboratory study in which iron-chloro-complexes were fractionated in 7 M HCl on an anion exchange resin (Anbar et al., 2000). This setup, which is similar to the one commonly used during sample preparation, was further refined by Roe et al. (2003) and the observed effect ascribed to equilibrium iron isotope fractionation. Another laboratory-based study reported strong kinetic isotope fractionation effects between different iron complexes in solution (Matthews et al., 2002).

The next important step to understand iron isotope geochemistry was achieved by the determination of an equilibrium isotope fractionation factor between ferrous and ferric iron in solution (Johnson et al., 2002). Some aspects in the interpretation of these initial experiments were questioned (Bullen et al., 2002), but subsequent experiments demonstrated that iron-aquo-complexes in a mixed-valence solution equilibrate toward a situation where ferrous iron is about 3 ‰ lighter in $\delta^{56}\text{Fe}$ than ferric iron (Welch et al., 2003). This finding has important implications because redox transformations are major processes in the biogeochemical iron cycle, as has been discussed in the previous chapter. However, the transfer of the equilibrium isotope fractionation factor, which was deduced from a specific laboratory system, to natural systems remains difficult. This is not only because many iron transformations in natural systems are kinetically controlled, but also because the presence of other reaction partners (e.g., organic ligands) could change the equilibrium fractionation factors. An important step of iron isotope geochemistry toward biological applications was done by the demonstration that human blood is strongly enriched in light isotopes by about 3 ‰ in $\delta^{56}\text{Fe}$ (Walczyk and von Blanckenburg, 2002). The isotope signature of the blood of males and females was found to be slightly different which was explained by the different iron metabolism. In the same study an initial survey on the iron isotope signatures of plants and animals was attempted pointing toward a general enrichment of biomass with light iron isotopes. The iron isotope signature of human blood was later shown to be stable over longer periods by measuring monthly blood samples from the same person (Ohno et al., 2004). An excellent overview on the variability of iron isotopes and potential pathways in the human body was provided by Walczyk and von Blanckenburg (2005).

The analytical work on iron isotope geochemistry was accompanied by studies which attempt to predict equilibrium iron isotope fractionations based on theoretical principles. First work in this direction was performed using data from Mössbauer spectroscopy (Polyakov, 1997; Polyakov and Mineev, 2000). Another approach using data from vibrational spectroscopy predicted significant equilibrium isotope fractionations between the two oxidation states of iron and between different bonding environments (Schauble et al., 2001). However, the predicted value for the Fe(II)-Fe(III)-aquo-complex system turned out to be considerably larger than the experimental value which was subsequently reported by Johnson et al. (2002). A new approach based on density functional theory (DFT) calculations provided theoretical predictions that were in better agreement with the experimental data (Jarzecki et al., 2004; Anbar et al., 2005). This technique will probably also prove to be helpful in systems with organic ligands but this potential is not fully explored up to now. The previous descriptions of the state of research on iron isotopes were focused mainly on studies about basic principles of iron isotope geochemistry. Selected studies, which are particularly important in the context of the presented thesis or otherwise relevant for soil systems, will be discussed briefly in the following paragraph. This selection leaves out the recent contributions to iron isotope research which are concerned with the study of cosmochemical, petrological, or marine systems and which were reviewed to a large extent by Dauphas and Rouxel (2006).

A first attempt to investigate iron isotope fractionation in soils was performed by the author of this thesis in a limited study on a seasonally reduced soil in Oregon (US) (Wiederhold, 2000). The project was performed in collaboration with Thomas Bullen (USGS) who measured iron isotope ratios in a small sample set by double-spike TIMS. Enrichments of light iron isotopes in soil solution contrasted with heavy iron isotope signatures of oxide-bound soil iron. However, methodological difficulties which may have created fractionation artifacts and the very limited dataset prevented a publication of the study. The dissolution of hornblende, an iron-containing silicate mineral, in the presence of aerobic soil bacteria (*Streptomyces* and *Arthrobacter*) was shown to result in the preferential release of light iron isotopes in solution by about 0.8 ‰ in $\delta^{56}\text{Fe}$ (Brantley et al., 2001). The same fractionation trend, though smaller in magnitude, was observed during hornblende dissolution in the presence of organic ligands (oxalate and the siderophore desferrioxamine mesylate). In the same

study, a soil sample from a B horizon of a hornblende-containing soil was investigated by two extraction procedures. An extraction with 1 M MgCl₂ was performed and iron in solution, which was referred to as exchangeable iron from cation exchange sites of the soil, was found to be isotopically lighter than oxide-bound iron which was separated by a dithionite-citrate extraction procedure. However, this approach can be questioned since exchangeable iron is a poorly-defined pool in oxic soil environments and secondary precipitation reactions may have affected the iron isotope data. The work was extended by including goethite dissolution in a second study (Brantley et al., 2004) where strong fractionation effects in the presence of *Bacillus* bacteria (-1.4 ‰ in $\delta^{56}\text{Fe}$), but no significant fractionation effect during goethite dissolution by desferrioxamine mesylate was reported in contrast to the experiments with hornblende. The difference was explained by the concept that hornblende develops a iron-depleted leached layer at the mineral surface in which heavy iron isotopes are preferentially retained, whereas such a surface layer was assumed to be absent in the case of goethite. This interpretation stands in contrast to experimental data that are presented in this thesis in chapter 6 and will be discussed in more detail there.

The observation that dissimilatory iron-reducing bacteria are preferentially using light iron isotopes (Beard et al., 1999) was investigated in more detail in subsequent studies. The light iron isotope signature of the solution was confirmed also with *Geobacter* species and different iron oxide phases (Beard et al., 2003; Crosby et al., 2005). However, since a significant fraction of ferrous iron which is produced during dissimilatory iron reduction readsorbs to mineral surfaces at the neutral pH of the experiments, the issue of iron isotope fractionation during adsorption reactions was raised. A first study on this subject pointed towards a significant iron isotope fractionation during adsorption of ferrous iron to ferric iron oxide phases (Icopini et al., 2004). However, the most important data points in this study were only inferred by calculations and many open question remained. A detailed field study on iron isotope fractionation during adsorption, observed after the injection of oxygen into a reduced groundwater aquifer, provided more evidence for the importance of adsorption processes in the interpretation of iron isotope signatures (Teutsch et al., 2005). However, the exact mechanisms and fractionation factors of iron isotope fractionation during adsorption processes are still poorly understood and need to be

investigated in more detail. It could be shown that iron isotope fractionation during dissimilatory iron reduction is certainly not caused primarily by adsorption effects and that equilibrium isotope effects during the iron redox transition probably play a dominant role in the fractionation mechanism (Crosby et al., 2005). Another important microbially-mediated iron transformation in natural environments is bacterial iron oxidation. The effect of this process on iron isotopes was investigated by Croal et al. (2004) using photoautotrophic bacteria. A strong enrichment of heavy iron isotopes by about 1.5 ‰ ($\delta^{56}\text{Fe}$) in the metabolic product, a poorly-crystalline ferric iron oxyhydroxide phase, was observed. Iron isotope fractionation during microbially-mediated iron oxidation was also recently investigated by Balci et al. (2006). However, the separation of biotic and abiotic processes during the oxidative precipitation of ferric iron phases remains difficult. Iron isotope fractionation during abiotic precipitation of iron was also demonstrated between ferric iron and hematite (Skulan et al., 2002). The effect was found to be dependent on the precipitation rate and attributed to both kinetic and equilibrium isotope fractionation. Isotopic zonation of hematite crystals was also discovered in this study by stepwise leaching of synthesized crystals. Another important finding of the study, which is consistent with results from this thesis presented in chapter 6, was the demonstration that dissolution of hematite in hydrochloric acid does not induce iron isotope fractionation. The exploration of potential iron isotope fractionation during the transformation of ferrihydrite to goethite crystals was attempted by Clayton et al. (2005). However, their interpretation of the limited data set is characterized by a complete disregard of basic mass balance considerations between the iron pools of the investigated system.

Iron isotope data from natural soil environments are still very limited. Significant iron isotope fractionation during lateral iron translocation at the landscape scale was investigated in the diploma work of the author of this thesis (Wiederhold, 2002). The assignment of the observed iron isotope variations to specific pedogenic processes was complicated by the fact that the field site was influenced concomitantly by strong acidity, high concentrations of organic ligands and reducing conditions due to water saturation (Wiederhold and von Blanckenburg, 2002). Similar problems arise in the interpretation of the data from Fantle and DePaolo (2004) who reported significant iron isotope fractionation between selected horizons of a soil profile in California (US). The iron isotope signature of total soil digests exhibited a range about 0.7 ‰ in

$\delta^{56}\text{Fe}$ but the pedogenic connection of the investigated horizons was poorly defined. The selected soil was probably both subject to podzolization processes and iron redox transformations due to seasonal water saturation of the subsoil. An extraction method with 0.5 M HCl was performed in addition to the bulk soil data in order to separate mobile iron phases from the soil. However, their heat treatment of the samples (600°C for 12-20 h) prior to the extraction has possibly changed the iron mineralogy of the samples and therefore makes a useful interpretation of the HCl-leaching data difficult. Iron isotope data of unfiltered river water samples presented in the same study suggested that continental weathering transports isotopically light iron into the oceans (Fantle and DePaolo, 2004). A recent study on iron isotopes in the Amazon river indicates that interactions between dissolved and suspended load, as well as the influence of organic ligands on the stabilization of iron in river waters, have to be taken into account in the interpretation of iron isotope signatures of continental weathering processes (Bergquist and Boyle, 2006). Emmanuel et al. (2005) measured iron isotope ratios in a Czech forest soil and an Israeli semi-arid soil and reported variations of about 0.35 ‰ in $\delta^{57}\text{Fe}$ in bulk soil samples. Based on these iron isotope data from total digestions and iron concentration data of a six-step sequential extraction procedure, they used a fixed end member mixing model to calculate iron isotope values of individual iron pools in the soil. The calculated values for organically-bound, oxide-bound and silicate-bound iron ranged over more than 1 ‰ in $\delta^{57}\text{Fe}$. However, their model is based on the assumption that the different iron mineral pools exhibit a constant iron isotope ratio over soil depth and that the different iron pools are not genetically related. This approach is highly questionable since the different iron mineral pools in the soil are developing from each other, as has been discussed in chapter 2. The transformation of iron phases from one pool into another (e.g., primary silicate mineral pool into pedogenic Fe oxide pool) will have an influence on the iron isotope ratio of both pools. The results from natural soil profiles that are presented in this thesis (chapter 4 and 5) indicate that the iron isotope signature of individual iron mineral pools in the soil exhibits significant variations over soil depth which are linked to the intensity of pedogenic processes in different soil horizons. Therefore, the approach taken by Emmanuel et al. (2005) to construct a preliminary mixing model for iron isotopes in soils possesses some severe methodological problems and will probably be of limited use toward a further

understanding of iron isotope fractionation in soils. The selected examples from the recent literature demonstrate that the interpretation of iron isotope signatures of natural soils is a challenging task and presents many potential pitfalls. In particular, the identification of processes and fractionation mechanisms responsible for iron isotope variations in natural soils proves to be difficult. The work presented in this thesis on iron isotope fractionation in soils intends to bridge this apparent gap between the observation of phenomena and the identification of the underlying processes and mechanisms.

REFERENCES

- Alam S, Kamei S, Kawai S (2005) Effectiveness of phytosiderophore in absorption and translocation of ^{59}Fe in barley in the presence of plant-borne, synthetic, and microbial chelators. *J. Plant Nutr.* **28**, 1709-1722
- Amonette JE, Kukkadapu RK, Alp EE, Sturhahn W, Toellner TS (2003) Heterogeneous electron-transfer kinetics with synchrotron Fe-57 Mössbauer spectroscopy. *Geochim. Cosmochim. Acta* **67**, 2109-2116.
- Anbar AD, Roe JE, Barling J, Nealson KH (2000) Nonbiological fractionation of iron isotopes. *Science* **288**, 126-128.
- Anbar AD (2004) Iron stable isotopes: beyond biosignatures. *Earth Planet. Sci. Lett.* **217**, 223–236.
- Anbar AD, Jarzecki AA, Spiro TG (2005) Theoretical investigation of iron isotope fractionation between $\text{Fe}(\text{H}_2\text{O})_6^{3+}$ and $\text{Fe}(\text{H}_2\text{O})_6^{2+}$: Implications for iron stable isotope geochemistry. *Geochim. Cosmochim. Acta* **69**, 825-837.
- Arnold GL, Weyer S, Anbar AD (2004) Fe isotope variations in natural materials measured using high mass resolution multiple collector ICPMS. *Anal. Chem.* **76**, 322-327.
- Beard BL, Johnson CM (1999) High precision iron isotope measurements of terrestrial and lunar materials. *Geochim. Cosmochim. Acta* **63**: 1653-1660.
- Beard BL, Johnson CM, Cox L, Sun H, Nealson KH, Aguilar C (1999) Iron isotope biosignatures. *Science* **285**: 1889-1896.
- Beard BL, Johnson CM, Skulan JL, Nealson KH, Cox L, Sun H (2003) Application of Fe isotopes to tracing the geochemical and biological cycling of Fe. *Chem. Geol.* **195**, 87-117.
- Beard BL, Johnson CM (2004) Fe isotope variations in the modern and ancient Earth and other planetary bodies. *Rev. Mineral. Geochem.* **55**, 319-357.
- Beard BL, Johnson CM (2006) Comment on “Heavy iron isotope composition of granites determined by high resolution MC-ICP-MS”, by F. Poitrasson and R. Freydier [Chem. Geol. 222 132–147]. *Chem. Geol.* **235**, 201-204 .

- Belshaw NS, Zhu XK, Guo Y, O'Nions RK (2000) High precision measurement of iron isotopes by plasma source mass spectrometry. *Int. J. Mass Spectrom.* **197**: 191-195.
- Bergquist BA, Boyle EA (2006) Iron isotopes in the Amazon River system: Weathering and transport signatures. *Earth Planet. Sci. Lett.* **248**, 39–53.
- Brantley SL, Liermann L, Bullen TD (2001) Fractionation of Fe isotopes by soil microbes and organic acids. *Geology* **29**, 535-538.
- Brantley SL, Liermann LJ, Guynn RL, Anbar A, Icopini GA, Barling J (2004) Fe isotopic fractionation during mineral dissolution with and without bacteria. *Geochim. Cosmochim Acta* **68**, 3189-3204.
- Bullen TD, McMahon PM (1998) Using stable Fe isotopes to assess microbially-mediated Fe³⁺ reduction in a jet-fuel contaminated aquifer. *Mineral. Mag.* **62A**: 255-256.
- Bullen TD, White AF, Childs CW, Vivit DV, Schulz MS (2001) Demonstration of significant abiotic iron isotope fractionation in nature. *Geology* **29**, 699-702.
- Bullen TD, White AF, Childs CW (2002) Comment on "Isotopic fractionation between Fe(III) and Fe(II) in aqueous solutions" by Clark Johnson et al., [Earth Planet. Sci. Lett. 195 (2002) 141-153]. *Earth Planet. Sci. Lett.* **206**, 229-232
- Clayton RE, Hudson-Edwards KA, Malinovsky D, Andersson P (2005) Fe isotope fractionation during the precipitation of ferrihydrite and transformation of ferrihydrite to goethite. *Mineral. Mag.* **69**, 667-676.
- Criss RE (1999) Principles of stable isotope distribution. Oxford University Press, New York, US.
- Croal LR, Johnson CM, Beard BL, Newman DK (2004) Iron isotope fractionation by Fe(II)-oxidizing photoautotrophic bacteria. *Geochim. Cosmochim. Acta* **68**, 1227-1242.
- Dauphas N, Janney PE, Mendybaev RA, Wadhwa M, Richter FM, Davis AM, van Zuilen M, Hines R, Foley CN (2004) Chromatographic separation and multicollection-ICPMS analysis of iron. Investigating mass-dependent and -independent isotope effects. *Anal. Chem.* **76**, 5855-5863.
- Dideriksen K, Baker JA, Stipp SLS (2003) Iron isotopes in natural carbonate minerals determined by MC-ICP-MS with a Fe-58-Fe-54 double spike. *Geochim. Cosmochim. Acta* **70**, 118-132.
- Dixon PR, Janecky DR, Perrin RE, Rokop DJ, Unkefer PL, Spall WD (1992) Unconventional stable isotopes: Iron. p. 915-918. In Kharaka YK, Maest AS (eds.) *Water-rock Interaction, Volume 2*, Balkema, Rotterdam, The Netherlands.
- Dixon PR, Perrin RE, Rokop DJ, Maeck R, Janecky DR, Banar JP (1993) Measurements of iron isotopes (⁵⁴Fe, ⁵⁶Fe, ⁵⁷Fe, and ⁵⁸Fe) in submicrogram quantities of iron. *Anal. chem.* **65**, 2125-2130.
- Dyar MD, Agresti DG, Schaefer MW, Grant CA, Sklute EC (2006) Mössbauer spectroscopy of earth and planetary materials. *Ann. Rev. Earth Planet. Sci.* **34**, 83-125.

- Emmanuel S, Erel Y, Matthews A, Teutsch N (2004) A preliminary mixing model for Fe isotopes in soils. *Chem. Geol.* **222**, 23-34.
- Fantle MS, DePaolo DJ (2004) Iron isotope fractionation during continental weathering. *Earth Planet. Sci. Lett.* **228**, 547–562.
- Feder F, Trolard F, Klingelhofer G, Bourrie G (2005) In situ Mössbauer spectroscopy: Evidence for green rust (fougerite) in a gleysol and its mineralogical transformations with time and depth. *Geochim. Cosmochim. Acta* **69**, 4463-4483
- Fischer AC, Wolterbeek HT, Kroon JJ, Gerringa LJA, Timmennans KR, van Elteren JT, Teunissen T (2006) On the use of iron radio-isotopes to study iron speciation kinetics in seawater: A column separation and off-line counting approach. *Sci. Tot. Environ.* **362**, 242-258.
- Gartenmann P, Schnabel C, Suter M, Synal HA (1997) Fe-60 measurements with an EN tandem accelerator. *Nucl. Instr. and Meth. B* **123**, 132-136.
- Goodman BA (1988) An introduction to physical and chemical principles. p. 19-36. In Stucki JW, Goodman BA, Schwertmann U (eds.) *Iron in soils and clay minerals*. D. Reidel, Dordrecht, The Netherlands.
- Graham S, Pearson N, Jackson S, Griffin W, O'Reilly SY (2004) Tracing Cu and Fe from source to porphyry: in situ determination of Cu and Fe isotope ratios in sulfides from the Grasberg Cu-Au deposit. *Chem. Geol.* **207**, 147-169.
- Halliday AN, Lee D-C, Christensen JN, Rehkämper M, Yi W, Luo X, Hall CM, Ballentine CJ, Pettke T, Stirling C (1998) Applications of multiple collector-ICPMS to cosmochemistry, geochemistry, and paleoceanography. *Geochim. Cosmochim. Acta* **62**, 919-940.
- Hirata T, Ohno T (2001) In-situ isotopic ratio analysis of iron using laser ablation-multiple collector-inductively coupled plasma mass spectrometry (LA-MC-ICP-MS). *J. Anal. Atom. Spec.* **16**, 487-491.
- Hirata T, Hayano Y, Ohno T (2003) Improvements in precision of isotopic ratio measurements using laser ablation-multiple collector-ICP-mass spectrometry: reduction of changes in measured isotopic ratios. *J. Anal. Atom. Spec.* **18**, 1283-1288.
- Hoefs, J. (2004) Stable isotope geochemistry. 5th edition. Springer, Berlin, Germany.
- Horn I, Schoenberg R, von Blanckenburg F (2006a) Comment on "Analysis of Fe isotopes in sulfides and iron meteorites by laser ablation high-mass resolution multi-collector-ICP mass spectrometry" by J. Kosler, R.B. Pedersen, C. Kruber and P.J. Sylvester. *J. Anal. Atom. Spec.* **21**, 211-213.
- Horn I, von Blanckenburg F, Schoenberg R, Steinhoefel G, Markl G (2006b) In situ iron isotope ratio determination using UV-femtosecond laser ablation with application to hydrothermal ore formation processes. *Geochim. Cosmochim. Acta* **70**, 3677-3688.
- Icopini GA, Anbar AD, Ruebush SS, Tien M, Brantley SL (2004) Iron isotope fractionation during microbial reduction of iron: The importance of adsorption. *Geology* **32**, 205-208.

- IRMM (1999) Certificate isotopic reference material IRMM-014. Institute for Reference Materials and Measurements, Geel, Belgium.
- Jarzecki AA, Anbar AD, Spiro TG (2004) DFT analysis of $\text{Fe}(\text{H}_2\text{O})_6^{3+}$ and $\text{Fe}(\text{H}_2\text{O})_6^{2+}$ structure and vibrations; implications for isotope fractionation. *J. Phys. Chem. A* **108**, 2726-2732.
- Johnson CM, Beard BL (1999) Correction of instrumentally produced mass fractionation during isotopic analysis of Fe by thermal ionization mass spectrometry *Int. J. Mass Spectrom.* **193**: 87-99.
- Johnson CM, Skulan JL, Beard BL, Sun H, Nealon KH, Braterman PS (2002) Isotopic fractionation between Fe(III) and Fe(II) in aqueous solutions. *Earth Planet. Sci. Lett.* **195**, 141-153.
- Johnson CM, Beard BL, Albarède F (2004a) (eds.) Geochemistry of non-traditional stable isotopes. Reviews in Mineralogy and Geochemistry 55. Mineralogical Society of America and Geochemical Society, Washington, DC, US.
- Johnson CM, Beard BL, Roden EE, Newman DK, Nealon KH (2004b) Isotopic constraints on biogeochemical cycling of Fe. *Rev. Mineral. Geochem.* **55**, 359-408.
- Kehm K, Hauri EH, Alexander CMO, Carlson RW (2003) High precision iron isotope measurements of meteoritic material by cold plasma ICP-MS. *Geochim. Cosmochim. Acta* **67**, 2879-2891.
- Knie K, Korschinek G, Faestermann T, Wallner C, Scholten J, Hillebrandt W (1999) Indication for supernova produced Fe-60 activity on earth. *Physical Rev. Lett.* **83**, 18-21.
- Kosler J, Pedersen RB, Kruber C, Sylvester PJ (2005) Analysis of Fe isotopes in sulfides and iron meteorites by laser ablation high-mass resolution multi-collector ICP mass spectrometry. *J. Anal. Atom. Spec.* **20**, 192-199.
- Kraus KA, Moore GE (1953) Anion exchange studies. VI. The divalent transition elements manganese to zinc in hydrochloric acid. *J. Am. Chem Soc.* **75**, 1460-1462.
- Malinovsky D, Stenberg A, Rodushkin I, Andren H, Ingri J, Ohlander B, Baxter DC (2003) Performance of high resolution MC-ICP-MS for Fe isotope ratio measurements in sedimentary geological materials. *J. Anal. Atom. Spec.* **18**, 687-695.
- Mandernack KW, Bazylnski DA, Shanks WC, Bullen TD (1999) Oxygen and iron isotope studies of magnetite produced by magnetotactic bacteria. *Science* **285**: 1892-1896.
- Matthews A, Zhu XK, O'Nions K (2001) Kinetic iron stable isotope fractionation between iron (-II) and (-III) complexes in solution. *Earth Planet. Sci. Lett.* **192**, 81-92.
- Montaser A (1998) Inductively coupled plasma mass spectrometry. Wiley-VCH, New York, US.
- Ohno T, Shinohara A, Kohge I, Chiba M, Hirata T (2004) Isotopic analysis of Fe in human red blood cells by multiple collector-ICP-mass spectrometry. *Anal. Sci.* **20**, 617-621.

- Pedersen HD, Postma D, Jakobsen R, Larsen O (2005) Fast transformation of iron oxyhydroxides by the catalytic action of aqueous Fe(II). *Geochim. Cosmochim. Acta* **69**, 3967-3977.
- Pedersen HD, Postma D, Jakobsen R (2006) Release of arsenic associated with the reduction and transformation of iron oxides. *Geochim. Cosmochim. Acta* **70**, 4116-4129.
- Poitrasson F, Halliday AN, Lee DC, Levasseur S, Teutsch N (2004) Iron isotope differences between Earth, Moon, Mars and Vesta as possible records of contrasted accretion mechanisms. *Earth Planet. Sci. Lett.* **223**, 253-266.
- Poitrasson F, Freydier R (2005) Heavy iron isotope composition of granites determined by high resolution MC-ICP-MS. *Chem. Geol.* **222**, 132-147.
- Poitrasson F (2006) On the iron isotope homogeneity level of the continental crust. *Chem. Geol.* **235**, 195-200.
- Polyakov VB (1997) Equilibrium fractionation of the iron isotopes: Estimation from Mössbauer spectroscopy data. *Geochim. Cosmochim. Acta* **61**, 4213-4217.
- Polyakov VB, Mineev SD (2000) The use of Mössbauer spectroscopy in stable isotope geochemistry. *Geochim. Cosmochim. Acta* **64**, 849-865.
- Quitté G, Meier M, Latkoczy C, Halliday AN, Gunther D (2006) Nickel isotopes in iron meteorites-nucleosynthetic anomalies in sulphides with no effects in metals and no trace of ^{60}Fe . *Earth Planet. Sci. Lett.* **242**, 16-25.
- Rehkämper M, Frank M, Hein JR, Porcelli D, Halliday A, Ingri J, Liebetrau V (2002) Thallium isotope variations in seawater and hydrogenetic, diagenetic, and hydrothermal ferromanganese deposits. *Earth Planet. Sci. Lett.* **197**, 65-81.
- Reichard PU (2005) Effects of microbial and plant siderophore ligands on the dissolution of iron oxides. Dissertation #15665 ETH Zurich, Zurich, Switzerland.
- Roden EE, Lovley DR (1992) Evaluation of ^{55}Fe as a tracer of Fe(III) reduction in aquatic sediments. *Geomicrobiol. J.* **11**, 49-56.
- Roe JE, Anbar AD, Barling J (2003) Nonbiological fractionation of Fe isotopes: evidence of an equilibrium isotope effect. *Chem. Geol.* **195**, 69-85.
- Schoenberg R, von Blanckenburg F (2005) An assessment of the accuracy of stable Fe isotope ratio measurements on samples with organic and inorganic matrices by high-resolution multicollector ICP-MS. *Int. J. Mass Spectrom.* **242**, 257-272.
- Skulan JL, Beard BL, Johnson CM (2002) Kinetic and equilibrium Fe isotope fractionation between aqueous Fe(III) and hematite. *Geochim. Cosmochim. Acta* **66**, 2995-3015.
- Strelow FEW (1980) Improved separation of iron from copper and other elements by anion-exchange chromatography on a 4% cross-linked resin with high concentrations of hydrochloric acid. *Talanta* **27**, 727-732.
- Taylor PDP, Valkiers S, Debievre P, Flegel U, Kruck T (1993) Stable-isotope analysis of iron by gas-phase electron-impact mass spectrometry. *Anal. Chem.* **65**, 3166-3167.

- Teutsch N, von Gunten U, Porcelli D, Cirpka OA, Halliday AN (2005) Adsorption as a cause for iron isotope fractionation in reduced groundwater. *Geochim. Cosmochim. Acta* **69**, 4175-4185.
- Van Der Zee C, Slomp CP, Rancourt DG, De Lange GJ, Van Raaphorst W (2005) A Mössbauer spectroscopic study of the iron redox transition in eastern Mediterranean sediments. *Geochim. Cosmochim. Acta* **69**, 441-453.
- Vogl J, Klingbeil P, Pritzkow W, Riebe G (2003) High accuracy measurements of Fe isotopes using hexapole collision cell MC-ICP-MS and isotope dilution for certification of reference materials. *J. Anal. Atom. Spec.* **18**, 1125-1132.
- Völkening, J, Papanastassiou DA (1989) Iron isotope anomalies. *Astrophys. J.* **347**, L43-L46.
- Walczyk T, von Blanckenburg F (2002) Natural iron isotope variations in human blood. *Science* **295**, 2065-2066.
- Walczyk T, von Blanckenburg F (2005) Deciphering the iron isotope message of the human body. *Int. J. Mass Spectrom.* **242**, 117-134.
- Walder AJ, Freedman PA (1992) Isotopic ratio measurement using a double focusing magnetic-sector mass analyzer with an inductively coupled plasma as an ion-source. *J. Anal. Atom. Spec.* **7**, 571-575.
- Warwick PE, Cundy AB, Croudace IW, Bains MED, Dale AA (2001) The uptake of iron-55 by marine sediment, macroalgae, and biota following discharge from a nuclear power station. *Environ. Sci. Technol.* **35**, 2171-2177.
- Welch SA, Beard BL, Johnson CM, Braterman PS (2003) Kinetic and equilibrium Fe isotope fractionation between aqueous Fe(II) and Fe(III). *Geochim. Cosmochim. Acta* **67**, 4231-4250.
- Weyer S, Schwieters J (2003) High precision Fe isotope measurements with high mass resolution MC-ICPMS. *Int. J. Mass Spectrom.* **226**, 355-368.
- Weyer S, Anbar AD, Brey GP, Munker C, Mezger K, Woodland AB (2005) Iron isotope fractionation during planetary differentiation. *Earth Planet. Sci. Lett.* **240**, 251-264.
- Wiederhold JG (2000) Iron isotope fractionation in a seasonally reduced soil. Project report, Department of Crop and Soil Science, Oregon State University, Corvallis, US.
- Wiederhold JG (2002) Fraktionierung von Eisen-Isotopen in einer Stagnogley-Ockererde-Catena auf Buntsandstein. Diploma thesis, Institute for Mineralogy and Geochemistry, University of Karlsruhe (TH), Germany.
- Wiederhold JG, von Blanckenburg F (2002) Iron isotope variations in a complete natural soil catena with lateral iron mobilization and reprecipitation. *Geochim. Cosmochim. Acta* **66**, A834.
- Williams AGB, Scherer MM (2004) Spectroscopic evidence for Fe(II)-Fe(III) electron transfer at the iron oxide-water interface. *Environ. Sci. Technol.* **38**, 4782-4790.
- Williams HM, McCammon CA, Peslier AH, Halliday AN, Teutsch N, Levasseur S, Burg J-P (2004) Iron isotope fractionation and the oxygen fugacity of the mantle. *Science* **304**, 1656-1659.

- Williams HM, Peslier AH, McCammon C, Halliday AN, Levasseur S, Teutsch N, Burg JP (2005) Systematic iron isotope variations in mantle rocks and minerals: The effects of partial melting and oxygen fugacity. *Earth Planet. Sci. Lett.* **235**, 435-452.
- Xie QL, Lu SY, Evans D, Dillon P, Hintelmann H (2005) High precision Hg isotope analysis of environmental samples using gold trap-MC-ICP-MS. *J. Anal. Atom. Spec.* **20**, 515-522.
- Young ED, Galy A, Nagahara H (2002) Kinetic and equilibrium mass-dependent isotope fractionation laws in nature and their geochemical and cosmochemical significance. *Geochim. Cosmochim. Acta* **66**, 1095-1104

4. IRON ISOTOPE FRACTIONATION IN OXIC SOILS BY MINERAL WEATHERING AND PODZOLIZATION

This chapter is submitted for publication:

Wiederhold JG, Teutsch N, Kraemer SM, Halliday AN, Kretzschmar R

Iron isotope fractionation in oxic soils by mineral weathering and podzolization

Abstract

Stable iron isotope ratios in three natural soil profiles were measured by MC-ICPMS to trace pedogenic iron transformation and translocation processes under oxic conditions. The motivation for this work was to elucidate the relationships between geochemical processes, responsible for mineral weathering and pedogenesis in oxic soils, and mass-dependent fractionations of iron isotopes. Two Podzols that are characterized by intense pedogenic vertical iron translocation within the soil profile and one Cambisol without pedogenic iron translocation were investigated. A three-step sequential extraction procedure was used to separate operationally-defined iron mineral pools (poorly-crystalline iron oxyhydroxides, crystalline iron oxides, silicate-bound iron) from the soil samples. Iron isotope ratios of total soil digests were compared to those of the separated iron mineral pools. Mass balance calculations demonstrate excellent agreement between results of sequential extractions and total soil digestions. Systematic variations in the iron isotope signature were found in the Podzol profiles that were formed by pedogenic vertical transport of iron under the influence of organic ligands and acidic conditions (soil pH < 4). An enrichment of light iron isotopes of about 0.6 ‰ in $\delta^{57}\text{Fe}$ was found in total soil digests of the illuvial Bh horizons which can be explained by preferential translocation of light iron isotopes. The separated iron mineral pools exhibit a wide range of $\delta^{57}\text{Fe}$ values of more than 3 ‰ in the Podzol profiles. Strong enrichments of heavy iron isotopes in silicate-bound iron, which constitutes the residue of weathering processes, indicate the preferential transformation of light iron isotopes during weathering. In contrast to the Podzol profiles, the Cambisol profile displayed uniform $\delta^{57}\text{Fe}$ values over soil depth and showed only a small enrichment of light iron

isotopes of about 0.4 ‰ in the poorly-crystalline iron oxide pool extracted by 0.5 M HCl. Iron isotope fractionation during podzolization is probably linked to the ligand-controlled iron translocation processes. This work demonstrates that significant iron isotope fractionations occur in nature not only by reductive iron transformations as shown previously, but also in oxic environments under the influence of organic ligands. These findings provide new insights into the fractionation mechanisms of iron isotopes and will help in the development of stable iron isotopes as a tracer for the biogeochemical iron cycle in nature.

4.1 INTRODUCTION

Stable iron isotopes provide a new tool to trace the biogeochemical iron cycle in nature (Anbar, 2004; Johnson et al., 2004a; Dauphas and Rouxel, 2006). Iron is not only an essential nutrient for almost all organisms, but it also influences the biogeochemical cycling of many nutrient and pollutant elements in soils (Stucki et al., 1988; Cornell and Schwertmann, 2003). Moreover, iron transformations and translocations are important processes in weathering and soil formation (van Breemen and Buurman, 2004). The analysis of stable isotope ratios of light elements (e.g., C, H, O, N, S) has been widely applied in the investigation of basic and applied problems of earth and environmental sciences (Hoefs, 2004). The development of new analytical methods, mainly multiple collector inductively coupled plasma mass spectrometry (MC-ICPMS), has recently expanded the potential of stable isotope studies to heavier elements including iron (Halliday et al., 1998; Johnson et al., 2004b).

Iron has four stable isotopes (percent natural abundance): ^{54}Fe (5.84 %), ^{56}Fe (91.76 %), ^{57}Fe (2.12 %), and ^{58}Fe (0.28 %). The δ -notation is commonly used to describe iron isotope fractionation relative to the international iron isotope standard IRMM-014 and is defined as

$$\delta^{56}\text{Fe} [\text{‰}] = \left(\frac{(^{56}\text{Fe}/^{54}\text{Fe})_{\text{sample}}}{(^{56}\text{Fe}/^{54}\text{Fe})_{\text{IRMM-014}}} - 1 \right) \cdot 10^3 \quad \text{or} \quad \delta^{57}\text{Fe} [\text{‰}] = \left(\frac{(^{57}\text{Fe}/^{54}\text{Fe})_{\text{sample}}}{(^{57}\text{Fe}/^{54}\text{Fe})_{\text{IRMM-014}}} - 1 \right) \cdot 10^3 .$$

The two values can be easily converted into each other by the approximation $\delta^{57}\text{Fe} = 1.5 \times \delta^{56}\text{Fe}$ because the observed fractionation effects are mass-dependent. Variations of $\delta^{56}\text{Fe}$ in bulk igneous rocks were found to be very small (Beard and

Johnson, 1999; Beard and Johnson, 2004). In contrast, significant iron isotope variations of several per mil were found in a variety of low-temperature environments (Dauphas and Rouxel, 2006). However, there is still very limited information available on iron isotope variations in soils and about the mechanisms responsible for the observed fractionations. Brantley et al. (2001 and 2004) studied iron isotope fractionation in a soil sample from the B horizon of a hornblende-containing soil and reported a strong enrichment of light isotopes in the “exchangeable” iron fraction compared to oxide-bound iron. Wiederhold and von Blanckenburg (2002) investigated iron isotope fractionation during lateral iron translocation under reducing conditions in a soil catena in the Black Forest (Germany) and found significant iron isotope variations indicating the preferential transport of light iron isotopes within the landscape. Fantle and DePaolo (2004) studied iron isotope variations in four selected horizons of a soil profile in northern California (USA) and reported variations of about 0.7 ‰ in $\delta^{56}\text{Fe}$ between bulk soil samples from different depths. Emmanuel et al. (2005) measured iron isotopes in a Czech forest soil and an Israeli semi-arid soil and reported variations of about 0.35 ‰ in $\delta^{57}\text{Fe}$ in bulk soil samples. However, the identification of fractionation mechanisms responsible for the observed iron isotope variations in soils remains unclear. This is not only due to the limited set of available data but also because most soils are highly heterogeneous natural systems and various iron transformation reactions are often occurring simultaneously.

Under atmospheric conditions, iron is thermodynamically stable in the ferric oxidation state (Fe^{III}). The weathering of primary silicate minerals in soils releases ferrous iron (Fe^{II}) that is oxidized followed by the precipitation of poorly-crystalline iron (oxyhydr)oxide minerals such as ferrihydrite. A transformation to more crystalline iron oxide mineral phases, such as goethite and hematite, takes place during further soil development. These pedogenic transformations are occurring in situ and do not result in significant iron redistribution within the soil profile. The development of brownish colors in the mineral soil typically indicates pedogenic formation of iron (oxyhydr)oxide minerals. Soils exhibiting only these features of incipient weathering are classified as Cambisol according to the World Reference Base for Soil Resources (WRB, 2006a). Cambisols (from the Latin word *cambiare* meaning “changing”) are among the most important soil groups covering an estimated area of about 1.5 billion hectares worldwide (WRB, 2006a). They occur in almost all climatic zones and are particularly widespread in landscape positions which prevent

uninterrupted soil development due to erosion processes, and on relatively young soil substrates. Cambisols are typically characterized by a brownish weathered Bw horizon below the A horizon, which exhibits organic matter enrichments from decaying plant material in the topsoil. In the US Soil Taxonomy, most Cambisols are classified as Inceptisols (USDA, 2006). With increasing soil age and under certain pedogenetic conditions, Cambisols can develop into other soil types such as Podzols.

Podzols are characterized by a vertical translocation of iron in the soil profile, together with aluminum and organic matter (Van Breemen and Buurman, 2004). There are 485 million hectares of Podzols worldwide occurring mainly in forested regions in a cool humid climate (WRB, 2006a). The name Podzol originates from the Russian words “pod zola” (under ash) (Lundström et al., 2000). In the US Soil Taxonomy, Podzols are classified as Spodosols (USDA, 2006). The typical horizon sequence of Podzols consists of a dark organic surface layer (O) on top, followed by a grey depleted eluvial horizon (E) and enriched illuvial B horizons that are colored by organic matter (Bh) and iron oxides (Bs). The pedogenic process leading to this horizon pattern is called podzolization and has been subject of numerous studies. However, the podzolization mechanisms are still debated intensively in the literature (Anderson et al., 1982; Lundström et al., 2000; Buurman and Jongmans, 2005; Jansen et al., 2005). General prerequisites for podzolization are a well-drained substrate that is poorly-buffered against acidification (typically quartz-rich sands or granite), a cool humid climate, and a vegetation producing litter that is only slowly biodegradable (typically coniferous forests or heath). Organic acids that are released from the organic surface layer (O horizon) under very acidic conditions ($\text{pH} < 4$) form complexes with iron and aluminum thereby leaching the upper mineral soil and creating the iron-depleted, grey E horizon. The iron-aluminum-organic complexes are then transported vertically downward until they re-precipitate in the B horizon. Often, an organic rich black Bh horizon is overlying a reddish sesquioxide-rich Bs horizon. The podzolization process has important consequences on many physical and chemical soil properties and influences ecosystem functions and land use. Podzolization also changes the element distribution of elements other than iron and aluminum (Tyler, 2004; Donisa et al., 2005). Besides the importance of podzolization for pedogenesis, it also represents an ideal system for the investigation of ligand-controlled iron translocation processes in nature.

The objective of this work was to investigate iron isotope fractionation during weathering and soil formation under oxic conditions. Therefore, we measured iron isotope ratios in soil samples of two Podzol and one Cambisol profiles with high spatial resolution. We chose these soils types due to the contrasting geochemical iron dynamics during their formation and because they are dominated by specific pedogenic processes. Hence, we were able to relate iron isotope fractionation and soil formation based on the involved geochemical processes. We focused on oxic soil environments in this study, which are dominated by protolytic weathering and ligand-controlled iron transformation processes, and in which reductive iron transformation processes are unlikely to play a significant role. Iron isotope ratios of total soil digests were measured and compared to isotope data of different Fe phases (poorly-crystalline iron oxyhydroxides, crystalline iron oxides, silicate-bound iron) separated by a three-step sequential extraction procedure. Thus, this work provides a comprehensive study of iron isotope variations in oxic soils aiming at a process-oriented understanding of Fe isotope fractionation during weathering reactions and soil formation in nature.

4.2 METHODS

4.2.1 Sampling sites

Soil samples were taken at three different sites in Germany representing two Podzol profiles and one Cambisol profile. All three investigated soils are well-drained and not influenced by groundwater. They are therefore well-aerated and exhibit oxic conditions year-round. No redoximorphic features such as iron and manganese mottles or concretions, which are characteristic for hydromorphic soils, are present. In consequence, it is unlikely that the pedogenesis of the investigated soils was influenced to a significant extent by reductive iron transformations due to temporarily water-saturated conditions.

The first Podzol profile, in the following referred to as Podzol A, was sampled in NW-Germany near Flaesheim / Westphalia (51°43' N, 7°12' E). The site has been previously used for studies of soil organic matter dynamics (Schmidt et al., 2000). The soil has developed on a Pleistocene eolian sand deposit and the vegetation is dominated by pine trees (*Pinus sylvestris*). Soil pH(CaCl₂) ranges from 3.1 in the upper mineral soil horizon (A_{he}) to 4.0 at a depth of 140 cm (Schmidt et al., 2000).

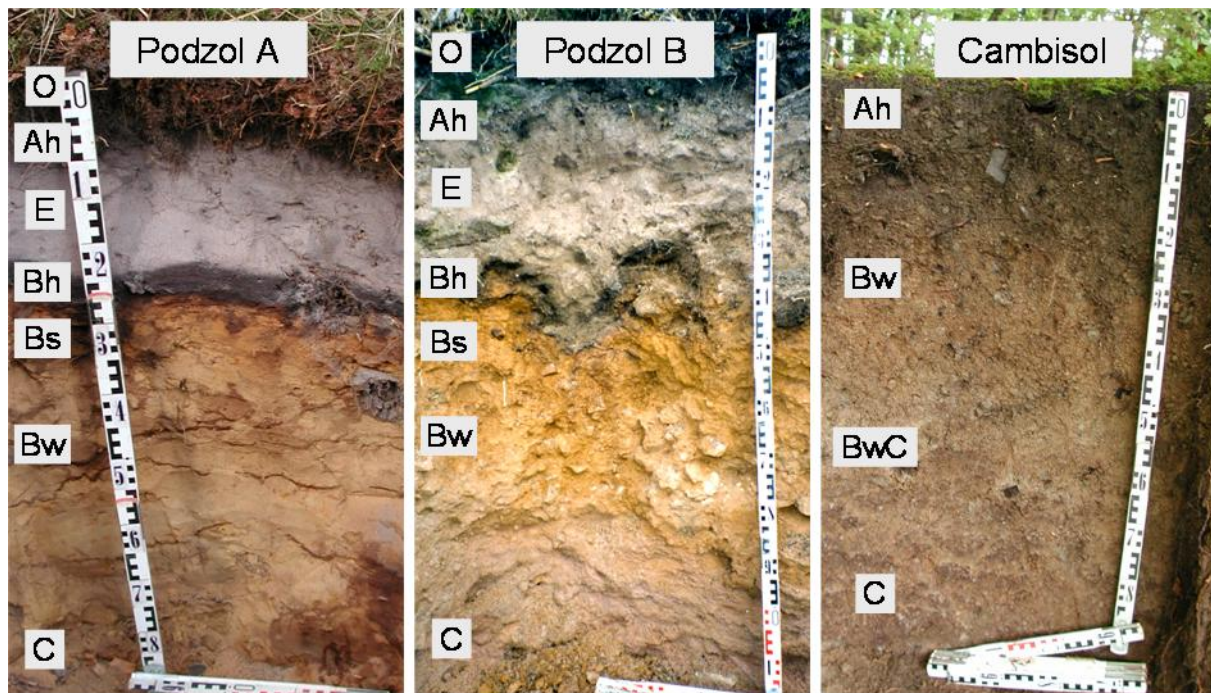


Figure 4.1 Photographs of the three investigated soil profiles. Podzol A (near Flaesheim, Westphalia, NW-Germany), Podzol B (near Klosterreichenbach, Black Forest, SW-Germany) and Cambisol (near Hewenegg, Hegau, SW-Germany). The horizon designations are consistent with the World Reference Base for Soil Resources (WRB, 2006b): O = organic surface layer (decomposing plant litter), Ah = organic-rich mineral horizon, E = eluvial horizon, Bh = illuvial organic-rich horizon, Bs = illuvial sesquioxide-rich horizon, Bw = weathered horizon, C = soil substrate, BwC = transition horizon.

The second Podzol profile, in the following referred to as Podzol B, was sampled in SW-Germany near Klosterreichenbach / Black Forest (48°31' N, 8°24' E) and has formed on Triassic hematitic sandstone (Buntsandstein) that was reworked by periglacial processes during the Pleistocene. The vegetation at this site is dominated by spruce (*Picea abies*) and pine (*Pinus sylvestris*) trees. Soil pH(CaCl₂) ranges from 2.7 in the upper mineral soil horizon (Ahe) to 4.6 at a depth of 120 cm (Sommer, 1992). Both Podzols are classified as Haplic Podzol according to the World Reference Base for Soil Resources (WRB, 2006a) or Typic Haplorthod according to US Soil Taxonomy (USDA, 2006).

The Cambisol profile was sampled in the Hegau region in SW-Germany near Immendingen (47°54' N, 8°44' E) situated within a tertiary volcanic complex (Hewenegg). We selected this soil as a reference profile exhibiting clear indications of chemical weathering but without pedogenic iron translocation within the profile.

The soil at this site is classified as Haplic Cambisol (eutric) according to the World Reference Base for Soil Resources (WRB, 2006a). This soil, in the following referred to as Cambisol, has formed on basaltic tuff and exhibits pH(CaCl₂) values between 5.5 and 5.9 (Jahn et al., 1997). The vegetation on the site is dominated by beech trees (*Fagus sylvatica*) which produce an easily-biodegradable litter compared to the pine and spruce trees at the two Podzol profile locations. Photographs of all three soil profiles with indications of pedogenic horizons are shown in Fig. 4.1 (Podzol A is also depicted on the front cover of this thesis).

4.2.2 Soil sampling and sample preparation

The soil profiles were sampled with a high vertical spatial resolution in order to resolve the different pedogenic horizons (12 depths per Podzol profile and 4 depths in the Cambisol profile). The samples were dried at 40°C in the laboratory and sieved through a 2 mm mesh. Aliquots of the samples were ground to a fine powder with a rotary disk mill. From this powder, wax pellets were produced to measure total element concentrations by energy-dispersive X-ray fluorescence analysis (Spectro-X-Lab 2000, Spectro, Germany). A small amount of the powdered samples (100 - 500 mg depending on iron content) was dissolved totally in a microwave digestion with HF-HNO₃-HCl (mixture 1:2:2). These samples represent the Fe_{total} pool of the soil samples. Samples rich in organic matter were pre-treated with 30% H₂O₂ prior to the digestion. The clear solutions after the digestion were evaporated in Teflon beakers on a hotplate to remove excess HF. The residue was redissolved in concentrated HNO₃ to ensure complete oxidation of ferrous to ferric iron. This solution was again evaporated and the residue taken up in 6 M HCl. All reagents used during sample preparation were at least *pro analysi* grade and prepared with ultrapure water (>18 MΩ). Hydrochloric and nitric acids were further purified by sub-boiling distillation. Hydrofluoric acid used during digestions was suprapure quality (MERCK, Germany).

In parallel, another aliquot of the dried and sieved soil samples was subjected to a three-step sequential extraction procedure to separate different Fe mineral pools (poorly-crystalline iron oxyhydroxides, crystalline iron oxides, silicate-bound iron) from the soil samples. In the first extraction step, 2 g of the soil material were weighed into 50 mL centrifuge tubes, 40 mL of 0.5 M HCl were added to the tubes and the samples were placed on an overhead shaker for 24 hours at room

temperature. Afterwards the tubes were centrifuged (3400g, 15 min) and the supernatants decanted and filtered through 0.45 μm Nylon membrane filters (Opti-Flow, WICOM, Germany). This solution is the Fe_{HCl} fraction of the soil. In the second extraction step, 40 mL of a 1 M $\text{NH}_2\text{OH}\text{-HCl}$ solution in 1 M HCl were added to the residue in the centrifuge tubes and shaken vigorously. The tubes were then placed in a hot water bath at 90°C with integrated horizontal shaker for four hours. Additionally, the samples were manually shaken overhead from time to time. Afterwards the tubes were again centrifuged (3400g, 15 min) and the supernatants decanted and filtered through 0.45 μm Nylon filters. This solution is the $\text{Fe}_{\text{NH}_2\text{OH-HCl}}$ fraction of the soil. The residue was washed twice with water, dried overnight at 105°C and then ground to a fine powder with a rotary disk mill. An aliquot of this powder, again depending on the Fe content between 100 and 500 mg, was then totally dissolved in a microwave digestion with $\text{HF-HNO}_3\text{-HCl}$ (mixture 1:2:2) and further treated similar to the total soil samples. The extracted solutions (Fe_{HCl} and $\text{Fe}_{\text{NH}_2\text{OH-HCl}}$) were also evaporated in Teflon beakers on a hotplate and oxidized with HNO_3 and H_2O_2 to destroy organic matter and hydroxylamine and to convert ferrous to ferric iron. The residue was then also taken up in 6 M HCl. The organic surface layer samples of the Podzol profiles were not subjected to the entire sequential extraction procedure since the method is only applicable for mineral soil samples. For these samples, only the total digestion and the first extraction step with 0.5 M HCl were performed.

Iron concentrations of all samples were measured by atomic absorption spectrometry (AAS, SpectrAA 220, Varian, Australia). Further sample preparation took place in a clean chemistry laboratory. Teflon micro-columns filled with about 1 mL anion exchange resin (Bio-Rad AG1 X4, 200-400 mesh) were used to separate iron from matrix elements of the sample. In 6 M HCl ferric iron is present as FeCl_4^- anion. The iron complex is retained on the resin while the sample matrix is washed out by repeated additions of 6 M HCl. Elution of iron from the columns was achieved with 0.05 M HCl. The eluates were again evaporated and finally taken up in 0.05 M HCl as solution matrix for the iron isotope measurements.

4.2.3 Iron isotope measurement

Iron isotope ratios were determined by multiple collector inductively coupled plasma mass spectrometry (MC-ICPMS, Nu Plasma, Nu instruments, UK). A

comprehensive description of iron isotope analytical methods was recently published by Schoenberg and von Blanckenburg (2005). The analytical procedures for iron isotope measurements in our laboratory have been previously described in detail (Williams et al., 2004; Teutsch et al., 2005). Briefly, a standard-bracketing approach was used to correct for machine drift and instrumental mass bias. A membrane desolvating system (MCN-6000, Cetac, USA) was used to minimize argide interferences (ArN^+ , ArO^+ , ArOH^+) to insignificant levels (background to signal ratio typically < 0.001). The $^{57}\text{Fe}/^{54}\text{Fe}$ and $^{56}\text{Fe}/^{54}\text{Fe}$ ratios were measured simultaneously and all data plot on the theoretical mass fractionation line demonstrating the absence of isobaric interferences. A Cr correction was performed by monitoring mass 52 or 53 to calculate the potential influence of ^{54}Cr on ^{54}Fe . However, our purified solutions did not contain significant amounts of Cr and the Cr corrected and uncorrected $\delta^{57}\text{Fe}$ values differed by less than ± 0.02 ‰ for all samples. All masses were collected in Faraday cups equipped with $10^{11} \Omega$ resistors except mass 56 which was collected in a Faraday cup equipped with a $10^9 \Omega$ resistor. This allowed measurements at relatively high Fe concentrations (8 ppm) but it also affected the precision of the $^{56}\text{Fe}/^{54}\text{Fe}$ measurement. Therefore, given the smaller analytical error for the $^{57}\text{Fe}/^{54}\text{Fe}$ ratio, the results are expressed as $\delta^{57}\text{Fe}$. Samples were only measured after several stable isotope measurements of an internal house standard against IRMM-014. This standard was again measured after every six samples and at the end of the analytical run. The long term reproducibility of $\delta^{57}\text{Fe}$ of our internal house standard is better than ± 0.15 ‰ (2SD). Samples were measured several times and the error bars for $\delta^{57}\text{Fe}$ represent either the reproducibility (2SD) of replicate sample measurements or, in case of fewer measurements ($n < 3$), the reproducibility (2SD) of our internal house standard during the same analytical session. A mass balance approach was used to verify the iron concentration and iron isotope results of the different iron fractions. The isotope mass balance was calculated according to the following formula, where $[\text{Fe}]_n$ is the iron concentration in pool n,

$$\delta^{57}\text{Fe}_{total, calc.} \cdot [\text{Fe}]_{total, calc.} = \delta^{57}\text{Fe}_{HCl} \cdot [\text{Fe}]_{HCl} + \delta^{57}\text{Fe}_{NH_2OH-HCl} \cdot [\text{Fe}]_{NH_2OH-HCl} + \delta^{57}\text{Fe}_{residue} \cdot [\text{Fe}]_{residue} .$$

The error bars of the calculated total Fe value were determined with the following

$$\text{formula } 2SD_{total, calc.} = \sqrt{(2SD_{HCl})^2 + (2SD_{NH_2OH-HCl})^2 + (2SD_{residue})^2} .$$

4.3 RESULTS AND DISCUSSION

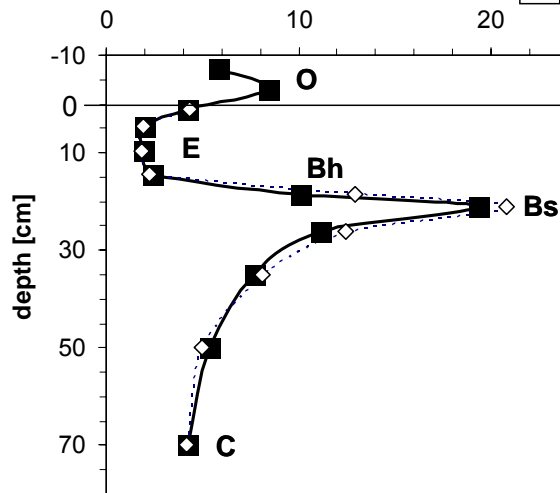
4.3.1 Iron concentration profiles in total soil digests

The typical vertical horizon sequence of Podzols is clearly visible in the soil profiles (Fig. 4.1). Depth profiles of the total iron concentrations (Fig. 4.2 A+B) reflect the pedogenic iron translocation process. The highest total iron concentrations are found in the black Bh and reddish-brown Bs horizon, whereas the lowest iron concentrations are found in the grey E horizon. The iron concentration slowly decreases below the enriched B horizons towards geogenic background values in the C horizon. The results of the XRF measurements, which were used to obtain depth profiles of the total concentrations of other elements, are summarized in the Electronic Annex. Uniform depth profiles of Ti and Zr concentrations indicate the geologic homogeneity of the parent material of Podzol A, which consists of a Pleistocene eolian sand deposit. The parent material of Podzol B is slightly less homogeneous, probably due to periglacial mixing of slope debris. However, the distinct iron depth distribution in both Podzol profiles clearly originates from pedogenic translocation processes and there is no indication of a significant influence by geological substrate heterogeneity.

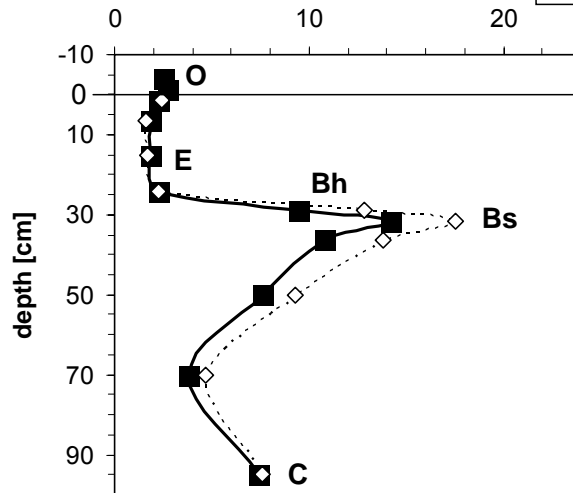
The iron concentration depth profile of the Cambisol are shown in Fig. 4.2 C. The uniform total iron concentrations over soil depth indicate the absence of vertical iron translocation. Although the basaltic tuff substrate weathers relatively rapidly, iron transformations from primary silicate minerals to secondary iron (oxyhydr)oxide phases occur mainly in situ. The warmer and drier climate prevailing at this site compared to those of the two Podzol profiles, the vegetation that produces well-degradable litter, and the higher buffer capacity of the parent material against acidification, explain the absence of podzolization processes in this soil profile.

Figure 4.2 Depth profiles of iron concentrations in total soil digests of the three investigated soil profiles. The pedogenic iron depletion in the E horizon and the iron enrichment in the Bh and Bs horizons are clearly visible in both Podzol profiles (Fig. 4.2 A+B). The uniform depth profile in the Cambisol profile (Fig. 4.2 C) confirms the absence of pedogenic iron translocation. Open symbols indicate the calculated sum of the three iron fractions that were separated by sequential extraction (Fig. 4.4). Zero values on depth axes indicate top of mineral soil. Lines serve as eye guides. Letters indicate selected pedogenic horizons (see Fig. 4.1).

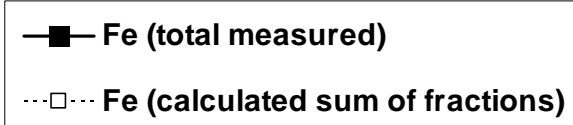
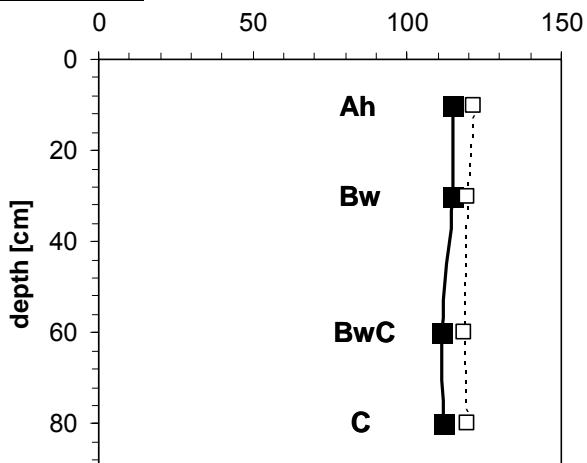
Podzol A **A**



Podzol B **B**



Cambisol **C**

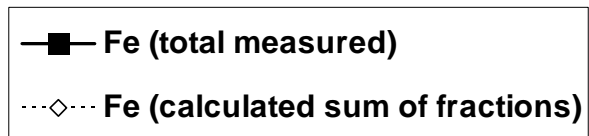
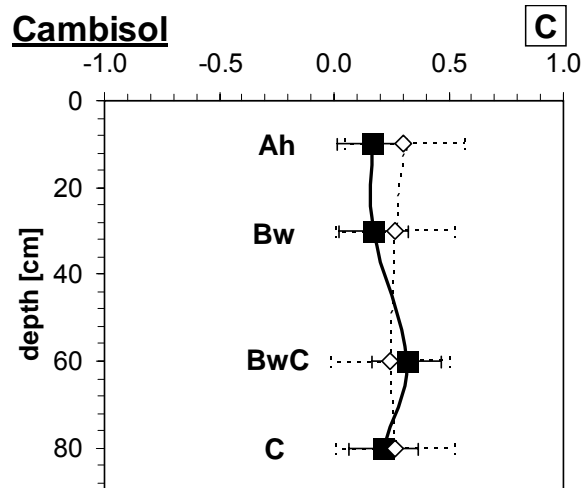
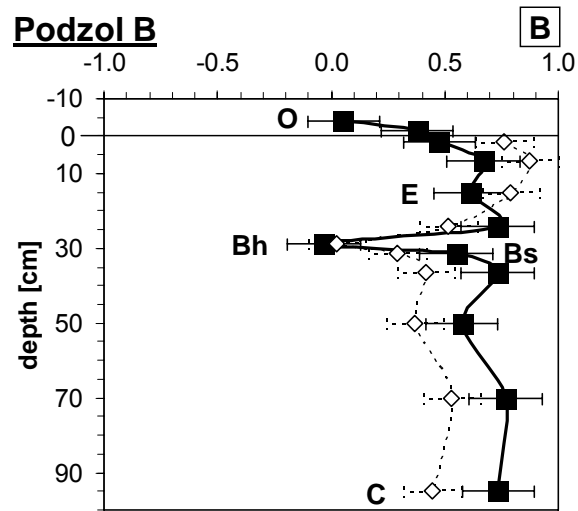
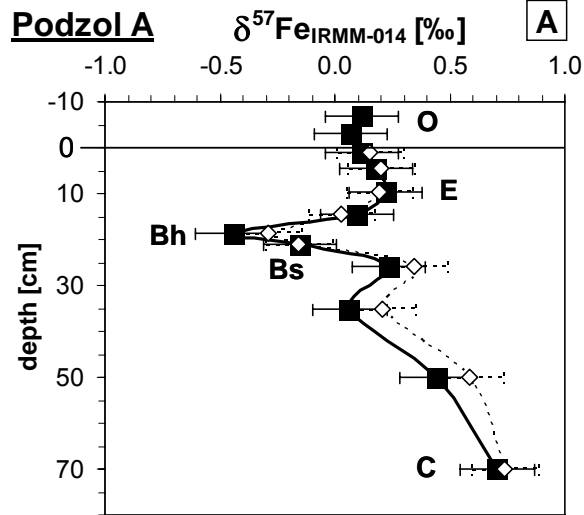


4.3.2 Iron isotope ratios in total soil digests

The results of the iron isotope measurements of the total soil digests (Fe_{total}) of the two Podzol profiles are displayed in Fig. 4.3 A+B. Both profiles exhibit a distinct peak toward lighter iron isotope ratios in the dark, iron-enriched Bh horizon. In contrast, the iron-depleted E horizons show slightly positive $\delta^{57}\text{Fe}$ values. The difference in $\delta^{57}\text{Fe}$ between the E and Bh horizons of both profiles is about 0.6 ‰ which is a clear indication of iron isotope fractionation during pedogenic iron translocation in Podzols. It is interesting that the strongest isotope effect is present in the Bh horizon although the highest iron concentrations are present in the Bs horizon below (Fig. 4.2A+B). However, the Bs horizon also exhibits a lighter iron isotope signature compared to the E horizon samples. Since the Bh horizon is not only enriched in iron but also characterized by high contents of organic matter causing the dark color of the horizon, it is likely that the iron isotope fractionation process is linked to the organic matter dynamics during the podzolization process.

The organic surface layer samples of Podzol A do not exhibit a significant isotope fractionation compared to the mineral soil horizons directly below. However, the results from Podzol B exhibit $\delta^{57}\text{Fe}$ values in the organic surface layer horizons that are lower by up to 0.5 ‰ compared to the underlying mineral soil horizons. This could indicate that organically bound iron in the plant litter at this site is enriched in light isotopes. The C horizons, which represent the least-transformed parent material of the soils, exhibit iron isotope signatures that are heavy compared to IRMM-014 at both sites. We do not have a good explanation for the increase of $\delta^{57}\text{Fe}$ in the two lowest horizons of Podzol A. A lithogenic origin seems unlikely considering the concentration profiles of iron and immobile elements such as Ti and Zr, as discussed in the previous section.

Figure 4.3 Depth profiles of $\delta^{57}\text{Fe}$ values in total soil digests of the three investigated soil profiles. The negative peaks of $\delta^{57}\text{Fe}$ in the Bh horizon of both Podzol profiles (Fig. 4.3 A+B) indicate iron isotope fractionation during pedogenic iron translocation. The Cambisol data display no significant variations in $\delta^{57}\text{Fe}$ over soil depth (Fig. 4.3 C). Open symbols indicate the calculated isotope mass balance based on the iron concentrations and isotope signatures of the three iron fractions that were separated by sequential extraction (Fig. 4.4 and Fig. 4.5). Zero values on depth axes indicate top of mineral soil. Lines serve as eye guides. Letters indicate selected pedogenic horizons (see Fig. 4.1).



A pedogenic origin of the observed enrichment of heavier isotopes could be caused by preferential removal of light iron isotopes. However, this explanation is not supported by the available information on the pedogenesis of the soil profile. The relatively heavy $\delta^{57}\text{Fe}$ values in the subsoil of Podzol B, which has formed on Triassic hematitic sandstone (Buntsandstein), can be compared with a recent study of Markl et al. (2006) in which a $\delta^{57}\text{Fe}$ value of +0.35 ‰ was reported for a similar geological unit in the Black Forest.

The iron isotope ratios of the total digestions from the Cambisol profile on basaltic tuff exhibit no significant fractionation over the soil depth (Fig. 4.3 C). All samples display $\delta^{57}\text{Fe}$ values around +0.2 ‰ relative to IRMM-014 which is identical within error to the terrestrial baseline of igneous rocks (Beard and Johnson, 2004). The uniform depth distribution of iron isotope ratios is consistent with pedogenic conditions that do not induce iron translocations within the profile but rather in situ transformations of iron minerals.

4.3.3 Sequential extraction methods in iron isotope studies

Iron in soils is present in a variety of different phases such as silicate minerals, clay minerals, iron (oxyhydr)oxide minerals of different crystallinity, as well as organically bound iron (Stucki et al., 1988). The analysis of iron isotopes in total soil digestions yields only information about the average isotope ratio of all these different phases. Thus, it is desirable to develop methods to separate different iron-containing phases from soil samples in order to investigate the iron isotope signature of the individual phases. Physical methods such as sieving, density separation or handpicking under a microscope, which are used for instance to separate mineral phases from rock samples, are not applicable in most cases due to the small size of most iron compounds in soils and the heterogeneity of natural soil samples. Therefore, chemical separation methods, based on the sequential dissolution of specific iron phases from soil samples, have to be used. A wide range of sequential extraction methods has been developed and applied to separate different iron mineral pools from soil samples (e.g., Chao and Zhou, 1983; Borggaard, 1988; Heron et al., 1994; LaForce and Fendorf, 2000). However, these iron pools are only operationally defined because of the insufficient specificity of extraction methods for individual mineral phases from soil samples. We have selected a three-step sequential extraction procedure in our study. The first extraction step by hydrochloric

acid (0.5 M, 24 h, 25°C) dissolves poorly-crystalline iron oxide minerals such as ferrihydrite as well as adsorbed and organically-bound iron. The second extraction step with hydroxylamine-hydrochloride (1 M, 4 h, 90°C) achieves a complete reductive dissolution of all crystalline iron oxides such as goethite and hematite. In the third step all remaining soil material containing iron in primary silicates and clay minerals is totally dissolved by a microwave digestion procedure with HF-HNO₃-HCl. We decided to use this extraction scheme rather than other procedures, such as the commonly applied oxalate and dithionite methods, for several reasons discussed below.

First, isotope fractionation artifacts can be introduced by incomplete removal of certain mineral phases during dissolution. Since a quantitative extraction of selected mineral pools from a natural soil sample is difficult to verify, it is preferable to use only extraction methods that do not cause iron isotope effects even during incomplete dissolution. We have shown recently that the dissolution of goethite in the presence of oxalate, either by photochemical reductive or ligand-controlled mechanisms, results in significant iron isotope fractionation (see chapter 6 of this thesis). Moreover, the effect was found to vary between different stages of the dissolution reaction. In contrast, no iron isotope fractionation was observed during the stepwise dissolution of goethite by 0.5 M HCl, which is consistent with previous studies on hematite dissolution in HCl (Skulan et al., 2002).

A second consideration in the selection of extraction methods for isotope studies is the matrix that is introduced to the samples during the procedure. Since isotope measurements by MC-ICPMS are very sensitive to matrix effects and require highly purified solutions, organic compounds need to be destroyed by complete oxidation prior to removal of inorganic matrix elements by column separation methods. Some methods for the selective dissolution of iron phases from soils contain matrix components (such as sulfur in dithionite), which may complicate sample preparation for iron isotope analysis to a great extent.

A third requirement for the selection of sequential extraction methods in iron isotope studies is the absence of secondary precipitation reactions. Partial precipitation or adsorption reactions of iron-containing phases from the extraction solution could introduce fractionation artifacts compromising the data. The three-step sequential extraction procedure used in this study was designed to meet all criteria discussed above.

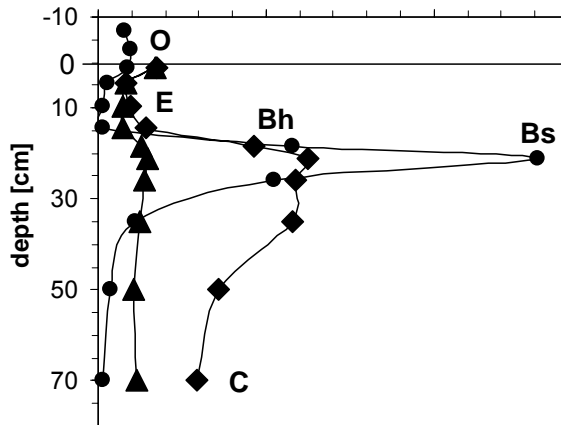
We used 0.5 M HCl for the first extraction step in our study because it dissolves the most labile soil iron phases (poorly-crystalline iron oxyhydroxides, adsorbed and organically-bound iron) and does not result in isotope fractionation artifacts even during incomplete dissolution (Skulan et al., 2002, chapter 6 of this thesis). We focused on the complete removal of all crystalline iron oxide minerals in the development of our second extraction step. This can be achieved by reductive dissolution at acidic pH, which also prevents re-precipitation and does not require the presence of a complexing agent to stabilize the dissolved iron in solution. We tested the procedure with 1 M hydroxylamine-hydrochloride in 1 M HCl at 90°C (modified after Ribet et al., 1995) and found a complete reductive dissolution of iron oxide minerals including hematite after four hours of extraction time. It is possible that some iron that was bound in the structure of clay minerals or other silicate minerals was extracted as well during this extraction step. Thus, a small bias may have been introduced into the isotope data of the last two steps of the sequential extraction procedure. The last extraction step (total dissolution by HF-HNO₃-HCl) was done similar to the total digestions of the soil samples. This parallel performance of total digestions and sequential extractions provided us with the possibility of establishing an isotope mass balance between the sum of the three extractions and the total digestion. The excellent agreement between the measured and calculated total iron isotope data (open symbols in Figs. 4.2 and 4.3) confirms the high data quality of the results from the sequential extraction procedure.

4.3.4 Iron concentration profiles in sequential extraction samples

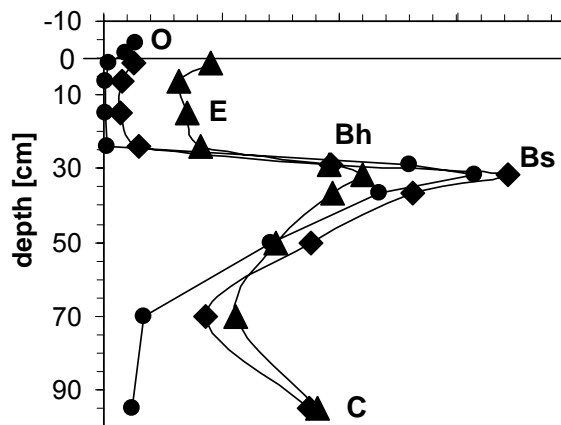
Fig. 4.4 A+B display the depth profiles of the different iron fractions in Podzols A and B that were separated by a three-step chemical extraction procedure.

Figure 4.4 Depth profiles of iron concentrations in the three iron mineral pools Fe_{HCl} , $Fe_{NH_2OH-HCl}$ and $Fe_{residue}$ which were separated by sequential extraction in the three investigated soil profiles. Pedogenic iron translocation in Podzol A is dominated by oxide-bound iron phases (Fe_{HCl} and $Fe_{NH_2OH-HCl}$) (Fig. 4.4 A), whereas all three fractions are affected in Podzol B (Fig. 4.4 B). Crystalline iron oxides ($Fe_{NH_2OH-HCl}$) are the dominant iron mineral pool in the Cambisol profile (Fig. 4.4 C). The calculated sum of the three fractions is shown in Fig. 4.2 in comparison to the total digests. Zero values on depth axes indicate top of mineral soil. Lines serve as eye guides. Letters indicate pedogenic horizons (see Fig. 4.1).

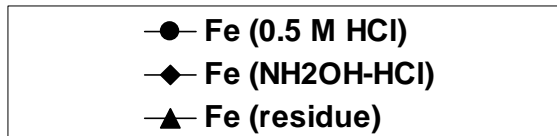
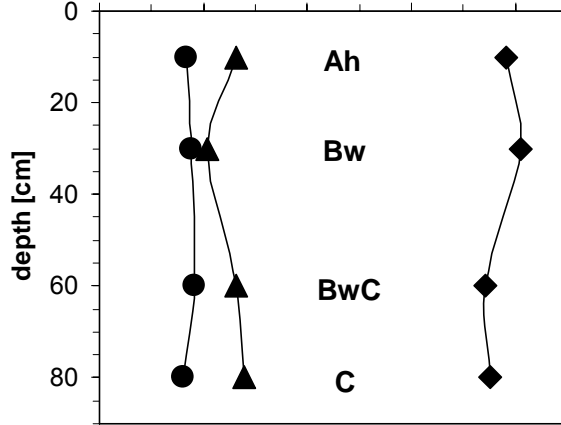
Podzol A Fe [mg/g] **A**



Podzol B **B**



Cambisol **C**

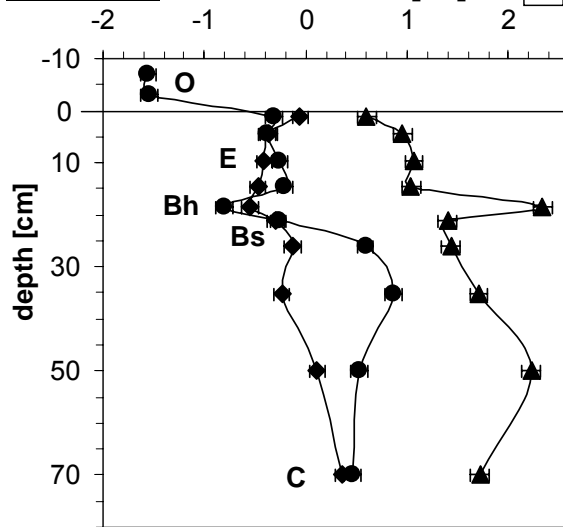


In Podzol A, the Fe_{HCl} fraction shows a very sharp enrichment peak in the Bs horizon, whereas the $Fe_{NH_2OH-HCl}$ fraction dominates in the lower horizons indicating the presence of crystalline iron oxides. The $Fe_{residue}$ fraction of Podzol A, containing iron in silicate minerals, shows only a depletion in the E horizon but no enrichment in the lower horizons. In Podzol B, the pedogenic iron translocation is visible in all three fractions which are about similar in size. However, the $Fe_{residue}$ fraction is the dominant iron pool in the depleted E horizon, whereas the Fe_{HCl} fraction makes up the smallest iron pool in the lower horizons. The sum of the three separated iron fractions is depicted with open symbols in Fig. 4.2. The close match between the total digestion value (Fe_{total}) and the calculated sum indicates an excellent iron mass balance during the sequential extraction procedure.

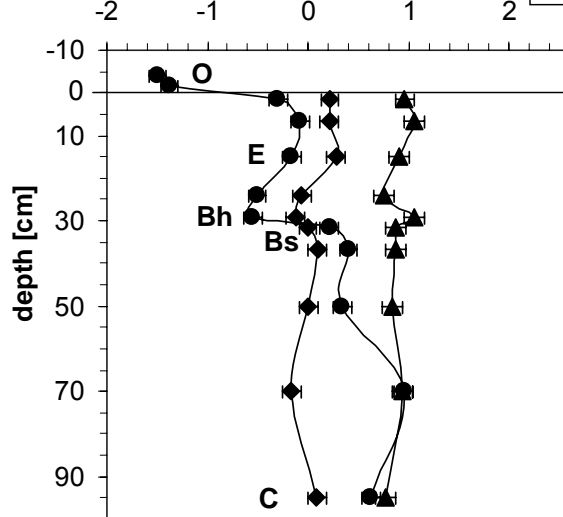
The iron concentration depth profiles of the three iron mineral pools separated by sequential extraction of the Cambisol are shown in Fig. 4.4 C. The distributions of the three fractions are uniform over soil depth, corresponding to the total iron concentration profile without iron translocation. Crystalline iron oxides ($Fe_{NH_2OH-HCl}$) are the dominant iron mineral pool over the whole profile depth which indicates an intense pedogenic formation of secondary iron(oxyhydr)oxide minerals. The highest crystalline iron oxide content ($Fe_{NH_2OH-HCl}$) was found in the Bw horizon at 30 cm depth where a correspondingly small depletion of the silicate iron pool ($Fe_{residue}$) is present. The Fe_{HCl} fraction is the smallest iron pool indicating that poorly-crystalline iron(oxyhydr)oxide minerals transform readily into more crystalline iron oxide minerals during pedogenesis of the soil.

Figure 4.5 Depth profiles of $\delta^{57}Fe$ values in the three iron mineral pools Fe_{HCl} , $Fe_{NH_2OH-HCL}$ and $Fe_{residue}$ which were separated by sequential extraction in the three investigated soil profiles. Pedogenic processes result in a similar pattern in the two Podzol profiles (Fig. 4.5 A+B) with lighter $\delta^{57}Fe$ values in the oxide-bound iron pool (Fe_{HCl} and $Fe_{NH_2OH-HCl}$) and strong enrichments of heavy isotopes in the silicate-bound iron pool ($Fe_{residue}$). Please note the different scale of $\delta^{57}Fe$ in the Cambisol profile (Fig. 4.5 C) exhibiting a small enrichment of light iron isotopes in the poorly-crystalline iron oxyhydroxide pool (Fe_{HCl}). The calculated sum of the three fractions based on iron concentration and isotope mass balance is shown in Fig. 4.3 in comparison to isotope data of the total soil digests. Zero values on depth axes indicate top of mineral soil. Lines serve as eye guides. Letters indicate selected pedogenic horizons (see Fig. 4.1).

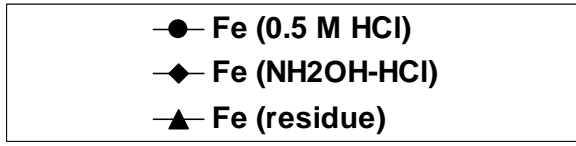
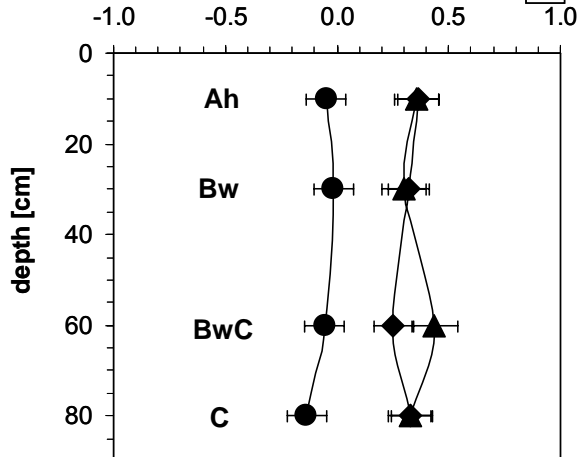
Podzol A $\delta^{57}\text{Fe}_{\text{IRMM-014}} [\text{‰}]$ **A**



Podzol B **B**



Cambisol **C**



4.3.5 Iron isotope ratios in sequential extraction samples

The results of the iron isotope measurements of the separated iron fractions of the two Podzol profiles are shown in Fig. 4.5 A+B. First of all, it is apparent that the range of iron isotope ratios is much wider compared to the total soil digestion data and extends over more than 3 ‰ in $\delta^{57}\text{Fe}$. Iron isotope fractionation is not only occurring between different soil horizons but also among different iron pools of the soil. The Fe_{HCl} fractions exhibit the strongest iron isotope variation in both Podzol profiles. The lowest $\delta^{57}\text{Fe}$ values were found in the Fe_{HCl} fraction of the organic surface layers (O horizons) with $\delta^{57}\text{Fe}$ values of around -1.5 ‰, indicating the enrichment of light iron isotopes in labile organically bound iron of the plant litter. The negative $\delta^{57}\text{Fe}$ peak in the Bh horizon that was found in the depth profile of the total soil digestions is also evident in the Fe_{HCl} fraction which makes up the largest iron pool in this horizon (Fig. 4.4 A+B). The $\delta^{57}\text{Fe}$ values of -0.8 ‰ in Podzol A and -0.6 ‰ in Podzol B clearly point toward a genetic relationship between organic matter enrichment and light iron isotope signatures in this horizon.

The crystalline iron oxide pool ($\text{Fe}_{\text{NH}_2\text{OH-HCl}}$) displays a smaller range of $\delta^{57}\text{Fe}$ within the two Podzol profiles. However, the lowest iron isotope ratios are again found in the Bh horizon. The $\text{Fe}_{\text{residue}}$ fraction in both Podzol profiles exhibit heavy $\delta^{57}\text{Fe}$ values (Fig. 4.4 A+B). These results probably indicate that light iron isotopes have been preferentially removed during weathering of iron-bearing silicate minerals which is consistent with the results of hornblende dissolution studies in the presence of different organic ligands (Brantley et al., 2001 and 2004). The highest iron isotope ratios were measured in the $\text{Fe}_{\text{residue}}$ fraction of the organic matter enriched Bh horizon with $\delta^{57}\text{Fe}$ values of +2.3 ‰ in Podzol A and +1.1 ‰ in Podzol B. These strong enrichments of heavy iron isotopes probably constitute the residue of intense silicate weathering processes which favor the transformation of light iron isotopes.

In contrast to the strong iron isotope fractionation in the two Podzol profiles, much smaller effects were found in the Cambisol profile (Fig. 4.5 C). The Fe_{HCl} fraction, which is the smallest iron pool in the soil profile, displays $\delta^{57}\text{Fe}$ values that are lighter by about 0.4 ‰ compared to the other two iron mineral pools. The $\text{Fe}_{\text{NH}_2\text{OH-HCl}}$ and $\text{Fe}_{\text{residue}}$ fractions are very similar and slightly heavier compared to the total soil digests. The enrichment of light iron isotopes in the Fe_{HCl} fraction, which is consistent with the data of the two Podzol profiles, could be explained by the

preferential weathering of light iron isotopes from primary silicate minerals and the subsequent pedogenic formation of poorly-crystalline iron oxyhydroxide minerals, or additionally by the presence of isotopically light organically-bound iron in the Fe_{HCl} fraction.

4.3.6 Comparison with available literature data

Iron isotope variations in soil samples have been observed in previous studies (Brantley et al., 2001; Brantley et al., 2004; Fantle and DePaolo, 2004; Emmanuel et al., 2005). However, the available data are still limited and the descriptions of the investigated samples were often not well defined in terms of their pedogenetic development. In addition, some of the applied methods to study iron isotopes in soil samples possess methodological problems, which hamper the interpretation of the results. Therefore, a brief discussion of the available data from previous publications will be presented in the following section.

Brantley et al. (2001 and 2004) extracted “exchangeable” iron with 1 M MgCl_2 from a soil sample of the B horizon of a hornblende-containing soil and reported light iron isotope ratios in this fraction compared to the oxide-bound fraction dissolved by a citrate-dithionite extraction. Exchangeable iron is difficult to measure in oxic soil environments due to the very low solubility of ferric iron. Re-precipitation of iron after the replacement by magnesium ions at cation exchange sites of the soil is likely, except under extremely acidic conditions. No discussion of this effect and its consequences on the isotope data or information about soil pH, redox conditions, and about the degree of hornblende weathering in terms of relative pool sizes of oxide-bound and silicate-bound iron was included. However, the presented data clearly indicate that different iron pool in soils may have distinct iron isotope signatures and, together with the results of the dissolution experiments presented in the same publication, point toward the importance of organically-complexed iron for iron isotope fractionation in soils.

Fantle and DePaolo (2004) studied iron isotope variations in four selected horizons of a soil profile in northern California (USA) and reported variations of about 0.7 ‰ in $\delta^{56}\text{Fe}$ between bulk soil samples from different depths. Their site belongs to a soil series which is classified as Plinthic Haplohumult according to the US Soil Taxonomy (USDA, 2006). The sampled horizons were influenced by different soil forming processes but their pedogenetic connection was poorly described. The

information provided indicates that the upper mineral horizon was subject to iron eluviation by podzolization or clay migration. The lowest mineral horizon was influenced by seasonal water saturation and contains redoximorphic features such as nodules. The horizon sampled in-between exhibits consolidated iron enrichments (plinthite), which could be genetically connected both to the upper eluvial horizon and the lower redoximorphic horizon. In addition to the bulk analyses, a 0.5 M HCl extraction method was used to separate iron phases from the soil that are more mobile, conceptually similar to the approach used in our study. However, the heat treatment of the samples to destroy organic matter (600°C for 12-20 h) prior to the extraction has possibly changed the iron mineralogy of the samples and therefore renders the interpretation of HCl-leaching data difficult. The observed variations of about 0.7 ‰ in $\delta^{56}\text{Fe}$ in the total soil digests with negative values in the upper two horizons and slightly positive values in the lower two horizons indicate unambiguously that iron isotope fractionations occur in natural soils.

Emmanuel et al. (2005) measured iron isotopes in bulk samples of two soil profiles and reported variations of 0.35 ‰ ($\delta^{57}\text{Fe}$) in a Czech forest soil and of 0.12 ‰ ($\delta^{57}\text{Fe}$) in an Israeli semi-arid soil. The Czech forest soil was classified as Haplorthod according to US Soil taxonomy (USDA, 2006), which corresponds to a Podzol in the WRB nomenclature (WRB, 2006a). The sampling was confined to three organic surface layers (O horizons), a transition horizon OA, and two lower mineral horizons denoted as BC. The characteristic pedogenic horizons which define a Podzol, such as eluvial E and illuvial Bh or Bs horizons, are not mentioned in the publication. The Israeli semi-arid soil was classified as shallow Terra rossa (Haploxerept) on a bedrock of limestone and dolomite. Three horizons (one A horizon and two C horizons) were sampled exhibiting iron isotope signature that are identical within the analytical error. Based on iron isotope data from the total digests and iron concentration data of a six-step sequential extraction procedure, Emmanuel et al. (2005) applied a fixed end member mixing model to calculate iron isotope values of individual iron pools in the soil. However, their model is based on the assumption that the different iron end member pools exhibit a constant iron isotope value over soil depth. This approach is highly questionable since the different iron mineral pools in the soil develop from each other. Transformations of iron phases from one pool into another (e.g., primary silicate mineral pool into pedogenic

iron oxide pool) potentially affect the iron isotope ratio of both pools. This effect is apparent in the results of our study, demonstrating that iron isotope data from individual iron fractions (e.g., Fe_{HCl}) display a strong variability over soil depth that is linked to pedogenic processes which have influenced the different soil horizons to a varying extent. Therefore, the modeling approach taken by Emmanuel et al. (2005) to construct a preliminary mixing model for iron isotopes in soils is based on questionable assumptions and will probably be of limited use towards a further understanding of iron isotope fractionation in soils.

Clearly, the available data from previous studies do indicate the presence of iron isotope variations in soils. The described partial shortcomings of previous studies illustrate the importance of careful method development, selection and description of field sites with well-defined pedogenesis, detailed sampling of complete soil profiles, and the investigation of individual iron pools in the soil. Hence, we tried to perform a comprehensive approach in our study, which avoids the above mentioned problems and aims at a process-oriented understanding of iron isotope fractionation in soils.

4.3.7 Fractionation mechanisms

The iron isotope data of the two Podzol profiles exhibit significant variations in $\delta^{57}\text{Fe}$ that are clearly linked to pedogenic processes. Reductive iron transformations are not likely to play a significant role in the investigated soil profiles due to the well-drained and oxic conditions year-round. The observation of significant iron isotope variations in a system that is not significantly influenced by reductive iron transformation processes is an important finding, because iron redox transformations are often believed to be the major source of iron isotope variability in nature. The results demonstrate unequivocally that iron isotopes are fractionated during podzolization, a process where pedogenic vertical iron translocation is driven by organic ligands at very acidic pH. Our data show that this process results in a preferential translocation of lighter iron isotopes within the soil. The observed fractionation could be explained by a kinetic isotope effect during the pedogenic iron translocation. In a recent laboratory study, iron isotope fractionation during ligand-controlled dissolution of goethite was found to result in kinetic iron isotope effects that changed systematically over the course of the dissolution reaction (chapter 6 of this thesis). Preferential leaching of light iron isotopes from hornblende by organic ligands

was also reported by Brantley et al. (2001 and 2004). Since ligand-controlled dissolution is one of the main processes involved in podzolization, we believe that this process is also involved in the observed iron isotope fractionation in natural Podzol profiles. High concentrations of various ligands such as low molecular weight organic acids (Lundström et al., 2000) and even low concentrations of siderophores (Essen et al., 2006) were found in natural Podzol profiles. In general, the precipitation step during the podzolization process could also cause iron isotope effects. However, since precipitation of iron in the Bh and Bs horizons of Podzols probably proceeds nearly quantitatively, these potential fractionations are less likely to be preserved in the iron isotope signature of soils compared to the effects of partial dissolution processes during iron mobilization. An additional fractionation mechanism of iron isotopes in soils could be the preferential uptake of light isotopes by plants which could explain the light $\delta^{57}\text{Fe}$ values in the organic surface layers of the Podzol profiles. This proposed fractionation mechanism is consistent with the findings of Walczyk and von Blanckenburg (2002) who reported that plant biomass is enriched in light iron isotopes.

4.4 CONCLUSIONS

The iron isotope data of two Podzol and one Cambisol soil profiles exhibit significant variations that are clearly linked to pedogenic processes. A broad range in $\delta^{57}\text{Fe}$ values of more than one per mil between bulk soil samples and of more than three per mil between individual iron mineral pools was found. This study demonstrates that geochemical processes in oxic soils result in systematic variations of $\delta^{57}\text{Fe}$ values within soil profiles. The high-resolution sampling of soil profiles combined with sequential extractions revealed a systematic pattern of iron isotope signatures between different pedogenic horizons and among different iron mineral pools in Podzols. The observed light iron isotope ratios in the Bh horizons, which are enriched in organic matter, point toward the importance of organic ligands in the iron isotope fractionation process. Ligand-controlled dissolution of iron oxide minerals is likely an important mechanism to induce the observed isotope fractionation effects in Podzols. In addition, preferential uptake of light iron isotopes by plants could also have an effect on the iron isotope signature of soils. The Cambisol data indicate that oxic weathering reactions in the absence of high concentrations of organic ligands

and strongly acidic soil pH result only in small iron isotope fractionation effects. In contrast, the strongly acidic conditions (soil pH < 4) and the high concentrations of organic ligands in Podzols exert a much stronger impact on iron isotope ratios within the soil. Weathering residues tend to be enriched in heavy iron isotopes as highlighted by the positive $\delta^{57}\text{Fe}$ values of the silicate-bound iron pool in weathered soil horizons. The results of our study emphasize that reductive iron transformations are not a prerequisite for significant iron isotope fractionation in nature. These findings provide new important insights into the behavior of iron isotopes in nature and the corresponding fractionation mechanisms. Therefore, we hope that this work contributes to the further development of stable iron isotopes as a tracer for the biogeochemical iron cycle in soils and other natural systems.

ACKNOWLEDGEMENTS

We thank Tim Mansfeldt (University of Cologne, Germany) for his help during the field sampling, Kurt Barmettler for support in the soil chemistry laboratory, and the staff of the ETH MC-ICPMS laboratory for excellent maintenance and support. This research was funded by ETH Research Grant No. 01927.

REFERENCES

- Anbar AD (2004) Iron stable isotopes: beyond biosignatures. *Earth Planet. Sci. Lett.* **217**, 223–236.
- Anderson HA, Berrow ML, Farmer VC, Hepburn A, Russell JD, Walker AD (1982) A reassessment of podzol formation processes. *J. Soil. Sci.* **33**, 125-136.
- Beard BL, Johnson CM (1999) High precision iron isotope measurements of terrestrial and lunar materials. *Geochim. Cosmochim. Acta* **63**: 1653-1660.
- Beard BL, Johnson CM (2004) Fe isotope variations in the modern and ancient Earth and other planetary bodies. *Rev. Mineral. Geochem.* **55**, 319-357.
- Borggaard OK (1988) Phase identification by selective dissolution techniques. p.83-97. In Stucki JW, Goodman BA, Schwertmann U (eds.) *Iron in soils and clay minerals*. D. Reidel, Dordrecht, The Netherlands.
- Brantley SL, Liermann L, Bullen TD (2001) Fractionation of Fe isotopes by soil microbes and organic acids. *Geology* **29**, 535-538.
- Brantley SL, Liermann LJ, Guynn RL, Anbar A, Icopini GA, Barling J (2004) Fe isotopic fractionation during mineral dissolution with and without bacteria. *Geochim. Cosmochim Acta* **68**, 3189-3204.

- Buurman P, Jongmans AG (2005) Podzolisation and soil organic matter dynamics. *Geoderma* **125**, 71-83.
- Chao TT, Zhou L (1983) Extraction techniques for selective dissolution of amorphous iron oxides from soils and sediments. *Soil Sci. Soc. Am. J.* **47**: 225-232.
- Cornell RM, Schwertmann U (2003) The iron oxides – structure, properties, reactions, occurrence and uses. Second edition. VCH, Weinheim, Germany.
- Dauphas N, Rouxel O (2006) Mass spectrometry and natural variations of iron isotopes. *Mass Spec. Rev.* **25**, 515-550.
- Donisa C, Steinnes E, Sjobakk TE (2005) Nitric-acid soluble fractions of 21 elements in Norwegian podzols: Factors affecting regional differences in vertical distribution. *Appl. Geochem.* **20**, 1258-1267.
- Emmanuel S, Erel Y, Matthews A, Teutsch N (2004) A preliminary mixing model for Fe isotopes in soils. *Chem. Geol.* **222**, 23-34.
- Essen SA, Bylund D, Holmstrom SJM, Moberg M, Lundstrom US (2006) Quantification of hydroxamate siderophores in soil solutions of podzolic soil profiles in Sweden. *Biometals* **19**, 269-282
- Fantle MS, DePaolo DJ (2004) Iron isotope fractionation during continental weathering. *Earth Planet. Sci. Lett.* **228**, 547–562.
- Halliday AN, Lee D-C, Christensen JN, Rehkämper M, Yi W, Luo X, Hall CM, Ballentine CJ, Pettke T, Stirling C (1998) Applications of multiple collector-ICPMS to cosmochemistry, geochemistry, and paleoceanography. *Geochim. Cosmochim. Acta* **62**, 919-940.
- Heron G, Crouzet C, Bourg ACM, Christensen TH (1994) Speciation of Fe(II) and Fe(III) in contaminated aquifer sediments using chemical extraction techniques. *Environ. Sci. Tech.* **28**: 1698-1705.
- Hoefs, J. (2004) Stable isotope geochemistry. 5th edition. Springer, Berlin, Germany.
- Jahn R, Kunold W, Hermann L, Papenfuss KH, Ehrmann O, Stahr K (1997) Querschnitt durch den Hegau und seine Randgebiete. Exkursion D 3. *Mitteilungen der Deutschen Bodenkundlichen Gesellschaft* **82**, 213-250.
- Jansen B, Nierop KGJ, Verstraten JM (2005) Mechanisms controlling the mobility of dissolved organic matter, aluminium and iron in podzol B horizons. *Eur. J. Soil. Sci.* **56**, 537-550.
- Johnson CM, Beard BL, Albarède F (2004a) (eds.) Geochemistry of non-traditional stable isotopes. Reviews in Mineralogy and Geochemistry 55. Mineralogical Society of America and Geochemical Society, Washington, DC, US.
- Johnson CM, Beard BL, Roden EE, Newman DK, Nealson KH (2004b) Isotopic constraints on biogeochemical cycling of Fe. *Rev. Mineral. Geochem.* **55**, 359-408.
- La Force MJ, Fendorf S (2000) Solid-phase iron characterization during common selective sequential extractions. *Soil Sci. Soc. Am. J.* **64**, 1608-1615.
- Lundström US, van Breeman N, Bain D (2000) The podzolization process - a review. *Geoderma* **94**: 91-107.

- Markl G, von Blanckenburg F, Wagner T (2006) Iron isotope fractionation during hydrothermal ore deposition and alteration. *Geochim. Cosmochim. Acta* **70**, 3011-3030.
- Ribet I, Ptacek CJ, Blowes DW, Jambor JL (1995) The potential for metal release by reductive dissolution of weathered mine tailings. *J. Contam. Hydrol.* **17**, 239-273.
- Schmidt MWI, Knicker H, Kögel-Knabner I. (2000) Organic matter accumulating in Aeh and Bh horizons of a Podzol - chemical characterization in primary organo-mineral associations. *Org. Geochem.* **31**, 727-734.
- Schoenberg R, von Blanckenburg F (2005) An assessment of the accuracy of stable Fe isotope ratio measurements on samples with organic and inorganic matrices by high-resolution multicollector ICP-MS. *Int. J. Mass. Spec.* **242**, 257-272.
- Skulan JL, Beard BL, Johnson CM (2002) Kinetic and equilibrium Fe isotope fractionation between aqueous Fe(III) and hematite. *Geochim. Cosmochim. Acta* **66**, 2995-3015.
- Sommer M (1992) Musterbildung und Stofftransporte in Bodengesellschaften Baden-Württembergs. Hohenheimer Bodenkundliche Hefte 4, Stuttgart, Germany.
- Stucki JW, Goodman, BA, Schwertmann U (eds.) 1988. Iron in soils and clay minerals. D. Reidel, Dordrecht, The Netherlands.
- Teutsch N, von Gunten U, Porcelli D, Cirpka OA, Halliday AN (2005) Adsorption as a cause for iron isotope fractionation in reduced groundwater. *Geochim. Cosmochim. Acta* **69**, 4175-4185.
- Tyler G (2004) Vertical distribution of major, minor, and rare elements in a Haplic Podzol. *Geoderma* **119**, 277-290.
- USDA (2006) Keys to soil taxonomy. Tenth edition. United States Department of Agriculture, Washington, DC, US.
- van Breemen N, Buurman P. (2004) Soil Formation. Second edition. Kluwer Academic, Dordrecht, The Netherlands.
- Walczyk T, von Blanckenburg F (2002) Natural iron isotope variations in human blood. *Science* **295**, 2065-2066.
- Wiederhold JG, von Blanckenburg F (2002) Iron isotope variations in a complete natural soil catena with lateral iron mobilization and reprecipitation. *Geochim. Cosmochim. Acta* **66**, A834.
- Williams HM, McCammon CA, Peslier AH, Halliday AN, Teutsch N, Levasseur S, Burg J-P (2004) Iron isotope fractionation and the oxygen fugacity of the mantle. *Science* **304**, 1656-1659.
- WRB (2006a) World Reference Base for Soil Resources 2006 - a framework for international classification, correlation and communication. World Soil resources reports 103. Food and Agriculture Organization of the United Nations, Rome, Italy.
- WRB (2006b) Guidelines for soil description. Fourth edition. Food and Agriculture Organization of the United Nations, Rome, Italy.

5. IRON ISOTOPE FRACTIONATION DURING PEDOGENESIS IN REDOXIMORPHIC SOILS

This chapter is submitted for publication:

Wiederhold JG, Teutsch N, Kraemer SM, Halliday AN, Kretzschmar R

Iron isotope fractionation during pedogenesis in redoximorphic soils

Abstract

Stable iron isotopes provide a new potential tool for tracing the biogeochemical cycle of iron in soils. Iron isotope ratios in two redoximorphic soils were measured by multicollector ICP-MS to study the relationships between pedogenic iron transformation and redistribution processes, and mass-dependent fractionations of iron isotopes. Redoximorphic iron depletion and enrichment zones were sampled separately to the bulk soil samples. A three-step sequential extraction procedure was used to separate different iron pools, which were examined in parallel to total soil digests. Significant enrichments of heavy iron isotopes in total soil digests of iron-depleted zones compared to bulk soil samples of about 0.3 ‰ in $\delta^{57}\text{Fe}$ were found and explained by the preferential removal of light isotopes during microbially-mediated iron oxide dissolution under anoxic conditions. Accordingly, pedogenic iron enrichment zones were found to be slightly enriched in light iron isotopes. Distinct iron isotope variations of more than 1 ‰ in $\delta^{57}\text{Fe}$ were found between different iron pools within soil samples. Enrichments of light isotopes in pedogenic oxides contrasted to heavy isotope signatures of residual silicate-bound iron. Our data demonstrate that pedogenic iron transformations in redoximorphic soils are linked to iron isotope fractionation, revealing a higher mobility of lighter relative to heavier iron isotopes during pedogenesis. However, no simple quantitative relationship between iron depletion and isotope fractionation can be inferred. Our findings provide new insights into the behavior of iron isotopes in soil environments and contribute to the development of iron isotopes as a tracer for the biogeochemical iron cycle in nature.

5.1 INTRODUCTION

Iron is not only an essential nutrient element for almost all organisms, but also exerts a major influence on the mobility of nutrient and pollutant elements in soils (Stucki et al., 1988). Redox transformations between ferrous (Fe^{II}) and ferric (Fe^{III}) iron play an important role in the biogeochemical cycle of iron. Moreover, iron transformations and translocations are key processes in soil formation and soil classification (van Breemen and Buurman, 2004). Iron in soils occurs in a variety of different phases such as primary silicate minerals, clay minerals, iron (oxyhydr)oxide minerals of different crystallinity, as well as organically-bound iron (Stucki et al., 1988). Under atmospheric conditions, ferric iron is the thermodynamically stable oxidation state. The weathering of primary silicate minerals in soils releases ferrous iron that is rapidly oxidized followed by the precipitation of poorly-crystalline iron (oxyhydr)oxide minerals such as ferrihydrite. A transformation to better crystallized iron oxide minerals, such as goethite and hematite, takes place during further soil development. Under atmospheric conditions, these phases are characterized by a very low solubility (Cornell & Schwertmann, 2003). However, under anaerobic conditions in water-saturated soils, ferric iron is used as an alternate electron acceptor by dissimilatory-iron reducing bacteria (Lovley et al., 2004). This process results in the formation of soluble ferrous iron in soil solution which is transported within the soil by advective and diffusive processes. Reprecipitation of iron(oxyhydr)oxide minerals occurs as soon as this mobile $\text{Fe}(\text{II})$ pool comes into contact with oxygen. This happens, depending on the temporal and spatial variability of the soil water regime, in characteristic horizons of the soil profile and results in the formation of typical iron depletion and enrichment zones. The corresponding soils are generally referred to as redoximorphic or hydromorphic soils (Schlichting and Schwertmann, 1973). They are formed by pedogenic processes that are summarized by the term redoximorphosis, and they are characterized by typical redoximorphic features (Vepraskas, 1996). In soils that are permanently water-saturated, mainly at locations with a high groundwater table, iron enrichments occur in a distinct horizon corresponding to the capillary fringe, whereas iron depletion zones are found predominantly in the soil horizons below the ground water table. In contrast, soils that are only seasonally water-saturated, typically due to stagnant water above a dense layer which inhibits vertical drainage, exhibit a different pattern of redoximorphic

features. Here the depletion zones are mainly found in the vicinity of larger pores and along preferential flow paths where water infiltrates rapidly and reducing conditions are generated first. The enrichment zones are then mainly found in the interior of soil aggregates and in the soil matrix where remaining oxygen results in the precipitation of iron (oxyhydr)oxide minerals, often in the form of nodules or concretions (Vepraskas, 1996). These pedogenic redistribution processes of iron within hydromorphic soils are not only interesting in terms of soil morphology and classification but also influence the fate of other elements of environmental interest such as arsenic (Cummings et al., 1999) and phosphorus (Szilas et al., 1998). Despite extensive research over the last few decades on biogeochemical iron cycling in soils, there are still many unsolved issues. These include, for instance, the importance of different iron (oxyhydr)oxide minerals as electron acceptors for bacterial respiration in natural environments or mineral dissolution kinetics and mechanisms which influence nutrient and pollutant element cycling.

The analysis of stable isotope ratios represents an important method to elucidate biogeochemical reactions and element cycles in the environment (Hoefs, 2004). However, until recently this approach was confined to lighter isotopes (e.g., C, O, H, N, S) which can be measured in the gas phase. The development of new analytical methods, mainly multiple collector inductively coupled plasma mass spectrometry (MC-ICPMS), has expanded this range to heavier elements such as iron and opened up a new field of isotope geochemistry (Halliday et al., 1998; Johnson et al., 2004a). Iron isotopes may provide a new tool to trace the biogeochemical iron cycle of soils. Iron has four stable isotopes (percent natural abundance): ^{54}Fe (5.84 %), ^{56}Fe (91.76 %), ^{57}Fe (2.12 %), and ^{58}Fe (0.28 %). The δ -notation is commonly used to describe iron isotope fractionation relative to the international iron isotope standard IRMM-014 and is defined as

$$\delta^{56}\text{Fe} [\text{‰}] = \left(\frac{(^{56}\text{Fe}/^{54}\text{Fe})_{\text{sample}}}{(^{56}\text{Fe}/^{54}\text{Fe})_{\text{IRMM-014}}} - 1 \right) \cdot 10^3 \quad \text{or} \quad \delta^{57}\text{Fe} [\text{‰}] = \left(\frac{(^{57}\text{Fe}/^{54}\text{Fe})_{\text{sample}}}{(^{57}\text{Fe}/^{54}\text{Fe})_{\text{IRMM-014}}} - 1 \right) \cdot 10^3 .$$

The two values can be easily converted into each other by the approximation $\delta^{57}\text{Fe} = 1.5 \times \delta^{56}\text{Fe}$ because the observed fractionation effects are mass-dependent (Dauphas and Rouxel, 2006). Variations of $\delta^{56}\text{Fe}$ in bulk igneous rocks were found to be very small (Beard and Johnson, 1999; Beard and Johnson, 2004). In contrast, significant deviations from this average terrestrial background ratio of about four

per mil occur in various low temperature environments such as sediments or soils (Brantley et al., 2001; Wiederhold and von Blanckenburg, 2002; Fantle and DePaolo, 2004; Matthews et al., 2004; Emmanuel et al., 2005). It was shown that iron isotopes can be fractionated by kinetic and equilibrium isotope effects during both biotic and abiotic reactions (Anbar, 2004; Johnson et al., 2004b; Dauphas and Rouxel, 2006). Laboratory studies have shown that dissolution of iron (oxyhydr)oxide minerals by dissimilatory iron-reducing bacteria results in an enrichment of light iron isotopes in solution (Beard et al., 1999; Crosby et al., 2005). The abiotic dissolution of goethite in the presence of oxalate both by a photochemical reductive and a ligand-controlled mechanism was shown to enrich light iron isotopes in the first dissolved fractions (chapter 6 of this thesis). In contrast, the abiotic oxidative precipitation of ferrihydrite has been shown to favor heavy iron isotopes in the reaction product (Bullen et al., 2001). Furthermore, fractionation of iron isotopes during adsorption processes in reduced groundwater systems was investigated by Teutsch et al. (2005). They found a preferential adsorption of heavy iron isotopes during the reaction of dissolved ferrous iron with ferric iron (oxyhydr)oxide minerals in a natural aquifer. Iron isotope fractionations along redox gradients in marine sediments were recently reported by Severmann et al. (2006) and Staubwasser et al. (2006) with enrichments of light iron isotopes in extracts of the reactive iron mineral pools. However, the mechanisms that govern the distribution of iron isotopes during redox processes in natural environments are still poorly understood. So far, there are no data published on iron isotope fractionation in redoximorphic soils. Thus, this study represents the first attempt to relate the fractionation of iron isotopes to pedogenic processes in redoximorphic soils.

The objective of our study was to investigate the fractionation of iron isotopes in natural soil environments with distinct iron redox dynamics. Therefore, we performed a detailed study of the spatial distribution of iron isotope ratios in relation to hydromorphic properties in two soils exhibiting contrasting soil pH and seasonal water regimes. The first soil was seasonally saturated by stagnant water and strongly acidic, while the second soil was permanently water-saturated in the subsoil due to groundwater and had a neutral soil pH. Separation of iron depletion and enrichment zones during sampling enabled a detailed investigation of small-scale variations during redox transformations. In addition, the separation of different iron pools by sequential extractions and their subsequent iron isotope analysis in addition to total

soil digests provided further insights into the variability and fractionation of iron isotopes in redoximorphic soils.

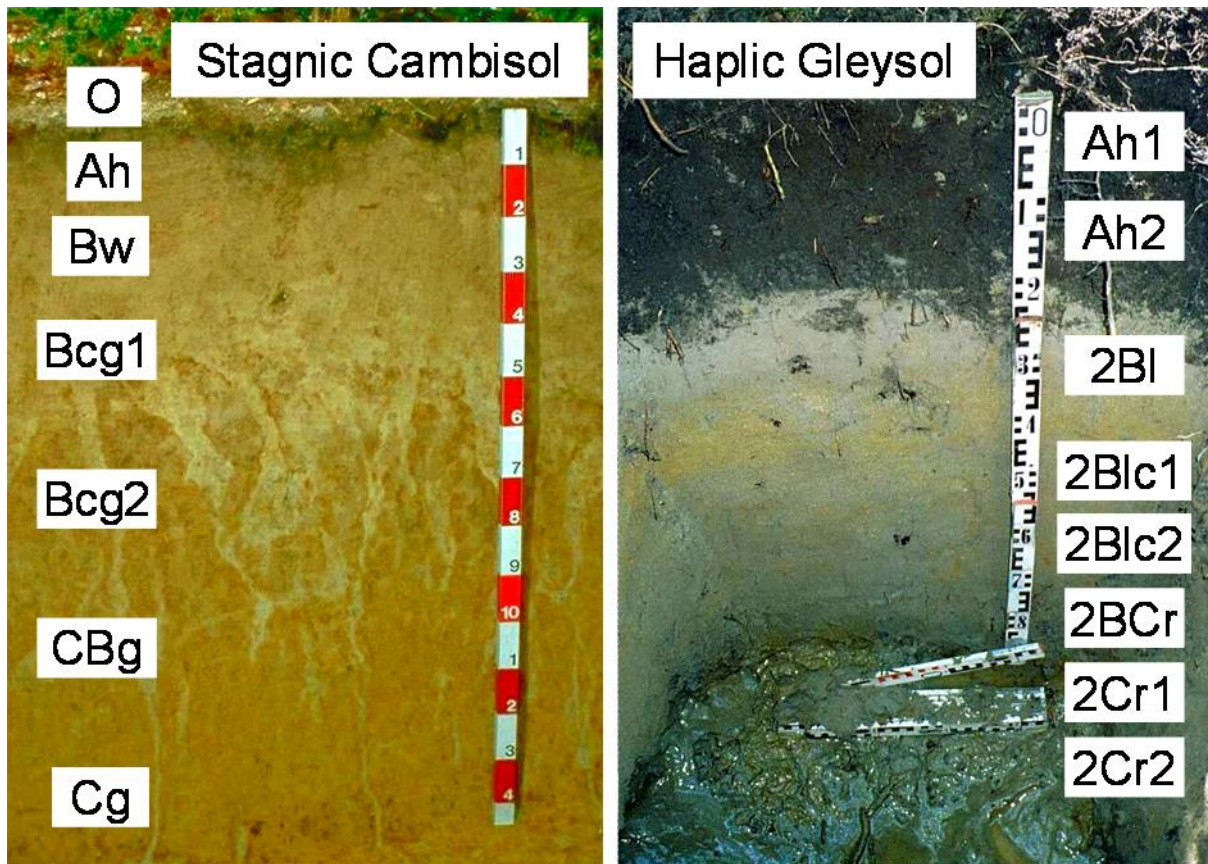


Figure 5.1 Pictures of the Stagnic Cambisol (near Rafz, Switzerland) and the Haplic Gleysol (near Tettngang, Germany). Both profiles exhibit clear redoximorphic features. Horizon designations correspond to the World Reference Base for Soil Resources (WRB, 2006b) (O = organic surface layer, Ah = organic-rich mineral horizon, Bw = weathered horizon, C = soil substrate, c = concretions or nodules, g = stagnic conditions, l = capillary fringe mottling (gleying), r = strong reduction; prefix numbers indicate lithogenic discontinuities, suffix numbers indicate vertical subdivision of horizon).

5.2 MATERIALS AND METHODS

5.2.1 Sampling sites

Soil samples were taken at two sites representing a strongly acidic, seasonally water-saturated soil and a neutral soil which is permanently water-saturated in the subsoil horizons. The two soils are classified as Typic Epiaquept and Typic Humaquept according to US Soil Taxonomy (USDA, 2006), respectively. According to the World Reference Base for Soil Resources (WRB, 2006a), the profiles are

classified as Stagnic Cambisol and Haplic Gleysol, respectively. The WRB nomenclature for soil types and horizon designations will be used in the following. The two sampled profiles are depicted in Fig. 5.1 along with designations of the pedogenic horizons. The first soil (Stagnic Cambisol) was sampled in Northern Switzerland near Rafz, Canton Zurich (47°37' N, 8°32' E). The soil has formed on a glacial moraine deposit that was possibly admixed with eolian silt (loess) in the upper part of the profile. The vegetation is dominated by spruce trees (*Picea abies*). This site was not covered by ice during the last glaciation period because it is located north of the alpine end moraines, resulting in a relatively long period of continuous soil development of about 100,000 years (Gimmi et al., 1997). This has led to considerable leaching and acidification of the soil. Soil pH(CaCl₂) ranges from 3.4 in the upper mineral soil horizon (Ah) to 4.1 at a depth of 140 cm, which is classified as extremely acidic (USDA, 1993). A distinct organic surface layer (O horizon) is present on top of the mineral soil because of the acidity and the poorly-degradable plant litter which inhibit the decomposition of organic matter. The glacial moraine deposit serving as soil substrate has a high bulk density (1.75 g/cm³), which inhibits vertical water drainage. In consequence, the soil is water-saturated for prolonged periods of the year resulting in seasonally anoxic conditions. Characteristic redoximorphic features with distinct iron depletion and enrichment zones are apparent below a depth of about 40 cm (Fig. 5.1, see also closeup picture in chapter 2, Fig. 2.1).

The second soil profile (Haplic Gleysol) was sampled in Southern Germany near Tettwang, Upper Swabia (47°39' N, 9°33' E). It has formed on carbonate-rich sandy sediments that were deposited by fluvial processes during the Pleistocene and later covered by a layer of loamy sediments that makes up the upper part of the soil profile (Kösel und Vogl, 1997). The vegetation at this site is dominated by deciduous trees (*Fraxinus excelsior*, *Alnus glutinosa*, *Quercus robur*). No organic surface layer horizon exists because the high biological activity and easily-degradable plant litter prevent accumulation of organic matter. Soil pH(CaCl₂) ranges from 5.9 in the upper mineral soil horizon (Ah) to 7.7 at a depth of 120 cm which is classified as moderately acidic to slightly alkaline (USDA, 1993). Carbonate is present below a depth of about 40 cm buffering the soil pH to values above 7.5. The lower soil horizons are permanently saturated by groundwater and the capillary fringe is situated at a depth of about 50 cm with little seasonal variations. In consequence, the lower soil horizons are subjected to reducing conditions, which has led to significant iron mobilization

and subsequent development of matrix depletion features. Iron enrichment zones are prominent at depths around 50 cm to 70 cm, where the reaction of mobilized ferrous iron with atmospheric oxygen results in oxidative precipitation of ferric iron (oxyhydr)oxide minerals. Table 5.1 lists selected soil properties including soil colors of the two investigated soil profiles.

Table 5.1 Selected soil properties of the two sampled profiles. Soil colors are described with hue, value, and chroma according to the Munsell Soil Color charts (WRB, 2006b)

Stagnic Cambisol (near Rafz / Switzerland) (Data from Gimmi et al., 1997)

horizon	depth [cm]	pH (CaCl ₂)	color (Munsell)	bulk density [g/cm ³]	sand	silt	clay
					[g/kg]		
Ah	0-3	3.4	10YR 3/2	1.25	300	550	150
Bw	3-30	4.0	10YR 5/5	1.29	260	550	200
Bcg1	30-55	3.9	2.5Y 5/4	1.36	280	540	180
Bcg2	55-100	3.9	10YR 4/6 *	1.65	290	500	210
CBg	100+	4.1	10YR 5/8 *	1.75	180	540	270

* colors listed in table refer to bulk soil samples; colors of redoximorphic features: depletion zones: 2.5YR 6/2, enrichment zones: 7.5YR 5/8

Haplic Gleysol (near Tett nang / Germany) (Data from Kösel and Vogl, 1997)

horizon	depth [cm]	pH (CaCl ₂)	color (Munsell)	bulk density [g/cm ³]	sand	silt	clay
					[g/kg]		
Ah	0-14	6.1	10YR 3/1	0.80	490	320	190
Ah2	14-26	6.6	10YR 3/1	0.98	500	320	180
2BI1	26-37	7.5	5Y 6/2	1.53	320	470	210
2BI2	37-46	7.6	7.5YR 6/1	1.50	400	500	100
2BIc	46-109	7.6	10Y 6/1 **	n.d.	810	160	30
2Cr	109+	7.6	10Y 5/1	n.d.	830	150	20

** color listed in table refers to bulk soil sample; color of enrichment zones: 10YR 5/8
n.d. = not determined

5.2.2 Soil sampling and sample preparation

The soil profiles were sampled with a high vertical spatial resolution tracing the different pedogenic horizons (8 depths per profiles). Additionally, two horizons with distinct redoximorphic features were chosen in each profile for detailed sampling. In the Stagnic Cambisol profile, the Bcg2 horizon (~80 cm) and the CBg horizon (~120 cm) exhibiting distinct iron depletion and enrichment zones, were selected. At these depths, samples of the grey depleted zones and the brown enriched zones were taken separately to the bulk soil samples. For the Haplic Gleysol profile, the brown redoximorphic enrichment zones of the 2B1c1 horizon (~50 cm) and the 2B1c2 horizon (~70 cm) were separated from the bulk soil matrix samples. No specific iron depletion zones could be sampled because the whole soil matrix is depleted in these horizons. The soil samples were dried at 40°C in the laboratory and sieved through a 2 mm mesh. An aliquot of the samples was ground to a fine powder with a rotary disk mill. From this powder, wax pellets were produced to measure total element concentrations by energy-dispersive X-ray fluorescence analysis (Spectro-X-Lab 2000, Spectro, Germany). A small amount of the powdered samples (100 - 500 mg depending on iron content) was dissolved totally in a microwave digestion with HF-HNO₃-HCl (mixture 1:2:2). These samples represent the Fe_{total} pool of the soil samples. Samples rich in organic matter were pre-treated with 30% H₂O₂ prior to the digestion. The clear solutions after the digestion were evaporated in Teflon beakers on a hotplate to remove excess HF. The residue was redissolved in concentrated HNO₃ to ensure complete oxidation of ferrous to ferric iron. This solution was again evaporated and the residue taken up in 6 M HCl. All reagents used during sample preparation were at least *per analysi* grade and prepared with ultrapure water (>18 MΩ). Hydrochloric and nitric acids were further purified by sub-boiling distillation. Hydrofluoric acid used during digestions was suprapure quality (MERCK, Germany).

In parallel, another aliquot of the dried and sieved soil samples was subjected to a three-step sequential extraction procedure in order to separate different Fe mineral pools (poorly-crystalline iron oxyhydroxides, crystalline iron oxides, silicate-bound iron) from the soil samples. In the first extraction step, 2 g of the soil material were weighed into 50 mL centrifuge tubes, 40 mL of 0.5 M HCl were added to the tubes and the samples were placed on an overhead shaker for 24 h at room temperature. Afterwards the tubes were centrifuged (3400g, 15 min) and the supernatants

decanted and filtered through 0.45 µm Nylon membrane filters (Opti-Flow, WICOM, Germany). This solution is the Fe_{HCl} fraction of the soil. In the second extraction step, 40 mL of a 1 M $\text{NH}_2\text{OH-HCl}$ solution in 1 M HCl were added to the residue in the centrifuge tubes and shaken vigorously. The tubes were then placed in a hot water bath at 90°C with integrated horizontal shaker for 4 hours. During this time the samples were additionally manually shaken overhead from time to time. Afterwards the tubes were centrifuged (3400g, 15 min) and the supernatants decanted and filtered through 0.45 µm Nylon filters. This solution is the $\text{Fe}_{\text{NH}_2\text{OH-HCl}}$ fraction of the soil. The residue was washed twice with water, dried overnight at 105°C and then ground to a fine powder with a rotary disk mill. An aliquot of this powder, again depending on the Fe content between 100 and 500 mg, was then totally dissolved in a microwave digestion with $\text{HF-HNO}_3\text{-HCl}$ (mixture 1:2:2) and further treated similar to the total iron samples. The extraction solutions (Fe_{HCl} and $\text{Fe}_{\text{NH}_2\text{OH-HCl}}$) were also evaporated in Teflon beakers on a hotplate and oxidized with HNO_3 and H_2O_2 to destroy organic matter and hydroxylamine and to convert ferrous to ferric iron. The residue was then also taken up in 6 M HCl.

Iron concentrations of all samples were measured by atomic absorption spectrometry (AAS, SpectrAA 220, Varian, Australia). The organic surface layer samples of the Stagnic Cambisol profile were not subjected to the entire sequential extraction procedure since the method is only applicable for mineral soil samples. For these samples, only the total digestion and the first extraction step with 0.5 M HCl were performed. Further sample preparation took place in a clean chemistry laboratory. Teflon microcolumns filled with about 1 mL anion exchange resin (Bio-Rad AG1 X4, 200-400 mesh) were used to separate iron in the samples from matrix elements. In 6 M HCl ferric iron is present as FeCl_4^- anion. The iron complex is retained on the resin while the sample matrix is washed out by repeated additions of 6 M HCl. Elution of iron from the columns was achieved with 0.05 M HCl. The eluates were again evaporated and finally taken up in 0.05 M HCl as solution matrix for the iron isotope measurement.

5.2.3 Iron isotope measurement

Iron isotope ratios were determined by multiple collector inductively coupled plasma mass spectrometry (MC-ICPMS, Nu Plasma, Nu instruments, UK). A comprehensive description of iron isotope analytical methods was recently published by Schoenberg and von Blanckenburg (2005). The analytical procedures for iron isotope measurement in our laboratory have been previously described in detail (Williams et al., 2004; Teutsch et al., 2005). Briefly, a standard-bracketing approach was used to correct for machine drift and instrumental mass bias. A membrane desolvation system (MCN-6000, Cetac, US) was used to minimize argide interferences (ArN^+ , ArO^+ , ArOH^+) to insignificant levels (background to signal ratio typically < 0.001). The $^{57}\text{Fe}/^{54}\text{Fe}$ and $^{56}\text{Fe}/^{54}\text{Fe}$ ratios were measured simultaneously and all data plot on the theoretical mass fractionation line demonstrating the absence of isobaric interferences. A Cr correction was performed by monitoring mass 52 or 53 to calculate the potential influence of ^{54}Cr on ^{54}Fe . However, our purified solutions did not contain significant amounts of Cr and the Cr corrected and uncorrected $\delta^{57}\text{Fe}$ values differed by less than ± 0.02 ‰ for all samples. All masses were collected in Faraday cups equipped with $10^{11} \Omega$ resistors except mass 56 which was collected in a Faraday cup equipped with a $10^9 \Omega$ resistor. This allowed to run solutions with relatively high Fe concentrations (8 ppm) but affected the precision of the $^{56}\text{Fe}/^{54}\text{Fe}$ measurement. Therefore, due to the smaller analytical error for the $^{57}\text{Fe}/^{54}\text{Fe}$ ratio, the results are expressed as $\delta^{57}\text{Fe}$. Samples were only measured after several stable isotope measurements of an internal house standard against IRMM-014. This standard was again measured after every six samples and at the end of the analytical run. The long term reproducibility of $\delta^{57}\text{Fe}$ of our internal house standard is better than ± 0.15 ‰ (2SD). Samples were measured several times and the error bars for $\delta^{57}\text{Fe}$ represent either the reproducibility (2SD) of replicate sample measurements or, in case of fewer measurements ($n < 3$), the reproducibility (2SD) of our internal house standard during the same analytical session. A mass balance approach was used to verify the iron concentration and iron isotope results of the different iron fractions. The isotope mass balance was calculated according to the following formula, where $[\text{Fe}]_n$ is the iron concentration in pool n,

$$\delta^{57}\text{Fe}_{total} \times [\text{Fe}]_{total} = \delta^{57}\text{Fe}_{\text{HCl}} \times [\text{Fe}]_{\text{HCl}} + \delta^{57}\text{Fe}_{\text{NH}_2\text{OH}-\text{HCl}} \times [\text{Fe}]_{\text{NH}_2\text{OH}-\text{HCl}} + \delta^{57}\text{Fe}_{residue} \times [\text{Fe}]_{residue} .$$

The error bars of the calculated total Fe value were adapted with the following formula

$$2SD_{total,calc.} = \sqrt{(2SD_{HCl})^2 + (2SD_{NH_2OH-HCl})^2 + (2SD_{residue})^2}.$$

Iron isotope fractionation of depleted or enriched zones relative to bulk soil is denoted as $\Delta^{57}Fe_{depleted-bulk} = \delta^{57}Fe_{depleted} - \delta^{57}Fe_{bulk}$ or $\Delta^{57}Fe_{enriched-bulk} = \delta^{57}Fe_{enriched} - \delta^{57}Fe_{bulk}$. Error bars of $\Delta^{57}Fe$ values were adapted according to the following formulas, where $2SD[\delta^{57}Fe_n]$ indicates the double standard deviation of the isotope ratio of pool n,

$$2SD[\Delta^{57}Fe_{depleted-bulk}] = \sqrt{(2SD[\delta^{57}Fe_{bulk}])^2 + (2SD[\delta^{57}Fe_{depleted}])^2} \quad \text{or}$$

$$2SD[\Delta^{57}Fe_{enriched-bulk}] = \sqrt{(2SD[\delta^{57}Fe_{bulk}])^2 + (2SD[\delta^{57}Fe_{enriched}])^2}.$$

5.3 RESULTS AND DISCUSSION

5.3.1 Iron concentration profiles in total soil digests

Both studied soil profiles exhibited pronounced redoximorphic features such as iron mottling and manganese concretions (Fig. 5.1). The depth profiles of total iron concentration in the two soil profiles are presented in Fig. 5.2. The Stagnic Cambisol profile displayed higher total iron concentrations in the subsoil horizons compared to the topsoil horizons. This difference is probably not caused by pedogenic processes and may instead be explained by a lower initial iron content of the parent material due to loess deposition. The lowest total iron concentrations were present in the two organic surface layer samples which is consistent with the low iron content of plant litter compared to the mineral soil material. The expected iron concentration differences were found in the enriched and depleted zones compared to the bulk soil samples in the seasonally water-saturated Bcg2 and CBg horizons. The grey depleted zones contained considerable less iron than the bulk soil samples, while the brown enrichment zones were slightly higher in iron concentration. The data indicate that about 30 % of the total iron has been leached from the depleted zones. We were not able to perform a quantitative mass balance of iron fluxes within the profile because the relative proportions of depleted and enriched zones are difficult to quantify and because the soil is an open system from which some iron may have been lost during soil formation. Some iron which was mobilized during anoxic periods

has presumably left the soil profile by vertical or lateral transport. In any case, the significant concentration differences are clear indications of pedogenic iron redistribution as a result of iron redox transformations. Other elements besides iron were also strongly influenced by the described redox cycling, which was confirmed by X-ray fluorescence analysis of depleted and enriched zones (see Appendix 2, Fig. A2.1). Elements such as manganese, arsenic, phosphorus, and lead showed similar depletion and enrichment patterns compared to iron, corresponding either to their own redox chemistry or because they are bound to iron minerals. In contrast, no significant concentration differences between iron-depleted and iron-enriched zones were found for redox-insensitive elements such as silicon, aluminum, calcium, sodium, and titanium.

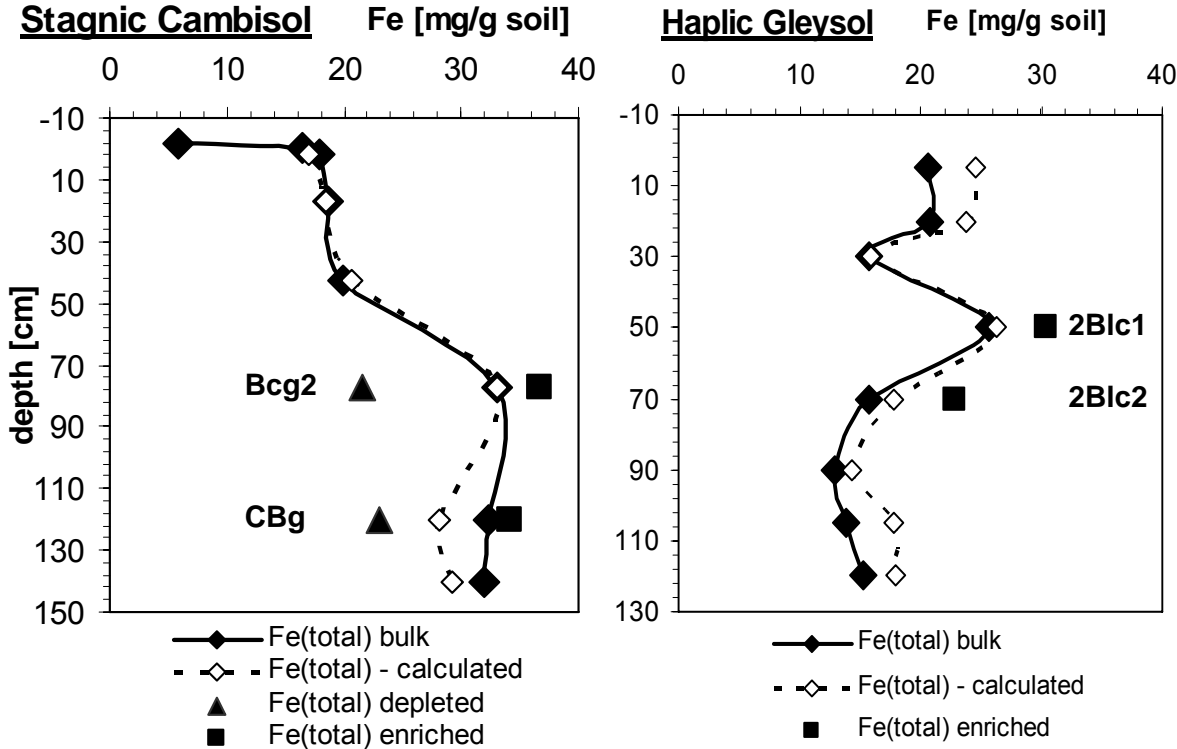


Figure 5.2 Depth profiles of total iron concentration in the two soil profiles. The redoximorphic features of the Bcg2 and the CBg horizon of the Stagnic Cambisol and of the 2B1c1 and the 2B1c2 horizon of the Haplic Gleysol were sampled separately. Open symbols indicate the calculated sum of the three iron fractions that were separated by sequential extractions (Fig. 5.4). Lines serve as eye guides. Letters indicate selected pedogenic horizons (see Fig. 5.1).

The total iron concentrations of the Haplic Gleysol (Fig. 5.2) displayed the typical depth profile of permanently water-saturated soils exhibiting lower iron contents in the subsoil and a distinct iron enrichment peak corresponding to the average position of the capillary fringe above the groundwater table at a depth of about 50 cm. Iron concentrations decreased again above this horizon. The two topsoil horizon samples (Ah1 and Ah2) consisted of a genetically different parent material (loamy cover sediment) (Kösel and Vogl, 1997), which was also apparent by the concentration profiles of immobile elements, such as Ti and Zr, measured by XRF (see Appendix 2, Table A2.3.1). Therefore, the total iron concentration of the upper two horizons cannot be directly compared to the soil horizons below. The brown iron enrichment zones that were separated from the depleted soil matrix exhibited a relative increase in total iron concentrations of 19 % in the 2B1c1 horizon and of 45 % in the Gro horizon compared to the bulk soil samples. However, it is apparent that the sampling procedure achieved only a partial separation of the iron enriched zones and the depleted bulk matrix because the bulk soil matrix samples contained still higher total iron concentrations compared to the permanently reduced soil horizons below.

5.3.2 Iron isotope ratios in total soil digests

The results of the iron isotope measurements of the total soil digestions are displayed in Fig. 5.3. The bulk soil data of the Stagnic Cambisol profile exhibited a relatively narrow range with $\delta^{57}\text{Fe}$ values of 0.0 to +0.2 ‰ relative to IRMM-014. However, the depleted zones of the Bcg2 and CBg horizons had a significantly heavier iron isotope signature with $\delta^{57}\text{Fe}$ values of +0.4 ‰ and +0.5 ‰, respectively. The enriched zones of the two horizons were not significantly fractionated relative to the bulk soil samples. This corresponds to the iron concentration data (Fig. 5.2), where the depleted zones also showed more pronounced changes compared to the bulk soil samples. The heavier $\delta^{57}\text{Fe}$ values in the depleted zones are consistent with the concept of the preferential removal of light iron isotopes during microbial dissimilatory iron reduction (Beard et al., 1999, Crosby et al., 2005), which results in a relative enrichment of heavy isotopes and thus higher $\delta^{57}\text{Fe}$ values. The bulk soil data of the Haplic Gleysol profile showed a very similar range of $\delta^{57}\text{Fe}$ values of 0.0 to +0.2 ‰, except for the two top horizons Ah1 and Ah2, which exhibited $\delta^{57}\text{Fe}$ values of +0.3 ‰ and +0.4 ‰, respectively. As mentioned before, these horizons

consist of a genetically different parent material and cannot be directly compared to the soil material below. The sample collected from the enriched zone of the 2B1c2 horizon at 70 cm depth had a significantly lighter Fe isotope signature of -0.15 ‰. This effect was probably caused by the preferential mobilization of light iron isotopes from the subsoil and quantitative oxidative precipitation of this light iron pool in the enrichment zone of the soil profile. However, the enriched zone of the second horizon (2B1c1) did not exhibit a significant iron isotope fractionation relative to the bulk soil. Iron isotope ratios of the bulk soil samples seem to increase slightly with increasing depth from +0.01 ‰ at 50 cm to +0.18 ‰ at 110 cm. This is consistent with the upward transport of isotopically light iron during pedogenic iron transformation under reducing conditions in the subsoil.

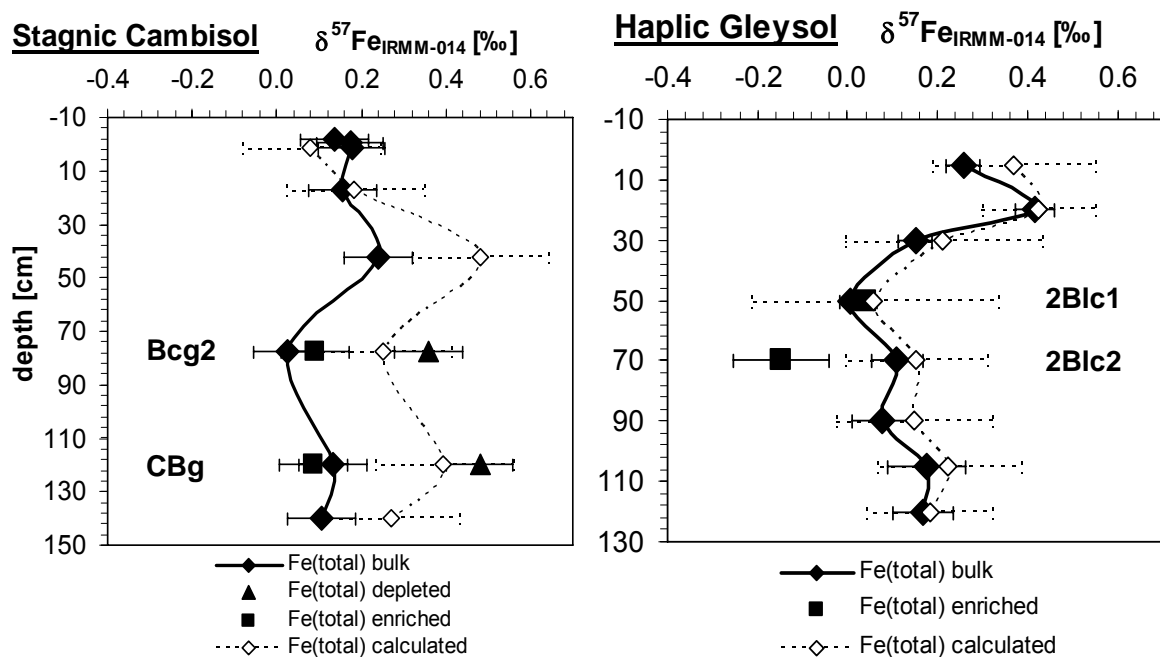


Figure 5.3 Depth profiles of $\delta^{57}\text{Fe}$ values in total soil digests of the two soil profiles. The redoximorphic features of the Bcg2 and the CBg horizon of the Stagnic Cambisol and of the 2B1c1 and the 2B1c2 horizon of the Haplic Gleysol were sampled separately. Open symbols indicate the calculated isotope mass balance of the three iron fractions that were separated by sequential extractions (Figs. 5.4 and 5.5). Lines serve as eye guides.

5.3.3 Sequential extraction methods in iron isotope studies

The analysis of iron isotopes in total soil digests only yields information about the average isotope ratio of all iron-bearing phases in the soil. Thus, it is desirable to develop complementary methods which separate these different phases in soil samples. Thereby, it is possible to investigate the iron isotope signature of different mineral phases or at least operationally defined iron pools. Chemical extractions are widely used to achieve this goal. A wide range of sequential extraction methods for iron has been developed and applied for soil samples (e.g., Chao and Zhou, 1983; Borggaard, 1988; Heron et al., 1994; LaForce and Fendorf, 2000). However, the application of sequential extraction methods in iron isotope studies needs to be evaluated carefully to avoid isotope fractionation artifacts induced by the procedure. A detailed discussion on the problems and pitfalls of sequential extraction methods in iron isotope studies is provided in chapter 4 of this thesis and is briefly summarized below. Besides the desired selectivity for specific mineral phases, a sequential extraction method should not induce kinetic isotope fractionation effects during partial dissolution since a quantitative extraction of a certain target pool is difficult to verify in natural samples. In addition, the use of extraction procedures, which complicate the sample preparation for iron isotope analysis because of difficult matrix components (e.g., dithionite-citrate), should be avoided. Moreover, secondary precipitation reactions of mobilized iron need to be eliminated due to the risk of isotope fractionation artifacts.

We decided to use a newly developed three-step sequential extraction procedure in our study, rather than the classical oxalate and dithionite methods. The first extraction step by hydrochloric acid (0.5 M, 24 h, 25°C) dissolves poorly-crystalline iron oxide minerals such as ferrihydrite as well as adsorbed and organically-bound iron, similar to the common oxalate extraction. While the dissolution of goethite in the presence of oxalate can result in significant iron isotope fractionation, no iron isotope fractionation was observed during the stepwise dissolution of goethite by 0.5 M HCl (chapter 6 of this thesis). This is in agreement with previous studies on hematite dissolution in HCl (Skulan et al., 2002).

The second extraction step with hydroxylamine-hydrochloride (1 M, 4 h, 90°C, modified after Ribet et al., 1995) was tested to achieve a complete reductive dissolution of all crystalline iron oxides such as goethite and hematite. However, it is possible that some iron that was bound to clay minerals or other silicate minerals was

extracted as well during this extraction step. Thus, a small bias may have been introduced into the isotope data of the last two steps of the sequential extraction procedure.

In the third step, all remaining soil material, which still contained iron in silicate minerals, was totally dissolved by a microwave digestion procedure with HF-HNO₃-HCl. The sequential extractions were done in parallel to the total soil digests, which allowed us to perform an isotope mass balance between the sum of the three extractions and the total digests.

5.3.4 Iron concentration profiles in sequential extraction samples

The results of the iron concentration measurements of the three-step sequential extraction procedure are displayed in Fig. 5.4. Please note the different scale bars for iron concentration of the three fractions. In both soil profiles, the crystalline iron oxide fraction ($Fe_{NH_2OH-HCl}$) exhibited the strongest variability within the profile reflecting the pedogenic iron transformation processes (Fig. 5.4 B and 5.4 E). The iron enrichment at the capillary fringe of the Haplic Gleysol profile was clearly dominated by this pool. In the Stagnic Cambisol profile, the $Fe_{NH_2OH-HCl}$ fraction even represented the dominant iron pool in all horizons. The relatively low proportion of silicate-bound iron ($Fe_{residue}$, Fig. 5.4 C) compared to oxide-bound iron can be explained by the intense weathering in the Stagnic Cambisol profile due to the high acidity and the age of the soil. In contrast, silicate-bound iron still represented the dominant iron pool in the subsoil of the Haplic Gleysol (Fig. 5.4 F), where the extent of weathering was less intense due to the neutral pH and the lower age of the soil. The $Fe_{residue}$ fractions of both soil profiles showed an increasing trend with soil depth, which can be explained by more intense weathering in the upper soil horizons. In contrast to this trend, the two topsoil horizons of the Haplic Gleysol profile exhibited a higher $Fe_{residue}$ content. However, this is probably caused by the different parent material compared to the underlying sandy horizons. The lower age of the cover sediment is consistent with the observed lower degree of silicate weathering. The Fe_{HCl} fraction, which mainly consists of poorly-crystalline iron (oxyhydr)oxide minerals such as ferrihydrite, was the smallest iron pool in most soil samples. It showed almost no variation with soil depth in the Stagnic Cambisol profile (Fig. 5.4 A) except for the uppermost organic surface layers.

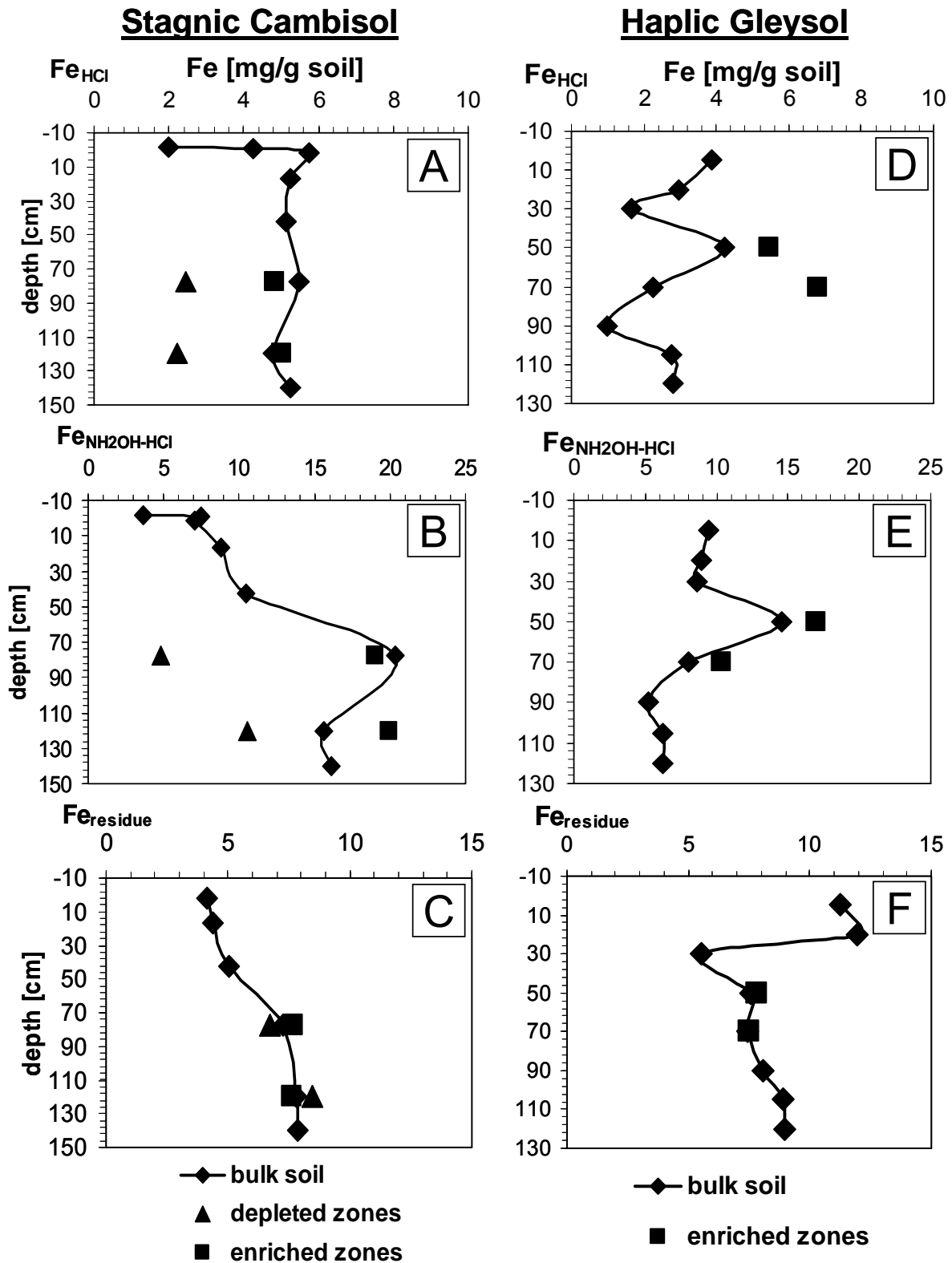


Figure 5.4 Depth profiles of iron concentrations for the three iron fractions Fe_{HCl} , $Fe_{NH_2OH-HCl}$, and $Fe_{residue}$ for bulk soil samples, depleted and enriched zones. Please note different concentration scale bars. Lines serve as eye guides. (A-C: Stagnic Cambisol, D-F: Haplic Gleysol)

In contrast, the pedogenic iron enrichment at about 50 cm soil depth of the Haplic Gleysol profile (Fig. 5.4 D) was clearly apparent in the Fe_{HCl} fraction indicating that poorly-crystalline iron oxides are partly responsible for the higher iron content of this horizon. Mass balance considerations dictate that the sum of the iron concentrations of the three sequential extractions corresponds to the iron content of the total soil digestion. The open symbols in Fig. 5.2 represent the calculated sum of the three separated iron fractions. The close match with the measured total iron values demonstrates the excellent agreement of the two datasets confirming the validity of our separation procedure.

The iron concentrations of the three soil iron pools in the separated depletion and enrichment zones of the selected horizons are depicted with triangles and squares in Fig. 5.4. The strongest redoximorphic effect is apparent in the Fe_{HCl} and $Fe_{NH_2OH-HCl}$ fractions of the Stagnic Cambisol profile with distinctly lower iron concentrations in the depleted zones compared to the bulk soil. The enriched zones of the Haplic Gleysol profile exhibited higher iron concentrations in the Fe_{HCl} and $Fe_{NH_2OH-HCl}$ fractions compared to the bulk soil. No significant concentration differences between depletion or enrichment zones and the bulk soil samples were found in the $Fe_{residue}$ fraction, which indicates that silicate-bound iron does not play a significant role in the redoximorphic iron redistribution within this soil profile.

5.3.5 Iron isotope ratios in sequential extraction samples

The $\delta^{57}Fe$ values of the three fractions Fe_{HCl} , $Fe_{NH_2OH-HCl}$, and $Fe_{residue}$, which were separated by sequential extractions, are presented in Fig. 5.5. The range of observed iron isotope ratios is much wider in this data set compared to the total digestion samples. This indicates that iron isotope fractionation does not only occur between different zones and horizons of the soil but also among different iron mineral pools. The calculated isotope mass balance from the sum of the three fractions separated by sequential extractions (indicated by open symbols and dashed lines in Fig. 5.3) showed an excellent agreement with the measured bulk soil data in the case of the Haplic Gleysol profile. The data from the lower horizons of the Stagnic Cambisol profile are less congruent and displayed a slight offset between measured and calculated values. However, the difference of about 0.2 ‰ is relatively small compared to the range of fractionations observed in the sequential extraction samples.

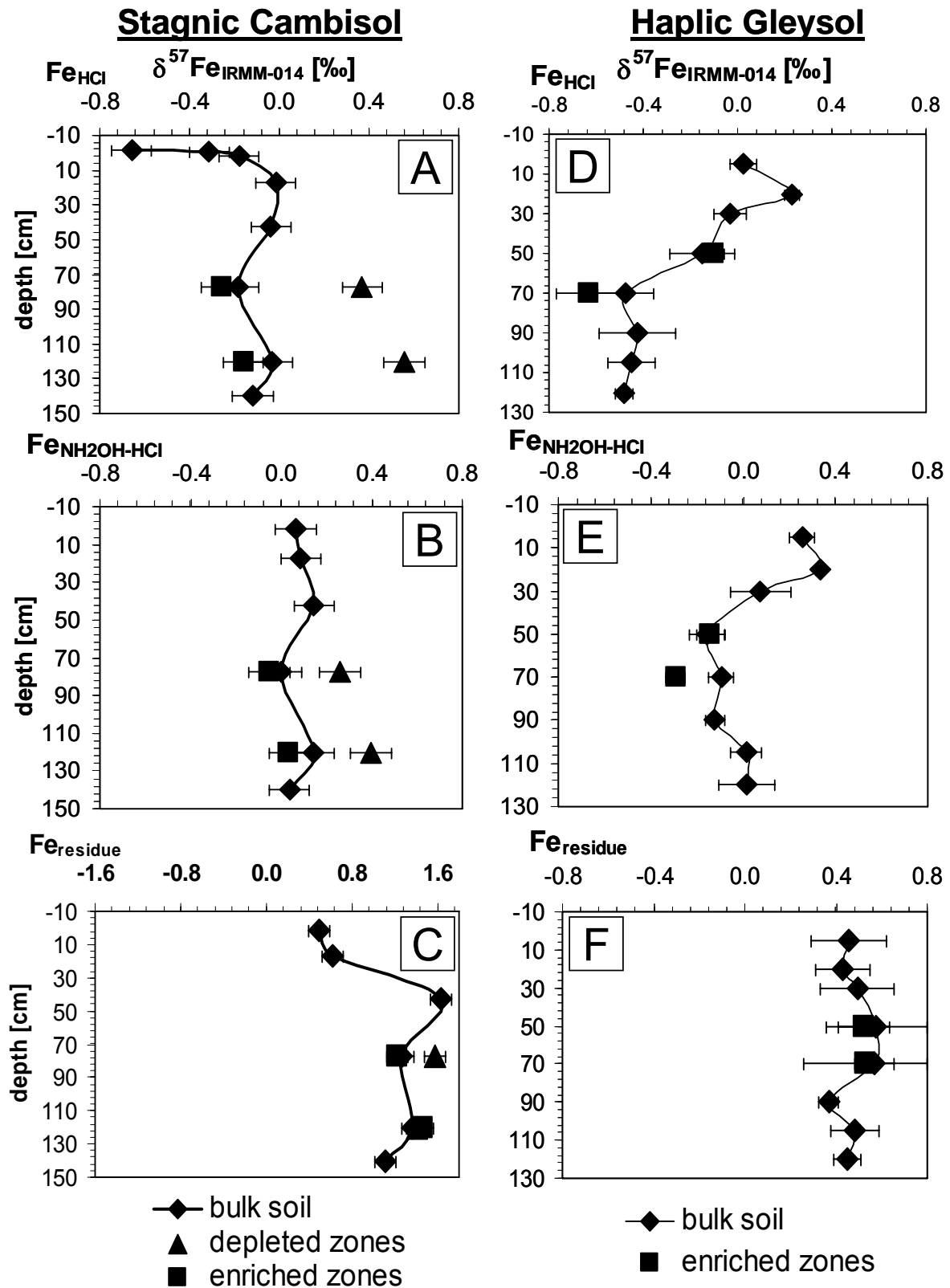


Figure 5.5 Depth profiles of $\delta^{57}\text{Fe}$ for the three iron fractions Fe_{HCl} , $\text{Fe}_{\text{NH}_2\text{OH-HCl}}$, and $\text{Fe}_{\text{residue}}$ for bulk soil samples, depleted and enriched zones. Please note different $\delta^{57}\text{Fe}$ scale in Fig. 5.5 C. Lines serve as eye guides. (A-C: Stagnic Cambisol, D-F: Haplic Gleysol)

The Fe_{HCl} and $\text{Fe}_{\text{NH}_2\text{OH-HCl}}$ fractions of the Stagnic Cambisol profile had $\delta^{57}\text{Fe}$ values close to IRMM-014 (Fig. 5.5 A and 5.5 B). The Fe_{HCl} fraction is isotopically a little lighter than the $\text{Fe}_{\text{NH}_2\text{OH-HCl}}$ fraction over the whole soil depth. The Fe_{HCl} fraction of the organic surface layer samples exhibited very light $\delta^{57}\text{Fe}$ values of up to -0.7‰ which may be explained by the preferential incorporation of light iron isotopes into plant biomass, which constitutes the source of the organic surface layer. This hypothesis is consistent with the finding of Walczyk and von Blanckenburg (2002) who reported that plant biomass was enriched in light iron isotopes. A strong enrichment of heavy isotopes was found in the $\text{Fe}_{\text{residue}}$ fraction which exhibits $\delta^{57}\text{Fe}$ values of up to $+1.6\text{‰}$ (Fig. 5.5 C). These pronounced enrichments of heavy isotopes point toward a high extent of silicate weathering due to the acidity and the age of the soil profile. The preferential transformation of light iron isotopes during weathering processes results in relative enrichments of heavy iron isotopes in the residue. The iron concentration data of the separated iron mineral pools (Fig. 5.4 A-C) indicated that the largest proportion of the iron in the soil has already been transformed to secondary mineral phases during pedogenesis.

The Haplic Gleysol data showed a similar succession of increasing $\delta^{57}\text{Fe}$ values along the sequential extraction procedure as in the Stagnic Cambisol. The difference between the iron fractions was most pronounced in the lower soil horizons with $\delta^{57}\text{Fe}$ values of around -0.5‰ in the Fe_{HCl} fraction (Fig. 5.5 D), of around 0.0‰ in the $\text{Fe}_{\text{NH}_2\text{OH-HCl}}$ fraction (Fig. 5.5 E), and of around $+0.5\text{‰}$ in the $\text{Fe}_{\text{residue}}$ fraction (Fig. 5.5 F). This trend is consistent with the concept of preferential mobilization of light iron isotopes during pedogenesis, since the light Fe_{HCl} fraction corresponds to the least-stable and youngest iron pool. In contrast, the heavy $\text{Fe}_{\text{residue}}$ fraction is made up of iron in silicate minerals which constitute the depleted residual product of weathering and soil formation processes. The younger cover sediment layer, which makes up the two top horizons of the Haplic Gleysol profile (Ah1 and Ah2), exhibited a smaller range in $\delta^{57}\text{Fe}$ with values between 0‰ and 0.5‰ . This can be explained by the lower degree of weathering due to the lower age but also by the absence of redoximorphic iron transformations in these oxic upper soil horizons. Significant iron isotope fractionations were also found between the individual iron mineral pools of the samples from the redoximorphic iron depletion and enrichment zones (Fig. 5.5). A strong enrichment of heavy iron isotopes was found in the $\text{Fe}_{\text{residue}}$ fraction similar

to the bulk soil samples. The Fe_{HCl} fraction and the $\text{Fe}_{\text{NH}_2\text{OH-HCl}}$ fraction of the Stagnic Cambisol profile exhibited systematic differences in $\delta^{57}\text{Fe}$ compared to IRMM-014 with enrichments of heavy iron isotopes in the samples from the depleted zones. In contrast, an enrichment of light iron isotopes was found in the Fe_{HCl} fraction of the enriched zones in the Stagnic Cambisol profile. The same effect was observed in the samples of the Haplic Gleysol profile with light iron isotope signatures in the Fe_{HCl} fraction of the enriched zones of up to -0.6‰ in $\delta^{57}\text{Fe}$ relative to IRMM-014.

5.3.6 Interpretation of iron isotope effects

The comparison of iron concentration data and iron isotope ratios in iron-enriched and iron-depleted zones plotted relative to the bulk soil data is shown in Fig. 5.6 for the Stagnic Cambisol profile. The link between pedogenic iron redistribution and iron isotope fractionation is evident.

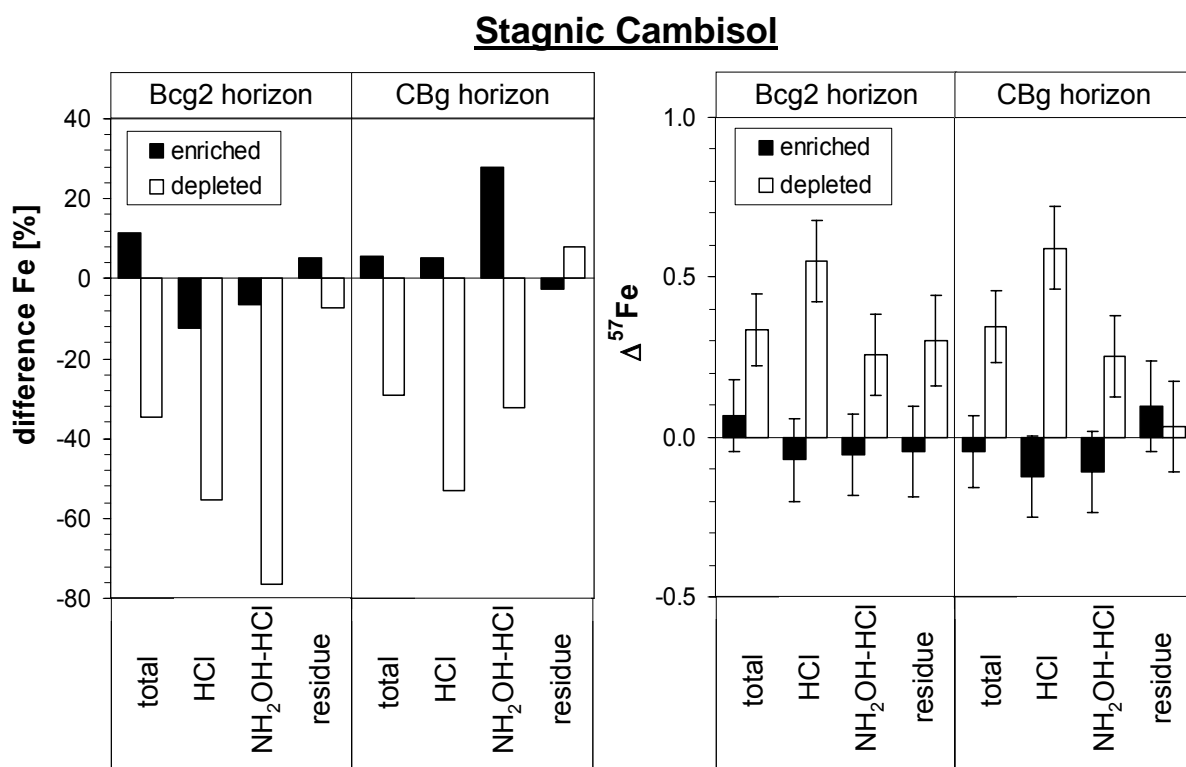


Figure 5.6 Difference in iron concentration [%] and iron isotope ratios in the enriched and depleted zones of the Stagnic Cambisol profile relative to bulk soil samples. $\Delta^{57}\text{Fe}$ represents iron isotope fractionation relative to the bulk soil sample ($\Delta^{57}\text{Fe} = \delta^{57}\text{Fe}_{\text{depleted}} - \delta^{57}\text{Fe}_{\text{bulk}}$ or $\Delta^{57}\text{Fe} = \delta^{57}\text{Fe}_{\text{enriched}} - \delta^{57}\text{Fe}_{\text{bulk}}$). Error bars of $\Delta^{57}\text{Fe}$ were adapted according to the formulas given at the end of the Materials and Methods section.

Iron depletion zones exhibit depletions of light iron isotopes and consequently relative enrichments of heavy iron isotopes, whereas iron enrichment zones tend to be slightly enriched in light iron isotopes. The Stagnic Cambisol profile showed the highest iron depletion effect in the $\text{Fe}_{\text{NH}_2\text{OH-HCl}}$ fraction of the Bcg2 horizon with concentration differences of 77 % relative to the bulk soil. This sample also displayed a significant iron isotope fractionation effect with an enrichment of heavy isotopes by 0.26 ‰ in $\delta^{57}\text{Fe}$ relative to the bulk soil. The strongest iron isotope effects were found in the Fe_{HCl} fraction of the depleted zones with enrichments of heavy isotopes of 0.55 ‰ and 0.59 ‰ in $\delta^{57}\text{Fe}$ corresponding to iron depletions of 55 % and 53 %, respectively. Fig. 5.7 presents the relative differences in iron concentration and iron isotope ratios between the enrichment zones and the bulk soil samples of the Haplic Gleysol profile. The pedogenic enrichment zones had higher iron concentrations relative to the bulk soil of up to 200 % in the Fe_{HCl} fraction of the 2B1c2 horizon. The corresponding iron isotope ratio exhibited an enrichment of light iron isotopes of 0.15 ‰ in $\delta^{57}\text{Fe}$. However, it is apparent that no simple quantitative relationship between iron concentration differences and iron isotope ratios in redoximorphic soils exist.

Iron isotope variations in soil samples have been observed in previous studies (Brantley et al., 2001; Brantley et al., 2004; Fantle and DePaolo, 2004; Emmanuel et al., 2005). A discussion of available data and methodical approaches used in previous studies is presented in chapter 4 of this thesis. The iron isotope study described here and the parallel study on oxic soils (chapter 4 of this thesis) apply a comprehensive approach aiming at a process-oriented understanding of iron isotope fractionation in soils and between individual iron mineral fractions. This study demonstrates for the first time that iron isotope variations in redoximorphic soils are clearly linked to pedogenic iron transformation and redistribution processes. The heavier $\delta^{57}\text{Fe}$ values in the depleted zones of the Stagnic Cambisol profile are caused by preferential removal of light iron isotopes. Accordingly, the lighter $\delta^{57}\text{Fe}$ values in the enrichment zones of the Haplic Gleysol profile are explained by the preferential mobilization of light iron isotopes from the subsoil and quantitative oxidative precipitation of this light iron pool in the enrichment zone of the soil profile.

Haplic Gleysol

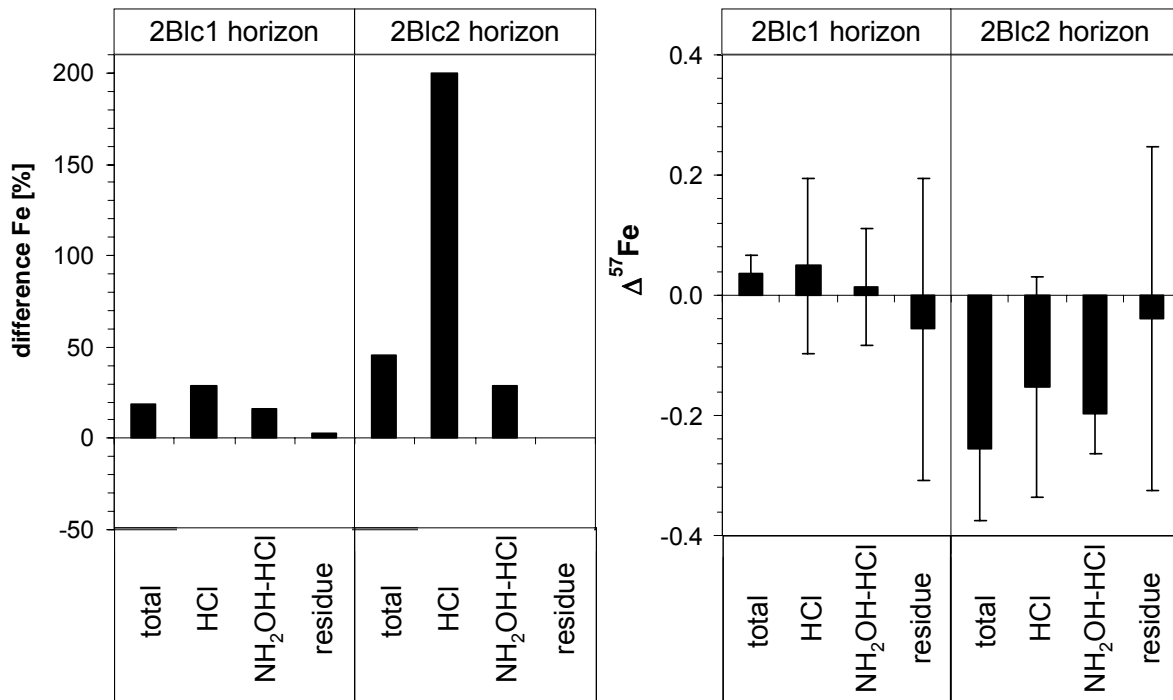


Figure 5.7 Difference in iron concentration [%] and iron isotope ratios in the enriched zones of the Haplic Gleysol profile relative to bulk soil samples. $\Delta^{57}\text{Fe}$ represents iron isotope fractionation relative to the bulk soil sample ($\Delta^{57}\text{Fe} = \delta^{57}\text{Fe}_{\text{enriched}} - \delta^{57}\text{Fe}_{\text{bulk}}$). Error bars of $\Delta^{57}\text{Fe}$ were adapted according to the formula given at the end of the Materials and Methods section.

The pedogenic iron depletion under seasonally water-saturated conditions is mediated by dissimilatory iron-reducing bacteria which are able to use ferric iron as alternate terminal electron acceptor (Lovley et al., 2004). The observed isotope effect is consistent with the observations from previous studies reporting a light iron isotope signature of the solution in laboratory experiments with dissimilatory iron-reducing bacteria (Beard et al., 1999; Crosby et al., 2005). The magnitude of the iron isotope fractionation effects between iron depleted and enriched zones of redoximorphic soils presented in this study is about 0.5 ‰ in $\delta^{57}\text{Fe}$. This is considerably smaller than the measured fractionation effects between substrate and solution in laboratory studies of about 1.3 ‰ in $\delta^{56}\text{Fe}$ (Johnson et al., 2004b). However, it is important to keep in mind that we focused on the iron isotope variations between solid iron phases in our field study. Although the depleted zones of our soil constitute the substrate of the

microbial iron reduction, the magnitude of the fractionation effects can not be directly compared with the laboratory studies. This is on the one hand because the solid mineral iron phases in a soil sample are very big iron pools compared to the small amounts of iron which is present in the soil solution at a given time. Mass balance considerations illustrate that the isotope signature of a big pool changes much less compared to a small pool during a fractionating reaction. On the other hand, dissolution reactions occur predominantly at mineral surfaces and the isotope signature of the depleted residue changes only along this reaction front at the surface (chapter 6 of this thesis). Therefore, the smaller magnitude of iron isotope fractionation found in this study does not contradict the finding of previous laboratory studies. However, our results indicate that for these reasons quantitative applications of experimentally-determined fractionation factors to isotope signatures from natural systems prove to be difficult. Nevertheless, the performance of laboratory experiments to elucidate specific iron isotope fractionation factors and mechanisms is certainly required to further understand the behavior of iron isotopes in nature.

5.4 CONCLUSIONS

The biogeochemical iron cycle in hydromorphic soils results in intense transformations of iron minerals within the soil profile. Our results show that the pedogenic transformation and redistribution processes of iron in such systems are linked to significant iron isotope fractionation. The data indicate that the reductive mobilization of ferric iron from iron (oxyhydr)oxide minerals under anoxic conditions favors the light iron isotopes, which is in good agreement with findings from laboratory studies with microorganisms (Beard et al., 1999; Crosby et al., 2005) and photoreductive dissolution experiments of iron oxide minerals (chapter 6 of this thesis). As a result of this process, iron-depleted zones are enriched in heavy iron isotopes whereas iron-enriched zones exhibit enrichments of light iron isotopes. The stronger fractionation effects were found in the Stagnic Cambisol profile which may be explained by the fact that this soil has developed over a longer time compared to the Haplic Gleysol. In addition, mineral transformation reactions and the associated isotope fractionation effects are probably enhanced by the acidic pH of the Stagnic Cambisol profile. The smaller magnitude of iron isotope variations between the separated iron pools in the topsoil of the Haplic Gleysol profile compared to the

subsoil horizons can be explained by two reasons. On the one hand, the topsoil material has a lower age, corresponding to a smaller degree of weathering and pedogenesis, and hence less iron isotope fractionation. On the other hand, the redoximorphic processes, which proceed only in the subsoil, are the main driving force for iron transformation and redistribution processes in the profile, thereby increasing the extent of iron isotope variations between the different iron pools in the soil. A distinct qualitative relationship between iron concentration changes and iron isotope fractionation in redoximorphic soils was revealed in our study, indicating a higher mobility of lighter relative to heavier iron isotopes during pedogenesis. However, it is not possible to perform a simple quantitative correlation based only on these two parameters. This can be explained by the characteristics of isotope fractionation effects during dissolution reactions, which occur mainly on surfaces and exert a smaller influence on the isotope distribution of the bulk mineral. The application of iron isotopes as a tracer in natural systems is still restrained by the incomplete understanding of iron isotope fractionation mechanisms. Nevertheless, the potential of this new isotopic tool for soil environments was clearly demonstrated.

ACKNOWLEDGEMENTS

We thank Kurt Barmettler for support in the soil chemistry laboratory, and the staff of the ETH MC-ICPMS laboratory for excellent maintenance and support. This research was funded by ETH research grant No. 01927.

REFERENCES

- Anbar AD (2004) Iron stable isotopes: beyond biosignatures. *Earth Planet. Sci. Lett.* **217**, 223–236.
- Beard BL, Johnson CM (1999) High precision iron isotope measurements of terrestrial and lunar materials. *Geochim. Cosmochim. Acta* **63**: 1653-1660.
- Beard BL, Johnson CM, Cox L, Sun H, Nealson KH, Aguilar C (1999) Iron isotope biosignatures. *Science* **285**: 1889-1896.
- Beard BL, Johnson CM (2004) Fe isotope variations in the modern and ancient Earth and other planetary bodies. *Rev. Mineral. Geochem.* **55**, 319-357.
- Borggaard OK (1988) Phase identification by selective dissolution techniques. p.83-97. In Stucki JW, Goodman BA, Schwertmann U. (eds.) *Iron in soils and clay minerals*. D. Reidel, Dordrecht, The Netherlands.

- Brantley SL, Liermann LJ, Guynn RL, Anbar A, Icopini GA, Barling J (2004) Fe isotopic fractionation during mineral dissolution with and without bacteria. *Geochim. Cosmochim Acta* **68**, 3189-3204.
- Brantley SL, Liermann L, Bullen TD (2001) Fractionation of Fe isotopes by soil microbes and organic acids. *Geology* **29**, 535-538.
- Chao TT, Zhou L (1983) Extraction techniques for selective dissolution of amorphous iron oxides from soils and sediments. *Soil Sci. Soc. Am. J.* **47**: 225-232.
- Crosby HA, Johnson CM, Roden EE, Beard BL (2005) Coupled Fe(II)-Fe(III) electron and atom exchange as a mechanism for Fe isotope fractionation during dissimilatory iron oxide reduction. *Environ. Sci. Technol.* **39**, 6698-6704.
- Cornell RM, Schwertmann U (2003) The iron oxides – structure, properties, reactions, occurrence and uses. Second edition. VCH, Weinheim, Germany.
- Cummings DE, Caccavo, Jr. F, Fendorf S, Rosenzweig RF (1999) Arsenic mobilization by the dissimilatory Fe(III)-reducing bacterium *Shewanella alga* BrY. *Environ. Sci. Technol.* **33**, 723-729.
- Dauphas N, Rouxel O (2006) Mass spectrometry and natural variations of iron isotopes. *Mass Spec. Rev.* **25**, 515-550.
- Emmanuel S, Erel Y, Matthews A, Teutsch N (2004) A preliminary mixing model for Fe isotopes in soils. *Chem. Geol.* **222**, 23-34.
- Fantle MS, DePaolo DJ (2004) Iron isotope fractionation during continental weathering. *Earth Planet. Sci. Lett.* **228**, 547–562.
- Gimmi T., Kretzschmar. R., Papritz, A., Flüher, H. (1997) Zürich Nord. Exkursion CH 1. *Mitteilungen der Deutschen Bodenkundlichen Gesellschaft* **82**, 169-186.
- Halliday AN, Lee D-C, Christensen JN, Rehkämper M, Yi W, Luo X, Hall CM, Ballentine CJ, Pettke T, Stirling C (1998) Applications of multiple collector-ICPMS to cosmochemistry, geochemistry, and paleoceanography. *Geochim. Cosmochim. Acta* **62**, 919-940.
- Heron G, Crouzet C, Bourg ACM, Christensen TH (1994) Speciation of Fe(II) and Fe(III) in contaminated aquifer sediments using chemical extraction techniques. *Environ. Sci. Tech.* **28**: 1698-1705.
- Hoefs, J. (2004) Stable isotope geochemistry. 5th edition. Springer, Berlin, Germany.
- Johnson CM, Beard BL, Albarède F (2004a) (eds.) Geochemistry of non-traditional stable isotopes. *Reviews in Mineralogy and Geochemistry* 55. Mineralogical Society of America and Geochemical Society, Washington, DC, US.
- Johnson CM, Beard BL, Roden EE, Newman DK, Nealson KH (2004b) Isotopic constraints on biogeochemical cycling of Fe. *Rev. Mineral. Geochem.* **55**, 359-408.
- Kösel M, Vogl W (1997) Schussenbecken. Exkursion D7. *Mitteilungen der Deutschen Bodenkundlichen Gesellschaft* **82**, 349-382.

- La Force MJ, Fendorf S (2000) Solid-phase iron characterization during common selective sequential extractions. *Soil Sci. Soc. Am. J.* **64**, 1608-1615.
- Lovley DR, Holmes DE, Nevin KP (2004) Dissimilatory Fe(III) and Mn(IV) reduction. *Adv. Microb. Physiol.* **49**, 219-286.
- Matthews A, Morgans-Bell HS, Emmanuel S, Jenkyns HC, Erel Y, Halicz L (2004) Controls on iron-isotope fractionation in organic-rich sediments (Kimmeridge Clay, Upper Jurassic, Southern England). *Geochim. Cosmochim. Acta* **68**, 3107-3123.
- Ribet I, Ptacek CJ, Blowes DW, Jambor JL (1995) The potential for metal release by reductive dissolution of weathered mine tailings. *J. Contam. Hydrol.* **17**, 239-273.
- Severmann S, Johnson CM, Beard BL, McManus J (2006) The effect of early diagenesis on the Fe isotope compositions of porewaters and authigenic minerals in continental margin sediments. *Geochim. Cosmochim. Acta* **70**, 2006-2022.
- Schlichting E, Schwertmann U (eds.) 1973. Pseudogley and Gley - Genesis and use of hydromorphic soils. VCH, Weinheim, Germany.
- Schoenberg R, von Blanckenburg F (2005) An assessment of the accuracy of stable Fe isotope ratio measurements on samples with organic and inorganic matrices by high-resolution multicollector ICP-MS. *Int. J. Mass. Spec.* **242**, 257-272.
- Skulan JL, Beard BL, Johnson CM (2002) Kinetic and equilibrium Fe isotope fractionation between aqueous Fe(III) and hematite. *Geochim. Cosmochim. Acta* **66**, 2995-3015.
- Staubwasser M, von Blanckenburg F, Schoenberg R (2006) Iron isotopes in the early marine diagenetic iron cycle. *Geology* **34**, 629-632.
- Stucki JW, Goodman, BA, Schwertmann U (eds.) 1988. Iron in soils and clay minerals. D. Reidel, Dordrecht, The Netherlands.
- Szilas CP, Borggaard OK, Hansen HCB, Rauer J (1998) Potential iron and phosphate mobilization during flooding of soil material. *Water, Air, and Soil Pollution* **106**: 97-109.
- Teutsch N, von Gunten U, Porcelli D, Cirpka OA, Halliday AN (2005) Adsorption as a cause for iron isotope fractionation in reduced groundwater. *Geochim. Cosmochim. Acta* **69**, 4175-4185.
- USDA (1993) Soil Survey Manual. United States Department of Agriculture. Handbook No. 18. Washington, USA.
- USDA (2006) Keys to soil taxonomy. Tenth edition. United States Department of Agriculture, Washington, USA.
- van Breemen N, Buurman, P (2004) Soil Formation. Second edition. Kluwer Academic, Dordrecht, The Netherlands.

- Vepraskas MJ (1996) Redoximorphic features for identifying aquic conditions. North Carolina Agricultural Research Service, Technical Bulletin 301, Raleigh, North Carolina, US.
- Walczyk T, von Blanckenburg F (2002) Natural iron isotope variations in human blood. *Science* **295**, 2065-2066.
- Wiederhold JG, von Blanckenburg F (2002) Iron isotope variations in a complete natural soil catena with lateral iron mobilization and reprecipitation. *Geochim. Cosmochim. Acta* **66**, A834.
- Williams HM, McCammon CA, Peslier AH, Halliday AN, Teutsch N, Levasseur S, Burg J-P (2004) Iron isotope fractionation and the oxygen fugacity of the mantle. *Science* **304**, 1656-1659.
- WRB (2006a) World Reference Base for Soil Resources 2006 - a framework for international classification, correlation and communication. World Soil resources reports 103. Food and Agriculture Organization of the United Nations, Rome, Italy.
- WRB (2006b) Guidelines for soil description. Fourth edition. Food and Agriculture Organization of the United Nations, Rome, Italy.

6. IRON ISOTOPE FRACTIONATION DURING PROTON-PROMOTED, LIGAND-CONTROLLED, AND REDUCTIVE DISSOLUTION OF GOETHITE

This chapter was published in June 2006 in Environmental Science and Technology:

Wiederhold JG, Kraemer SM, Teutsch N, Borer PM, Halliday AN, Kretzschmar R (2006) Iron isotope fractionation during proton-promoted, ligand-controlled, and reductive dissolution of goethite. Environ. Sci. Technol. 40, 3787-3793.

Abstract

Iron isotope fractionation during dissolution of goethite (α -FeOOH) was studied in laboratory batch experiments. Proton-promoted (HCl), ligand-controlled (oxalate dark) and reductive (oxalate light) dissolution mechanisms were compared in order to understand the behavior of iron isotopes during natural weathering reactions. Multicollector ICP-MS was used to measure iron isotope ratios of dissolved iron in solution. The influence of kinetic and equilibrium isotope fractionation during different timescales of dissolution was investigated. Proton-promoted dissolution did not cause iron isotope fractionation, concurrently demonstrating the isotopic homogeneity of the goethite substrate. In contrast, both ligand-controlled and reductive dissolution of goethite resulted in significant iron isotope fractionation. The kinetic isotope effect, which caused an enrichment of light isotopes in the early dissolved fractions, was modeled with an enrichment factor for the $^{57}\text{Fe}/^{54}\text{Fe}$ ratio of -2.6 ‰ between reactive surface sites and solution. Later dissolved fractions of the ligand-controlled experiments exhibit a reverse trend with a depletion of light isotopes of ~0.5 ‰ in solution. We interpret this as an equilibrium isotope effect between Fe(III)-oxalate complexes in solution and the goethite surface. In conclusion, different dissolution mechanisms cause diverse iron isotope fractionation effects and likely influence the iron isotope signature of natural soil and weathering environments.

6.1 INTRODUCTION

Iron is an essential nutrient for almost all organisms and the Fe(II)/Fe(III) redox couple is a key factor in the regulation of various biogeochemical processes. The biogeochemical iron cycle is closely interlinked with natural cycles of many other nutrient and pollutant elements of environmental interest. Stable isotopes have been very helpful in studying transport and transformation processes of various elements in natural ecosystems (Hoefs, 2004). However, until recently this application was confined mainly to light elements that could be measured in the gas phase (e.g., H, C, O, N, and S). The development of new analytical techniques within the last decade, especially multiple-collector inductively-coupled-plasma mass-spectrometry (MC-ICPMS), has expanded this range to heavier elements (Halliday et al., 1998). High precision data of transition metal isotope ratios in environmental samples are now becoming more and more available, opening up a new promising and fast growing research area of isotope geochemistry (Johnson et al., 2004a).

Due to its unique importance in natural systems, iron has attracted particular attention (Anbar, 2004), and iron isotopes now provide a new tool to trace the biogeochemical iron cycle (Johnson et al., 2004b). Iron has four stable isotopes (percent natural abundance): ^{54}Fe (5.8%), ^{56}Fe (91.8%), ^{57}Fe (2.1%), and ^{58}Fe (0.3%). The δ -notation is commonly used to describe iron isotope fractionation relative to the international iron isotope standard IRMM-014 and is defined as

$$\delta^{56}\text{Fe} [\text{‰}] = \left(\frac{(^{56}\text{Fe}/^{54}\text{Fe})_{\text{sample}}}{(^{56}\text{Fe}/^{54}\text{Fe})_{\text{IRMM-014}}} - 1 \right) \cdot 10^3 \quad \text{or} \quad \delta^{57}\text{Fe} [\text{‰}] = \left(\frac{(^{57}\text{Fe}/^{54}\text{Fe})_{\text{sample}}}{(^{57}\text{Fe}/^{54}\text{Fe})_{\text{IRMM-014}}} - 1 \right) \cdot 10^3 .$$

The two values can be easily converted into each other by the approximation $\delta^{57}\text{Fe} = 1.5 \times \delta^{56}\text{Fe}$ because the observed fractionation effects are mass-dependent. Variations of $\delta^{56}\text{Fe}$ in bulk igneous rocks were found to be very small (Beard and Johnson, 2004). In contrast, significant iron isotope variations of more than one per mil were found in a variety of low-temperature environments including sediments and soils (Fantle and DePaolo, 2004; Matthews et al., 2004; Wiederhold et al., 2004). Iron isotope fractionations have been attributed to biotic or abiotic processes including bacterial dissimilatory iron reduction (Beard et al., 1999), precipitation (Bullen et al., 2001), and adsorption (Teutsch et al., 2005), and have been explained by kinetic or equilibrium fractionation effects (Anbar, 2004; Johnson et al., 2004; Beard and

Johnson, 2004). However, the exact fractionation mechanisms governing the distribution of iron isotopes in nature still remain largely unclear.

Only limited data are available on iron isotope fractionation during abiotic mineral dissolution reactions. No fractionation was observed during hematite dissolution in hydrochloric acid (Skulan et al., 2002; Johnson et al., 2004b). In contrast, significant iron isotope fractionation was observed during dissolution of hornblende in the presence of different organic ligands including oxalate (Brantley et al., 2001; Brantley et al., 2004). The solution was found to be enriched in light isotopes and the extent of fractionation correlated with the association constants of the organic ligands with ferric iron. The fractionation was attributed predominantly to the retention of heavy iron isotopes in a leached layer that forms on the surface of the hornblende minerals.

Iron isotope ratios from natural soil profiles with pedogenic iron translocation exhibit significant variations (Wiederhold et al., 2004). The light isotopes are preferentially transported during both podzolization in very acidic, oxic soils (ligand-controlled process) and the formation of redoximorphic features in seasonally anoxic soils (redox-controlled process). However, the interpretation of iron isotope field data and the assignment of the observed effects to specific fractionation reactions remain difficult. Therefore, controlled laboratory experiments focusing on single reaction mechanisms are required to elucidate the key mechanisms of iron isotope fractionation during mineral dissolution.

Goethite (α -FeOOH) is one of the most important Fe oxide minerals in soils and sediments (Cornell and Schwertmann, 2003). It is formed during pedogenesis and weathering. The dissolution behavior of iron oxides such as goethite is a key factor in controlling iron bioavailability for plants and microorganisms (Reichard et al., 2005). Iron oxide minerals dissolve by three different mechanisms: proton-promoted, ligand-controlled, and reductive dissolution, which have been studied in detail (Zinder et al., 1986; Cornell and Schwertmann, 2003). Proton-promoted dissolution is a slow process except at very acidic pH and plays only a minor role in iron mobilization in nature. The presence of molecules that form stable Fe(III)-ligand complexes (e.g., organic acids and siderophores (Cheah et al., 2003; Kraemer, 2004)) can strongly accelerate the dissolution of iron oxides. The ligand molecules adsorb to the iron oxide and form surface complexes (Persson and Axe, 2005). The subsequent

detachment of these surface complexes and release of Fe(III)-ligand-complexes represents the rate-limiting step for ligand-controlled dissolution (Zinder et al., 1986). In soils and sediments, ligand-controlled dissolution can have a major influence on iron cycling especially in organic-rich systems (e.g., podzols). The third mechanism, reductive dissolution, is the most important iron oxide dissolution mechanism in nature. Electron transfer to Fe(III)-atoms on the oxide surface produces ferrous iron which is readily released into solution. Reductive dissolution can be mediated by both biotic and abiotic processes. Dissimilatory iron reducing bacteria couple the oxidation of organic matter to the reduction of iron oxides by using ferric iron as terminal electron acceptor (Lovley et al., 2004). This reaction has been shown to fractionate iron isotopes by producing ferrous iron in solution that is enriched in light isotopes (Beard et al., 1999; Crosby et al., 2005). Besides microbially-mediated reactions, reductive dissolution of iron oxides can also occur non-enzymatically with a variety of different electron donors (e.g., phenolic compounds, LaKind and Stone, 1989) and is promoted by photochemical processes (Sulzberger and Laubscher, 1995; Borer et al., 2005). In the presence of light, photolysis of Fe(III)-ligand-complexes results in electron transfer reactions and the formation of soluble ferrous iron. Reductive dissolution of iron oxides is strongly accelerated in the presence of ferrous iron or Fe(II)-ligand-complexes (Suter et al., 1988).

Oxalate ($C_2O_4^{2-}$) is a ubiquitous organic acid anion and plays an important role in mineral weathering (Drever and Stillings, 1997). It is formed as a product of organic matter decomposition or is exuded by plant roots and microorganisms into soils and weathering environments. Oxalate concentrations in soil solution are highly variable. Typical values are on the order of a few μM but can be as high as several hundreds of μM (Jones, 1998). Oxalate can dissolve iron oxides by both ligand-controlled and photochemical reductive dissolution mechanisms. In the dark, oxalate dissolves goethite by a ligand-controlled process releasing Fe(III)-oxalate complexes into solution (Zinder et al., 1986). In the presence of light, oxalate dissolves goethite by a photochemical reductive mechanism producing aqueous Fe(II) and CO_2 (Sulzberger and Laubscher, 1995). We have taken advantage of this interesting property of oxalate to study iron isotope fractionation during mineral dissolution by both mechanisms using the same reagent.

The objective of this work is to explore iron isotope fractionation during mineral dissolution by different dissolution mechanisms. We investigated goethite dissolution in batch experiments comparing proton-promoted, ligand-controlled, and reductive dissolution by measuring iron isotope ratios in the dissolved phase. With this approach, we obtain insight into the fractionation mechanisms of iron isotopes during mineral dissolution and contribute to the development of iron isotopes as a tracer for biogeochemical iron cycling in natural systems such as soils.

6.2 EXPERIMENTAL SECTION

6.2.1 Materials and reagents

Goethite was synthesized following the method of Schwertmann and Cornell (2000). The crystal structure of the material was checked by powder X-ray diffraction (XRD) and the surface area was determined to be 38 m²/g (N₂-BET method). The same goethite has been used in previous studies (Reichard et al., 2005; Borer et al., 2005). All reagents were p.a. quality and prepared with ultrapure H₂O (>18 MΩ). Polyethylene labware was precleaned with 3 M HNO₃ and rinsed with ultrapure H₂O prior to use. Teflon beakers (Savillex, US) were cleaned with concentrated HNO₃ followed by rinsing with ultrapure H₂O.

6.2.2 Setup of batch dissolution experiments

The ligand-controlled dissolution experiments (oxalate dark) were performed in polyethylene bottles wrapped with aluminum foil. Concentrations of 2.5 – 5 g/L goethite and 5 mM oxalic acid were used. The pH of the suspension was adjusted to 3.0 at the beginning of the experiment by addition of small amounts of potassium hydroxide. The well mixed suspension was filled into a series of bottles that were placed on an overhead-shaker. After predefined time steps (5 min to 315 days), bottles were removed from the shaker, centrifuged (3400 x g, 15 min) and carefully decanted. The decanted solution was then immediately filtered through a 0.025 μm cellulose nitrate membrane filter (Schleicher & Schuell, Germany) and acidified with distilled concentrated HNO₃. The pH in the suspension increased to 3.9 after 95 days and to 4.1 after 315 days of dissolution due to the consumption of protons during goethite dissolution. Dissolution was stopped after 315 days. The residue was then washed with water (acidified to pH 4) and afterwards leached twice with 0.5 M HCl

(leach 1: 15 min, leach 2: 90 min). The remaining residue was totally dissolved in 6 M HCl.

The proton-promoted dissolution experiments were carried out with 0.5 M HCl. A lower pH of ~ 0.3 was chosen because proton-promoted dissolution at pH 3 is too slow to produce enough dissolved iron for isotope measurements in a reasonable timeframe (Cornell and Schwertmann, 2003). The experimental setup was similar to the oxalate dark experiments. The reaction time ranged from 3 min to 24 h and the goethite solid concentration from 2.5 g/L to 12.5 g/L. The higher solid concentration was necessary to obtain sufficient amounts of iron for isotope analysis from a small dissolved fraction.

The reductive dissolution experiments (oxalate light) were performed in a Pyrex glass vessel that was irradiated by a solar simulator (high pressure Xenon lamp, OSRAM, Germany) producing a spectrum similar to sunlight and a light energy of 1200 W/m^2 at the sample (Borer et al., 2005). The vessel was water-cooled to constant temperature ($25 \pm 1 \text{ }^\circ\text{C}$), stirred by a magnetic Teflon-coated stirring bar, and constantly purged with nitrogen gas to prevent re-oxidation of ferrous iron by oxygen. The experimental setup is depicted on the back cover of this thesis. A lower goethite solid concentration of 0.5 g/L was used to assure sufficient light penetration. At the beginning of the experiment the oxalic acid concentration was 1 mM. The pH in the suspension increased from 3.0 to 5.1 at the end of the experiment. Adsorption of Fe(II) to the goethite surface is negligible below pH 5 (Silvester et al., 2005), which is important as adsorption reactions could induce additional isotope fractionation effects (Teutsch et al., 2005). The suspension was sampled with a syringe after predefined dissolution times (5 min to 7.5 h), immediately filtered ($0.025 \text{ }\mu\text{m}$) and acidified with HNO_3 .

Finally, the remaining goethite solid material of all dissolution experiments and the unreacted goethite were completely dissolved in 6 M HCl to measure the iron isotope composition of the bulk solid and to assess the isotopic homogeneity of the goethite material.

6.2.3 Sample preparation for isotope analysis

Sample preparation took place in a clean chemistry laboratory and the detailed methods have been previously described (Teutsch et al., 2005). Sample solutions

(up to 240 mL) were evaporated on a hotplate in Teflon beakers and treated several times with 30% H₂O₂ and concentrated HNO₃ to oxidize oxalate to CO₂ and ferrous iron to ferric iron. Subsequently, the samples were re-dissolved in 6 M HCl, purified in Teflon columns on anion-exchange resin (Bio-Rad AG1 X4, 200-400 mesh) with quantitative recovery, again evaporated and finally diluted to 8 ppm Fe in 0.05 M HCl.

6.2.4 Analytical Methods

Iron concentrations were measured by atomic absorption spectrometry (AAS, SpectrAA 220, Varian, Australia). Iron isotope ratios were measured by multiple-collector inductively-coupled-plasma mass-spectrometry (MC-ICPMS, Nu Plasma, Nu instruments, UK). The analytical procedures for iron isotope measurement have been previously described in detail (Teutsch et al., 2005; Williams et al., 2004). Briefly, a standard-bracketing approach with IRMM-014 was used to correct for machine drift and instrumental mass bias (Schoenberg and von Blanckenburg, 2005). A membrane desolvation system (MCN-6000, Cetac, US) was used to minimize argide interferences (ArN⁺, ArO⁺, ArOH⁺) to insignificant levels (background to signal ratio typically < 0.001). The ⁵⁷Fe/⁵⁴Fe and ⁵⁶Fe/⁵⁴Fe ratios were measured simultaneously and all data plot on the theoretical mass fractionation line demonstrating the absence of isobaric interferences. A Cr correction was performed by monitoring mass 52 or 53 to calculate the potential influence of ⁵⁴Cr on ⁵⁴Fe. However, our purified solutions did not contain significant amounts of Cr and the Cr corrected and uncorrected $\delta^{57}\text{Fe}$ values differed by less than ± 0.01 ‰. All masses were collected in Faraday cups equipped with 10¹¹ Ω resistors except mass 56 which was collected in a Faraday cup equipped with a 10⁹ Ω resistor. This allowed to run solutions with relatively high Fe concentrations (8 ppm) but affected the precision of the ⁵⁶Fe/⁵⁴Fe measurement. Therefore, due to the smaller analytical error for the ⁵⁷Fe/⁵⁴Fe ratio, the results are expressed as $\delta^{57}\text{Fe}$ with a long-term reproducibility of $\pm \leq 0.15$ ‰ (2SD). Samples were only measured after several stable isotope measurements of an internal house standard against IRMM-014. This standard was again measured after every six samples and at the end of the analytical run. All data in this paper are reported as $\Delta^{57}\text{Fe}$ relative to the isotopic composition of the bulk goethite ($\Delta^{57}\text{Fe} = \delta^{57}\text{Fe}_{\text{IRMM}} - \delta^{57}\text{Fe}_{\text{bulk goethite}}$), which has a $\delta^{57}\text{Fe}$ value of $+0.54 \pm 0.15$ ‰ (n = 11) and was processed identically to all other samples.

6.2.5 Modeling approach.

Isotope fractionation during dissolution can not be described by a simple Rayleigh fractionation model because dissolution reactions only proceed at the surface of the mineral. Therefore, only a small pool of the substrate participates in the reaction at any given time. The size of the total surface site pool (i.e. one monolayer) of the goethite was calculated from the N₂-BET surface area (38 m²/g) combined with an estimated surface site density of 4.35 Fe atoms per nm² based on a detailed study of goethite surface structure (Koretsky et al., 1998) considering that the (010) face is the most relevant goethite surface for dissolution (Cornell et al., 1974). Accordingly, the total surface site pool makes up ~2.4 % of the total iron atoms in the goethite. Furthermore, dissolution of surface atoms from a mineral such as goethite is dominated by a subset of highly reactive surface sites (Wehrli et al., 1990). Specifically, monatomic steps on the surface expose iron octahedra that are not fully coordinated and more susceptible to proton or ligand attack (Figure 6.1, Casey and Ludwig, 1996). These reactive sites are self-reproducing because new octahedra are constantly exposed as dissolution proceeds along double chains of iron (oxy)hydroxide octahedra. The rate of dissolution of an exposed octahedron may be influenced by the isotopic mass of the central iron atom. If one isotope is preferentially dissolved, the other isotopes are subsequently enriched on the remaining surface while the bulk of the mineral phase remains unchanged. We developed a kinetic fractionation model based on dissolution of reactive surface sites that accounts for this surface enrichment effect. Our model is conceptually similar to the model used by Brantley et al. to describe the distribution of ⁵⁶Fe and ⁵⁴Fe within a leached layer at the surface of hornblende minerals (Brantley et al., 2004). While goethite does not develop a leached layer, iron isotope fractionation occurs between a reactive surface site pool of constant size and the solution. Our model considers all four iron isotopes (⁵⁴Fe, ⁵⁶Fe, ⁵⁷Fe, and ⁵⁸Fe) with their relative mass differences, abundances and interactions. We modeled the dissolution of the reactive surface site pool (rss) with a preferential release of the lighter isotopes (fixed enrichment factor $\varepsilon = \Delta^{57}\text{Fe}_{\text{sol}} - \Delta^{57}\text{Fe}_{\text{rss}}$) and subsequent replenishment of the depleted residual reactive surface site pool with unfractionated bulk material. A detailed description of our model is provided in the supporting material.

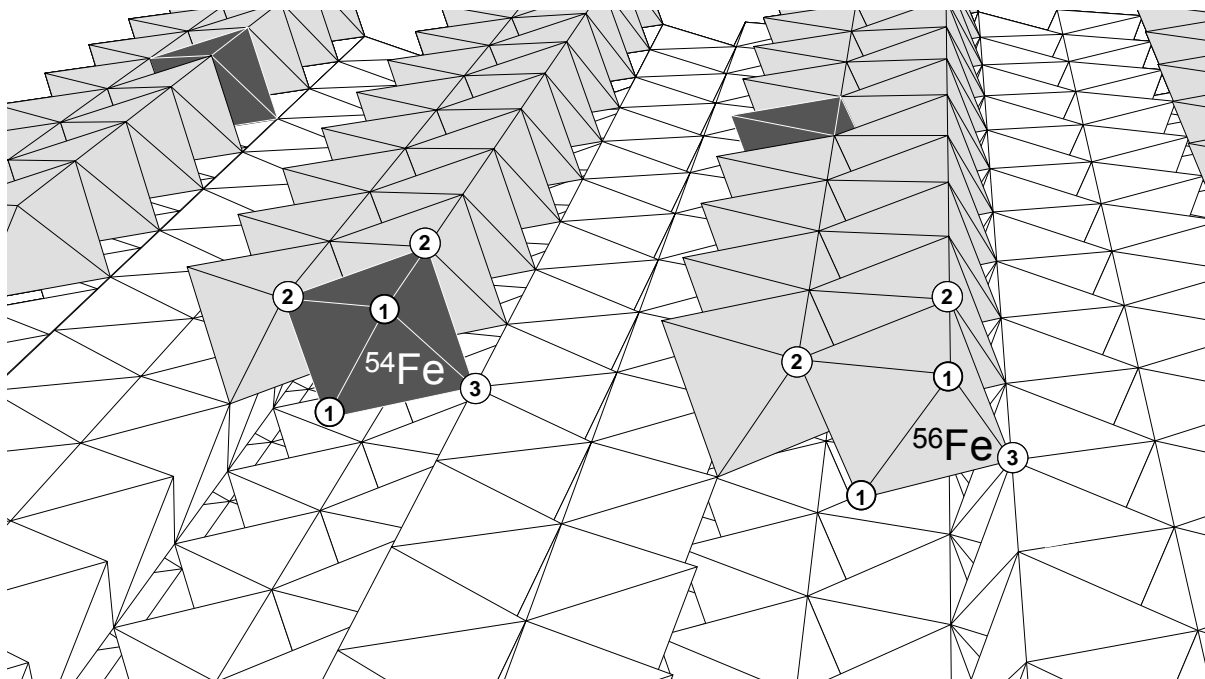


Figure 6.1 Dissolution of goethite at monatomic steps (modified after Casey and Ludwig, 1996). Iron is octahedrally coordinated to six oxygen atoms that are partially protonated. Dissolution proceeds at monatomic steps along double chains of ^{54}Fe (black) and ^{56}Fe (grey) octahedra at the mineral surface (^{57}Fe and ^{58}Fe are not considered for simplicity). Bulk Fe octahedra below are shown in white without indication of isotopic masses. Bidentate ligands such as oxalate can only attack iron octahedra with at least two singly-coordinated oxygens (marked as 1) (Holmen and Casey, 1996). These dissolution active sites constitute only a small fraction of the total surface sites. Iron isotope ratios in solution only change if doubly and triply coordinated oxygen atoms (marked at 2 and 3) remain at the surface, i.e., if bonds between the detaching iron atom and 2 and 3 are broken in the dissolution reaction. In this case, dissolution of ^{54}Fe sites proceeds faster than dissolution of ^{56}Fe sites.

6.3 RESULTS AND DISCUSSION

6.3.1 Dissolution kinetics

The dissolution kinetics of goethite during proton-promoted (0.5 M HCl), ligand-controlled (oxalate dark) and reductive dissolution (oxalate light) are illustrated in Figure 6.2. Proton-promoted dissolution was the slowest process, even at the lower pH of 0.3 compared to pH 3 in the other two experiments. Reductive dissolution

(oxalate light) exhibited by far the fastest dissolution rate achieving a dissolved fraction of 13.8 % in five hours, whereas ligand-controlled dissolution dissolved only 6.3% of the goethite in 315 days. An amount of iron corresponding to a single surface monolayer (~2.4 % of total Fe) dissolved in less than 90 minutes by reductive dissolution and in about four weeks by ligand-controlled dissolution. Dissolution rates changed slightly over the course of the experiments. The increase in dissolution rate in the oxalate light experiments can be explained by the autocatalytic effect of increasing ferrous iron concentrations on the reductive dissolution (Suter et al., 1988; Sulzberger and Laubscher, 1995). A decrease in reaction rates at the end of the oxalate dark experiments occurred as the reaction approached chemical equilibrium.

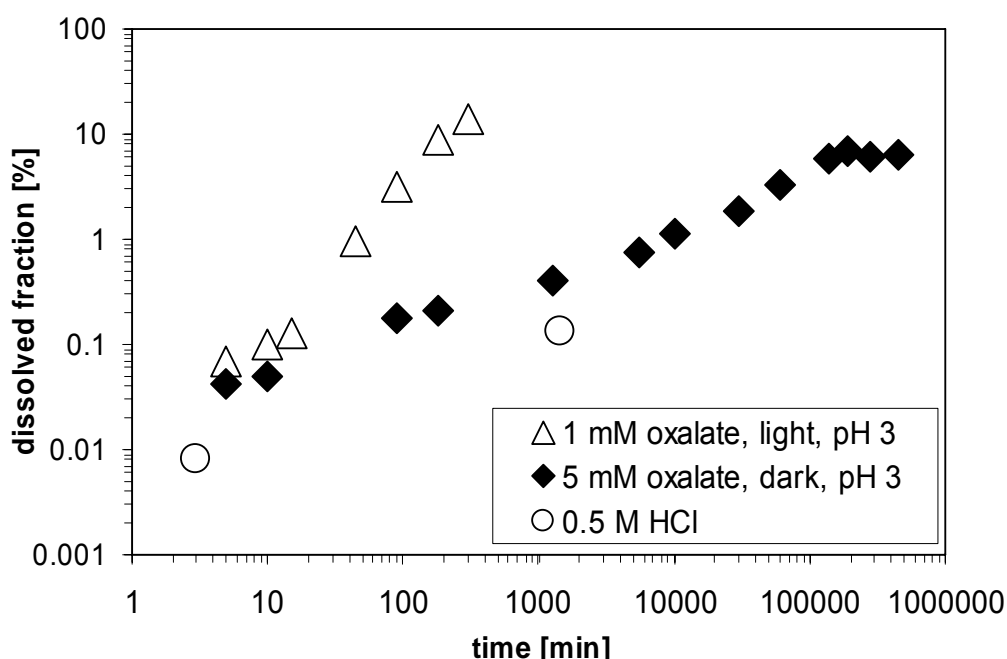


Figure 6.2 Dissolution of goethite during the three batch experiments. The dissolved fraction in the oxalate dark experiments (ligand-controlled dissolution) did not increase after about four months of reaction indicating that the solution was saturated and a chemical equilibrium approached.

6.3.2 Iron isotopes

Figure 6.3 shows the iron isotope composition in solution as a function of the dissolution time. It is important to note that all data points show accumulated values because samples were taken from independent parallel bottles (0.5 M HCl and oxalate dark) or from one batch where only small aliquots were sampled over time (oxalate light). Therefore, the iron isotope ratio in solution at a given time represents

the average of dissolved iron up to the sampling time. In the 0.5 M HCl experiments, $\Delta^{57}\text{Fe}$ in solution did not vary between dissolved fractions and was not statistically different from the bulk value obtained by total dissolution in 6 M HCl. Hence, proton-promoted dissolution with 0.5 M HCl does not induce fractionation of iron isotopes. This result is in agreement with previous studies on hematite dissolution by HCl where no iron isotope fractionation was reported (Skulan et al., 2002; Johnson et al., 2004b) and confirms that the goethite is not isotopically zoned.

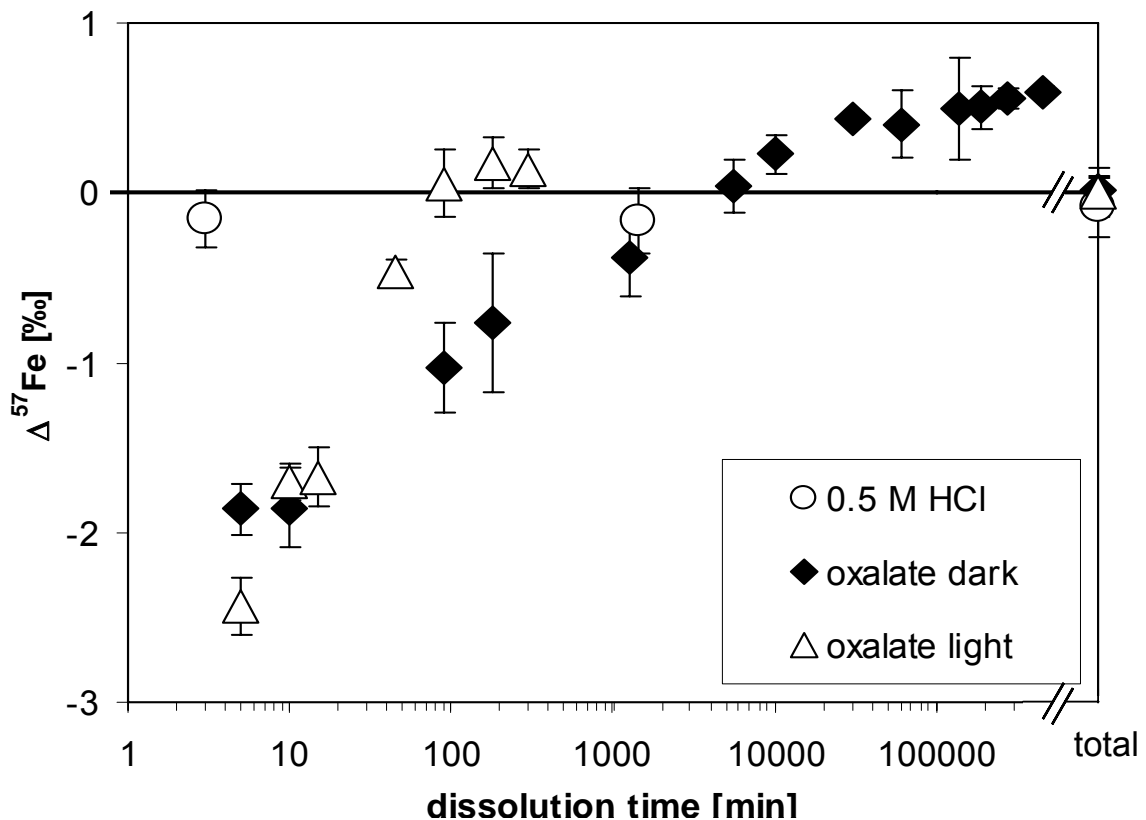


Figure 6.3 Iron isotopes in solution as a function of the dissolution time. Total dissolution of remaining solids was achieved in 6 M HCl. Error bars indicate 2SD of replicate measurements ($n = 3 - 6$).

In contrast, both ligand-controlled and reductive dissolution experiments result in significant fractionation of iron isotopes. In order to interpret these data, the course of the dissolution process is divided into an early and a late stage. The early dissolved fractions show a strong enrichment in the light isotope ^{54}Fe with $\Delta^{57}\text{Fe}$ values of -1.8 ‰ and -2.5 ‰ in the ligand-controlled and reductive dissolution experiments, respectively. A faster dissolution rate of light ^{54}Fe atoms compared to heavier ^{57}Fe atoms can explain the observed $\Delta^{57}\text{Fe}$ values in solution. This effect

diminishes over the course of the experiment and $\Delta^{57}\text{Fe}$ values gradually increase towards the isotopic composition of the bulk goethite (0 ‰) in later dissolved fractions. Preferential dissolution of light isotopes concurrently causes the remaining surface (and only the surface) to become depleted in light isotopes. Dissolution of a progressively heavier substrate results in the release of increasingly heavier iron from the surface until the released iron has the same isotopic composition as the bulk mineral phase at steady-state conditions (Brantley et al., 2004), while the reactive surface sites are enriched in heavy isotopes.

6.3.3 Model results

Figure 6.4 shows the model results of the kinetic isotope effect in the early-stage dissolution where $\Delta^{57}\text{Fe}$ is plotted as a function of dissolved fraction. We achieved the best fit for both ligand-controlled and reductive dissolution experiments using an enrichment factor ε of -2.6 ‰ for the $^{57}\text{Fe}/^{54}\text{Fe}$ ratio. This corresponds to -1.7 ‰ for the $^{56}\text{Fe}/^{54}\text{Fe}$ ratio. The size of the reactive surface site pool was fitted to be 2.4 % and 5.9 % of the monolayer for ligand-controlled and reductive dissolution, respectively. The higher value for the oxalate light experiments seems to indicate that photochemical reductive dissolution could occur on crystallographic sites that are not reactive in ligand-controlled dissolution. For example, ferrous iron released during reductive dissolution may form ternary surface complexes to oxalate adsorbed to the goethite surface (Suter et al., 1988) and electron transfer through the bridging ligand could result in reduction and subsequent release of Fe atoms at the goethite surface even from less labile crystallographic positions. The lack of independent information about the exact size of the reactive surface site pool certainly restricts the precision of our model. Information on the sensitivity of our model towards the size of the reactive surface site pool and the enrichment factor can be found in the supporting material. The resulting enrichment factor of -2.6 ‰ for both ligand-controlled and reductive dissolution corresponds to a fractionation factor $\alpha_{\text{goethite-solution}}$ of 1.0026 for the $^{57}\text{Fe}/^{54}\text{Fe}$ ratio. The enrichment factor equals $\Delta^{57}\text{Fe}$ in solution at the onset of the dissolution reaction. Our first samples were taken when surface depletion of the light isotope was already ongoing. However, $\Delta^{57}\text{Fe}$ values of the first dissolved fractions (-1.8 ‰ for oxalate dark and -2.5 ‰ for oxalate light) provide minimum estimates for the enrichment factor.

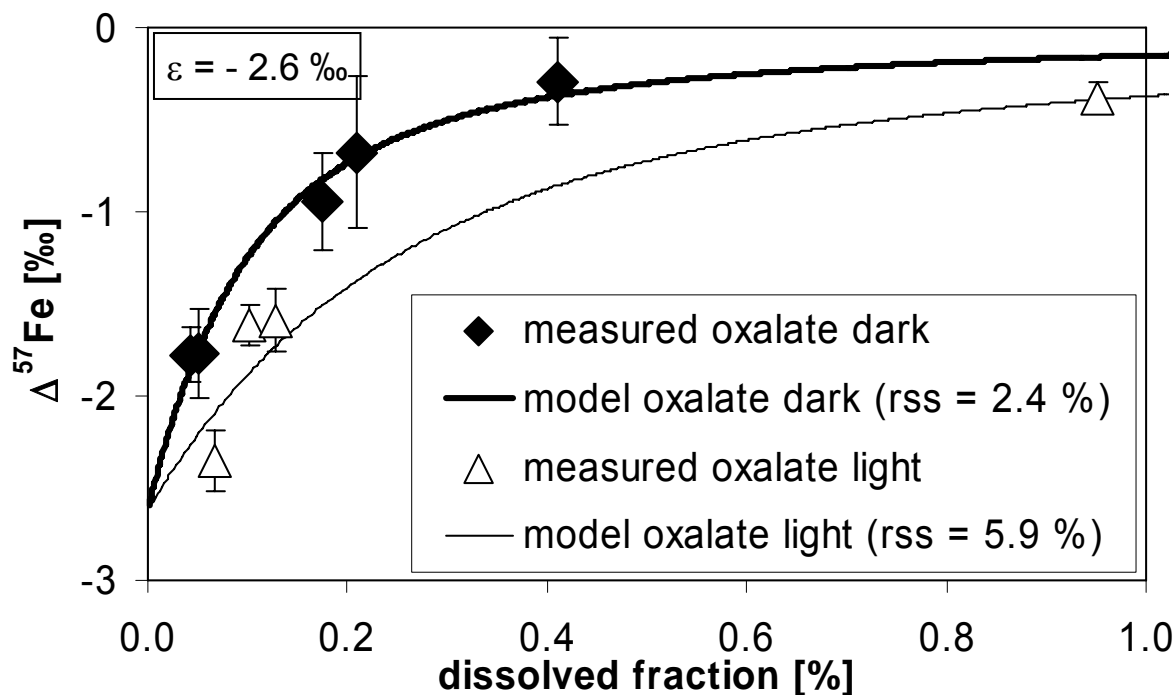


Figure 6.4 Modeling results of kinetic isotope effect during early dissolved fraction. The best fit was achieved with an enrichment factor ϵ of -2.6 ‰ and a size of the reactive surface site pool (rss) of 2.4 % of the surface monolayer for the oxalate dark experiments (ligand-controlled dissolution) and 5.9 % for the oxalate light experiments (reductive dissolution). A detailed description of the model is presented in Appendix 3 of this thesis.

6.3.4 Fractionation mechanism

The close proximity of iron isotope fractionation factors in ligand-controlled and reductive dissolution is interesting considering the different mechanisms and end products of the reactions. Ligand-controlled dissolution releases Fe(III)-ligand-complexes into solution whereas reductive dissolution produces aqueous Fe(II). However, in both cases the rate determining step is the detachment of the dissolving iron ions from the goethite surface. We propose that this step is responsible for the observed kinetic iron isotope fractionation. Several Fe-O bonds of the goethite lattice have to be broken during the detachment of iron from the surface (Figure 6.1). The bond energy differs between different iron isotopes and it is energetically easier to break a bond with a lighter ^{54}Fe isotope. This effect can explain the enrichment of light iron isotopes in solution during the kinetically controlled early stage dissolution.

However, $\Delta^{57}\text{Fe}$ in solution can only change if the mass of the detaching iron atom is causing the isotope effect. If the detaching iron atom carries along its coordinating oxygens of the lattice, i.e. if the detachment involves breaking of the bonds between the coordinating oxygen and adjacent iron atoms, no isotope fractionation is expected because the isotopic mass of the detaching iron has little effect on the bond breakage. The difference of iron isotope fractionation in proton-promoted and ligand-controlled dissolution may therefore be a consequence of differences in the nature of the bond exchange mechanism. Ligands such as oxalate directly attack the detaching iron atom, thereby weakening the bonds between the detaching iron atom and coordinating oxygen atoms (Holmen et al., 1996). We suggest that this induces breakage of these bonds and results in iron isotope fractionation. However, protonation of lattice oxygen atoms weakens the bonds to both detaching and adjacent iron atoms. It is unknown whether the detaching or remaining iron atoms get oxygen atoms from dissociating water molecules to reconstitute the octahedral coordination sphere of iron during proton-promoted dissolution (Casey and Ludwig, 1996). Lack of observed iron isotope fractionation may indicate bond breakage between oxygen and adjacent iron atoms during detachment.

Brantley et al. (2004) reported no significant iron isotope fractionation during ligand-controlled goethite dissolution in the presence of a siderophore, which was based on iron isotope measurements from a single dissolved fraction. Considering the evolution of $\Delta^{57}\text{Fe}$ in solution during dissolution, the results depend heavily on the sampling strategy and it is difficult to compare their results with ours.

6.3.5 Late stage dissolution

The kinetic fractionation model only explains the data of the early dissolved fractions within one surface monolayer. The model predicts the convergence of the iron isotope ratio in solution with the composition of the bulk solid ($\Delta^{57}\text{Fe} = 0 \text{ ‰}$) as the reaction proceeds. However, we observed an increase of $\Delta^{57}\text{Fe}$ in solution with increasing dissolution time exceeding the value of the bulk goethite (Figure 6.3). The solution of the ligand-controlled experiments (oxalate dark) reaches a plateau of $\Delta^{57}\text{Fe}$ at approximately +0.5 ‰ relative to the bulk goethite. A similar but smaller effect was observed during the reductive dissolution (oxalate light) with $\Delta^{57}\text{Fe}$ values of about +0.2 ‰.

Solubility calculations of Fe(III)-oxalate indicated that chemical equilibrium in our system was not reached before approximately three surface monolayers were dissolved (solubility and hydrolysis constants taken from Kraemer, 2004). However, no significant change in the isotopic composition of the solution was observed between the dissolution of the first surface monolayer (after four weeks) and the last measurement (after 315 days) when the system was very close to chemical equilibrium. Therefore, the attainment of the $\Delta^{57}\text{Fe}$ plateau value in solution of +0.5 ‰ in the ligand-controlled experiments did occur somewhat before the chemical equilibrium of the dissolution reaction was reached. However, the time scales to reach chemical and isotopic equilibrium can differ substantially (Beard and Johnson, 2004; Barling and Anbar, 2004). Mass balance considerations dictate that if the solution is enriched in heavy isotopes, the mineral surface must be enriched in light isotopes. Figure 6.5 shows the results of the leaching experiment with 0.5 M HCl that was performed at the end of the oxalate dark experiments after 315 days. Negative $\Delta^{57}\text{Fe}$ values in the leach solutions indicate the presence of an isotopically light surface iron pool on the goethite surface. In any case, the enrichment of heavy isotopes in the product of the reaction and the constant solution value over very long time periods (several months) suggests that equilibrium isotope fractionation rather than a kinetic effect is dominating the late stage dissolution of the ligand-controlled experiment.

Kinetic isotope effects can only be observed in incomplete and unidirectional reactions (Hoefs, 2004). However, if the dissolution reaction is approaching equilibrium and the back reaction is gaining in importance, kinetic isotope effects will eventually disappear. Then equilibrium isotope fractionation sets in, which is governed by energetic differences in the bonding environment of the reactant and the product (Hoefs, 2004). Isotope fractionation theory predicts that equilibrium fractionation enriches the heavier isotope in the stronger bonding environment (Schauble, 2004). It is possible that kinetic and equilibrium fractionation in the same system result in opposite effects especially if the product of the reaction provides a stronger bonding environment compared to the reactant. This seems to be the case for ligand-controlled dissolution where the main driving force of the reaction is the formation of iron-ligand complexes. Iron(III)-oxalate complexes in solution probably provide a stronger bonding environment than the goethite surface causing an

enrichment of heavy isotopes in the product of the reaction and positive $\Delta^{57}\text{Fe}$ values in solution. Consequently, an equilibrium isotope effect dominates during late stage dissolution leading to the enrichment of the heavy isotopes in solution. This hypothesis is supported by the observation of an isotopically light surface iron pool during the leach experiments. However, further work is certainly needed to confirm the equilibrium isotope effect. It is probable that different ligand complexes could have different equilibrium fractionation factors.

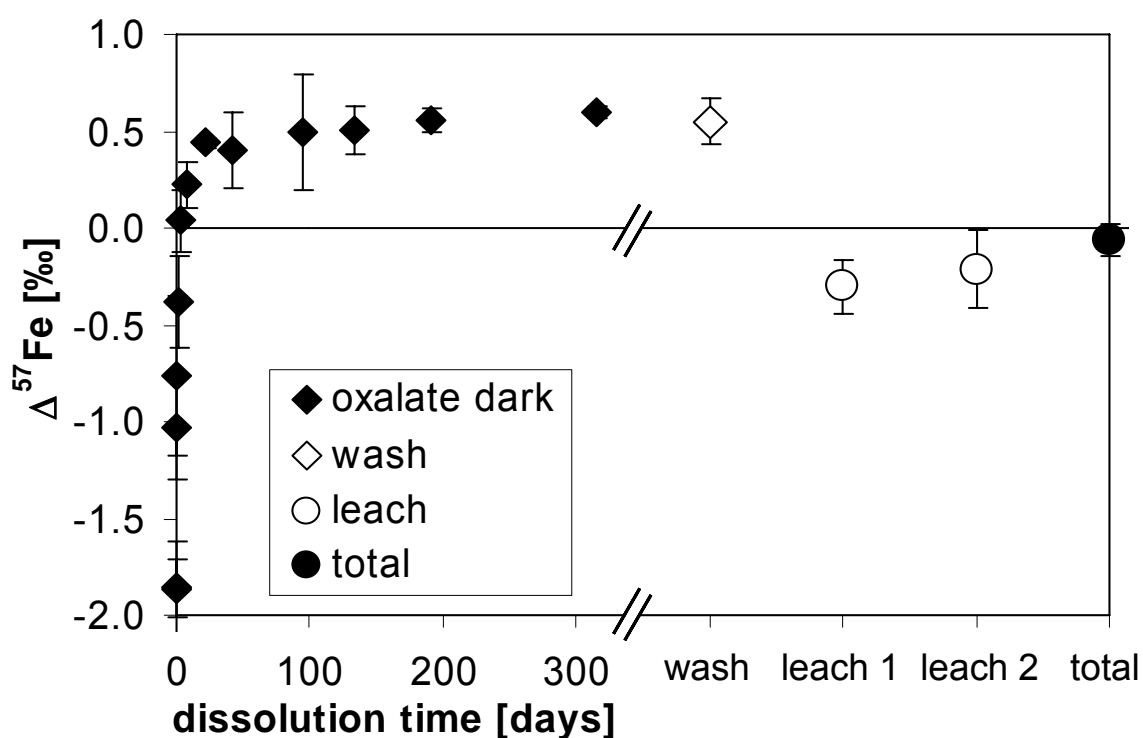


Figure 6.5 Late stage dissolution (oxalate dark) and leaching experiment. Dissolution was stopped after 315 days. The residue was washed with water (acidified to pH 4) and afterwards leached twice with 0.5 M HCl (leach 1: 15 min, leach 2: 90 min). The remaining residue was totally dissolved in 6 M HCl. Negative $\Delta^{57}\text{Fe}$ values of leach samples indicate the presence of an isotopically light surface iron pool. This is consistent with the concept of equilibrium isotope fractionation between “heavy” Fe(III)-oxalate-complexes in solution and a “light” goethite surface.

6.3.6 Environmental significance.

The dissolution of kinetically stable mineral phases in soils is often sustained by persistent strong disequilibria with the soil solution. Thus, it can be assumed that kinetic isotope effects dominate during dissolution reactions of iron oxide minerals in soils and sediments especially if a physical separation of reactant and product is taking place. However, it is possible that under certain conditions equilibrium fractionation effects become important in nature. Our finding of an inverse fractionation effect between kinetic early-stage and equilibrium late-stage processes during mineral dissolution may have important implications for the interpretation of iron isotope data in natural systems such as soils with highly heterogeneous solution chemistry at a small scale. In addition, our results indicate that oxalate extractions which are widely used to separate poorly-crystalline iron oxides from soil or sediment samples (Cornell and Schwertmann, 2003) are inappropriate for iron isotope studies. Extractions with 0.5 M HCl should be preferred due to the absence of isotope fractionation artifacts during the procedure. In summary, we have demonstrated that iron isotopes are significantly fractionated during dissolution of goethite by ligand-controlled and reductive dissolution, but not by proton-promoted dissolution. This work provides a detailed examination of iron isotope fractionation during mineral dissolution by different mechanisms. Our results will help to further develop iron isotopes as a powerful tool for the study of the biogeochemical iron cycle in nature.

ACKNOWLEDGEMENTS

We thank Kurt Barmettler for support in the laboratory, Nicholas Chambers for help during sampling and sample preparation, and the staff of the ETH MC-ICPMS lab for excellent maintenance and support. Ariel Anbar, Thomas D. Bullen, and two anonymous reviewers are thanked for their helpful comments. This research was funded by ETH Research Grant No. 01927.

SUPPORTING INFORMATION AVAILABLE

Additional data tables and a detailed model description are provided in Appendix 3.

REFERENCES

- Anbar AD (2004) Iron stable isotopes: beyond biosignatures. *Earth Planet. Sci. Lett.* **217**, 223–236.
- Barling J, Anbar AD (2004) Molybdenum isotope fractionation during adsorption by manganese oxides. *Earth Planet. Sci. Lett.* **217**, 315–329.
- Beard BL, Johnson CM, Cox L, Sun H, Neelson KH, Aguilar C (1999) Iron isotope biosignatures. *Science* **285**: 1889-1896.
- Beard BL, Johnson CM (2004) Fe isotope variations in the modern and ancient Earth and other planetary bodies. *Rev. Mineral. Geochem.* **55**, 319-357.
- Borer PM, Sulzberger B, Reichard P, Kraemer SM (2005) Effect of siderophores on the light-induced dissolution of colloidal iron(III) (hydr)oxides. *Mar. Chem.* **93**, 179-193.
- Brantley SL, Liermann L, Bullen TD (2001) Fractionation of Fe isotopes by soil microbes and organic acids. *Geology* **29**, 535-538.
- Brantley SL, Liermann LJ, Guynn RL, Anbar A, Icopini GA, Barling J (2004) Fe isotopic fractionation during mineral dissolution with and without bacteria. *Geochim. Cosmochim Acta* **68**, 3189-3204.
- Bullen TD, White AF, Childs CW, Vivit DV, Schulz MS (2001) Demonstration of significant abiotic iron isotope fractionation in nature. *Geology* **29**, 699-702.
- Casey WH, Ludwig C (1996) The mechanism of dissolution of oxide minerals. *Nature* **381**, 506-509.
- Cheah SF, Kraemer SM, Cervini-Silva J, Sposito G (2003) Steady-state dissolution kinetics of goethite in the presence of desferrioxamine B and oxalate ligands: implications for the microbial acquisition of iron. *Chem. Geol.* **198**, 63–75.
- Cornell RM, Posner AM, Quirk JP (1974) Crystal morphology and the dissolution of goethite. *J. Inorg. Nucl. Chem.* **36**, 1937-1946.
- Cornell RM, Schwertmann U (2003) The iron oxides – structure, properties, reactions, occurrence and uses. Second edition. VCH, Weinheim, Germany.
- Crosby HA, Johnson CM, Roden EE, Beard BL (2005) Coupled Fe(II)-Fe(III) electron and atom exchange as a mechanism for Fe isotope fractionation during dissimilatory iron oxide reduction. *Environ. Sci. Technol.* **39**, 6698-6704.
- Drever JI, Stillings LL (1997) The role of organic acids in mineral weathering. *Colloids and Surfaces A: Physicochemical and Engineering Aspects* **120**, 167-181.
- Fantle MS, DePaolo DJ (2004) Iron isotope fractionation during continental weathering. *Earth Planet. Sci. Lett.* **228**, 547–562.
- Halliday AN, Lee D-C, Christensen JN, Rehkämper M, Yi W, Luo X, Hall CM, Ballentine CJ, Pettke T, Stirling C (1998) Applications of multiple collector-ICPMS to cosmochemistry, geochemistry, and paleoceanography. *Geochim. Cosmochim. Acta* **62**, 919-940.
- Hoefs, J. (2004) Stable isotope geochemistry. 5th edition. Springer, Berlin, Germany.

- Holmen BA, Casey WH (1996) Hydroxamate ligands, surface chemistry, and the mechanism of ligand-promoted dissolution of goethite [α -FeOOH(s)]. *Geochim. Cosmochim. Acta* **60**, 4403-4416.
- Johnson CM, Beard BL, Albarède F (2004a) (eds.) Geochemistry of non-traditional stable isotopes. Reviews in Mineralogy and Geochemistry 55. Mineralogical Society of America and Geochemical Society, Washington, DC, US.
- Johnson CM, Beard BL, Roden EE, Newman DK, Nealson KH (2004b) Isotopic constraints on biogeochemical cycling of Fe. *Rev. Mineral. Geochem.* **55**, 359-408.
- Jones DL (1998) Organic acids in the rhizosphere – a critical review. *Plant Soil* **205**, 25-44.
- Koretsky CM, Sverjensky DA, Sahai N (1998) Surface site types on oxide and silicate minerals based on crystal chemistry: Implications for site types and densities, multi-site adsorption, surface infrared spectroscopy, and dissolution kinetics. *Amer. J. Sci.* **298**, 349-438.
- Kraemer SM (2004) Iron oxide dissolution and solubility in the presence of siderophores. *Aquat. Sci.* **66**, 3-18.
- LaKind JS, Stone AT (1989) Reductive dissolution of goethite by phenolic reductants. *Geochim. Cosmochim. Acta* **53**, 961-971.
- Lovley DR, Holmes DE, Nevin KP (2004) Dissimilatory Fe(III) and Mn(IV) reduction. *Adv. Microb. Physiol.* **49**, 219-286.
- Matthews A, Morgans-Bell HS, Emmanuel S, Jenkyns HC, Erel Y, Halicz L (2004) Controls on iron-isotope fractionation in organic-rich sediments (Kimmeridge Clay, Upper Jurassic, Southern England). *Geochim. Cosmochim. Acta* **68**, 3107-3123.
- Persson P, Axe K (2005) Adsorption of oxalate and malonate at the water-goethite interface: molecular surface speciation from IR spectroscopy. *Geochim. Cosmochim. Acta* **69**, 541-552.
- Reichard PU, Kraemer SM, Frazier S, Kretzschmar R (2005) Goethite dissolution in the presence of phytosiderophores: rates, mechanisms, and the synergistic effect of oxalate. *Plant Soil* **276**, 115-132.
- Schauble E (2005) Applying stable isotope fractionation theory to new systems. *Rev. Mineral. Geochem.* **55**, 65-111.
- Schoenberg R, von Blanckenburg F (2005) An assessment of the accuracy of stable Fe isotope ratio measurements on samples with organic and inorganic matrices by high-resolution multicollector ICP-MS. *Int. J. Mass. Spec.* **242**, 257-272.
- Schwertmann U, Cornell RM (2000) Iron oxides in the laboratory – preparation and characterization. Second edition. Wiley-VCH, Weinheim, Germany.
- Silvester E, Charlet L, Tournassat C, Géhin A, Grenèche J-M, Liger E (2005) Redox potential measurements and Mössbauer spectrometry of Fe^{II} adsorbed onto Fe^{III} (oxyhydr)oxides. *Geochim. Cosmochim. Acta* **69**, 4801-4815.
- Skulan JL, Beard BL, Johnson CM (2002) Kinetic and equilibrium Fe isotope fractionation between aqueous Fe(III) and hematite. *Geochim. Cosmochim. Acta* **66**, 2995-3015.

- Sulzberger B, Laubscher H (1995) Reactivity of various types of iron(III) (hydr)oxides towards light-induced dissolution. *Mar. Chem.* **50**, 103-115.
- Suter D, Siffert C, Sulzberger B, Stumm W (1988) Catalytic dissolution of iron(III) (hydr)oxides by oxalic acid in the presence of Fe(II). *Naturwissenschaften* **75**, 571-573.
- Teutsch N, von Gunten U, Porcelli D, Cirpka OA, Halliday AN (2005) Adsorption as a cause for iron isotope fractionation in reduced groundwater. *Geochim. Cosmochim. Acta* **69**, 4175-4185.
- Wehrli B, Wieland E, Furrer G (1990) Chemical mechanisms in the dissolution kinetics of minerals; the aspect of active sites. *Aquat. Sci.* **52**, 3-31.
- Wiederhold JG, Teutsch N, Kretzschmar R, Kraemer SM, Halliday AN (2004) Iron isotope fractionation during soil formation – comparison of ligand and redox controlled processes. *Geochim. Cosmochim. Acta* **68**, 11S: A415.
- Williams HM, McCammon CA, Peslier AH, Halliday AN, Teutsch N, Levasseur S, Burg J-P (2004) Iron isotope fractionation and the oxygen fugacity of the mantle. *Science* **304**, 1656-1659.
- Zinder B, Furrer G, Stumm W (1986) The coordination chemistry of weathering: II. Dissolution of Fe(III) oxides. *Geochim. Cosmochim. Acta* **50**, 1861–1869.

7. CONCLUSIONS

In the following section, a short overview on the most important findings and conclusions of this thesis will be given. In addition, a brief discussion of current trends and research needs of iron isotope geochemistry in soils is attempted.

The results of this thesis demonstrate unequivocally that iron isotopes are fractionated to a significant extent during pedogenic processes in soils. The magnitude of the observed fractionation effects is much higher than the limited range of iron isotope distributions in igneous rocks and similar to other low-temperature environments such as sediments and presumably the biosphere. The analysis of bulk soil samples exhibits variations of more than one per mil in $\delta^{57}\text{Fe}$ between different soil profiles or between different pedogenic horizons or zones of a single soil profile. The separation of iron in soil samples into individual mineral pools by the means of chemical extractions reveals that the variability of iron isotopes in soils is even considerably larger. It amounts to more than three per mil in $\delta^{57}\text{Fe}$ ranging from -1.55 ‰ relative to IRMM-014 in the HCl extract of an organic surface layer to +2.34 ‰ in the residual silicate fraction of a pedogenic B horizon. Iron isotope fractionations were observed during pedogenic iron transformations both under strongly acidic conditions in the presence of organic ligands and under variable redox conditions induced by water-saturation. The isotope effects observed in redoximorphic soils are probably mediated by the activity of microorganisms, whereas the isotope fractionation during podzolization is caused by abiotic processes under the influence of organic ligands. There is no evidence for a systematic difference in magnitude or direction between biotic and abiotic, or better between enzymatic and non-enzymatic, iron isotope effects in soils. This is important because the use of iron isotopes as a biosignature to differentiate biotic and abiotic processes had been proposed, as discussed in chapter 3. The concept of using iron isotope as a signature for microbial activity or other specific biogeochemical iron transformations might still be possible in certain cases. However, the application will be limited to circumstances in which the geochemical conditions are already reasonably well-constrained and the influence of other potential fractionating reaction can be excluded. Nevertheless, the results of this thesis also demonstrate that iron isotope fractionations in soils result in systematic patterns which are linked to specific pedogenic processes. The laboratory experiments, presented in chapter 6, have

shown that different dissolution mechanisms are causing iron isotope effects that are clearly distinct from each other. The strong iron isotope effects during ligand-controlled and reductive iron oxide dissolution contrast to the absence of iron isotope fractionation during proton-promoted dissolution, which may be explained by a different bond-breakage scheme compared to the other two mechanisms. Unfortunately, the magnitude and direction of ligand-controlled and reductive dissolution observed during goethite dissolution is fairly similar. Therefore, it will be difficult to differentiate iron transformations induced by ligand-controlled processes and reductive iron transformations based on their iron isotope signature. The soil profile data presented in chapter 4 and 5 indicate that light iron isotopes are preferentially translocated both during podzolization and under the influence of reductive iron transformations. However, the observed fractionation effects seem to be generally linked to the intensity of the pedogenetic transformations and the degree of soil development and mineral weathering. The strongest iron isotope fractionation effects were found in the Podzol profiles and the Stagnic Cambisol profile, which were both formed under extremely acidic conditions and can be considered as soils in a mature stage of soil development. In contrast, the iron isotope effects observed in the pedogenetically younger and less-developed Haplic Gleysol and Cambisol profile are smaller in magnitude. It is reasonable to assume that iron isotope fractionation effects in soils and between different iron mineral phases increase with the extent of soil formation. This trend is already apparent in the smaller range of iron isotope ratios between oxide-bound and silicate-bound iron phases in the younger cover sediment, which forms the upper two horizons of the Haplic Gleysol profile, compared to the slightly older material, which constitutes the lower horizons of the soil. However, a quantitative assessment of iron isotope fractionation effects in natural soil environments remains difficult. It is for instance not possible to construct a direct correlation between the extent of iron depletion and the associated iron isotope effect, which is discussed in chapter 5. This is mainly due to the fact that dissolution reactions are occurring only within a moving reaction front at the mineral surface. Therefore, the effect on the isotope ratio of the bulk material is not directly proportional to the overall extent of dissolution but rather dominated by transient surface effects. However, these surface effects are certainly not negligible in soil environments in which iron-bearing mineral phases are often characterized by small particle sizes and high specific surface areas. The development of iron isotope ratios

in solution during different dissolution stages of the laboratory experiments (chapter 6) display the variability of such a dynamic system. The enrichment of heavy iron isotopes in solution during the late stage of the dissolution experiments points towards the importance of possible equilibrium fractionation effects. Despite the general preference of light iron isotopes during pedogenetic iron transformations, which may be interpreted as indication for a control by kinetic effects, it can not be excluded that equilibrium isotope fractionation plays a significant role for iron isotope fractionation in soils or other natural environments.

In fact, the differentiation between kinetic and equilibrium isotope effects probably presents one of the major challenges of future work on iron isotope geochemistry. The interpretation of iron isotope signatures from natural environments requires a detailed understanding of fractionation mechanisms and their control by kinetic or thermodynamic constraints. The determination of equilibrium fractionation factors for a wide range of specific processes and reactions involving iron will be necessary in order to advance the scientific development of iron isotope geochemistry. This includes for instance solid-solution equilibria of a variety of mineral phases and solution species during precipitation and adsorption reactions. Adsorption reactions may certainly be of importance for iron isotope fractionation in natural systems, but the understanding of the involved mechanisms is still very limited. Research on equilibrium fractionations of iron isotopes has mainly focused on iron redox transformations. However, the different bonding environments which are for instance provided by organic complexes in solution may as well generate significant iron isotope effects. The theoretical prediction of equilibrium isotope fractionation, using computational approaches based on density functional theory or similar ab-initio methods, will certainly be useful in the future development of the scientific field. The predicted values will provide important hints for the interpretation of measured iron isotope data and contribute to the understanding of the fundamental principles behind iron isotope fractionation. Nevertheless, the validation of the predicted fractionation factors and the elucidation of the involved reaction mechanisms can only be achieved by careful laboratory work. Theoretical predictions for kinetic isotope effects are probably not possible in a quantitative manner. However, understanding the influence of kinetic effects on the iron isotope signature of natural samples might be at least equally important to equilibrium effects. It has

been shown for instance that iron isotope fractionation during precipitation of iron (oxyhydr)oxide phases is not only governed by equilibrium fractionation factors between solid and solution species, but also depend on the precipitation rate, hence the kinetics of the reaction. Another important aspect of future iron isotope research will probably focus on biosphere-geosphere interactions. The iron isotope signature of plants and other organisms is still almost completely unexplored. Initial trends indicate an enrichment of iron isotope along the food chain, but the behavior of iron isotopes in biological systems needs to be studied in more detail. A possible application in the context of soil systems presents the study of different iron acquisition strategies of plants in the rhizosphere. However, considering the importance of iron for biological systems, other important applications of iron isotopes as a useful tracer are likely to exist and to be explored in the future.

Despite the complexity of the involved mechanisms which are influencing the distribution of iron isotopes in natural environments, the analysis of iron isotope ratios will certainly be able to provide important clues for the understanding of the biogeochemical iron cycle in nature. The interpretations of iron isotope signatures of natural samples will become easier and more reliable in the future as a result of the current endeavors to disentangle the involved processes and mechanisms. These future developments should be seen in relation to the progress in the stable isotope geochemistry of light elements which has evolved over many decades and now proves to be useful in many applications. This certainly also includes applications which were not foreseen in the pioneering days of scientific development in the field. Moreover, it needs to be mentioned that iron isotopes are only one of several novel tools of stable isotope geochemistry. The analysis of stable isotope ratios of other elements (e.g., Mg, Si, Ca, Cr, Cu, Zn, Ge, Se, Mo, Cd, Sb, Te, Hg), which are still largely unexplored due to previous analytical limitations, represents a vast research field offering immense possibilities and prospects for earth and environmental sciences. In many cases, a multi-tracer approach, which is not build solely upon a single isotope system, will yield the best results.

Appendix 1

(referring to work presented in chapter 4)

Table A1.1 Iron concentrations and iron isotope ratios for Podzol A
(near Flaesheim / Westphalia, NW-Germany)

Iron concentrations

horizon German	horizons WRB	depth [cm]	Fe _{total} measured [mg/g soil]	Fe _{HCl} [mg/g soil]	Fe _{NH₂OH-HCl} [mg/g soil]	Fe _{residue} [mg/g soil]	Fe _{total} calculated [mg/g soil]
O _L	O1	-7	5.88	0.79	-	-	-
O _F	O2	-3	8.45	0.97	-	-	-
Ahe	Ah	1	4.23	0.88	1.74	1.70	4.31
Ae1	E1	4.5	2.00	0.28	0.84	0.84	1.97
Ae2	E2	9.5	1.94	0.15	0.95	0.73	1.84
Ae3	E3	14.5	2.40	0.13	1.41	0.73	2.27
Bh	Bh	18.5	10.13	5.77	4.63	1.27	11.66
Bs1	Bs1	21	19.36	13.07	6.25	1.49	20.81
Bs2	Bs2	26	11.16	5.22	5.85	1.36	12.43
ICv1	Bw	35	7.70	1.10	5.78	1.22	8.10
ICv2	BC	50	5.36	0.35	3.59	1.05	4.98
ICv3	C	70	4.22	0.13	2.92	1.15	4.20

Iron isotope ratios

horizon German	horizons WRB	depth [cm]	δ ⁵⁷ Fe _{total} measured [‰]	δ ⁵⁷ Fe _{HCl} [‰]	δ ⁵⁷ Fe _{NH₂OH-HCl} [‰]	δ ⁵⁷ Fe _{residue} [‰]	δ ⁵⁷ Fe _{total} calculated [‰]
O _L	O1	-7	0.12	-1.55	-	-	-
O _F	O2	-3	0.07	-1.54	-	-	-
Ahe	Ah	1	0.12	-0.31	-0.06	0.60	0.15
Ae1	E1	4.5	0.18	-0.38	-0.37	0.96	0.20
Ae2	E2	9.5	0.22	-0.26	-0.41	1.07	0.19
Ae3	E3	14.5	0.10	-0.21	-0.47	1.04	0.03
Bh	Bh	18.5	-0.44	-0.80	-0.55	2.34	-0.36
Bs1	Bs1	21	-0.15	-0.27	-0.30	1.40	-0.16
Bs2	Bs2	26	0.23	0.59	-0.13	1.43	0.34
ICv1	Bw	35	0.06	0.86	-0.24	1.71	0.21
ICv2	BC	50	0.44	0.53	0.11	2.22	0.59
ICv3	C	70	0.71	0.46	0.37	1.72	0.74

Table A1.2 Iron concentrations and iron isotope ratios for Podzol B
(near Klosterreichenbach / Black Forest, SW-Germany)

Iron concentrations

horizon German	horizons WRB	depth [cm]	Fe _{total} measured [mg/g soil]	Fe _{HCl} [mg/g soil]	Fe _{NH₂OH-HCl} [mg/g soil]	Fe _{residue} [mg/g soil]	Fe _{total} calculated [mg/g soil]
O _L	O1	-4	2.51	0.54	-	-	-
O _F	O2	-1.5	2.78	0.36	-	-	-
Ah	Ah	1.5	2.26	0.09	0.51	1.83	2.43
Ae1	E1	6.5	1.89	0.03	0.30	1.26	1.60
Ae2	E2	15	1.90	0.02	0.27	1.43	1.72
Ae3	E3	24	2.28	0.05	0.58	1.64	2.28
Bh	Bh	29	9.44	5.19	3.86	3.83	12.88
Bs1	Bs1	31.5	14.24	6.29	6.86	4.39	17.54
Bs2	Bs2	36.5	10.81	4.70	5.25	3.89	13.84
Bv1	Bw1	50	7.57	2.84	3.51	2.92	9.26
Bv2	Bw2	70	3.79	0.67	1.73	2.25	4.65
iiCv	C	95	7.43	0.49	3.49	3.62	7.60

Iron isotope ratios

horizon German	horizons WRB	depth [cm]	δ ⁵⁷ Fe _{total} measured [‰]	δ ⁵⁷ Fe _{HCl} [‰]	δ ⁵⁷ Fe _{NH₂OH-HCl} [‰]	δ ⁵⁷ Fe _{residue} [‰]	δ ⁵⁷ Fe _{total} calculated [‰]
O _L	O1	-4	0.06	-1.50	-	-	-
O _F	O2	-1.5	0.38	-1.38	-	-	-
Ah	Ah	1.5	0.48	-0.30	0.22	0.96	0.76
Ae1	E1	6.5	0.67	-0.08	0.21	1.06	0.88
Ae2	E2	15	0.61	-0.16	0.28	0.90	0.79
Ae3	E3	24	0.73	-0.50	-0.06	0.75	0.51
Bh	Bh	29	-0.03	-0.55	-0.13	1.06	0.06
Bs1	Bs1	31.5	0.55	0.21	0.00	0.87	0.29
Bs2	Bs2	36.5	0.73	0.40	0.10	0.87	0.42
Bv1	Bw1	50	0.58	0.34	0.00	0.83	0.37
Bv2	Bw2	70	0.77	0.95	-0.17	0.94	0.53
iiCv	C	95	0.74	0.63	0.09	0.77	0.45

Table A1.3 Iron concentrations and iron isotope ratios for Cambisol
(near Hewenegg / Hegau, SW-Germany)

Iron concentrations

horizon German	horizons WRB	depth [cm]	Fe _{total} measured [mg/g soil]	Fe _{HCl} [mg/g soil]	Fe _{NH₂OH-HCl} [mg/g soil]	Fe _{residue} [mg/g soil]	Fe _{total} calculated [mg/g soil]
Ah	Ah	10	114.80	16.82	78.23	26.40	121.45
Bv	Bw	30	115.00	17.56	81.13	20.74	119.43
iiCv1	BwC	60	111.35	18.28	74.15	26.20	118.63
iiCv2	C	80	111.62	16.23	75.05	27.99	119.27

Iron isotope ratios

horizon German	horizons WRB	depth [cm]	δ ⁵⁷ Fe _{total} measured [‰]	δ ⁵⁷ Fe _{HCl} [‰]	δ ⁵⁷ Fe _{NH₂OH-HCl} [‰]	δ ⁵⁷ Fe _{residue} [‰]	δ ⁵⁷ Fe _{total} calculated [‰]
Ah	Ah	10	0.17	-0.05	0.36	0.36	0.31
Bv	Bw	30	0.17	-0.02	0.32	0.30	0.27
iiCv1	BwC	60	0.32	-0.06	0.25	0.44	0.25
iiCv2	C	80	0.22	-0.13	0.33	0.33	0.27

Table A1.4.1 XRF measurements (Podzol A, Podzol B, Cambisol)
(err indicates absolute error in same unit as concentration value)

horizon	horizon	depth	Fe	Fe	Mn	Mn	Al	Al	Si	Si	Ti	Ti	Zr	Zr		
German	WRB	[cm]	%	err	%	err	%	err	%	err	%	err	µg/g	err		
Podzol A																
O _L	O1	-7	0.503	0.001	0.0126	0.0001	0.333	0.004	7.51	0.01	0.051	0.000	104.1	0.4		
O _F	O2	-3	0.744	0.002	0.0111	0.0001	0.484	0.005	7.10	0.01	0.055	0.000	84.9	0.4		
Ahe	Ah	1	0.329	0.002	0.0042	0.0001	0.443	0.008	40.38	0.05	0.137	0.001	322.2	0.8		
Ae1	E1	4.5	0.186	0.001	0.0043	0.0001	0.280	0.007	41.98	0.05	0.129	0.001	293.6	0.7		
Ae2	E2	9.5	0.153	0.001	0.0035	0.0000	0.275	0.007	42.64	0.06	0.128	0.001	293.6	0.7		
Ae3	E3	14.5	0.190	0.001	0.0029	0.0000	0.209	0.006	43.10	0.06	0.128	0.001	297.7	0.7		
Bh	Bh	18.5	0.820	0.002	0.0031	0.0000	0.737	0.009	36.85	0.05	0.139	0.001	256.7	0.7		
Bs1	Bs1	21	1.587	0.003	0.0087	0.0001	0.707	0.010	37.65	0.05	0.135	0.001	285.7	0.7		
Bs2	Bs2	26	0.866	0.003	0.0043	0.0001	0.876	0.011	40.12	0.05	0.129	0.001	269.5	0.7		
ICv1	Bw	35	0.569	0.002	0.0041	0.0001	0.844	0.010	41.26	0.05	0.119	0.000	272.6	0.7		
ICv2	BC	50	0.391	0.002	0.0037	0.0001	0.631	0.010	41.96	0.05	0.115	0.000	299.8	0.7		
ICv3	C	70	0.319	0.002	0.0031	0.0000	0.543	0.009	42.23	0.05	0.107	0.000	292.6	0.7		
Podzol B																
O _L	O1	-4	0.244	0.001	0.0157	0.0001	0.334	0.003	5.30	0.01	0.048	0.000	48.7	0.3		
O _F	O2	-1.5	0.545	0.002	0.0137	0.0001	0.794	0.007	19.68	0.03	0.126	0.000	110.1	0.5		
Ahe	Ah	1.5	0.242	0.001	0.0037	0.0001	0.707	0.010	40.15	0.05	0.143	0.001	190.1	0.6		
Ae1	E1	6.5	0.168	0.001	0.0023	0.0000	0.593	0.009	42.14	0.05	0.108	0.001	161.8	0.6		
Ae2	E2	15	0.220	0.001	0.0043	0.0001	0.661	0.010	42.20	0.05	0.113	0.001	172.4	0.6		
Ae3	E3	24	0.223	0.001	0.0032	0.0000	1.019	0.011	41.49	0.05	0.124	0.001	175.2	0.6		
Bh	Bh	29	1.304	0.003	0.0139	0.0001	2.597	0.014	33.91	0.05	0.156	0.001	153.4	0.6		
Bs1	Bs1	31.5	1.455	0.003	0.0080	0.0001	3.902	0.016	32.21	0.04	0.142	0.001	129.4	0.5		
Bs2	Bs2	36.5	1.123	0.003	0.0073	0.0001	4.100	0.017	33.23	0.04	0.128	0.001	124.5	0.5		
ICv1	Bw	50	0.844	0.002	0.0113	0.0001	3.456	0.016	34.56	0.05	0.101	0.001	125.4	0.5		
ICv2	BC	70	0.442	0.002	0.0135	0.0001	2.697	0.015	37.15	0.05	0.055	0.000	90.7	0.5		
ICv3	C	95	0.692	0.002	0.0129	0.0001	3.387	0.016	37.14	0.05	0.077	0.000	92.8	0.5		
Cambisol																
Ah	Ah	10	9.138	0.011	0.2290	0.0006	4.511	0.020	17.87	0.03	2.267	0.003	437.5	1.3		
Bv	Bw	30	9.439	0.011	0.2165	0.0005	5.834	0.023	17.55	0.03	2.003	0.003	367.9	1.2		
iICv1	BwC	60	9.148	0.011	0.3165	0.0006	6.333	0.023	17.62	0.03	1.625	0.003	313.3	1.1		
iICv2	C	80	9.129	0.011	0.2719	0.0006	5.988	0.023	17.76	0.03	1.663	0.003	315.0	1.2		
Podzol A																
O _L	O1	-7	0.139	0.001	0.584	0.001	< 0.071	-0.05	0.12	0.01	77.9	1.4	5.4	0.2	13.8	0.2
O _F	O2	-3	0.149	0.001	1.077	0.002	< 0.078	0.00	0.21	0.01	100.4	1.4	5.8	0.2	16.6	0.2
Ahe	Ah	1	0.146	0.001	0.029	0.000	< 0.16	0.00	< 0.032	0.00	77.0	1.4	5.6	0.2	12.1	0.2
Ae1	E1	4.5	0.103	0.001	0.018	0.000	< 0.16	-0.05	< 0.033	0.00	52.8	1.4	3	0.2	9.2	0.2
Ae2	E2	9.5	0.089	0.001	0.012	0.000	< 0.16	0.00	0.03	0.00	64.4	1.4	2.8	0.2	8.7	0.2
Ae3	E3	14.5	0.108	0.001	0.009	0.000	< 0.16	-0.09	< 0.033	-0.02	55.9	1.4	4	0.2	9.5	0.2
Bh	Bh	18.5	0.200	0.001	0.037	0.000	< 0.15	0.00	0.06	0.01	87.6	1.5	8.7	0.2	14.1	0.2
Bs1	Bs1	21	0.261	0.001	0.035	0.000	< 0.16	0.00	0.04	0.01	100.1	1.5	11.4	0.3	15.8	0.3
Bs2	Bs2	26	0.269	0.001	0.031	0.000	< 0.16	0.00	0.07	0.01	89.6	1.4	10.9	0.3	15.7	0.3
ICv1	Bw	35	0.251	0.001	0.025	0.000	0.27	0.06	< 0.033	-0.03	78.7	1.4	9.9	0.2	14.9	0.3
ICv2	BC	50	0.187	0.001	0.010	0.000	< 0.16	-0.07	0.09	0.01	65.0	1.4	8.2	0.2	11.8	0.2
ICv3	C	70	0.166	0.001	0.007	0.000	< 0.16	0.00	0.04	0.01	61.0	1.4	6.9	0.2	11	0.2
Podzol B																
O _L	O1	-4	0.209	0.001	0.607	0.001	< 0.060	-0.03	0.08	0.01	100.2	1.4	8.7	0.2	24.8	0.2
O _F	O2	-1.5	0.563	0.002	0.155	0.001	0.10	0.03	0.10	0.01	134.4	1.6	17.1	0.2	27.5	0.3
Ahe	Ah	1.5	0.591	0.002	0.013	0.000	< 0.15	-0.12	0.06	0.01	127.3	1.5	21.5	0.3	28.5	0.3
Ae1	E1	6.5	0.511	0.002	0.008	0.000	< 0.16	0.00	< 0.034	-0.01	110.0	1.5	18.4	0.3	22.2	0.3
Ae2	E2	15	0.566	0.002	0.007	0.000	< 0.16	0.00	0.05	0.01	115.9	1.5	20.6	0.3	23.2	0.3
Ae3	E3	24	0.810	0.002	0.008	0.001	< 0.16	0.00	< 0.033	-0.03	161.0	1.6	32.6	0.3	29.4	0.3
Bh	Bh	29	1.254	0.003	0.012	0.001	< 0.15	-0.07	0.11	0.01	242.7	1.7	73.9	0.4	44.2	0.3
Bs1	Bs1	31.5	1.442	0.003	0.016	0.001	< 0.14	-0.09	0.14	0.01	277.5	1.7	79.4	0.5	43.1	0.3
Bs2	Bs2	36.5	1.557	0.003	0.018	0.001	< 0.14	-0.11	0.14	0.01	290.4	1.7	75.6	0.5	41.7	0.3
ICv1	Bw	50	1.752	0.004	0.016	0.001	< 0.15	0.00	0.13	0.01	315.9	1.8	71.2	0.4	43.6	0.3
ICv2	BC	70	1.944	0.004	0.009	0.001	< 0.15	0.00	0.07	0.01	359.2	1.8	66.9	0.4	40.2	0.3
ICv3	C	95	2.335	0.004	0.009	0.001	< 0.15	-0.13	0.15	0.01	424.6	1.9	90	0.5	53.8	0.4
Cambisol																
Ah	Ah	10	0.547	0.003	2.687	0.005	< 0.19	0.00	1.96	0.03	954.5	2.7	65.8	0.6	220.9	0.9
Bv	Bw	30	0.396	0.002	1.970	0.004	< 0.18	0.00	2.56	0.03	1048.0	3.0	64.5	0.6	250.8	1
iICv1	BwC	60	0.410	0.002	2.581	0.005	< 0.19	0.00	2.45	0.03	861.6	2.6	69.8	0.6	314.6	1.1
iICv2	C	80	0.330	0.002	3.354	0.006	< 0.18	0.00	2.58	0.03	766.4	2.5	58.7	0.6	420.3	1.3

Table A1.4.2

XRF measurements (Podzol A, Podzol B, Cambisol)
(err indicates absolute error in same unit as concentration value)

horizon	horizon	depth	As	As	Sb	Sb	Sn	Sn	Br	Br	Y	Y	Nb	Nb	La	La	Ce	Ce
German	WRB	[cm]	µg/g	err	µg/g	err	µg/g	err	µg/g	err	µg/g	err	µg/g	err	µg/g	err	µg/g	err
Podzol A																		
O _L	O1	-7	4.5	0.5	4.2	0.2	3	0.1	14.8	0.2	1.7	0.2	0.6	0.1	12	1.7	20.1	2.4
O _F	O2	-3	6.4	0.7	4.8	0.2	6.5	0.2	17.8	0.3	1.8	0.2	1.4	0.1	11	1.7	20	2.4
Ahe	Ah	1	6.8	0.5	1.7	0.2	2.8	0.1	5.6	0.3	8.1	0.3	4.4	0.1	9.1	1.7	20	2.5
Ae1	E1	4.5	3.2	0.3	1	0.2	1.1	0.1	3.3	0.2	6.2	0.3	4.1	0.1	12.5	1.8	21.6	2.5
Ae2	E2	9.5	2.2	0.2	1.4	0.2	1.3	0.1	2	0.3	6.3	0.3	3.7	0.1	35.8	1.8	62.4	2.5
Ae3	E3	14.5	2.7	0.2	< 0.3	0	0.9	0.1	2.3	0.2	5.9	0.3	3.8	0.1	16.7	1.8	31.1	2.4
Bh	Bh	18.5	4	0.3	< 0.3	0	1.1	0.1	33.7	0.4	5.9	0.3	3.8	0.1	8.2	1.7	23.9	2.5
Bs1	Bs1	21	3.7	0.3	0.3	0.2	0.8	0.1	15.4	0.3	6.2	0.3	3	0.1	27.7	1.9	48	2.5
Bs2	Bs2	26	3.1	0.2	0.5	0.2	0.7	0.1	14.5	0.3	5.4	0.3	2.7	0.1	14.3	1.8	27.2	2.5
ICv1	Bw	35	2.3	0.2	< 0.3	0	0.9	0.1	8.9	0.3	5.2	0.3	3.7	0.1	6.5	1.7	16	2.5
ICv2	BC	50	1.5	0.1	0.7	0.2	0.6	0.1	4.7	0.3	4.7	0.3	3.3	0.1	5.7	1.6	15.2	2.4
ICv3	C	70	1.5	0.1	< 0.3	0	1	0.1	3.4	0.2	4.7	0.3	2.6	0.1	8.1	1.7	19.5	2.4
Podzol B																		
O _L	O1	-4	4.5	0.4	2.3	0.2	2.6	0.1	12.5	0.2	1.5	0.2	< 0.3	-0.1	10.3	1.6	25.4	2.3
O _F	O2	-1.5	4.6	0.5	2.6	0.2	3.3	0.1	10.3	0.3	5.9	0.3	2.1	0.1	18.9	1.9	31.4	2.6
Ahe	Ah	1.5	2.2	0.2	0.8	0.2	1.4	0.1	3.2	0.3	8.5	0.3	5.6	0.1	7.5	1.7	18.9	2.4
Ae1	E1	6.5	1.8	0.1	< 0.3	0	1.1	0.1	2.8	0.2	7.1	0.3	4.6	0.1	15.3	1.8	24.5	2.5
Ae2	E2	15	2.3	0.2	0.9	0.2	1.5	0.1	1.9	0.2	7.6	0.3	3.9	0.1	12.2	1.7	20.9	2.4
Ae3	E3	24	1.9	0.2	< 0.3	0	1.3	0.1	3.1	0.3	7.8	0.3	4.8	0.1	7.6	1.7	18.5	2.5
Bh	Bh	29	9.5	0.5	1.3	0.2	2.5	0.1	9.2	0.3	7.9	0.4	6.3	0.2	12.6	1.8	30.2	2.6
Bs1	Bs1	31.5	8.1	0.4	1.1	0.2	2.6	0.1	21.8	0.4	7.9	0.4	7.8	0.2	14.5	1.8	32.2	2.6
Bs2	Bs2	36.5	7.6	0.4	1.3	0.2	1.9	0.1	21.4	0.4	7.7	0.4	6.4	0.2	15.2	1.8	28.1	2.5
ICv1	Bw	50	5.3	0.3	1.5	0.2	1.9	0.1	11.7	0.3	6.6	0.3	5.6	0.2	10.7	1.7	21.4	2.5
ICv2	BC	70	3.7	0.3	1.2	0.2	1.7	0.1	10.3	0.3	4.6	0.3	3.5	0.1	8.1	1.7	12.5	2.4
ICv3	C	95	5.5	0.3	1	0.2	1.9	0.1	7.3	0.3	5.5	0.4	3.9	0.1	4.9	1.5	17.4	2.5
Cambisol																		
Ah	Ah	10	7.9	0.7	< 0.4	0	3.1	0.2	4	0.3	28.6	0.6	158.5	0.5	107.7	2.1	246.4	2.9
Bv	Bw	30	6.2	0.6	< 0.4	0	3.2	0.2	6.3	0.3	20.6	0.5	128.8	0.5	74.7	2.1	224.3	2.9
ilCv1	BwC	60	5.3	0.6	< 0.4	0	3.2	0.2	6	0.3	33.6	0.6	101.5	0.4	98.6	2.2	228.4	3
ilCv2	C	80	5.3	0.5	< 0.4	0	2.9	0.2	5.5	0.3	35.2	0.6	104.8	0.5	99.2	2.2	206.3	2.9
Podzol A																		
O _L	O1	-7	27.9	4.9	8.9	0.2	1.1	0.2	121.4	1	< 0.6	0	0.114	0.001	3009	7	334.2	1.7
O _F	O2	-3	18.1	4.7	8.3	0.2	0.8	0.2	178.2	1.2	< 0.7	0	0.106	0.001	2973	7	412.4	1.9
Ahe	Ah	1	15.1	4.8	11.3	0.3	4	0.4	55.8	0.9	4.9	0.3	0.012	0.000	234.6	3.3	39.5	0.9
Ae1	E1	4.5	17.7	4.9	11.3	0.3	3	0.3	15.6	0.7	2.2	0.3	< 0.0013	0.000	192.4	2.8	43.3	1
Ae2	E2	9.5	90.0	5.2	11.4	0.3	2.3	0.3	7.1	0.6	2.5	0.3	< 0.0017	0.000	< 20	0	122.8	1.9
Ae3	E3	14.5	33.5	5.0	11.3	0.3	3.1	0.3	5.1	0.6	2.4	0.3	< 0.0013	0.000	< 20	0	< 10	0
Bh	Bh	18.5	< 9.2	0.0	11.8	0.3	1.8	0.3	12.6	0.6	3.5	0.3	0.054	0.001	206.1	2.9	67	1.2
Bs1	Bs1	21	67.7	5.3	13.2	0.3	2.6	0.3	7.3	0.6	2.8	0.3	0.195	0.002	87	1.5	120.7	1.8
Bs2	Bs2	26	25.8	5.0	12.6	0.3	2.6	0.3	5.6	0.6	2.5	0.3	0.103	0.001	< 20	-16	70.2	1.3
ICv1	Bw	35	9.6	4.6	12.1	0.3	2.6	0.3	4.4	0.6	2.9	0.3	0.028	0.001	< 20	0	161.4	2.3
ICv2	BC	50	< 9.1	0.0	12.1	0.3	2.7	0.3	4.6	0.6	3	0.3	0.006	0.000	< 20	0	9.7	0.3
ICv3	C	70	26.3	5.0	11.8	0.3	2.6	0.3	4.4	0.6	2.6	0.3	< 0.0015	0.000	< 20	0	13.2	0.4
Podzol B																		
O _L	O1	-4	28.1	4.7	7.5	0.2	< 0.5	0	76.3	0.8	2.3	0.2	0.079	0.001	1961	5	325.7	1.5
O _F	O2	-1.5	< 9.8	0.0	10.9	0.3	1.6	0.3	58.1	0.9	4.7	0.3	0.081	0.001	2158	8	333	2.2
Ahe	Ah	1.5	11.9	4.5	11.2	0.3	2.7	0.3	12.9	0.6	4.3	0.3	0.003	0.000	91.2	1.6	59.3	1.2
Ae1	E1	6.5	26.1	5.0	10.4	0.3	2.7	0.3	5.5	0.6	2.8	0.3	< 0.0016	0.000	< 20	0	48.9	1.1
Ae2	E2	15	19.9	4.8	10.4	0.3	3.3	0.3	4	0.6	3.5	0.3	< 0.0017	0.000	< 20	0	49.2	1.1
Ae3	E3	24	19.5	4.9	11.5	0.3	2.5	0.3	6.6	0.6	4.6	0.3	< 0.0015	0.000	< 20	0	61.3	1.2
Bh	Bh	29	26.6	5.1	12.8	0.3	2.3	0.3	24.4	0.8	4.6	0.4	0.020	0.001	138.5	2.2	92.6	1.6
Bs1	Bs1	31.5	18.6	4.8	13.1	0.4	2.3	0.3	21	0.8	4	0.4	0.026	0.001	182.2	2.5	171	2.1
Bs2	Bs2	36.5	21.4	4.8	12.9	0.4	2.3	0.3	14.1	0.7	5.5	0.4	0.022	0.001	154	2.3	145.5	1.9
ICv1	Bw	50	12.9	4.4	12.4	0.4	2.5	0.3	10	0.6	4.4	0.4	0.017	0.000	52.3	1	135.6	1.8
ICv2	BC	70	< 9.2	0.0	11.5	0.4	2.2	0.3	8.4	0.6	3.4	0.3	0.008	0.000	< 20	0	138.9	2
ICv3	C	95	< 9.4	-8.4	12.7	0.4	2.6	0.3	9.6	0.7	4.6	0.4	< 0.0013	0.000	< 20	0	131.6	1.9
Cambisol																		
Ah	Ah	10	139.0	5.6	17.6	0.7	1.6	0.5	25.3	1.1	12.8	0.6	0.306	0.002	335.8	4.5	83.4	1.7
Bv	Bw	30	51.8	5.2	28.7	0.8	< 1.2	0	16.3	1	13.6	0.6	0.293	0.002	64.2	1.4	32.5	0.9
ilCv1	BwC	60	57.9	5.3	34.7	0.8	1.5	0.5	17.4	1	12.9	0.6	0.281	0.002	< 20	-14	14	0.5
ilCv2	C	80	78.8	5.5	31.2	0.8	< 1.1	0	14.1	1	10.9	0.6	0.333	0.002	25.6	0.7	17.1	0.6

Table A1.4.3

XRF measurements (Podzol A, Podzol B, Cambisol)
(err indicates absolute error in same unit as concentration value)

horizon	horizon	depth	V	V	Cr	Cr	Co	Co	Ni	Ni	Cu	Cu	Zn	Zn	Ga	Ga	Ge	Ge
German	WRB	[cm]	µg/g	err	µg/g	err	µg/g	err	µg/g	err	µg/g	err	µg/g	err	µg/g	err	µg/g	err
Podzol A																		
O _L	O1	-7	29	0.9	30.4	0.4	9.8	1.4	9.1	0.6	18.6	0.5	90	0.8	2.4	0.2	<0.8	0
O _F	O2	-3	26.8	1.1	34.6	0.4	11.9	1.8	13.7	0.7	28.7	0.6	108.5	1	3.6	0.3	0.5	0.1
Ahe	Ah	1	28.9	1.6	31.7	0.5	109	2.8	3.5	0.8	30.6	1	17.1	1.1	3.8	0.3	5	0.5
Ae1	E1	4.5	22.3	1.5	32.1	0.5	124	2.5	3.4	0.8	6.9	0.6	8.4	0.8	3.8	0.3	4.2	0.4
Ae2	E2	9.5	19.1	1.5	29.4	0.5	117	2.4	2.3	0.6	3.4	0.4	6.1	0.7	2.9	0.3	4.6	0.4
Ae3	E3	14.5	20.9	1.5	31.4	0.5	113	2.5	<2.6	0	4.5	0.5	7.3	0.8	2.8	0.3	3.7	0.4
Bh	Bh	18.5	41.4	1.7	34.3	0.5	59	3.4	2.6	0.7	6.2	0.5	11.1	0.8	5	0.3	<2.1	-0.7
Bs1	Bs1	21	59.3	1.7	47.8	0.6	73.9	4.7	4.2	0.9	2.6	0.3	14.3	1	5	0.3	<2.5	-1.2
Bs2	Bs2	26	40	1.7	40.4	0.6	84.4	3.7	4.6	1	2.2	0.3	14.7	1	3.5	0.3	2	0.3
ICv1	Bw	35	36	1.6	35.6	0.6	96.8	3.3	5.4	1	3.5	0.4	13.8	1	4.1	0.3	3.2	0.4
ICv2	BC	50	38.5	1.6	38.3	0.6	103	2.9	6.1	1	3.4	0.4	13.6	1	3.6	0.3	3	0.3
ICv3	C	70	34.4	1.6	35.1	0.6	112	2.8	5.1	1	1.2	0.2	11.7	0.9	3.6	0.3	5.9	0.5
Podzol B																		
O _L	O1	-4	9.1	0.8	13.5	0.3	3.1	0.6	4.6	0.5	9.4	0.4	61.8	0.7	2	0.2	0.7	0.2
O _F	O2	-1.5	13.8	1.4	30.6	0.4	4.9	1.5	4.9	0.8	8.2	0.5	34.2	0.8	2.8	0.2	1.1	0.2
Ahe	Ah	1.5	8.9	1.4	19.3	0.4	96.5	2.5	4	0.8	4	0.4	11.3	0.9	3.9	0.3	4.6	0.4
Ae1	E1	6.5	6.6	1.2	17.9	0.4	120	2.4	3.4	0.8	2.7	0.3	7.3	0.8	3	0.3	4.7	0.4
Ae2	E2	15	9	1.3	21.2	0.4	116	2.6	4.6	0.9	1	0.2	5.7	0.7	3.5	0.3	5	0.5
Ae3	E3	24	7.1	1.3	20.4	0.4	129	2.7	3.9	0.8	2.5	0.3	5.4	0.7	5.2	0.4	5.8	0.5
Bh	Bh	29	37	1.9	43	0.6	61.2	4.1	6	1	3.5	0.4	9.4	0.8	10.4	0.5	2.5	0.3
Bs1	Bs1	31.5	32.2	1.8	36.7	0.6	59.8	4.4	7.5	1.1	3	0.3	11.1	0.9	10.3	0.4	2.5	0.3
Bs2	Bs2	36.5	26.2	1.8	31.5	0.5	61.6	4	7.7	1.1	2.7	0.3	13.3	0.9	8.9	0.4	<2.2	-1.3
ICv1	Bw	50	21	1.6	31.7	0.5	56.7	3.5	6.8	1	3.6	0.4	10.8	0.8	6	0.4	2.9	0.4
ICv2	BC	70	12.9	1.3	18	0.4	55.9	2.7	4.8	0.9	1.7	0.2	6.5	0.7	4.5	0.3	<2.2	-1
ICv3	C	95	21.4	1.6	21.8	0.5	83.9	3.5	5.1	1	3.9	0.4	8.2	0.9	7.2	0.4	3.9	0.4
Cambisol																		
Ah	Ah	10	1202	11	882.9	4.2	62.6	7.2	221.1	3.8	63.8	1.7	110.4	1.8	17.1	0.8	<1.4	0
Bv	Bw	30	1485	11	580.3	3.4	63.8	7.3	343.9	4.5	94.1	2	106.1	1.7	22.4	0.8	2.3	0.5
iICv1	BwC	60	1532	10	508.8	3.3	33.7	4.3	280.1	4	89.1	2	100.8	1.7	22.4	0.8	0.8	0.4
iICv2	C	80	1485	11	472	3.2	25.9	3.8	270.5	4	90.7	2	104.9	1.7	20.8	0.8	1	0.4
Podzol A																		
O _L	O1	-7	0.7	0.2	2.5	0.3	0.3	0.1	0.8	0.1	<0.2	0	<0.3	0	7	0.5	3.5	0.8
O _F	O2	-3	1.3	0.2	2.4	0.2	0.9	0.1	0.8	0.1	<0.2	0	0.7	0.2	10.9	0.5	2.1	0.7
Ahe	Ah	1	1.4	0.6	1.7	0.4	<0.2	0	0.5	0.1	<0.2	0	<0.3	0	3.5	0.5	3.3	0.9
Ae1	E1	4.5	2.3	0.6	0.5	0.2	<0.2	0	<0.2	0	0.3	0.1	<0.3	0	<0.9	-0.3	2.2	0.8
Ae2	E2	9.5	1.7	0.6	<0.8	0	<0.2	0	<0.2	0	0.2	0.1	1.1	0.2	3.9	0.5	9.8	0.9
Ae3	E3	14.5	<1.0	0	0.8	0.3	<0.2	0	<0.2	0	<0.2	0	<0.3	0	<0.8	0	4.6	0.9
Bh	Bh	18.5	1.8	0.4	0.7	0.3	<0.2	0	0.2	0.1	0.3	0.1	<0.3	0	11.7	0.6	<1.6	0
Bs1	Bs1	21	1.9	0.5	0.4	0.2	<0.2	0	0.2	0.1	<0.2	0	<0.3	0	8.7	0.5	5.8	0.9
Bs2	Bs2	26	1.6	0.5	0.6	0.2	<0.2	0	<0.2	0	<0.2	0	<0.3	0	6.2	0.5	3.3	0.8
ICv1	Bw	35	<0.9	0	0.8	0.3	<0.2	0	<0.2	0	0.2	0.1	<0.3	0	2.6	0.5	1.4	0.7
ICv2	BC	50	<0.9	0	1	0.3	<0.2	0	<0.2	0	<0.2	0	0.6	0.2	1.3	0.5	<1.6	0
ICv3	C	70	<1.0	0	0.6	0.2	<0.2	-0.1	<0.2	-0.1	<0.2	0	<0.3	0	<0.8	0	<1.6	-0.7
Podzol B																		
O _L	O1	-4	0.2	0.1	0.3	0.1	<0.1	0	0.7	0.1	<0.1	0	<0.3	0	5.3	0.5	2.5	0.7
O _F	O2	-1.5	0.4	0.2	1.1	0.2	0.5	0.1	0.4	0.1	0.5	0.1	<0.3	0	4.9	0.6	3.8	0.8
Ahe	Ah	1.5	<1.0	-0.3	0.5	0.2	<0.2	0	0.2	0.1	<0.2	0	<0.3	0	0.7	0.5	<1.6	0
Ae1	E1	6.5	1.3	0.6	0.4	0.2	<0.2	0	0.3	0.1	<0.2	-0.1	<0.3	0	<0.8	0	4	0.8
Ae2	E2	15	1.9	0.6	0.6	0.2	<0.2	0	<0.2	0	<0.2	0	<0.3	0	<0.8	0	1.2	0.6
Ae3	E3	24	<1.1	0	0.7	0.2	0.2	0.1	<0.2	0	<0.2	0	<0.3	0	<0.9	0	1.4	0.6
Bh	Bh	29	<0.8	0	0.7	0.2	0.3	0.1	0.3	0.1	<0.2	0	<0.3	0	2.5	0.6	5.1	0.8
Bs1	Bs1	31.5	1.2	0.4	<0.6	-0.2	<0.2	0	<0.2	-0.1	<0.2	0	0.4	0.2	7.8	0.6	4.9	0.8
Bs2	Bs2	36.5	0.9	0.4	0.5	0.2	<0.2	0	<0.2	-0.1	0.3	0.1	0.5	0.2	9.1	0.6	3.6	0.7
ICv1	Bw	50	1.5	0.4	0.5	0.2	<0.2	0	<0.2	-0.1	<0.2	0	<0.3	0	4	0.6	1.5	0.5
ICv2	BC	70	1.4	0.4	<0.5	0	<0.2	0	<0.2	0	0.5	0.1	<0.3	0	<0.9	0	1.7	0.5
ICv3	C	95	1.1	0.6	0.4	0.1	<0.2	0	<0.2	0	<0.2	0	<0.3	-0.2	<0.9	0	1.2	0.4
Cambisol																		
Ah	Ah	10	1	0.3	1.8	0.5	<0.3	0	0.3	0.1	0.7	0.2	<0.3	0	<1.1	0	<2.0	0
Bv	Bw	30	1.1	0.3	1.3	0.4	<0.3	0	0.7	0.1	<0.3	0	<0.3	0	<1.1	0	<2.0	0
iICv1	BwC	60	0.4	0.2	1.3	0.4	<0.3	0	0.7	0.1	0.5	0.1	<0.3	0	<1.1	0	<2.0	-0.5
iICv2	C	80	<0.4	0	1.4	0.4	<0.3	0	0.5	0.1	<0.3	0	<0.3	0	<1.1	0	2.8	0.5

Table A1.4.4 XRF measurements (Podzol A, Podzol B, Cambisol)
(err indicates absolute error in same unit as concentration value)

*samples were prepared in W-carbide mill

horizon	horizon	depth	Pr	Pr	Hf	Hf	Ta	Ta	W*	W	Hg	Hg	Bi	Bi	U	U
German	WRB	[cm]	µg/g	err	µg/g	err	µg/g	err	µg/g	err	µg/g	err	µg/g	err	µg/g	err
Podzol A																
O _L	O1	-7	< 6.9	0	1.9	0.4	< 3.1	0	183.2	2.3	0.7	0.7	< 0.6	0	< 0.6	0
O _F	O2	-3	16.4	3.9	1.1	0.3	< 3.9	0	190.6	2.5	< 1.3	0	< 0.7	0	< 0.7	0
Ahe	Ah	1	11.2	4	< 2.9	0	< 7.1	0	1739	8	5.6	2.6	< 1.0	0	< 0.8	0
Ae1	E1	4.5	14.3	4.1	< 2.4	0	< 6.3	0	1877	9	< 4.6	0	< 0.9	0	< 0.8	-0.3
Ae2	E2	9.5	78.4	4	< 2.3	0	< 5.9	0	1804	8	5.9	2.6	< 0.9	0	< 0.8	0
Ae3	E3	14.5	23.5	4	< 2.2	0	< 6.0	0	1726	8	< 4.4	0	< 0.9	0	0.4	0.3
Bh	Bh	18.5	12.8	4.1	< 2.2	0	< 4.7	-3.4	874.8	5.9	< 3.2	0	< 0.8	0	< 0.9	0
Bs1	Bs1	21	50.8	4.1	< 2.2	0	< 5.2	-1.9	1103	7	7.6	2.2	< 0.9	0	< 1.0	0
Bs2	Bs2	26	< 7.0	0	< 2.1	0	< 5.4	-4.6	1323	7	6.4	2.3	< 0.9	0	< 0.9	0
ICv1	Bw	35	< 7.1	0	< 2.3	0	< 5.6	0	1453	8	< 4.1	0	< 0.9	0	< 0.9	0
ICv2	BC	50	< 7.0	0	< 2.2	0	< 5.8	0	1573	8	6.1	2.5	< 0.9	0	< 0.9	0
ICv3	C	70	6.5	4	< 2.2	0	< 5.7	-2.5	1690	8	3.7	2.6	< 0.9	0	< 0.9	0
Podzol B																
O _L	O1	-4	25.1	3.8	0.6	0.2	< 2.3	-0.8	118.1	1.8	< 1.0	0	< 0.5	0	< 0.6	0
O _F	O2	-1.5	21.2	4.3	1.8	0.4	< 3.4	-1.8	245.5	3.1	1.4	1	< 0.7	0	< 0.9	0
Ahe	Ah	1.5	< 6.9	0	< 2.3	0	< 6.0	0	1875	9	< 4.6	0	< 0.9	0	< 1.0	-0.2
Ae1	E1	6.5	15	4	< 2.3	0	< 6.0	0	2024	9	< 4.7	-3.6	< 0.9	0	< 1.0	0
Ae2	E2	15	< 6.9	0	< 2.3	0	6.8	1.2	1906	9	5.5	2.7	< 0.9	0	< 1.0	0
Ae3	E3	24	15.3	4	< 2.4	0	< 6.2	0	1993	9	4.5	2.8	< 1.0	0	< 1.1	0
Bh	Bh	29	9.9	3.9	< 2.3	0	4.3	1.1	1029	7	4.4	2.1	< 0.9	0	< 1.5	0
Bs1	Bs1	31.5	13	3.9	< 2.3	0	< 4.8	-2.7	918	6.2	5.5	2	< 0.9	0	< 1.5	0
Bs2	Bs2	36.5	< 7.1	0	< 2.2	0	< 4.8	-2.6	924.8	6.2	6.1	1.9	< 0.9	0	< 1.4	0
ICv1	Bw	50	< 7.1	0	< 2.2	0	4.6	1.2	907.7	6.1	4.6	1.9	< 0.8	0	< 1.4	0
ICv2	BC	70	12.5	3.8	< 2.1	0	4.6	1.2	949.6	6.2	5.4	1.9	< 0.8	0	< 1.4	0
ICv3	C	95	< 7.3	0	< 2.5	0	< 5.8	0	1443	8	4.5	2.5	< 0.9	0	< 1.6	0
Cambisol																
Ah	Ah	10	66.2	4.3	7.3	2.2	18	5.4	118.1	4.1	3.4	1.1	< 1.3	0	3.8	1.1
Bv	Bw	30	8.8	3.3	8.1	2.9	11.6	5.7	20.7	3.2	< 1.4	0	< 1.3	0	2.8	1.1
ilCv1	BwC	60	< 7.7	0	7.3	2.8	12.8	5.5	17.4	2.9	1.9	0.7	< 1.3	0	< 2.0	0
ilCv2	C	80	9.7	3.6	7.4	2.8	15.7	5.8	19.2	2.9	1.6	0.7	< 1.3	0	< 2.0	0

Appendix 2

(referring to work presented in chapter 5)

Table A2.1 Iron concentrations and iron isotope ratios for Stagnic Cambisol (near Rafz / Canton Zurich, Northern Switzerland)

Iron concentrations

horizon German	horizon WRB	~depth [cm]	Fe _{total measured} [mg/g soil]	Fe _{HCl} [mg/g soil]	Fe _{NH₂OH-HCl} [mg/g soil]	Fe _{residue} [mg/g soil]	Fe _{total calculated} [mg/g soil]
L	O1	-1.5	5.83	1.98	-	-	-
Of	O2	-0.5	16.52	4.25	-	-	-
Ah	Ah	1.5	17.96	5.73	7.06	4.12	16.91
SwBv	Bw	17	18.64	5.25	8.82	4.40	18.48
Sw	Bcg1	42.5	19.88	5.12	10.43	5.05	20.59
Sd	Bcg2	77.5	33.01	5.48	20.35	7.29	33.11
C-Sd1	CBg	120	32.41	4.77	15.60	7.81	28.18
C-Sd 140	Cg	140	32.00	5.27	16.13	7.83	29.23

redoximorphic zones:

depleted	Bcg2	77.5	21.55	2.44	4.78	6.75	13.97
enriched	Bcg2	77.5	36.76	4.81	19.00	7.67	31.48
depleted	CBg	120	22.93	2.23	10.56	8.44	21.23
enriched	CBg	120	34.17	5.02	19.92	7.62	32.56

Iron isotope ratios

horizon German	horizon WRB	~depth [cm]	$\delta^{57}\text{Fe}_{\text{total measured}}$ [‰]	$\delta^{57}\text{Fe}_{\text{HCl}}$ [‰]	$\delta^{57}\text{Fe}_{\text{NH}_2\text{OH-HCl}}$ [‰]	$\delta^{57}\text{Fe}_{\text{residue}}$ [‰]	$\delta^{57}\text{Fe}_{\text{total calculated}}$ [‰]
L	O1	-1.5	0.14	-0.66	-	-	-
Of	O2	-0.5	0.17	-0.31	-	-	-
Ah	Ah	1.5	0.18	-0.18	0.07	0.49	0.08
SwBv	Bw	17	0.16	-0.02	0.09	0.62	0.18
Sw	Bcg1	42.5	0.24	-0.04	0.15	1.63	0.48
Sd	Bcg2	77.5	0.03	-0.18	0.00	1.27	0.25
C-Sd1	CBg	120	0.13	-0.03	0.14	1.37	0.39
C-Sd 140	Cg	140	0.11	-0.12	0.04	1.11	0.27

redoximorphic zones:

depleted	Bcg2	77.5	0.36	0.37	0.26	1.57	0.59
enriched	Bcg2	77.5	0.09	-0.26	-0.05	1.23	0.20
depleted	CBg	120	0.48	0.56	0.40	1.40	0.75
enriched	CBg	120	0.09	-0.16	0.03	1.46	0.32

Table A2.2 Iron concentrations and iron isotope ratios for Haplic Gleysol (near Tettngang / Upper Swabia, Southern Germany)

Iron concentrations

horizon German	horizon WRB	~depth [cm]	soil pH [CaCl ₂]	Fe _{total} measured [mg/g soil]	Fe _{HCl} [mg/g soil]	Fe _{NH₂OH-HCl} [mg/g soil]	Fe _{residue} [mg/g soil]	Fe _{total} calculated [mg/g soil]
Ah1	Ah1	5	5.9	20.67	3.87	9.44	11.26	24.57
Ah2	Ah1	20	6.1	20.83	2.95	8.94	11.93	23.82
Go1	2Bl	30	6.4	15.71	1.65	8.66	5.54	15.85
Go2	2Blc1	50	7.5	25.65	4.22	14.56	7.59	26.37
Gro	2Blc2	70	7.8	15.71	2.27	8.00	7.46	17.73
Gor	2BCr	90	7.8	12.95	0.98	5.21	8.10	14.29
Gr1	2Cr1	105	7.9	13.91	2.75	6.18	8.89	17.82
Gr2	2Cr2	120	7.7	15.29	2.80	6.22	8.97	18.00

redoximorphic zones:

enriched	2Blc1	50	7.4	30.41	5.45	16.92	7.82	30.19
enriched	2Blc2	70	7.6	22.81	6.81	10.31	7.47	24.58

Iron isotope ratios

horizon German	horizon WRB	~depth [cm]	soil pH [CaCl ₂]	$\delta^{57}\text{Fe}_{\text{total}}$ measured [‰]	$\delta^{57}\text{Fe}_{\text{HCl}}$ [‰]	$\delta^{57}\text{Fe}_{\text{NH}_2\text{OH-HCl}}$ [‰]	$\delta^{57}\text{Fe}_{\text{residue}}$ [‰]	$\delta^{57}\text{Fe}_{\text{total}}$ calculated [‰]
Ah1	Ah1	5	5.9	0.26	0.03	0.26	0.46	0.37
Ah2	Ah1	20	6.1	0.42	0.23	0.34	0.43	0.42
Go1	2Bl	30	6.4	0.15	-0.03	0.07	0.49	0.21
Go2	2Blc1	50	7.5	0.01	-0.15	-0.16	0.58	0.06
Gro	2Blc2	70	7.8	0.11	-0.48	-0.10	0.57	0.15
Gor	2BCr	90	7.8	0.08	-0.43	-0.12	0.37	0.15
Gr1	2Cr1	105	7.9	0.18	-0.45	0.01	0.48	0.22
Gr2	2Cr2	120	7.7	0.17	-0.48	0.02	0.45	0.18

redoximorphic zones:

enriched	2Blc1	50	7.4	0.04	-0.10	-0.14	0.52	0.04
enriched	2Blc2	70	7.6	-0.15	-0.63	-0.29	0.53	-0.15

Table A2.3.1

XRF measurements (Stagnic Cambisol, Haplic Gleysol)
(err indicates absolute error in same unit as concentration value)

horizon	horizon	depth	Fe	Fe	Mn	Mn	Al	Al	Si	Si	Zr	Zr	Ti	Ti		
German	WRB	[cm]	%	err	%	err	%	err	%	err	µg/g	err	%	err		
Stagnic Cambisol																
L	O1	-2.5	0.504	0.001	0.2685	0.0004	0.754	0.005	5.52	0.01	74	0.3	0.068	0.000		
Of	O2	-0.5	1.545	0.003	0.1139	0.0003	3.500	0.014	22.90	0.03	298	0.8	0.286	0.001		
Ah	Ah	1.5	1.475	0.003	0.0326	0.0001	3.760	0.016	31.43	0.04	373	0.9	0.352	0.001		
SwBv	Bw	17	1.619	0.004	0.0681	0.0002	4.506	0.018	33.28	0.05	395	0.9	0.372	0.001		
Sw	Bcg1	42.5	1.743	0.004	0.0437	0.0002	4.898	0.019	32.71	0.04	384	0.9	0.383	0.001		
Sd	Bcg2	77.5	3.010	0.005	0.0439	0.0002	5.799	0.020	29.89	0.04	334	0.9	0.372	0.001		
C-Sd1	CBg	120	2.817	0.005	0.0416	0.0002	5.730	0.020	30.00	0.04	327	0.9	0.361	0.001		
C-Sd 140	Cg	140	3.009	0.005	0.0453	0.0002	5.936	0.020	29.54	0.04	324	0.9	0.361	0.001		
redoximorphic zones:																
depleted	Bcg2	77.5	1.925	0.004	0.0191	0.0001	5.756	0.020	31.43	0.04	353	0.9	0.374	0.001		
enriched	Bcg2	77.5	3.205	0.005	0.0748	0.0002	5.769	0.021	30.02	0.04	344	0.9	0.365	0.001		
depleted	CBg	120	2.135	0.004	0.0164	0.0001	6.593	0.021	29.47	0.04	312	0.8	0.375	0.001		
enriched	CBg	120	2.952	0.005	0.0523	0.0002	5.686	0.020	30.24	0.04	338	0.9	0.357	0.001		
Haplic Gleysol																
Ah1	Ah1	5	2.067	0.004	0.0777	0.0002	4.679	0.016	21.20	0.03	152	0.6	0.248	0.001		
Ah2	Ah1	20	2.083	0.004	0.0565	0.0002	5.241	0.018	23.33	0.03	189	0.7	0.280	0.001		
Go1	2Bl	30	1.404	0.003	0.0183	0.0001	4.241	0.017	32.76	0.04	76.7	0.5	0.138	0.001		
Go2	2Blc1	50	2.382	0.004	0.0332	0.0002	4.642	0.018	26.85	0.04	77.9	0.5	0.179	0.001		
Gro	2Blc2	70	1.422	0.003	0.0360	0.0002	3.315	0.015	22.90	0.03	84.5	0.6	0.147	0.001		
Gor	2BCr	90	1.211	0.003	0.0384	0.0002	2.531	0.013	21.22	0.03	112	0.7	0.155	0.001		
Gr1	2Cr1	105	1.306	0.003	0.0412	0.0002	2.772	0.013	19.64	0.03	145	0.7	0.166	0.001		
Gr2	2Cr2	120	1.548	0.004	0.0490	0.0003	2.738	0.013	19.23	0.03	116	0.7	0.163	0.001		
redoximorphic zones:																
enriched	2Blc1	50	3.102	0.005	0.0408	0.0002	4.940	0.018	26.65	0.04	76.9	0.5	0.191	0.001		
enriched	2Blc2	70	2.140	0.004	0.0397	0.0002	3.537	0.016	24.05	0.03	81.7	0.6	0.160	0.001		
Stagnic Cambisol																
L	O1	-2.5	0.3167	0.0013	0.7734	0.0017	0.061	0.021	0.138	0.006	112	1.3	19.1	0.2	27.8	0.2
Of	O2	-0.5	1.018	0.003	0.3379	0.0013	0.348	0.059	0.350	0.015	229	1.7	61.6	0.4	53.1	0.4
Ah	Ah	1.5	1.214	0.003	0.2119	0.0011	0.576	0.073	0.292	0.015	243	1.7	59.9	0.4	57.2	0.4
SwBv	Bw	17	1.33	0.003	0.2117	0.0012	0.541	0.074	0.445	0.018	279	1.7	70.3	0.5	60.1	0.4
Sw	Bcg1	42.5	1.415	0.003	0.2095	0.0012	0.700	0.080	0.511	0.019	319	1.8	76.8	0.5	60.8	0.4
Sd	Bcg2	77.5	1.518	0.003	0.2019	0.0012	0.600	0.080	0.717	0.021	337	1.8	88.7	0.5	66.2	0.4
C-Sd1	CBg	120	1.415	0.003	0.2394	0.0012	0.525	0.076	0.694	0.021	363	1.8	85.7	0.5	68	0.4
C-Sd 140	Cg	140	1.475	0.003	0.229	0.0012	0.561	0.077	0.681	0.021	373	1.9	87.9	0.5	68.4	0.4
redoximorphic zones:																
depleted	Bcg2	77.5	1.532	0.003	0.2032	0.0012	0.586	0.077	0.630	0.020	349	1.8	87.1	0.5	66.3	0.4
enriched	Bcg2	77.5	1.388	0.003	0.2105	0.0012	0.584	0.080	0.712	0.022	319	1.8	85.2	0.5	69.4	0.4
depleted	CBg	120	1.496	0.003	0.2423	0.0013	0.500	0.073	0.715	0.021	380	1.9	94.5	0.5	68.5	0.4
enriched	CBg	120	1.386	0.003	0.2254	0.0012	0.520	0.077	0.719	0.021	341	1.8	84.2	0.5	68.3	0.4
Haplic Gleysol																
Ah1	Ah1	5	1.189	0.003	1.286	0.003	0.340	0.062	0.569	0.017	308	1.8	68.2	0.4	89.8	0.5
Ah2	Ah1	20	1.283	0.003	1.193	0.003	0.506	0.069	0.683	0.019	332	1.8	68.5	0.4	96	0.5
Go1	2Bl	30	1.721	0.004	0.3787	0.0015	0.537	0.077	0.580	0.019	291	1.8	74.4	0.5	71.9	0.4
Go2	2Blc1	50	1.757	0.004	2.036	0.004	0.603	0.078	1.039	0.022	321	1.8	78.8	0.5	101	0.5
Gro	2Blc2	70	1.314	0.004	8.078	0.01	0.485	0.078	1.499	0.024	222	1.7	62.7	0.5	227	0.8
Gor	2BCr	90	1.041	0.004	10.46	0.01	0.345	0.074	1.662	0.025	180	1.6	49.2	0.4	286	0.9
Gr1	2Cr1	105	1.079	0.004	10.89	0.01	0.408	0.077	1.665	0.024	201	1.7	53.3	0.4	282	0.9
Gr2	2Cr2	120	1.077	0.004	10.58	0.01	0.335	0.074	1.684	0.025	213	1.7	54.6	0.4	277	0.9
redoximorphic zones:																
enriched	2Blc1	50	1.86	0.004	1.025	0.002	0.398	0.072	0.960	0.022	353	1.9	85.2	0.5	87.2	0.5
enriched	2Blc2	70	1.39	0.004	6.331	0.008	0.562	0.081	1.405	0.024	265	1.8	69	0.5	192	0.7

Table A2.3.2

XRF measurements (Stagnic Cambisol, Haplic Gleysol)
(err indicates absolute error in same unit as concentration value)

horizon	horizon	depth	As	As	Sb	Sb	Sn	Sn	Br	Br	Y	Y	Nb	Nb	La	La	Ce	Ce
German	WRB	[cm]	µg/g	err	µg/g	err	µg/g	err	µg/g	err	µg/g	err	µg/g	err	µg/g	err	µg/g	err
Stagnic Cambisol																		
L	O1	-2.5	3.5	0.3	<0.3	0	1.2	0.1	3.3	0.2	4.8	0.2	1.9	0.1	12.6	1.6	21.4	2.2
Of	O2	-0.5	7.5	0.6	1.8	0.2	4.3	0.2	6.7	0.2	19.6	0.4	12.2	0.2	26.5	1.9	58.2	2.7
Ah	Ah	1.5	7	0.6	1.1	0.2	3.7	0.2	5.8	0.3	20.3	0.4	13.7	0.2	25	1.9	59	2.6
SwBv	Bw	17	5.6	0.4	0.5	0.2	3.3	0.2	5.2	0.3	24.2	0.4	13.8	0.2	38.8	1.9	88.9	2.6
Sw	Bcg1	42.5	6	0.4	<0.3	0	2.5	0.1	3	0.2	24.7	0.4	13.2	0.2	51.4	1.9	98.9	2.6
Sd	Bcg2	77.5	13.9	0.5	0.7	0.2	3.6	0.2	1.1	0.2	29.6	0.5	13.7	0.2	36.9	1.9	78.4	2.6
C-Sd1	CBg	120	14.2	0.5	<0.3	0	4.1	0.2	1.1	0.2	33.9	0.5	14	0.2	73	2	131.8	2.6
C-Sd 140	Cg	140	15.2	0.5	2.1	0.2	3.5	0.2	1.4	0.2	31.9	0.5	13.8	0.2	60.1	2	114.9	2.7
redoximorphic zones:																		
depleted	Bcg2	77.5	7.2	0.4	0.6	0.2	3.2	0.2	1	0.2	29.8	0.4	14	0.2	49.7	2	90.7	2.6
enriched	Bcg2	77.5	14.3	0.6	1	0.2	5.9	0.2	0.5	0.2	32.1	0.5	13.1	0.2	37	2	88.2	2.7
depleted	CBg	120	6.8	0.4	<0.4	0	3.8	0.2	1.5	0.2	36.4	0.5	13.6	0.2	39.5	2	75.3	2.7
enriched	CBg	120	14.4	0.5	<0.3	0	3.2	0.2	1.2	0.2	33.7	0.5	13.3	0.2	57.9	2	115.6	2.6
Haplic Gleysol																		
Ah1	Ah1	5	13.7	0.6	<0.4	0	3.2	0.2	11	0.3	23.6	0.4	10.3	0.2	24	1.9	54	2.7
Ah2	Ah1	20	12.8	0.5	1.1	0.2	2.9	0.1	6.6	0.3	25.9	0.4	11.4	0.2	26.1	1.9	58.7	2.7
Go1	2Bl	30	5.3	0.4	<0.3	0	1.8	0.1	2.3	0.2	9.1	0.4	5.1	0.2	8.1	1.7	23	2.6
Go2	2Blc1	50	17.2	0.5	1.1	0.2	2.5	0.1	1.7	0.2	12.1	0.4	5.5	0.2	9.4	1.8	26	2.6
Gro	2Blc2	70	4.6	0.4	<0.3	0	1.9	0.1	0.6	0.2	11.5	0.4	4.9	0.2	8.2	1.7	22.4	2.5
Gor	2BCr	90	2.9	0.3	0.6	0.2	1.4	0.1	1.1	0.2	14.9	0.4	7.7	0.2	9.8	1.8	24.5	2.6
Gr1	2Cr1	105	4.1	0.4	0.7	0.2	1.7	0.1	1.3	0.2	14.5	0.4	5.9	0.2	8	1.8	30.6	2.6
Gr2	2Cr2	120	3.4	0.4	0.5	0.2	2.1	0.1	1.2	0.2	14.6	0.4	6	0.2	11.3	1.8	30.8	2.6
redoximorphic zones:																		
enriched	2Blc1	50	27.8	0.6	0.9	0.2	2.5	0.1	1.6	0.2	13.4	0.4	8.4	0.2	7.7	1.7	22.1	2.6
enriched	2Blc2	70	14.6	0.5	1.5	0.2	2.2	0.1	1.7	0.2	12.1	0.4	5.3	0.2	9.2	1.8	22.5	2.6
German																		
horizon	horizon	depth	Nd	Nd	Sm	Sm	Tl	Tl	Pb	Pb	Th	Th	P	P	S	S	Cl	Cl
German	WRB	[cm]	µg/g	err	µg/g	err	µg/g	err	µg/g	err	µg/g	err	%	err	µg/g	err	µg/g	err
Stagnic Cambisol																		
L	O1	-2.5	24.6	4.5	5.8	0.1	<0.4	0	24.4	0.6	1.2	0.2	0.095	0	1103	4	108.2	0.9
Of	O2	-0.5	35.1	5.2	13	0.3	1.7	0.4	52.3	0.9	8.7	0.4	0.131	0	1326	7	111.4	1.5
Ah	Ah	1.5	10.1	4.4	14.9	0.4	2.3	0.3	42	0.9	6.8	0.4	0.06	0	349	4	67.1	1.2
SwBv	Bw	17	48.4	5.1	14.8	0.4	1.5	0.3	17.6	0.7	9.5	0.4	0.062	0	53.2	1	38	0.8
Sw	Bcg1	42.5	89.5	5.3	15.3	0.4	1.7	0.3	14.1	0.7	9.6	0.4	0.051	0	33.8	0.7	29.7	0.7
Sd	Bcg2	77.5	40.3	5.1	18	0.4	1.6	0.4	17	0.8	11.7	0.4	0.055	0	20.7	0.4	28.7	0.7
C-Sd1	CBg	120	135.8	5.4	18.4	0.4	1.4	0.3	17.7	0.8	11.3	0.4	0.05	0	<20	0	<2.3	0
C-Sd 140	Cg	140	92.4	5.4	19	0.4	1.8	0.4	19	0.8	10.4	0.4	0.05	0	<20	0	<2.3	0
redoximorphic zones:																		
depleted	Bcg2	77.5	67.3	5.3	16.1	0.4	1.1	0.3	14.5	0.7	11.7	0.4	0.027	0	<20	0	10.1	0.3
enriched	Bcg2	77.5	33.5	5.1	18.6	0.4	1.1	0.3	20.9	0.8	11.4	0.4	0.057	0	<20	-11	<2.2	0
depleted	CBg	120	45.6	5.2	18	0.4	1.5	0.3	14	0.7	11.5	0.4	0.026	0	<20	0	21.8	0.5
enriched	CBg	120	93	5.3	17.3	0.4	1.9	0.4	18.7	0.8	9.4	0.4	0.054	0	<20	0	63.4	1.2
Haplic Gleysol																		
Ah1	Ah1	5	28.7	5.2	14.6	0.4	1.4	0.3	36.5	0.9	7.3	0.4	0.162	0	1490	8	47.9	0.9
Ah2	Ah1	20	24.1	5	15.2	0.4	1	0.3	27.6	0.8	9	0.4	0.141	0	1086	7	58.9	1
Go1	2Bl	30	<9.5	0	12.5	0.4	<1.0	0	13	0.7	4.5	0.4	0.016	0	<20	0	7.2	0.2
Go2	2Blc1	50	<9.6	0	13.9	0.4	0.7	0.2	13.7	0.7	4.3	0.3	0.035	0	<20	0	59.4	1.1
Gro	2Blc2	70	<9.2	-5.5	12.7	0.5	0.7	0.2	9.9	0.7	3.8	0.4	0.030	0	<2.5	0	20.3	0.6
Gor	2BCr	90	16.3	4.8	13.3	0.6	1.3	0.3	8.7	0.7	3.4	0.4	0.032	0	10.1	0.3	52.3	1.1
Gr1	2Cr1	105	16.7	4.9	14.5	0.6	1	0.3	9.5	0.7	4.5	0.4	0.035	0	97.1	1.9	91.1	1.5
Gr2	2Cr2	120	10.6	4.6	14	0.6	0.7	0.2	10.3	0.7	4.1	0.4	0.035	0	100	1.9	43	1
redoximorphic zones:																		
enriched	2Blc1	50	16.3	4.7	14.9	0.4	1.4	0.3	14.6	0.7	3.6	0.3	0.034	0	<20	0	39.7	0.8
enriched	2Blc2	70	9.4	4.4	13.1	0.5	<1.0	0	11.3	0.7	4	0.4	0.029	0	39.7	0.9	68.9	1.3

Table A2.3.3

XRF measurements (Stagnic Cambisol, Haplic Gleysol)
(err indicates absolute error in same unit as concentration value)

horizon	horizon	depth	V	V	Cr	Cr	Co	Co	Ni	Ni	Cu	Cu	Zn	Zn	Ga	Ga	Ge	Ge
German	WRB	[cm]	µg/g	err	µg/g	err	µg/g	err	µg/g	err	µg/g	err	µg/g	err	µg/g	err	µg/g	err
Stagnic Cambisol																		
L	O1	-2.5	14.3	1.2	23.3	0.5	< 2.7	0	10.5	0.6	10.3	0.4	91.8	0.8	2.4	0.2	< 0.6	0
Of	O2	-0.5	38.8	2.4	63.8	0.8	< 7.1	0	19.6	1.1	14.6	0.7	81.3	1.1	7.9	0.4	1.5	0.3
Ah	Ah	1.5	35.7	2.5	71	0.8	40.3	4	17.1	1.3	8.4	0.6	45.2	1.1	9.6	0.5	< 1.9	-0.9
SwBv	Bw	17	35.2	2.7	78.9	0.9	37.1	3.7	17.4	1.3	7	0.5	44	1.1	10.5	0.5	< 1.9	0
Sw	Bcg1	42.5	39.1	2.7	80.4	0.9	40.3	4.3	23.6	1.4	9.4	0.6	55.5	1.2	12.4	0.5	1.9	0.3
Sd	Bcg2	77.5	71.9	3	97.9	1	42.4	5.4	33.8	1.6	18.3	0.8	55.7	1.2	13.4	0.5	2.4	0.4
C-Sd1	CBg	120	63.2	2.9	97.5	0.9	38	5.2	35.9	1.6	16.1	0.8	55	1.2	13.5	0.5	3.7	0.5
C-Sd 140	Cg	140	67.6	3	97.5	1	40.2	5.3	36.8	1.6	17.5	0.8	56.2	1.2	13.9	0.5	1.8	0.4
redoximorphic zones:																		
depleted	Bcg2	77.5	58.2	2.9	93.7	0.9	42.1	4.8	27.6	1.4	12.4	0.7	53.2	1.2	13.1	0.5	< 1.6	0
enriched	Bcg2	77.5	69.1	3	94.4	1	39	5	36	1.6	18.1	0.8	60.4	1.2	13.8	0.5	1.7	0.4
depleted	CBg	120	68.8	3	113.5	1	40.4	5	36.3	1.5	15.3	0.7	56	1.2	16.4	0.5	1	0.2
enriched	CBg	120	67.3	2.9	95.2	0.9	41.8	5.2	35.4	1.6	16.8	0.8	54.3	1.2	13	0.5	2.5	0.4
Haplic Gleysol																		
Ah1	Ah1	5	55.7	2.5	73.7	0.8	13.2	2.4	22.7	1.2	26	0.8	53.3	1	10	0.4	1.3	0.3
Ah2	Ah1	20	57.9	2.7	76.6	0.8	18.6	3.2	24.4	1.3	25.3	0.9	49	1	11.6	0.5	1.6	0.3
Go1	2Bl	30	35.5	1.9	43.6	0.6	41.1	4.1	20.5	1.3	7.9	0.5	29.5	1	9.2	0.4	1.9	0.3
Go2	2Blc1	50	50.8	2.4	56.5	0.8	28.2	4.5	27.8	1.4	12.8	0.7	41.8	1.1	11.3	0.5	1.4	0.3
Gro	2Blc2	70	32.9	2.8	40.6	0.9	17.1	3	17.1	1.3	8.3	0.5	30.2	1	7.4	0.4	< 1.4	-0.4
Gor	2BCr	90	28.5	3	39.6	0.9	15.3	2.5	12.4	1.1	6.1	0.5	24.3	0.9	6.5	0.4	1	0.3
Gr1	2Cr1	105	32.2	3.2	43.3	1	16.7	2.7	15.7	1.2	10.1	0.6	27.7	0.9	7.4	0.4	1.2	0.3
Gr2	2Cr2	120	36.3	3.2	55.1	1.1	10	2.2	17.5	1.3	10.1	0.6	29.2	0.9	7.6	0.4	1.8	0.4
redoximorphic zones:																		
enriched	2Blc1	50	61.1	2.4	70.3	0.8	35.5	5.2	31.8	1.5	15.9	0.7	48.9	1.1	12.8	0.5	2.1	0.4
enriched	2Blc2	70	45.2	2.8	49.4	0.9	32.6	4.4	22.8	1.4	14.4	0.8	36.1	1.1	8.9	0.4	< 1.7	-0.8
Stagnic Cambisol																		
L	O1	-2.5	< 0.2	0	0.5	0.1	< 0.1	0	0.1	0.1	< 0.1	0	< 0.3	0	1.4	0.5	1	0.6
Of	O2	-0.5	0.8	0.2	0.9	0.3	< 0.2	0	< 0.2	0	< 0.2	0	< 0.3	0	3.1	0.6	< 1.7	0
Ah	Ah	1.5	< 0.6	0	< 1.0	-0.4	0.3	0.1	0.2	0.1	0.5	0.1	< 0.3	0	< 0.9	0	< 1.7	0
SwBv	Bw	17	1	0.4	< 1.0	0	< 0.2	0	< 0.2	0	< 0.2	0	< 0.3	-0.1	3.3	0.6	< 1.7	-0.5
Sw	Bcg1	42.5	0.5	0.3	0.5	0.3	< 0.2	0	< 0.2	0	< 0.2	0	< 0.3	0	2.9	0.6	3.1	0.7
Sd	Bcg2	77.5	0.7	0.3	< 0.9	0	0.2	0.1	< 0.2	-0.1	< 0.2	0	< 0.3	-0.3	< 0.9	0	< 1.7	0
C-Sd1	CBg	120	< 0.6	0	1.3	0.4	0.3	0.1	< 0.2	0	< 0.2	0	< 0.3	0	2.8	0.6	8.4	0.8
C-Sd 140	Cg	140	< 0.5	-0.2	1.1	0.4	0.3	0.1	< 0.2	-0.1	< 0.2	0	0.9	0.2	2.1	0.6	4.4	0.7
redoximorphic zones:																		
depleted	Bcg2	77.5	0.5	0.3	1	0.4	< 0.2	0	0.2	0.1	< 0.2	0	< 0.3	-0.2	< 0.9	0	2.6	0.6
enriched	Bcg2	77.5	0.6	0.3	2.4	0.5	< 0.2	0	< 0.2	-0.1	< 0.2	0	< 0.3	0	< 0.9	0	< 1.7	0
depleted	CBg	120	< 0.6	-0.3	< 0.9	0	< 0.2	0	< 0.2	0	< 0.2	0	< 0.3	0	< 1.0	0	< 1.7	0
enriched	CBg	120	< 0.5	0	1	0.3	< 0.2	0	< 0.2	0	0.3	0.1	< 0.3	0	< 0.9	0	3.3	0.7
Haplic Gleysol																		
Ah1	Ah1	5	< 0.4	0	1.7	0.4	< 0.2	0	0.8	0.1	< 0.2	0	0.5	0.2	8.2	0.6	< 1.7	0
Ah2	Ah1	20	1.2	0.3	1.1	0.3	0.6	0.1	0.7	0.1	< 0.2	0	< 0.3	0	5.7	0.6	< 1.7	0
Go1	2Bl	30	0.9	0.4	< 0.6	-0.3	< 0.2	0	< 0.2	0	0.4	0.1	< 0.3	0	< 0.9	0	< 1.7	0
Go2	2Blc1	50	0.5	0.3	0.4	0.1	< 0.2	0	< 0.2	0	< 0.2	0	< 0.3	0	< 0.9	0	< 1.7	0
Gro	2Blc2	70	0.4	0.3	< 0.6	-0.2	< 0.2	0	< 0.2	0	< 0.2	0	< 0.3	0	< 0.9	0	< 1.6	0
Gor	2BCr	90	< 0.6	-0.2	0.7	0.2	< 0.2	0	< 0.2	-0.1	< 0.2	0	0.3	0.2	< 0.9	0	< 1.7	0
Gr1	2Cr1	105	< 0.5	0	< 0.7	-0.3	< 0.2	0	< 0.2	-0.2	< 0.2	0	< 0.3	0	< 0.9	0	< 1.7	0
Gr2	2Cr2	120	< 0.5	0	0.5	0.2	< 0.2	0	0.3	0.1	< 0.2	0	< 0.3	0	< 0.9	0	< 1.7	0
redoximorphic zones:																		
enriched	2Blc1	50	< 0.5	-0.1	1.2	0.2	0.4	0.1	0.5	0.1	0.5	0.1	< 0.3	0	< 0.9	0	< 1.7	0
enriched	2Blc2	70	< 0.6	0	1	0.2	< 0.2	0	< 0.2	-0.1	< 0.2	0	< 0.3	-0.1	< 0.9	0	< 1.7	0

Table A2.3.4 XRF measurements (Stagnic Cambisol, Haplic Gleysol)
(err indicates absolute error in same unit as concentration value)

*samples were prepared in W-carbide mill

horizon	horizon	depth	Pr	Pr	Hf	Hf	Ta	Ta	W*	W	Hg	Hg	Bi	Bi	U	U
German	WRB	[cm]	µg/g	err	µg/g	err	µg/g	err	µg/g	err	µg/g	err	µg/g	err	µg/g	err
Stagnic Cambisol																
L	O1	-2.5	9.9	3.6	1.7	0.4	4.7	1.2	112	1.8	< 0.9	0	< 0.4	0	< 0.7	0
Of	O2	-0.5	11.9	4.1	7.5	1.3	4.2	1.9	81.3	2.3	< 1.2	-0.4	< 0.8	0	< 1.4	-0.5
Ah	Ah	1.5	< 7.2	0	5.7	0.7	6.6	1.6	597	5.1	3.3	1.6	< 0.9	0	< 1.4	-0.6
SwBv	Bw	17	< 7.2	0	5.4	0.7	7.1	1.7	566	5.1	3.5	1.6	< 0.9	0	< 1.5	0
Sw	Bcg1	42.5	48.6	4.1	6	0.9	4.2	1.4	453	4.7	< 2.5	-1.4	< 0.9	0	< 1.5	0
Sd	Bcg2	77.5	10.7	3.9	5.7	1.2	5.6	2	306	4.1	< 2.2	-0.8	< 0.9	0	< 1.7	0
C-Sd1	CBg	120	85.6	4.1	6.7	1.1	< 5.3	-4.2	324	4.2	< 2.3	0	< 1.0	0	< 1.7	0
C-Sd 140	Cg	140	63.9	4.2	5	1	< 5.4	0	315	4.1	< 2.2	-0.7	< 0.9	0	< 1.7	0
redoximorphic zones:																
depleted	Bcg2	77.5	42.2	4.1	7.5	1.1	7.4	2	405	4.5	2.7	1.4	< 0.9	0	< 1.6	0
enriched	Bcg2	77.5	8	3.8	8.5	1.3	5.7	2	319	4.2	< 2.3	0	< 0.9	0	< 1.7	0
depleted	CBg	120	12.6	3.9	5.1	0.9	< 5.2	-2.7	382	4.4	< 2.3	0	< 0.8	0	< 1.7	-0.4
enriched	CBg	120	56.2	4.2	8.5	1.3	5.2	1.9	337	4.3	< 2.3	-0.5	< 0.9	0	< 1.7	0
Haplic Gleysol																
Ah1	Ah1	5	< 7.5	0	3.5	1	< 5.2	-1.4	152	2.9	< 1.6	0	< 0.9	0	12.9	0.9
Ah2	Ah1	20	10.6	3.9	4.6	1.1	< 5.3	-3	184	3.1	1.7	1	< 0.8	0	10.7	0.9
Go1	2Bl	30	< 7.3	0	< 2.4	0	6.4	1.6	593	5.2	< 2.8	0	< 0.8	0	< 1.5	0
Go2	2Blc1	50	< 7.4	0	< 2.7	0	6.3	1.9	332	4.1	< 2.2	0	< 0.9	0	< 1.6	0
Gro	2Blc2	70	< 7.2	0	< 2.7	-1.5	< 4.8	-3.4	278	3.9	1.7	1.2	< 0.8	0	< 1.5	0
Gor	2BCr	90	< 7.3	0	< 2.8	-0.9	4.1	1.6	331	4.3	< 2.3	0	< 0.9	0	< 1.5	0
Gr1	2Cr1	105	< 7.3	0	2.2	0.7	< 4.9	-3.4	264	3.9	< 2.1	0	< 0.9	0	< 1.5	0
Gr2	2Cr2	120	< 7.4	0	< 2.9	-1.2	< 5.0	-3.9	257	3.9	< 2.1	0	< 0.9	0	< 1.6	0
redoximorphic zones:																
enriched	2Blc1	50	< 7.4	-4.9	< 2.9	0	< 5.3	-1.4	328	4.2	< 2.3	0	< 0.9	0	< 1.7	0
enriched	2Blc2	70	< 7.4	-4	< 2.9	-1.5	6.5	2	394	4.6	< 2.5	0	< 0.9	0	< 1.6	0

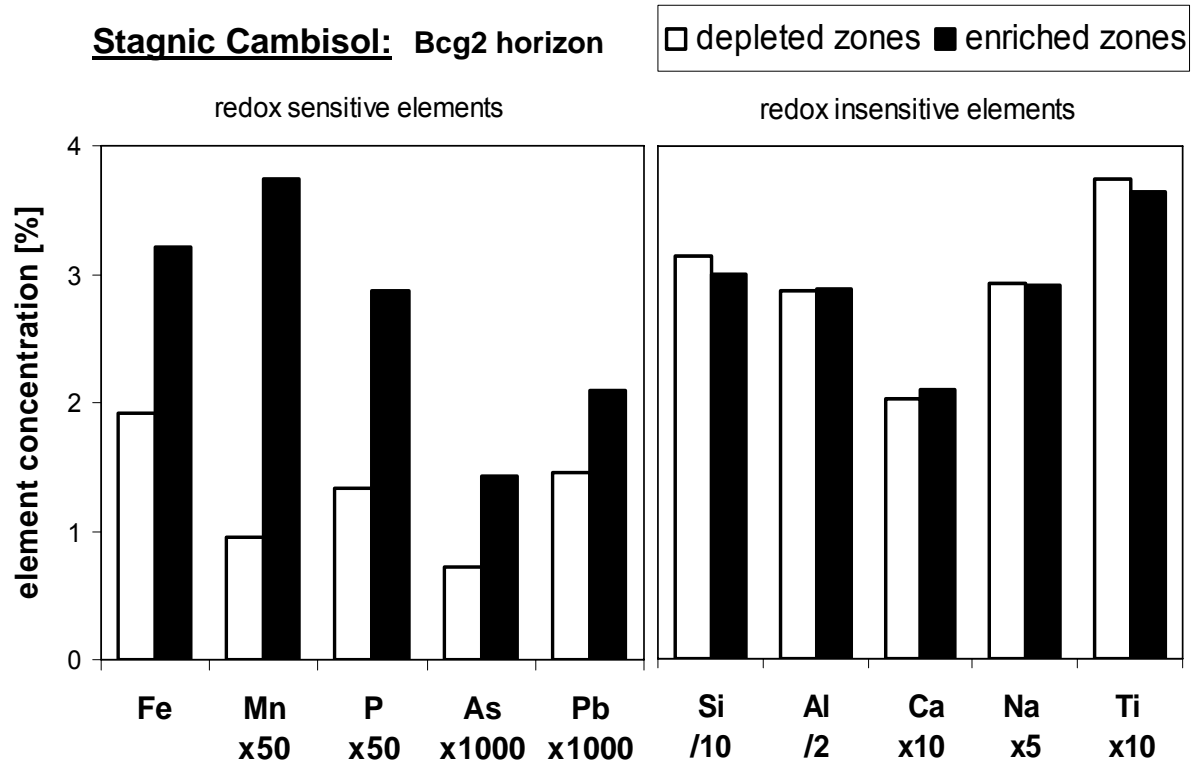


Figure A2.1 Comparison of total concentrations of selected redox sensitive and redox insensitive elements between enriched and depleted zones in the Bcg2 horizon of the Stagnic Cambisol profile measured by X-Ray fluorescence. Concentration values were scaled linearly by the indicated factors in order to allow easier comparisons.

Appendix 3

(referring to work presented in chapter 6)

Table A3.1 Experimental design of goethite batch dissolution experiments.

<u>mechanism</u>	<u>reagent</u>	<u>goethite</u>	<u>condition</u>	<u>product in solution</u>	<u>reaction time</u>	<u>initial pH</u>
proton-promoted	0.5 M HCl	2.5 – 12.5 g/L	dark	Fe(III)	3 min – 24 h	0.3
ligand-controlled	5 mM oxalate	2.5 g/L	dark	Fe(III)-oxalate	5 min – 315 d	3
reductive	1 mM oxalate	0.5 g/L	light	Fe(II)	5 min – 7.5 h	3

Table A3.2 Summary of results for dissolution experiments (chapter 6)

sample	dissolution time [min]	dissolved fraction [%]	$\delta^{57}\text{Fe}$ [‰] vs. IRMM-014	2SD	n	$\Delta^{57}\text{Fe}$ [‰] vs. bulk goethite
bulk goethite	-	100	0.54	0.15	11	0
dark 1	5	0.04	-1.32	0.15	3	-1.86
dark 2	10	0.05	-1.31	0.24	3	-1.85
dark 3	90	0.17	-0.49	0.26	4	-1.03
dark 4	180	0.21	-0.22	0.41	4	-0.76
dark 5	1260	0.41	0.16	0.24	4	-0.38
dark 6	5580	0.75	0.58	0.16	4	0.04
dark 7	10080	1.15	0.77	0.12	3	0.23
dark 8	30240	1.84	0.98	0.03	3	0.44
dark 9	60480	3.29	0.94	0.19	3	0.40
dark 10	136800	5.74	1.04	0.29	4	0.50
dark 11	191520	6.79	1.05	0.12	3	0.50
dark 12	275040	6.05	1.10	0.06	4	0.56
dark 13	453600	6.34	1.14	0.03	4	0.60
wash 1 (H ₂ O, pH 4)	-	0.13	1.09	0.12	4	0.55
leach 1 (0.5 M HCl)	15	0.17	0.24	0.14	4	-0.30
leach 2 (0.5 M HCl)	90	0.07	0.33	0.20	4	-0.21
dark total residue	-	100	0.48	0.08	4	-0.07
light 1	5	0.07	-1.90	0.17	4	-2.44
light 2	10	0.10	-1.16	0.11	4	-1.70
light 3	15	0.13	-1.14	0.17	4	-1.68
light 4	45	0.95	0.07	0.08	4	-0.47
light 5	90	3.15	0.60	0.20	4	0.06
light 6	180	8.72	0.71	0.15	4	0.17
light 7	300	13.8	0.68	0.11	3	0.14
light total residue	-	100	0.54	0.15	3	0.00
HCl 1	3	0.008	0.39	0.17	2	-0.15
HCl 2	1440	0.13	0.37	0.19	3	-0.17
HCl total residue	-	100	0.45	0.17	6	-0.09
dark B1	90	0.20	-0.56	0.05	3	-1.10
dark B2	1260	0.40	0.07	0.20	3	-0.47
dark B3	5580	0.74	0.53	0.08	3	-0.02
dark B4	10080	1.19	0.76	0.14	3	0.22
dark C2	1260	0.40	0.07	0.08	3	-0.47
dark C3	5580	0.74	0.46	0.06	3	-0.08
dark C4	10080	1.13	0.73	0.09	3	0.18
dark C5	136800	5.84	1.01	0.34	4	0.47
dark C6	191520	6.15	1.01	0.16	3	0.47
dark C7	275040	6.05	1.06	0.03	3	0.52
dark C total residue	-	100	0.56	0.08	3	0.02
dark D1 pH 4	90	0.14	-0.53	0.16	3	-1.07
dark D2 pH 4	1260	0.30	0.18	0.04	3	-0.36
dark D3 pH 4	5580	0.68	0.68	0.18	3	0.14
dark D4 pH 4	10080	0.85	0.78	0.16	3	0.24
dark D5 pH 4	30240	1.22	0.98	0.11	3	0.44
dark D6 pH 4	60480	1.96	1.07	0.19	3	0.52
light B1	30	0.59	-0.40	0.16	4	-0.94
light B2	80	1.56	0.30	0.15	4	-0.24
light B3	170	4.71	0.61	0.02	4	0.07
light B4	260	8.64	0.68	0.11	4	0.13
light B5	370	14.0	0.71	0.11	4	0.17
light B6	450	16.8	0.73	0.17	4	0.18

Samples marked B, C and D are additional sample series not discussed in the text. These data complement our main sample series and confirm the reproducibility of our results.

Description of kinetic fractionation model:

Calculation of total surface site pool (monolayer):

$$\boxed{\text{fraction of surface Fe atoms [\%]} = SSD \cdot SA \cdot M_{\text{goethite}} \cdot N_A^{-1} \cdot 100} \quad (1)$$

SSD [1/m²] = surface site density of Fe atoms

(4.35 sites/nm² from Koretsky et al., 1998, see chapter 6)

SA [m²/g] = surface area of goethite determined by N₂-BET-method (38 m²/g)

M_{goethite} [g/mol] = molar mass of goethite (FeOOH: 88.85 g/mol)

N_A [1/mol] = Avogadro number (6.02 · 10²³)

Table A3.3 Distribution of iron isotopes in IRMM-014 (IRMM, 1999, see chapter 3)

isotope ⁿ Fe	fraction (X _n)	exact mass (m)	mass difference (md _n)
⁵⁴ Fe	0.05845	53.9396147	-0.03412
⁵⁶ Fe	0.91754	55.9349418	0.00161
⁵⁷ Fe	0.021192	56.9353983	0.01952
⁵⁸ Fe	0.002818	57.9332801	0.03739
∅Fe	1.0000	55.8451479	0

mass difference of isotope ⁿFe to ∅Fe (n = 54, 56, 57, 58):

$$\boxed{md_n = \frac{m_n - m_{\emptyset\text{Fe}}}{m_{\emptyset\text{Fe}}}} \quad (2)$$

F = fractionation constant for specific reaction (independent of isotopic mass)

$$f_n = md_n \cdot F \quad (\text{note: } f_n \text{ is negative for } ^{54}\text{Fe} \text{ and positive for } ^{56}\text{Fe}, ^{57}\text{Fe} \text{ and } ^{58}\text{Fe}) \quad (3)$$

f_n determines the fractionation of isotope n relative to the average mass of iron (\bar{M}_{Fe}). We use this nomenclature rather than the commonly used fractionation factor α or enrichment factor ε because these values only refer to fractionation between two specific isotopes (e.g., ratio $^{57}\text{Fe}/^{54}\text{Fe}$), whereas f_n can be used for all four isotopes. However, the conversion of F to α and ε is shown in the following equations:

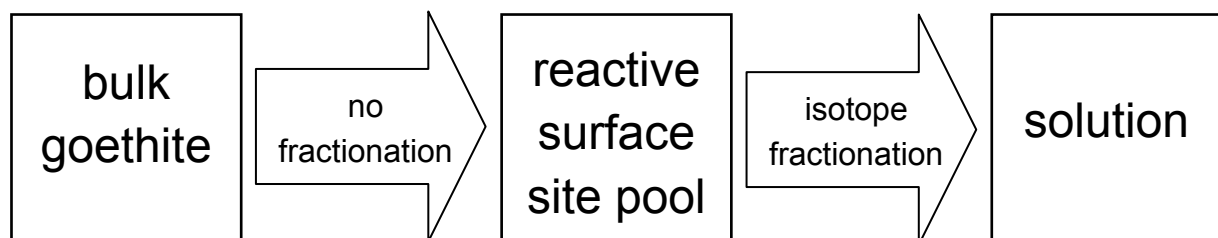
fractionation factor α for isotopes ^aFe and ^bFe ($a > b$): $\alpha = 1 + (md_a - md_b) \cdot F \quad (4)$

enrichment factor ε for isotopes ^aFe and ^bFe ($a > b$):

$$\varepsilon [\text{‰}] = (\alpha - 1) \cdot 10^3 = (md_a - md_b) \cdot F \cdot 10^3 \quad (5)$$

enrichment factor ε for the isotope ratio $^{57}\text{Fe}/^{54}\text{Fe}$: $\varepsilon [\text{‰}] = \Delta^{57}\text{Fe}_{\text{sol}} - \Delta^{57}\text{Fe}_{\text{rss}} \quad (6)$

Our model conceptually defines the following three compartments:



The size of the reactive surface site pool (rss) is constant due to self-replication of reactive surface sites during the dissolution reaction (number of Fe atoms dissolved equals number of Fe atoms replenished from bulk). Whereas the dissolution reaction differentiates between the different Fe isotopes, the self-replication of reactive surface sites from the bulk goethite is only dependent on the crystallographic position of the new reactive site and not on its isotopic mass. We express our model in terms of numbers of Fe atoms in a closed system. However, it could be easily converted into molar concentration units.

$[{}^n\text{Fe}]^{\text{bulk}}$ = number of atoms of isotope ${}^n\text{Fe}$ in bulk goethite (n = 54, 56, 57, 58)

$[{}^n\text{Fe}]^{\text{rss}}$ = number of atoms of isotope ${}^n\text{Fe}$ in reactive surface site pool
(n = 54, 56, 57, 58)

$[{}^n\text{Fe}]^{\text{sol}}$ = number of atoms of isotope ${}^n\text{Fe}$ in solution (n = 54, 56, 57, 58)

X_n = fraction of isotope n in bulk mineral (from Table A3.3) (n = 54, 56, 57, 58)

$$\boxed{[\text{Fe}]^{\text{tot}} = \sum_n [{}^n\text{Fe}]^{\text{bulk}} + \sum_n [{}^n\text{Fe}]^{\text{rss}} + \sum_n [{}^n\text{Fe}]^{\text{sol}}} \quad (7)$$

(total number of Fe atoms in system)

$$\boxed{\xi = \sum_n [{}^n\text{Fe}]^{\text{sol}} = [{}^{54}\text{Fe}]^{\text{sol}} + [{}^{56}\text{Fe}]^{\text{sol}} + [{}^{57}\text{Fe}]^{\text{sol}} + [{}^{58}\text{Fe}]^{\text{sol}}} \quad (8)$$

(ξ = reaction progress variable)

$$\text{dissolved fraction [\%]} = \frac{\xi \cdot 100}{[\text{Fe}]^{\text{tot}}}$$

$$\text{output of isotope n from rss} = \frac{(1-f_n)[{}^n\text{Fe}]^{\text{rss}}}{\sum_n (1-f_n)[{}^n\text{Fe}]^{\text{rss}}} \partial \xi \quad (\text{dissolution with isotope fractionation})$$

$$\text{input of isotope n to rss} = X_n \partial \xi \quad (\text{replenishment from bulk without isotope fractionation})$$

Differential equation describing the distribution of Fe isotopes in the reactive surface site pool:

$$\frac{\partial [{}^n Fe]^{rss}}{\partial \xi} = - \frac{(1 - f_n) [{}^n Fe]^{rss}}{\sum_n (1 - f_n) [{}^n Fe]^{rss}} + X_n \quad (9)$$

We developed a numerical model describing the system with 2 fitting parameters:

- fractionation constant F (can be converted to enrichment factor ε with equation 5)
- size of reactive surface site pool (rss)

The two parameters have a different influence on the model output. Whereas the fractionation constant F (or enrichment factor ε) is very sensitive at early dissolved fractions and defines the initial fractionation step, the size of the reactive surface site pool (rss) influences the surface depletion effect and is responsible for the shape of the curve at higher dissolved fractions. The best model fit was determined using the Solver tool of Microsoft EXCEL. First, we approximated our experimental data (only early-dissolved fractions with $\Delta^{57}Fe < 0 \text{ ‰}$) with simple logarithmic functions ($R^2 = 0.9903$ for oxalate dark and $R^2 = 0.9395$ for oxalate light). Solver was then used to find the best model fit by varying simultaneously the two fitting parameters (enrichment factor and size of reactive surface site pool) and thereby minimizing the sum of squared differences between our model and the approximated log functions within the range of dissolved fractions of our experimental data (0.04 – 0.41 % for oxalate dark and 0.07 – 0.95 % for oxalate light).

The following two figures S1 and S2 show the sensitivity of our model towards the two fitting parameters in the oxalate dark experiments.

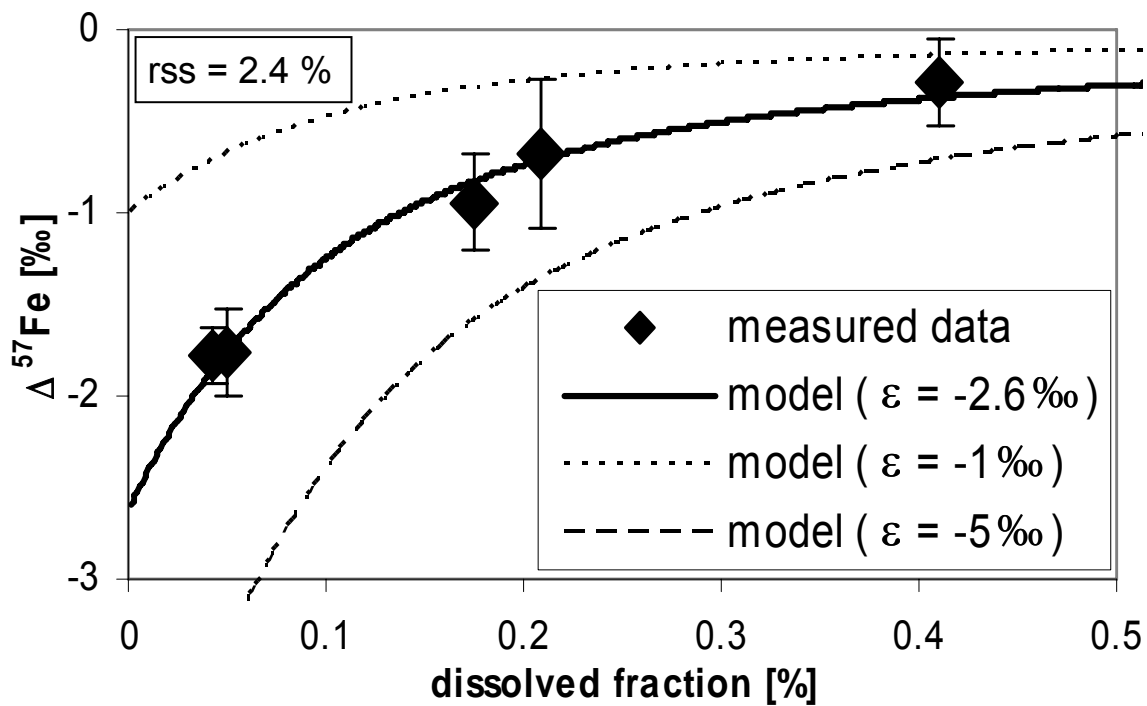


Figure A3.1 Model output with different enrichment factors ϵ and fixed size of reactive surface site pool (rss = 2.4 %)

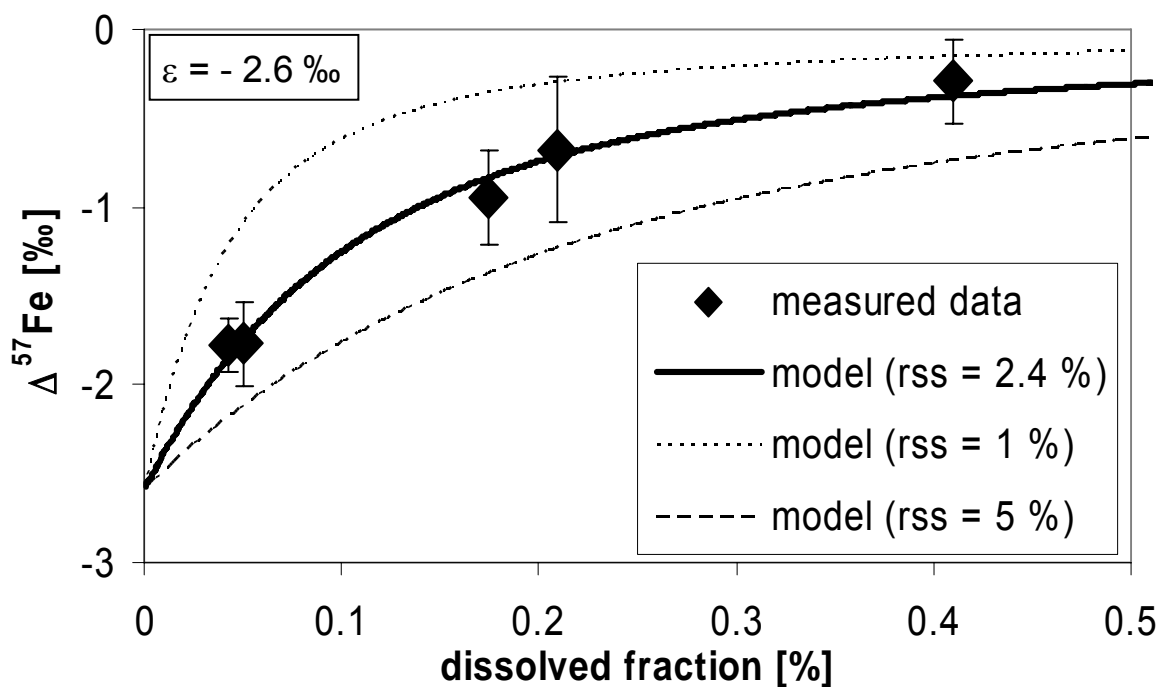


Figure A3.2 Model output with different sizes of reactive surface site pool and fixed enrichment factor ($\epsilon = -2.6\text{‰}$)

ACKNOWLEDGEMENTS

I would like to thank the following people for their help during my PhD studies:

- Prof. Dr. Ruben Kretzschmar, for giving me the possibility to work on this thesis, and for his sustained support during all phases of my project from field work to manuscript editing. Thanks for creating such a wonderful working environment and for always having time when needed!
- PD Dr. Stephan N. Kraemer, for his continuous support of my work, especially during the laboratory experiments and modeling development, for his contagious enthusiasm and many thoughtful discussions.
- Dr. Nadya Teutsch, for teaching me how to measure iron isotopes, for sharing all her analytical experience with me, and for her inspiring support of my project.
- Prof. Dr. Alex N. Halliday, for building an amazing isotope laboratory and assembling a great group, for his support of the project and his interest in my work.
- Dipl. Umwelt-Natw. ETH Paul Borer, for his help during the photoreductive dissolution experiments.
- Kurt Barmettler, for his skilled support in the soil chemistry laboratory and his uncomplicated manner of making things work.
- the whole staff of the ETH MC-ICPMS lab, especially Dr. Felix Oberli, for excellent maintenance and support in the isotope geochemistry laboratory.
- Nicholas Chambers, for his support in the lab during his stay in Zurich.
- Prof. Dr. Bernard Bourdon, for his interest in my work and the hospitality to finish my PhD work in his new lab and research group.
- Prof. Dr. Tim Mansfeldt, for guiding us to a fantastic Podzol profile.
- Charlotte Wüstholtz, for her reliable support in administrative issues.
- all members of the ETH soil chemistry and isotope geochemistry groups for a lot of help during my PhD studies and for a friendly and cooperative working atmosphere.
- last but not least, my parents, for their support during all my studies.

CURRICULUM VITAE

Jan Georg Wiederhold

born on September, 6th, 1975 in Kronberg, Germany

citizen of Germany

1981-1994 primary school and Gymnasium in Hofheim am Taunus, Germany

1994-1995 mandatory civil service, Naturschutzjugend Mainz, Germany

1995-1999 studies in geoecology, University of Karlsruhe, Germany

1999-2000 studies at Oregon State University, Corvallis, USA
with a scholarship of the German-American Fulbright commission

2000 degree “Master of Science”, Oregon State University, Corvallis, USA
(major: Soil Science, minor: Environmental Engineering)

2001-2002 diploma examinations and thesis, University of Karlsruhe, Germany

2002 degree “Diplom-Geoökologe”, University of Karlsruhe, Germany

2002-2006 PhD studies at the Institute of Biogeochemistry and Pollutant Dynamics (until May 2006: Institute of Terrestrial Ecology), Soil Chemistry Group of Prof. Ruben Kretzschmar and at the Institute of Isotope Geochemistry and Mineral Resources, Isotope Geochemistry Group of Prof. Alex Halliday (since October 2005: Prof. Bernard Bourdon), ETH Zurich, Switzerland

(private e-mail address: jan.wiederhold@gmx.net)

This PhD thesis is part of the ETH E-Collection
and available online in electronic format:
<http://e-collection.ethbib.ethz.ch/diss>

